T.C.
ISTANBUL OKAN UNIVERSITY
INSTITUTE OF GRADUATE SCIENCES

THESIS

FOR THE DEGREE OF

MASTER OF SCIENCE

IN AUTOMOTIVE MECHATRONICS AND INTELLIGENT VEHICLES PROGRAM

Abdelmounaim BENSABEUR

PREDICTING BATTERY STATE OF HEALTH: THE MACHINE LEARNING APPROACH

THESIS SUPERVISOR:

PROF. DR. Ramazan Nejat TUNCAY

ISTANBUL, 2024

T.C.
ISTANBUL OKAN UNIVERSITY
INSTITUTE OF GRADUATE SCIENCES

THESIS

FOR THE DEGREE OF

MASTER OF SCIENCE

IN AUTOMOTIVE MECHATRONICS AND INTELLIGENT VEHICLES PROGRAM

Abdelmounaim BENSABEUR

223005004

PREDICTING BATTERY STATE OF HEALTH: THE MACHINE LEARNING APPROACH

THESIS SUPERVISOR:

PROF. DR. Ramazan Nejat TUNCAY

ISTANBUL, 2024

T.C.
ISTANBUL OKAN UNIVERSITY
INSTITUTE OF GRADUATE SCIENCES

THESIS FOR THE DEGREE OF MASTER OF SCIENCE IN AUTOMOTIVE MECHATRONICS AND INTELLIGENT VEHICLES PROGRAM

Abdelmounaim BENSABEUR
223005004

Date Thesis Delivered to Institute:

Date of Thesis Defence:

Thesis Advisor: Prof. Dr. Ramazan Nejat TUNCAY

Jury Members: Assoc.Prof. Dr. Ömer Cihan KIVANÇ

Assoc. Prof. Dr. Salih Barış ÖZTÜRK

ISTANBUL, 2024

ABSTRACT

PREDICTING BATTERY HEALTH FOR ELECTRIC VEHICLES USING MACHINE LEARNING APPROACH

Research utilized data-driven models to investigate SoH estimation methodologies for lithium-ion batteries, particularly focusing on their effectiveness in capturing degradation trends. The study evaluated four different deep learning approaches-DNN, CNN, RNN, and LSTM-using various metrics, including MAE, RMSE, R^2, and validation loss. Results reveal that the LSTM model outperforms others, achieving the lowest MAE (0.1293), RMSE (0.1680), and validation loss (0.0282), with an R^2 of 0.9790, making it the most reliable predictor of battery SoH. The study highlights a strong linear correlation between SoH and parameters such as capacity and charge voltage, affirming their role as critical indicators of battery health. Conversely, temperature exhibited negligible impact on SoH within the narrow range studied, necessitating further research under diverse environmental conditions. Anomalies in terminal current during charge-discharge cycles suggest potential operational irregularities requiring deeper analysis. The study underscores the limitations of CNN in modeling temporal dependencies, advocating for hybrid architectures like CNN-LSTM for enhanced predictive accuracy. Findings also demonstrate consistent SoC transitions across cycles, emphasizing the stability of the battery's charge-discharge behavior and its implications for long-term durability. Recommendations include adopting LSTM-based models in battery management systems, refining anomaly detection mechanisms, and optimizing charge protocols to prevent premature degradation. The study's outcomes provide a robust framework for enhancing battery health monitoring and forecasting, contributing to the advancement of energy storage technologies. The focus of future research will be expanded thermal ranges, cutting-edge hybrid models, and the integration of real-world applications in validation of these findings. This shows potential value in using these findings for optimizations that affect the performance and life of LiBs, whether for EVs or renewable energy systems.

Keywords: Lithium Li-ion batteries, State of Health, State of Charge, Battery management system

ACKNOWLEDGMENT

I would like to express my profound gratitude and appreciation to my family for providing me with the unwavering support and motivation that has been instrumental in my academic pursuits. I am also grateful to my supervisor, Prof. Dr. Ramazan Nejat TUNCAY as well as Prof. Ömer Cihan Kıvanç , for their unceasing guidance and encouragement throughout my MSc studies and related work. Their invaluable insights and unflagging support have been of great benefit to me. Their constructive suggestions and consistent encouragement have been of significant assistance in the completion of this thesis. I would also like to express my gratitude to my colleagues for their assistance and for fostering a positive and collaborative work environment.

This research was made possible by the support of the Scientific and Technological Research Council of Turkey (TUBITAK) as well as MUTLU Co. R&D for their collaboration on conducting the tests. I am indebted to TUBITAK for its assistance in procuring the necessary hardware components through the national support programme of TUBITAK 5220028.

TABLE OF CONTENTS

LIST OF FIGURES

LIST OF TABLES

ABBREVIATIONS

LiB	Lithium Li-ion battery
CNN	Convolutional Neural Network
DNN	Deep Neural Network
RNN	Recurrent Neural Network
LSTM	Long Short-Term Memory
MAE	Mean Absolute Error
AE	Absolute Error
SoH	State of Health
SoC	State of Charge
BMS	Battery Management System
SVR	Support Vector Regression
RMSE	Root Mean Square Error
MSE	Mean Squared Error
EV	Electrical Vehicle
FOC	Fractional-Order Control
ECM	Equivalent Circuit Model
OCV	Open Circuit Voltage
EIS	Electrochemical Impedance Spectroscopy
KF	Kalman Filter
UKF	Unscented Kalman Filter
PF	Particle Filter
LR	Linear Regression
FFNN	Feedforward Neural Network
ANN	Artificial Neural Network
DTR	Decision Tree Regression
RFR	Random Forest Regression

KNN	K-Nearest Neighbors
LFP	Lithium Iron Phosphate
PBM	Physics-Based Model

CHAPTER 1
INTRODUCTION

1.1 INTRODUCTION

Electric vehicles (EVs) represent a crucial step in the global evolution toward sustainable and environmentally friendly transportation. Central to their operation is the lithium-ion (Li-ion) battery, a technology celebrated for its high energy density, longevity, and efficiency. However, as EV adoption accelerates, a pressing challenge emerges: the degradation of battery health over time. This deterioration directly impacts the vehicle's range, performance, and overall reliability, raising concerns for both manufacturers and consumers. Addressing this issue requires a robust methodology to predict the State of Health (SOH) of EV batteries, ensuring optimal performance and extending their usable lifespan. This study focuses on the development of a novel DNN model to predict battery health accurately, leveraging advanced data-driven techniques and experimental data.

Battery degradation is an inevitable phenomenon triggered by a mixture of chemical, thermal, and mechanical aspects [1]. These issues are exacerbated by real-world conditions such as extreme temperatures, frequent fast charging, and deep discharging cycles [2]. Effective management of these challenges demands a comprehensive understanding of the underlying mechanisms and a predictive framework to mitigate their impact [3]. Adding to the complexity is the variability in battery performance due to differences in manufacturing processes, usage patterns, and environmental conditions [4]. Achieving reliable SOH predictions requires integrating advanced sensing technologies with sophisticated computational models [5]. Traditional methods based on electrochemical principles, while accurate, often fall short in real-time applications due to their computational intensity [6]. In this context, data-driven approaches, particularly those leveraging ML and DL present a compelling alternative [7].

Li-ion batteries have significantly improved in terms of materials, designs, and management systems over time [8]. An emphasis has been placed on innovations like solid-state electrolytes and advanced cathode materials like nickel-manganese-cobalt (NMC) and lithium iron phosphate (LFP) in order to create greener and more sustainable batteries [9]. Even with these advancements, degradation is still a problem, requiring ongoing observation and forecasting of battery health [10]. The combination of data analytics and conventional battery modeling is one of the major advancements in battery management [11]. Global research endeavors are progressively centering on the advancement of hybrid methodologies that merge machine learning techniques with physics-based models [12]. Large datasets can be meaningfully analyzed thanks to this synergy, which opens the door to more precise and trustworthy SOH predictions [13].

Data driven models have transformed the battery health management domain completely utilizing huge volumes of operational data [14]. Machine learning proved capability in predicting the cycle life of batteries well before the onset of significant capacity degradation [15]. Assuming the voltage, current, temperature, and charging/discharging profiles, such models can be utilized for very accurate estimates of the remaining useful life of the batteries [16]. Due to its ability to derive complex non-linear data relationships, deep learning is arguably the most used of these machine learning methods [17]. The analysis of high-dimensional datasets has previously been achieved using DNN, CNN, and RNN models, which have given uncharted insight into battery behavior [18]. For instance, applications of machine-learning-based methods of SOH estimation found their way into real-life applications [19]. Long short-term memory (LSTM) networks also estimate battery health leveraging cut-off, time-based features showing how equitable these deep learning architectures are [20].

Despite the progress made, predicting battery health remains a challenging endeavor [21]. The dynamic nature of Li-ion batteries, influenced by factors such as aging, temperature variations, and cycling conditions, poses significant hurdles for model development [22]. There are limitations of existing approaches in capturing the intricate interplay between these variables, underscoring the need for more sophisticated modeling techniques [23]. Another

challenge lies in the availability and quality of data [24]. Comprehensive datasets that encompass diverse operating conditions are essential for training robust models [25]. The importance of standardized data collection protocols is stressed to facilitate the development of generalized models applicable across different battery chemistries and configurations [26].

This study suggests a DNN model intended to precisely approximate SOH of EV batteries as a solution to these problems [27]. The model predicts battery health with high precision by utilizing experimental data, such as voltage, current, temperature, and available health indicators [28]. The model uses cutting-edge feature extraction and optimization techniques in an effort to get beyond the drawbacks of conventional approaches and offer useful insights for battery management [29]. Transfer learning and hybrid modeling are the foundations of the suggested DNN framework [30]. It produces a reliable and scalable solution by fusing deep learning algorithms' predictive capability with domain expertise from electrochemical models [31]. Moreover, the architecture of the model is designed to manage extensive, high-dimensional datasets, guaranteeing its practicality in real-life situations [32].

The suggested methodology is consistent with the patterns noted in current research [33]. In order to predict battery health, feature selection and model optimization are crucial, and methods like random forest classification and DNNs play a significant part in this regard [34]. It is commonly known that data-driven approaches have the ability to increase the precision and dependability of SOH predictions [35]. Furthermore, a key component of the suggested remedy is the fusion of data-driven models with insights derived from physics [36]. The study intends to provide EV stakeholders with useful insights into battery behavior and a comprehensive understanding of battery behavior by merging the advantages of both methodologies [37].

This study aims to: (1) develop a DNN model for accurate prediction of the SOH of EV batteries, (2) leverage experimental data, including voltage, current, temperature, and health indicators, to train and validate the model, (3) integrate physics-based insights with data-driven methods to enhance the model’s predictive capabilities, (4) address the challenges of data variability and dynamic operating conditions through advanced feature extraction and optimization methods, and (5) provide actionable insights for battery

management, contributing to the longevity and reliability of EVs [38]. By achieving these objectives, the study seeks to advance the state of the art in battery health prediction, offering a scalable and practical solution for the growing EV market [39].

1.2 Application of Lithium Li-ion Batteries (LiB)

Indeed, lithium-ion batteries (LiBs) are ubiquitous in advanced technology and are extensively varied for applications in all types of industries. They provide power in today's consumer electronic devices and several renewable energy storage applications. These batteries have become the most preferred choice in many industries due to their long cycle life, high energy density, and very low self-discharge rate. To examine the various applications of LiBs through the lens of industry reports and scientific studies, this paper discusses data.

1.2.1 Consumer Electronics

In today's consumer electronics, Li-ion batteries are essential for powering gadgets like wearables, laptops, tablets, and smartphones. Li-ion batteries' high energy density makes them ideal for prolonged use, which is a crucial need for contemporary electronics. This technology greatly benefits smartphones because it permits lightweight designs without sacrificing battery life [1]. Li-ion batteries in smartphones are now even more useful thanks to fast charging capabilities, which satisfy users who need quick and effective recharging [2]. Li-ion batteries play a major role in the dependable performance and portability of laptops and tablets. High-performance computer tasks are supported by Li-ion batteries' energy efficiency, allowing users to work without constantly needing access to power outlets [3]. Tablets take advantage of these batteries' small size to create stylish designs that suit a variety of personal and business applications [4].

Human wearable devices such as smartwatches and fitness trackers also rely on Li-ion batteries for their operation. These devices demand compact, lightweight batteries with sufficient capacity to sustain continuous operation. Li-ion batteries meet these requirements, enabling functionalities like heart rate monitoring, GPS tracking, and real-time notifications [5]. Beyond their role in specific devices, Li-ion batteries have revolutionized the consumer

electronics industry by driving innovations in device design and functionality. Their efficiency and compact size have opened new possibilities for product development, allowing manufacturers to create thinner, lighter, and more versatile devices [6]. Additionally, the recyclability of Li-ion batteries aligns with sustainability goals, contributing to the reduction of electronic waste [7].

1.2.2 Electric Vehicles (EVs)

The electric vehicle (EV) revolution owes much of its success to the advancements in Li-ion battery technology. These batteries provide the high energy density and efficiency required to power EVs, making them the cornerstone of sustainable transportation. Li-ion batteries enable extended driving ranges, which is a critical factor for consumer adoption of EVs [8]. Moreover, their ability to handle fast charging enhances the convenience of owning an EV, reducing downtime for users [9]. Automakers are leveraging Li-ion technology to improve the performance and reliability of EVs. Innovations in battery design, such as the development of thermal management systems, have addressed challenges related to overheating, safeguarding the safety and longevity of the batteries [10]. Furthermore, improvements in energy density have allowed manufacturers to design vehicles with greater range without increasing the battery size or weight [11].

LiBs use in electric vehicles (EVs) is also in line with international initiatives to lower greenhouse gas emissions. A cleaner environment results from a reduced reliance on fossil fuels as EVs replace conventional internal combustion engine vehicles [12]. Li-ion battery demand is being further driven by governments and organizations around the world encouraging the use of EVs through infrastructure development and incentives [13]. Li-ion battery recycling and reuse are now essential components of the electric vehicle ecosystem. The environmental impact of battery production is lessened by efforts to create sustainable recycling methods that guarantee the recovery and reuse of valuable materials like cobalt and lithium [14]. Li-ion batteries are a sustainable option for EVs because of these initiatives, which not only support environmental goals but also address the financial aspects of resource management [15].

1.2.3 Renewable Energy Storage

Lithium-ion batteries are essential for storage renewable energies and to cope with their intermittency. These batteries can store the excess energy produced during its maximum production times to supply a regular and reliable energy source during low generation periods from the solar and wind systems [16]. This capability is called balancing between supply and demand, which is essential in integrating renewable energy resources into the grid [17]. Li-ion batteries, thus, can be said to be a part of grid-scale energy storage systems that build energy security while reducing the dependency upon fossil fuels. With the aid of these systems, utilities maximize the energy efficiency and reduce waste by storing excess renewable energy and discharging it during peak demand [18]. Li-ion battery systems can serve not only larger grid applications but also smaller community-based energy projects due to the scalability provision [19].

LiBs are frequently used with solar panels in residential settings. By storing energy during the day and using it at night, homeowners can lessen their reliance on the grid and cut their monthly electricity costs [20]. This application promotes energy independence and resilience against power outages in addition to its financial benefits [21]. Li-ion batteries are also utilized in microgrid applications, which provide electricity to isolated communities and commercial locations that are cut off from the main power system. They are a dependable option for these applications because of their effective energy storage and delivery capabilities, which guarantee a constant power supply [22]. Li-ion batteries are also becoming more and more viable for the storage of renewable energy due to advances in battery technology, such as longer cycle lives and higher energy efficiency [23].

1.2.4 Aerospace and Defense

In aerospace and defense, LiBs are valued for their lightweight nature, high energy output, and reliability. Satellites and spacecraft depend on Li-ion batteries to store solar energy, ensuring continuous operation during periods when sunlight is unavailable [24]. The ability to operate efficiently in extreme conditions makes these batteries indispensable for space exploration missions [25]. Drones and unmanned aerial vehicles (UAVs) used in defense applications rely on Li-ion batteries for power. These batteries provide the energy

needed for long flight durations and high-performance operations, making them critical for surveillance, reconnaissance, and combat missions [26]. Portable communication devices and radar systems also benefit from the compact and reliable power supply provided by Li-ion batteries, ensuring functionality in remote and challenging environments [27].

Innovations in Li-ion battery technology, such as improved thermal stability and energy density, have further enhanced their suitability for aerospace and defense applications. Research and development efforts continue to focus on making these batteries more robust and efficient, meeting the demanding requirements of these sectors [28]. The versatility and performance of Li-ion batteries have positioned them as a key enabler of advancements in aerospace and defense technologies [29].

1.2.5 Public Transportation

The introduction of electric buses and trains that run on Li-ion batteries is drastically altering public transportation networks. These batteries are suitable for the demanding requirements of public transportation operations because of their high energy density and effective rechargeability [30]. In line with international environmental goals, electric buses fitted with Li-ion batteries lower greenhouse gas emissions and enhance urban air quality [31]. Electric buses benefit greatly from Li-ion batteries' quick charging capability, which enables rapid turnaround times while in operation [32]. Improvements in battery technology, such as longer cycle life and better heat management, have increased the dependability and longevity of electric buses [33]. Li-ion technology also facilitates regenerative braking systems, which increase efficiency even further by recovering and storing energy during deceleration [34]. Li-ion batteries are utilized in commuter trains and light rail systems in addition to buses. These applications benefit from the scalability and efficiency of Li-ion technology, enabling sustainable and cost-effective public transportation [35]. The integration of Li-ion batteries into public transit systems represents a significant step toward reducing the carbon footprint of transportation while providing reliable and efficient mobility solutions for urban populations [36].

1.2.6 Industrial and Commercial Equipment

Li-ion batteries are becoming increasingly critical in industrial and commercial equipment, providing power for forklifts, cranes, automated guided vehicles (AGVs), and commercial cleaning machines. They are a great option for industrial settings where downtime must be kept to a minimum because of their high energy density and quick rechargeability [37]. Li-ion batteries provide longer cycle life and more energy efficiency than conventional lead-acid batteries, which lowers overall maintenance costs [38]. Li-ion batteries are used by forklifts and AGVs in warehouses and manufacturing facilities to ensure reliable performance and efficient operations. Their rapid recharging during breaks guarantees continuous workflow, thereby optimizing productivity [39]. These batteries provide dependable and transportable energy solutions for industrial uses, such as powering construction tools and cleaning equipment [40]. Li-ion technology is still essential to enabling effective and environmentally friendly operations as the need for sustainable energy solutions in industrial settings rises [41].

1.2.7 Telecommunications and Backup Power Systems

The telecommunications sector heavily depends on Li-ion batteries for reliable backup power solutions. Base stations, data centers, and telecommunication networks require consistent power to avoid disruptions, and Li-ion technology delivers this with high efficiency [42]. During power outages, Li-ion batteries ensure that communication systems remain operational, providing critical support in emergencies [43]. Li-ion batteries are preferred in telecommunication applications for their compact design, scalability, and ability to handle high energy demands. Data centers use Li-ion battery systems to power server operations during outages, reducing downtime and data loss risks [44]. As the reliance on telecommunication networks grows with the expansion of IoT and 5G technologies, the importance of resilient and efficient energy storage systems has increased, cementing Li-ion batteries as a critical component in this field [45].

1.2.8 Marine Applications and Shipping

The maritime industry is adopting Li-ion batteries for electric and hybrid vessels, ranging from small recreational boats to large cargo ships. These batteries contribute to

reducing emissions and improving fuel efficiency, addressing growing environmental regulations [46]. Hybrid systems in ships use Li-ion batteries for peak power demands, allowing for quieter and more efficient operations, especially in ports and ecologically sensitive areas [47]. Li-ion batteries are also instrumental in powering auxiliary systems in traditional ships, enhancing overall energy management. Their lightweight design and scalability make them suitable for various marine applications, supporting the transition toward greener maritime operations [48]. As global regulations tighten, Li-ion technology is expected to lead the way in transforming the shipping industry toward sustainability and reduced carbon footprints [49].

1.2.9 Agriculture and Farming Equipment

In modern agriculture, Li-ion batteries are becoming a cornerstone of innovative farming practices. They are used in electric tractors, harvesters, and drones for precision agriculture, enabling efficient monitoring and management of crops [50]. Li-ion batteries offer portability and long operational times, essential for remote and large-scale farming tasks [51]. Electric irrigation systems powered by Li-ion batteries reduce dependency on traditional energy sources, providing sustainable water management solutions. Moreover, drones equipped with Li-ion batteries aid in crop spraying, monitoring soil conditions, and assessing plant health, enhancing productivity and resource optimization [52]. As agriculture evolves toward sustainability and smart technologies, Li-ion batteries will continue to play a critical role in powering equipment that supports modern farming practices [53].

1.2.10 Wearable Technology and Implantable Medical Devices

Beyond portable electronics, Li-ion batteries power advanced wearable technologies such as augmented reality (AR) glasses and exoskeletons. In the medical field, these batteries are used in implantable devices such as pacemakers and neurostimulators, ensuring reliable operation over extended periods. The miniaturization of Li-ion batteries continues to open new possibilities for innovative wearable and medical applications, enhancing human health and performance. Li-ion batteries power a range of wearable technologies, including augmented reality (AR) glasses, fitness trackers, and exoskeletons. Their compact size and high energy density enable these devices to perform advanced functions such as real-time monitoring and enhanced

interactivity [54]. In the medical field, Li-ion batteries are used in implantable devices like pacemakers and neurostimulators, where long-term reliability is paramount. These batteries provide consistent power, ensuring the safety and efficacy of life-critical devices [55]. Miniaturization advancements in Li-ion technology continue to drive innovation, enabling the development of smaller, more efficient medical and wearable devices that enhance quality of life and expand the possibilities of health monitoring and treatment [56].

CHAPTER: 2

LITERATURE REVIEW

2.1 LITHIUM-ION BATTERY (LiB)

Transportation electrification and renewable energy integration are essential strategies. These approaches mitigate global warming and protect the environment [1]. Energy storage devices significantly influence system efficiency, robustness, and protection. Considerable progress has advanced reliable, cost-effective energy storage solutions recently. These advancements have fostered a diversity of energy storing technologies [2]. Lithium-ion batteries (LiBs) are the preferred choice commercially. They offer immense energy density, design diversity, and long lifecycle [3]. LiB dominate both energy storage markets and research landscapes. They provide significant advantages such as superior energy efficiency and minimal memory effects. These batteries also offer energy concentration suitable for large-scale energy systems. Additionally, they support battery and HEVs [4]. As a result, LiB production and usage have expanded rapidly. Their applications have become increasingly widespread worldwide [5]. LIBs are now critical for moveable electronics, EVs, and smart grids.

In practical use, battery systems consist of many interconnected cells. This setup ensures high output voltage and adequate energy storage. Across the value chain, data drives decisions during the battery lifecycle. It plays an essential role in design, production, sales, deployment, and management [6]. During the design phase, data accelerates innovation in components. Examples include electrodes, electrolytes, additives, and formation processes [7]. During sales, data helps classify batteries by expected lifespan. This improves reliability and consumer satisfaction [8]. Data is also essential during deployment for performance analysis. Insights cover battery chemistries, configurations, and manufacturer-specific details. This ensures batteries are matched to their operational requirements. Factors influencing selection include charge/discharge cycles and temperatures. Depth of discharge (DOD) and inactivity periods are additional considerations [9]. When in use, battery

management systems (BMS) ensure efficient operation. BMS depend heavily on data for their design and operational calibration.

BMS perform vital tasks like estimating charge and well-being states. The SOC ensures efficient battery operation and reliability. Monitoring the State of Health (SOH) improves system safety as well as longevity. LiB are favored for their high-capacity density and cycle life. Their advantages make them ideal for energy storage in EVs [10]. However, performance degradation occurs over time and with cycling. Degradation impacts energy and power capacities [11]. Battery aging reduces efficiency, driving range, and dynamic performance. These challenges pose risks for electric vehicles and reliability [12]. Correct SOH estimation is thus critically significant. SOH utilization ensures both operational safety and performance reliability [10]. Advanced data analytics and robust BMS technologies address aging issues effectively. These measures solidify LiB as leading energy storage solutions.

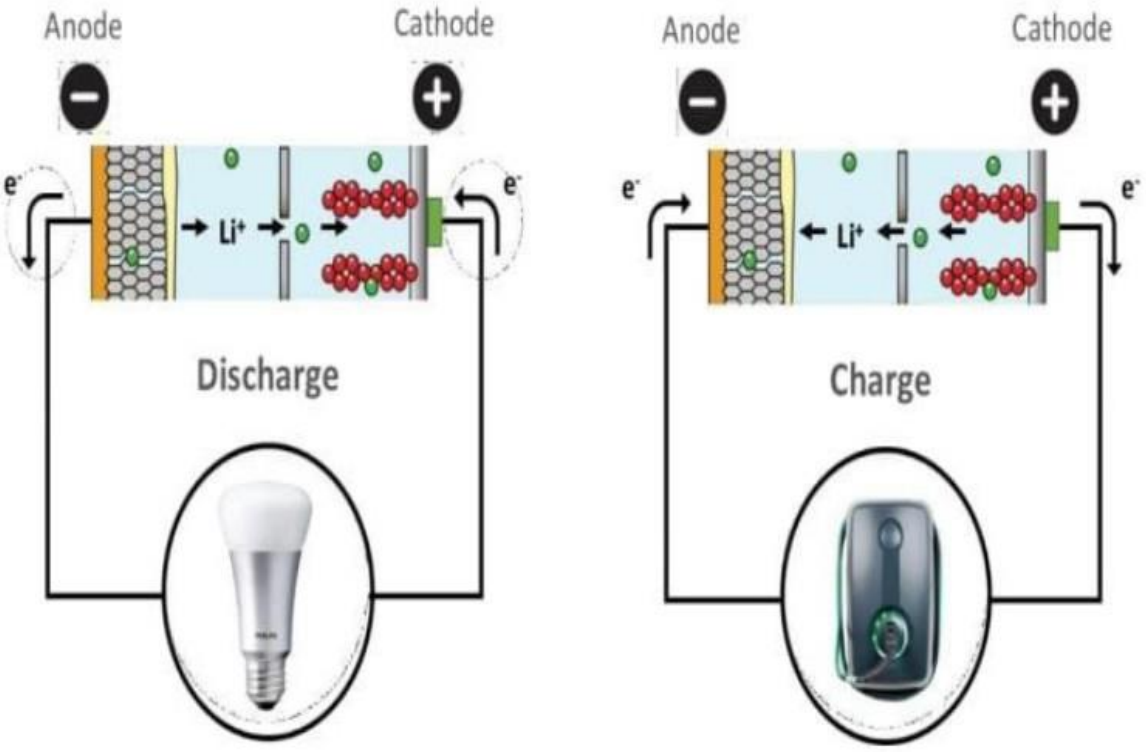

Figure 2.1.Lithium-Ion Battery Charging and Discharging [208]

LiB are rechargeable batteries with high energy density. They also offer an extended cycle life, making them reliable. The development of LiB has advanced rapidly. However, their lifespan is limited, and storage capacity decreases. This decline occurs with time and continuous usage. Therefore, assessing the SOH is crucial. SOH estimation helps in planning battery maintenance effectively. Reliable methods to estimate SOH ensure safe and efficient battery performance [13] analyzed regression techniques for estimating SoH. The study utilized multiple regression methods for this purpose. The various models are XGBoost, Support Vector Regression (SVR), random forest regression, Simple linear regression, Gradient-boosting regression, and Decision tree regression. NASA's Prognostics Data Repository provided data for the study. The method that proved the best among the tested ones was SVR. The results from SVR yielded RMSE, MSE, MAE, and MAPE values of 0.0226, 0.0005, 0.0208, and 0.0264, respectively. Hence, it can be said that SVR is a good estimator model for LiB SoH. This kind of advancement plays a major role in battery health management.

Following the research provided by [14] they suggested a data-driven SoH evaluation approach. This method used a simple yet effective health indicator (HI). The HI was extracted from a truncated 110-second discharge process. This approach addresses challenges in analyzing uncontrollable discharge processes. Unlike conventional HIs, the proposed HI uses different voltage ranges. This flexibility enhances its applicability to various scenarios. A (LSTM) deep learning model was employed. The LSTM learned the relationship between HI and practical SOH. Tests on an open dataset showed high estimation accuracy. This method requires no additional hardware or downtime for implementation. Such advancements simplify battery health monitoring and improve reliability. They developed another data-driven SOH estimation method. They introduced a novel energy-based health indicator (HI). This HI focuses on discharge processes that are less controllable. Unlike earlier methods, it combines voltage sequences and discharge rates. The inclusion of discharge rates improves the HI’s accuracy. The method allows online SOH estimation using offline training datasets. Validation on an open dataset reported an average RMSE of 1.23%. This demonstrates the effectiveness of this novel approach. These techniques offer significant potential for real-time applications.

In history, attention in cell chemistries and testing circumstances changed. These changes reflect advancements in battery technologies over time. NASA published the first public battery dataset in 2008. As new chemistries emerged, focus shifted from LFP to NMC and NCA batteries. Both NMC and NCA chemistries suit power tools, e-bikes, and EVs. They bargain higher detailed energy, decent power, and extended lifespans. The number of cells tested has significantly increased over time. This growth supports the study of complex battery interactions. NASA hosts couple of high-throughput battery datasets, totaling 62 cells. These datasets enable research on cell chemistry and testing conditions. They are essential for advancing LiB technology and diverse applications.

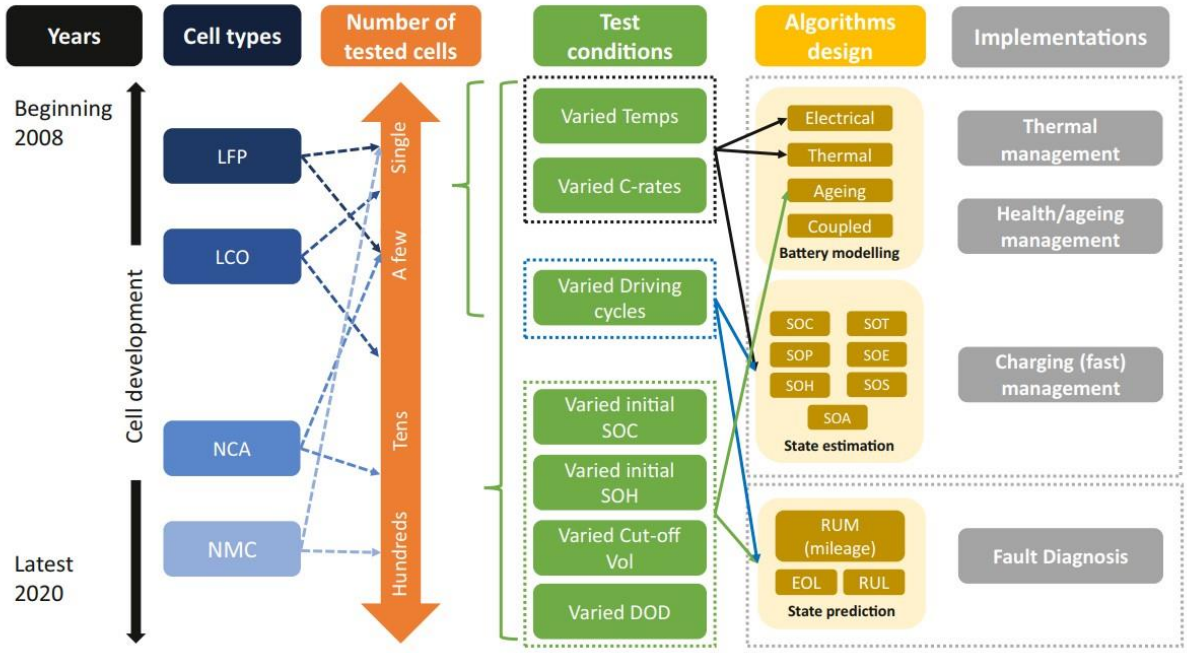

Figure 2.2.Historical Evolution of Dataset of Existing Batteries [16]

The literature highlights significant advancements in LiB technologies, particularly in SOH estimation methods, yet critical gaps remain in developing accurate, scalable, and real-time predictive models tailored for electric vehicle (EV) applications. Existing studies primarily focus on offline SOH estimation using controlled datasets, which do not adequately capture the dynamic and variable conditions of real-world EV operations. While data-driven techniques such as Support Vector Regression (SVR) and LSTM models have demonstrated

high accuracy, their reliance on laboratory datasets limits their applicability in operational EV scenarios. Furthermore, challenges persist in addressing uncontrollable discharge processes, with proposed health indicators (HIs) like voltage sequences and discharge rates still underexplored in practical contexts.

Another key gap lies in the adaptability of prediction models to emerging battery chemistries such as Nickel Manganese Cobalt (NMC) and Nickel Cobalt Aluminum (NCA), which exhibit unique degradation patterns under high energy and power demands. Although promising novel HIs have been introduced, their integration into real-world Battery Management Systems (BMS) for EVs remains limited. Additionally, current methods often require complex data inputs and computationally intensive processes, which may hinder scalability and cost-effectiveness, especially for large-scale EV fleets. Moreover, the long-term reliability of predictive models is affected by aging and performance degradation, yet there is insufficient research on how aging impacts prediction accuracy over extended battery lifespans. Lastly, real-world validation of these models is constrained by the availability of diverse datasets. Many studies rely on publicly available datasets such as those from NASA, which lack the variability of actual EV operational conditions, including temperature fluctuations, diverse driving behaviors, and environmental factors. Addressing these gaps requires the development of novel, real-time predictive models like a Deep Neural Network (DNN) that effectively utilize experimental data, as well as voltage, current, temperature, and advanced health indicators, to approximation SOH with higher accuracy and practical applicability in EV contexts.

2.2 LITHIUM IRON PHOSPHATE BATTERIES (LIPB)

Indeed, this is quite advantageous research. Many nations set active implement delinquent suppuration for electric vehicle (EV) development, of which lithium li-ion batteries (LiBs) form the essential influence source [16]. With a rapidly increasing demand for power LiBs, they are also becoming highly adept at making them [17]. However, commercial life span of these batteries is in the range of approximately 3 - 6 years; thus, the number of retired power batteries is increasing considerably [18]. Further, with the expected rapid growth of the EVs market, the enhancement of the importance and economic value

associated with battery recycling in the near future will be enhanced [19,20]. Recycling from retired power LiPBs is, therefore, strategically important to reduce production costs and resource conservation [21,22]. As to the cathode composition, lithium-ion batteries (LiBs) may be categorized under $LiFePO_4$, lithium cobalt oxide (LCO) batteries, lithium manganese oxide batteries (LMOB), lithium nickel cobalt manganese oxide batteries (NCMB), and lithium nickel cobalt aluminum oxide batteries (NCA). Among these, $LiFePO_4$ and NCMB batteries are the most used forms in the global electric vehicle (EV) industry [23].

In the context of an LFP battery, its discharge would include the following processes: electrons will break off from the lithium stored in the graphene layers of the negative electrode and form corresponding lithium ions. These travel through their separator to the positive pole, where they combine with iron phosphates. Going through the same steps as discharging, charging reverses that and lithium is blown up from the iron phosphate at the positive electrode, where it forms lithium ions and electrons in return traveling toward the negative electrode where it will reintegrate into the graphene layers. Some electrochemical reactions involved in these processes are shown in the table 2.1 below [24].

Table 2.1
Lithium iron phosphate (LiPB) battery during Electrochemical reactions [24]

Electrode	Electrochemical Reactions
Anode	LinC6 â† Li0C6 + nLi+ + neâˆ’
Cathode	Lim âˆ’ nFePO4 + nLi+ + neâˆ’ â† LimFePO4
Overall	LinC6 + Lim âˆ’ nFePO4 â† Li0C6 + LimFePO4

Lithium polymer batteries are quite common today because they have better thermal stability and cycling performance, are nonpoisonous, and are inexpensive. The increase in use has indeed resulted in the disposal of a huge number of spent batteries. Data as of 2020 from the CIAPS, for instance, indicated that NCM had accumulated total installed capacity of 61.1% and LiPB of 38.3% in China, by which time this figure had already increased considerably as a result of further development [25]. Based on installation data released, LiPB accounted for more than 51.7% of total installed capacity in vehicles by 2021, marking not just an improvement but surpassing NCM batteries as well [25]. LiPB batteries are popular in medium- and low-range vehicles because they extend battery life, have lower

costs, and are more environmentally friendly than NCM batteries [26,7]. LiPB battery main components are the shell, cathode electrode, anode electrode, electrolyte, and organic separator [27]. Structurally, the crystal framework of liPB batteries is formed by unit cells consisting of four LiFePO4 units that change from one LiFePO4 phase to a new LiFePO4 phase upon lithium removal [28]. The charge-discharge mechanism of LiPB batteries consists of two different phases: LiFePO4 and FePO4. In the charging process, LiFePO4 de-lithificates to convert into FePO4, while, in the discharging process, lithium ions re-embed into FePO4 to revert it to LiFePO4 [29]. This is how efficient energy storage and discharge become one of the reasons that make LiPB batteries a widely accepted devices choice in different applications.

Following the research conducted by [30] they evaluated on 160 Ah $LiFePO_4$ prismatic cells, evaluating their capacity, cycle life, and real-world road test performance for electric vehicle (EV) applications. The primary aim was to compare the performance of $LiFePO_4$ cells with $LiCoO_2$ cells, which had been previously deemed unsuitable for EV use. The capacity tests revealed that the $LiFePO_4$ cells maintained their full 160 Ah capacity, even after 50 cycles of testing. Road tests were performed on both types of cells under four ambient temperatures (-20°C, 0°C, +20°C, and +40°C), with each temperature condition tested four times. The results demonstrated that $LiFePO_4$ cells outperformed $LiCoO_2$ cells across all testing parameters, leading to the conclusion that $LiFePO_4$ cells are better suited for EV applications and should be considered in future designs.

Following the study by [31] they conducted a detailed analysis of waste LiPB battery treatment methods, emphasizing their impact across five critical dimensions: resources, energy, environment, economy, and society. The study highlighted that recycling waste LiPB batteries is vital for addressing the environmental hazards posed by their toxic components. Recycling also allows for the recovery of valuable materials, improving resource efficiency and reducing the demand for raw material extraction. Additionally, the study underscored the broader benefits of recycling, including fostering sustainable energy development, generating economic gains, supporting social progress, and creating employment opportunities.

Consequently, the recycling of discarded LiPB batteries is not only crucial but also inevitable for sustainable growth in the energy sector.

Following the work of [32] they proposed an innovative fast-charging strategy for high-power $LiFePO_4$ cells and conducted comprehensive evaluations to assess its impact on capacity fade, cycle life, and energy efficiency. The research adhered to the performance standards outlined by the U.S. Advanced Battery Consortium (USABC). The study's findings indicated that the fast-charging approach caused minimal degradation in the cells while maintaining high energy efficiency. Furthermore, the results showed that the observed performance losses were predominantly attributed to capacity fade rather than an increase in internal resistance. This underscores the method's practicality and its ability to preserve cell durability and efficiency, making it appropriate for real-world applications.

Another study structured by [33] they showcased the development of a thermally modulated lithium-ion phosphate battery (LiPB) designed to address range anxiety in electric vehicles (EVs). The battery provides an adequate cruising range per charge, with the capability to extend the range further with a 10-minute recharge under any climate condition. This thermally modulated battery operates at a stable working temperature of approximately 60°C, regardless of ambient conditions, making it a versatile powertrain solution for mass-market EVs. The study also revealed that low-surface-area graphite can be used when operating at high temperatures for brief periods, which could increase the EV's range to more than two million miles. These developments highlight the important breakthroughs in battery technology meant to improve the sustainability and performance of EVs.

Reference [34] considered a sustainable, scalable approach to selective lithium leaching from spent $LiFePO_4$ batteries. By optimally adjusting the oxidative state and proton activity of the leaching solution, it yielded very high lithium recovery efficiency while being selective to lithium. The research has revealed mechanisms for the selective reaction, and rate-controlling step in leaching kinetics. From the laboratory scale, continued into the development and simulation of a pilot batch process. Paved progressive mileages with regard to environmental friendliness and caution feasibility in accordance with the tenets of green chemistry. The process allowed for high-purity Li_2CO_3 (99.95 wt%) to be recovered at very

high recovery rates, and minimal environmental impact. Notably, this approach serves to boost the environmental sustainability of the LiB industry as well as increase recycling efficiency of metals from spent $LiFePO_4$ batteries. The research emphasizes the possibility of integrating green chemistry principles into battery recycling processes to promote circular economy practices and resource efficiency in the energy sector.

Despite significant advancements in LiPB for EVs, gaps persist in integrating predictive models for battery health management. While studies like [30] and [32] have examined performance and cycle life, limited research focuses on real-time SOH predictions. The present study introduces a Deep Neural Network (DNN) for SOH estimation using voltage, current, and temperature data, but its integration with recycling strategies, such as those by [34] and [31], remains unexplored. Predictive SOH modeling could optimize end-of-life recycling and material recovery efforts. Additionally, fast-charging impacts on SOH, as noted by [32], require predictive analytics to prevent degradation. Incorporating SOH models with thermal modulation data and recycling processes offers an opportunity for sustainable and efficient battery management in the EV sector.

2.3. MODELING OF LIB

Reference [209] provides a detailed categorization of methods used to estimate the State of Health (SOH) of a system, likely focusing on battery systems. These methods are divided into two primary categories: Experimental Methods and Model-Based Methods, each offering distinct approaches for health estimation. Under Experimental Methods, there are two subcategories: Direct Measurement Methods and Indirect Analysis Methods. Direct methods involve physically testing the system’s performance, such as Capacity Tests to measure charge storage, Impedance Spectroscopy to analyze the system's impedance, Cycle Counting to track charge-discharge cycles, and Coulomb Counting to measure the total charge flow. These methods provide direct insight into system health by monitoring fundamental parameters. In contrast, Indirect Analysis Methods offer techniques that infer health based on system behavior. This includes CC-CV Charging, a method that tests the system under constant current and voltage to assess performance indirectly, and Incremental Capacity Analysis, which examines small, incremental changes in capacity over time to

detect degradation patterns. On the other hand, Model-Based Methods leverage mathematical and computational models for estimating SOH. These are split into two subcategories: Adaptive Filtering Methods and Data Driven Methods. Adaptive Filtering Methods include approaches like Kalman Filters, Particle Filters, and Least Squares, all of which adapt model parameters based on incoming data to refine SOH predictions. These techniques are particularly useful for dynamic systems where the state is continuously evolving. In contrast, Data Driven Methods focus on leveraging large datasets and machine learning techniques to estimate SOH. This includes methods like Fuzzy Logic, which allows for dealing with uncertainties in system behavior, Neural Networks, which use deep learning models for predictive analysis, and Support Vector Machines, which perform classification and regression to estimate SOH. Together, these methods provide a comprehensive framework for assessing system health, ranging from simple experimental tests to advanced model-based predictions, offering flexibility in terms of complexity and accuracy based on the specific application.

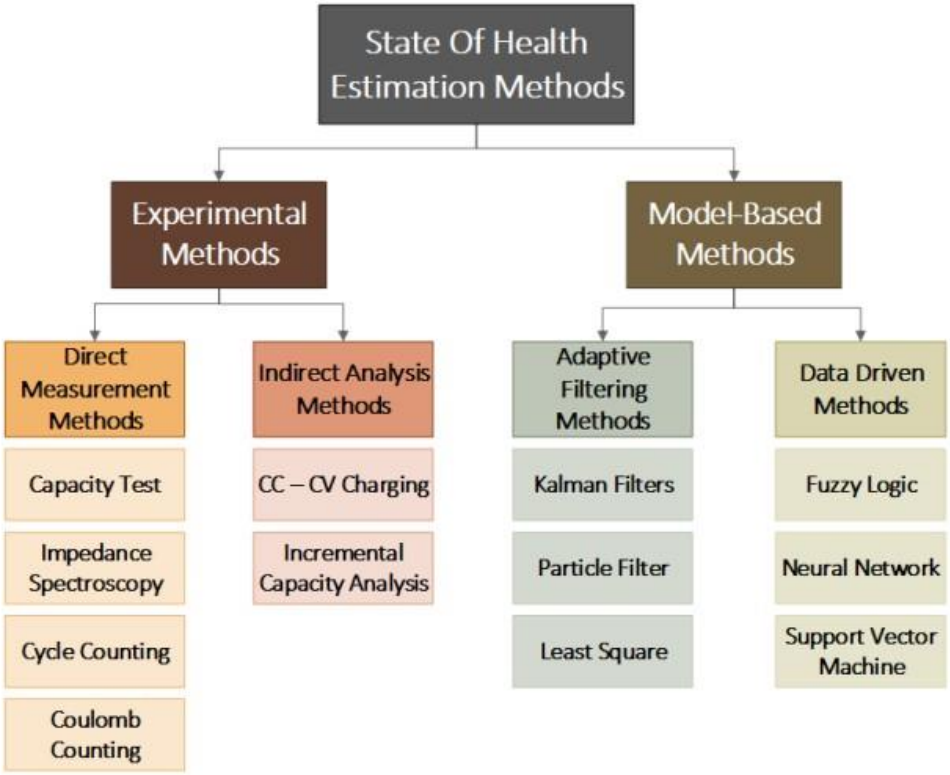

Figure 2.3 Different Methods of Measurement of SOH [209]

2.3.1 FRACTIONAL-ORDER CALCULUS (FOC)

First developed by Leibniz in 1695 when he introduced the non-integer orders of derivatives and integrals, fractional calculus has only recently peaked the interest of physical systems, specifically concerning mass transport, diffusion dynamics, memory, and hysteresis effects. Research indicates that modeling with fractional-order gives better results in representing real systems as permanent magnet synchronous motors and flexible robots whose control design relies on viscoelastic principles [36]. The improvement is attributed to the ability of the FOC to model distributed parameter systems, which closely approximates LiBs' characteristics. The important fractional-order derivatives are also converted into numerical implementation of FOC that considers approximating them for integer-order derivatives or state functions because of the necessity to apply FOC for practical applications. Apart from the definitions by Grünwald-Letnikov, definition criteria of fractional-order

derivatives include those of Riemann-Liouville and Caputo formulations. In this work, the definition used is that of Grünwald-Letnikov since it is the simplest definition that can readily be fitted within Kalman filtering techniques without much encumbrance for the subsequent integration with numerical models to give a more accurate presentation of the dynamic behavior of systems [37].

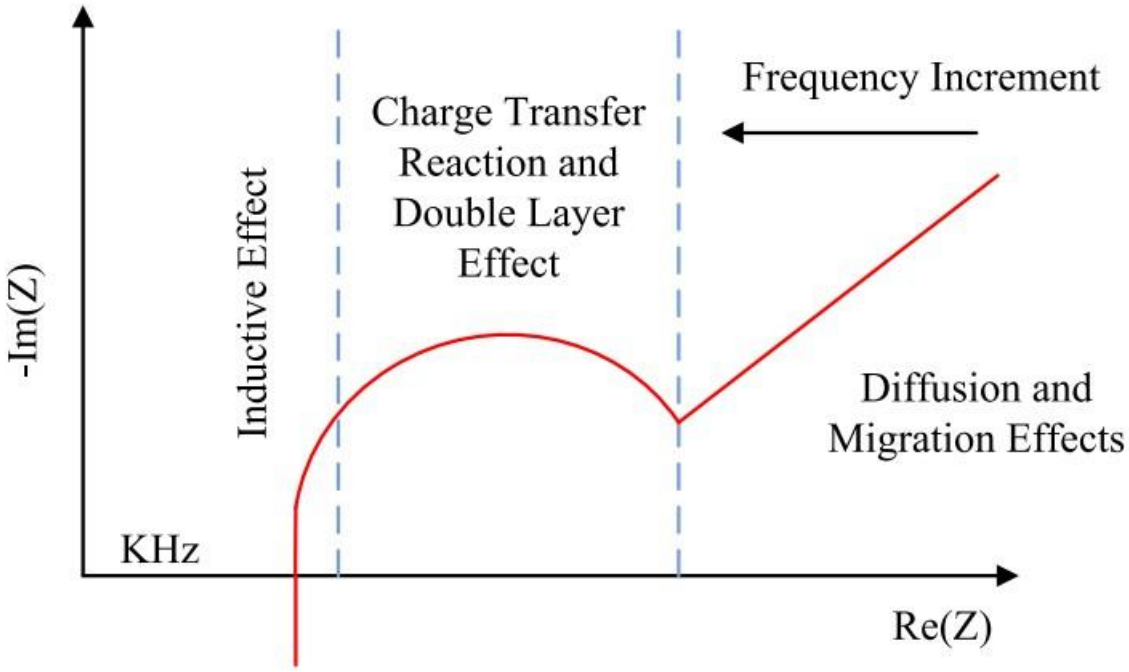

Figure 2.3.Charging effect of Lithium Li-Ion Battery [41]

Figure 2.3 actually depicts a skeptical view of an exponential map showed as a very versatile response of the complex impedance spectra of a Lithium Ion Battery with the x-axis portraying the real components of the impedance Re(Z) and y-axis negative imaginary components -Im(Z). These curves can generally reflect portions that represent an ongoing process; every segment shows different electrochemical processes in the battery. The extreme low-frequency right end of the graph reflects ionic diffusion and transport in the electrolyte and also in the materials of the electrodes. This indicates Warburg impedance, which is dominant at lower frequencies since lithium doesn't have fast diffusion. The two semisections towards the higher frequencies refer to the charge transport-reaction and double-layer

capacitance effects at the electrode-electrolyte interface: transfer-control resistance (Rct) and formation of the double-layer at the interface between which there interaction occurs between ions and electrode surfaces. In the leftmost end of the plot, that is, in the highest frequencies, the inductive effect dominates. It is due to inductances generally being parasitic current collectors, electrical connections, or other elements of the circuit. It shows the direction of increment in frequencies from the low-frequency domain onto the right, to the high one on the left. These different segments in the plot also represent different but multiplex processes within the battery towards which researchers can move closer to evaluating the important performance, degradation, as well as impedance parameters. These parameters help understand the health status and behavior of the battery.

2.3.2 FRACTIONAL-ORDER MODELING FOR LIBS

EIS is a powerful tool for probing LiBs and offers a comprehensive look at their internal action through impedance measurements over a wide frequency range. EIS is performed by applying a sinusoidal current signal of known amplitude to the battery and accurately measuring the voltage response across the battery terminals. The complex impedance, Z* is then obtained from the ratio of measured voltage to applied current. In order to obtain a complete impedance profile, measurements are made at different frequencies and plotted typically using a Nyquist plot showing the real vs. imaginary component of impedance as a function of frequency.

Figure 2.4 illustrates the relationship between the real and imaginary components of impedance, was conducted by [210]. This experiment likely involves impedance spectroscopy, where the real part of the impedance (Z real) represents resistance, and the imaginary part (Z imaginary) reflects reactance. The data shows a non-linear trend, with an initial stable region followed by a sudden increase in the impedance values, which may indicate a change in the system's behavior, such as a transition to a dominant capacitive or inductive effect. The reference [210] provides the source for this experimental setup and the data collected.

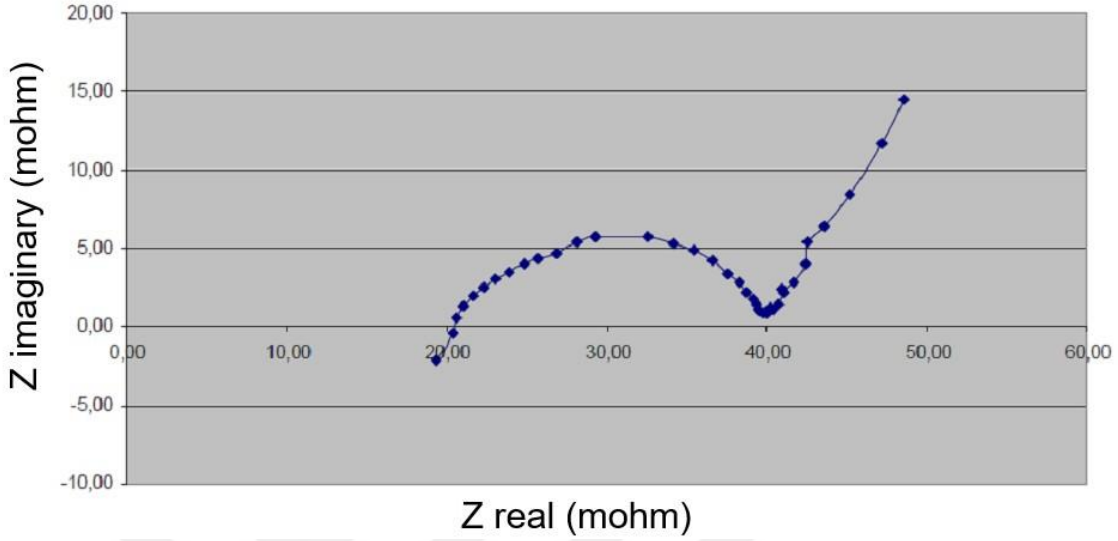

Figure 2.4.Nyquist diagram interpretation [210]

The Nyquist plot for a typical LIB, given in figure 2.4, can be divided into three major regions, namely low, mid, and high-frequency regions: the low-frequency region appears as a straight line of constant slope due to the diffusion of lithium ions within the electrodes; the mid-frequency range is characterized by a reduced semi-circle, which indicates the involvement of charge transfer and double-layer capacicitance phenomena [36]. The most important parameter displayed in Nyquist plot is the phase difference, determined by slope of the low-frequency line and the form of semi-circle in the mid-frequency region. A pure capacitance shows constant phase shift $\pi/2$ in accordance with plate hypothesis using battery electrodes according to [37].

Traditionally, second-order equivalent circuit models, or ECMs, make use of RC branches with simple capacitances so as to mimic the dynamics of Li-ion batteries. This approach does not effectively replicate the semi-circle shapes in the impedance spectra in the mid-frequency zone. This would be overcome by using a form of fractional-order capacitor called Constant Phase Element (CPE) which introduces a phase shift of $-\alpha\pi/2$, where α ranges between 0 and 1. This feature allows the model to better capture non-uniform boundaries and distributed intercalation/de-intercalation processes within porous electrodes [38,39]. Allowing the incorporation of CPE into ECMs greatly boosts the exercise of the ECM in

accurately modeling LIBs. The manpower and presentation of a CPE class as avowed [40] would constitute a solid foundation for interpreting these complex electrochemical dynamics. Hence, the equivalent circuit model with CPEs would be followed in this work to take LiB modeling to a higher point in accuracy and consistency.

$$Z(s) = 1/(Cs^{\alpha})$$

Where Z is the complex impedance, C is a constant representing the main capacitance effect, and s is a complex variable.

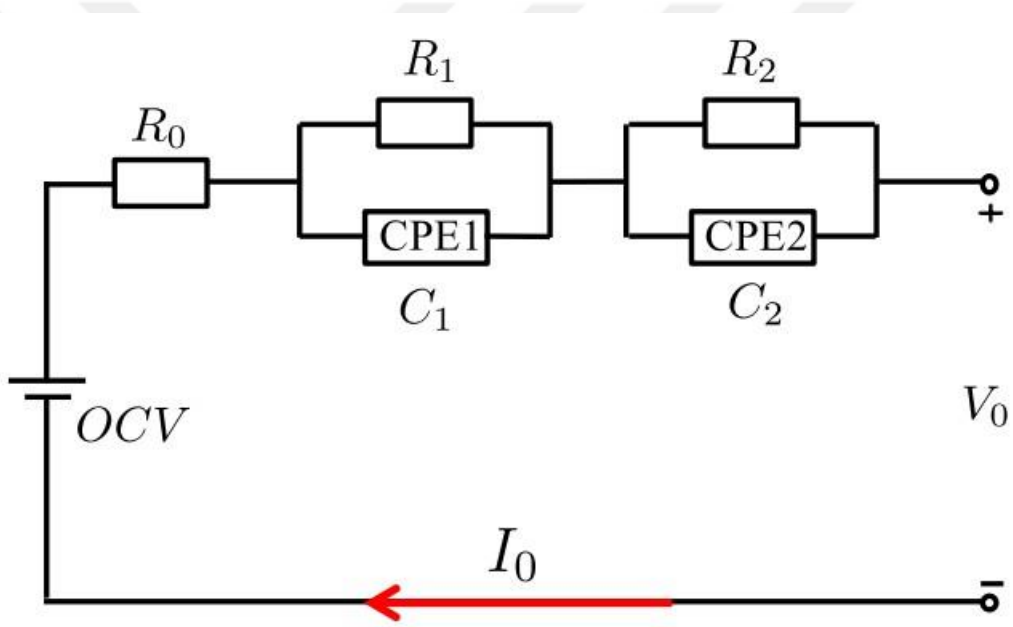

Figure 2.5.Fractional Order Modeling [41]

Figure 2.5 illustrates a Fractional Order Equivalent Circuit Model (FO-ECM) used for accurately representing the electrochemical behavior of LiB. This model integrates both traditional circuit components and fractional-order elements, offering enhanced precision in apprehending the multifaceted changing aspects of battery systems. The circuit begins with R_0, representing the internal ohmic resistance, which accounts for the immediate voltage drop caused by current flow through the electrolyte, electrodes, and internal components. Following this, a parallel combination of R_1 and CPE_1 (Constant Phase Element) models the charge transfer resistance and the double-layer capacitance at the electrode-electrolyte

interface. The use of a CPE, instead of an ideal capacitor, captures the frequency-dependent behavior of the interface, reflecting the non-ideal capacitive characteristics observed in real batteries.

Further along the circuit, another parallel combination of R_2 and CPE_2 represents slower processes such as ion diffusion and mass transport effects within the battery. These elements contribute to modeling the long-term electrochemical phenomena affecting battery performance. The model also includes the Open Circuit Voltage (OCV), which represents the battery's voltage in a no-load condition, and V_0, which denotes the output voltage under operating conditions. The current I_0 flows through the circuit, driving the system's overall dynamic response. This fractional-order approach provides significant advantages over traditional integer-order models by incorporating the frequency-dependent properties of real-world batteries, especially through the use of CPEs. It allows for more accurate modeling of processes like charge transfer, diffusion, and mass transport, making it highly suitable for applications such as SOH estimation, impedance spectroscopy, and predictive maintenance of batteries in various industrial and energy storage systems.

The application of fractional-order calculus (FOC) and fractional-order modeling has demonstrated significant potential in improving the accuracy of LiB models, particularly in capturing the complex internal processes and dynamics of LIBs. Techniques such as Electrochemical Impedance Spectroscopy (EIS) provide detailed insights into the battery's behavior across frequency domains, while fractional-order capacitors (CPEs) address limitations in traditional second-order equivalent circuit models (ECMs). Despite these advancements, critical gaps remain in the context of forecasting battery health for electric vehicles (EVs). While FOC-based approaches offer theoretical accuracy in modeling LIB behavior, their application in real-time SOH estimation for EVs remains underexplored. The inherent complexity of fractional-order models and their reliance on sophisticated computational techniques, such as Kalman filtering, pose challenges for practical implementation in dynamic EV environments.

Additionally, existing studies primarily focus on characterizing battery impedance and internal dynamics through controlled experimental setups. These approaches often lack

integration with real-world operational data, such as voltage, current, temperature, and evolving health indicators, which are crucial for SOH prediction in EVs. The reliance on parameters like Nyquist plots and impedance spectra also limits their scalability for large-scale deployment in EV fleets. Furthermore, fractional-order models, while effective in explaining charge transfer and diffusive properties, have not been directly linked to advanced data-driven techniques, such as Deep Neural Networks (DNNs), that can leverage diverse experimental data for predictive modeling. Finally, there is limited research bridging the gap between fractional-order modeling and the development of real-time, scalable, and cost-effective SOH estimation models for EVs. Addressing this gap through a novel DNN model that utilizes experimental data, including voltage, current, temperature, and health indicators, offers a promising solution to enhance prediction accuracy and practical applicability in dynamic EV environments.

2.3.3 ADVANCED ALGORITHMS FOR SOH ESTIMATION

With the rapid expansion of computational models and machine learning algorithms (MLA), several advanced methods have been introduced to estimate the SOH more accurately and in real-time. Among these, Kalman filtering (KF) and its variants, such as the unscented Kalman filter (UKF), are popular choices. Kalman filters provide an optimal solution to approximation the state of a system by combining noisy sensor data with a mathematical model. In the context of LiB, KF can estimate the SOH by incorporating charge-discharge data, temperature, and other operational parameters into a state-space model [109]. UKF, a more advanced variant of the Kalman filter, is particularly effective in non-linear systems, such as those found in battery modeling, where the battery's performance does not follow linear dynamics. The particle filter (PF) is another promising approach used for SOH estimation. Unlike Kalman filters, which rely on linear models, particle filters can handle highly nonlinear and non-Gaussian systems by using Monte Carlo sampling methods to approximate the distribution of the system states. Particle filters have been successfully functional to estimate SOH in LiB, particularly in dynamic environments where the battery's health changes rapidly due to varying load conditions [146]. This method is robust against

measurement noise and can provide reliable estimates even when only limited data is available.

2.3.3.1 KAMLAN FILTERS

Kalman Filtering (KF) is a widely employed recursive algorithm that optimally estimates the state of a dynamic system by integrating sensor data, potentially afflicted by noise, with a mathematical model. It functions within a linear state-space paradigm, seeking to minimize the mean squared error of state estimation. In battery management, Kalman Filtering (KF) has been widely employed for state-of-health (SOH) estimation by incorporating multiple operational parameters, including charge-discharge cycles, voltage, current, and temperature [109]. The algorithm's capacity for recursive state estimate updates renders it appropriate for real-time applications. Nonetheless, numerous battery systems demonstrate nonlinear characteristics, particularly regarding performance fluctuations over time. To mitigate these non-linearities, sophisticated adaptations of the Kalman Filter, including the Unscented Kalman Filter (UKF), have been created.

UKF is especially proficient for systems exhibiting nonlinear dynamics, as it employs a selection of meticulously chosen sample points, referred to as sigma points, to approximate the nonlinear transformations of the system. This approach yields more precise state estimations than the conventional Kalman Filter when the system's behavior markedly diverges from linearity [109]. The UKF is particularly advantageous for modeling battery performance under diverse conditions, including variable loads, temperatures, and charge-discharge cycles. A prevalent method for managing non-linear systems is the Extended Kalman Filter (EKF). The EKF linearizes the system through a first-order Taylor expansion to approximate nonlinear behavior [109]. Although effective, the EKF may encounter inaccuracies when the system displays pronounced nonlinear characteristics. The particle filter (PF) algorithm can integrate components of the EKF or UKF to enhance performance. In the context of PF, the importance density function is frequently derived using the EKF. This entails updating the sampled particles using the EKF algorithm, resampling them according to their revised weights, and producing new particles via the importance density function. Conversely, the UKF can be integrated into the PF framework by utilizing

its unscented transformation, which circumvents linearization and incorporates higher-order terms. This method guarantees that the mean and covariance estimations retain exceptional precision, even in nonlinear systems. The UKF updates particles by computing their mean and variance, which are subsequently employed in the following iterations of the particle filter.

The Regularized Particle Filter (RPF) algorithm employs an enhanced resampling technique to mitigate the problem of particle diversity degradation, a prevalent issue in conventional particle filters. By augmenting particle diversity during resampling, the RPF preserves the accuracy and robustness of the particle filter, rendering it especially effective for applications involving intricate and nonlinear battery dynamics. Advanced filtering techniques, such as UKF, EKF, and RPF, provide effective means for enhancing the accuracy and reliability of State of Health assessment in LiB.

2.3.3.2 LINEAR REGRESSION (LR)

LR is a statistical method employed to forecast a target variable by modeling it as a weighted amount of input features. The linear nature of the relationship between the inputs and the target makes the model straightforward to interpret. This simplicity has made linear regression a widely used method among statisticians, computer scientists, and professionals dealing with quantitative analysis across various domains. LR model for the population can be represented by

$$y_i = \beta_0 + \beta_1 x_1 + \text{"; "} \text{ belongs to } N(0; \sigma^2)$$

Since the equation represents the population distribution, the regression model derived from a sample can be expressed as follows. LR model is used to examine and quantify the impact of one independent variable on a dependent variable. It estimates the relationship between these variables based on observed data, allowing predictions and insights about how changes in the IV influence the DV.

$$\hat{y}_i = \hat{\beta}0 + \hat{\beta}_1 x_1 + \text{"; "} \text{ belongs to } N(0; \sigma^2)$$

The goal of LR is to determine regression coefficients that minimize the sum of squared errors (SSE). Ang and Paw [147] showed that a linear regression model trained on discharge voltage data can estimate battery SOH with a root mean square error (RMSE) of less than 12%. However, this technique has limitations, as it requires a complete discharge voltage profile until the battery reaches the end of its SOC for SOH estimation. This means that the SOH can only be estimated after a full discharge cycle has been completed. Consequently, the SOH estimate provided by this model reflects the battery's condition based solely on the most recently completed discharge cycle.

This delay in SOH estimation poses two significant challenges. First, in scenarios where there is a prolonged storage period between the previous and current usage cycles, the SOH estimated from the last discharge cycle may no longer be accurate. During storage, the battery could experience significant degradation due to suboptimal storage conditions [56]. Second, the need for a complete discharge profile necessitates the battery to be fully charged and then fully discharged for data collection, which limits the method's practicality in real-world engineering applications. Batteries in operational systems, such as electric vehicles (EVs), often do not undergo full charge or discharge cycles in every use case [119,97].

LR remains one of the simplest and most frequently used MLM for SOH estimation. This statistical method accepts a linear relationship between the dependent variable (e.g., battery health) and one or more independent variables, such as voltage, current, temperature, and cycle count. Despite its simplicity, linear regression is effective in identifying trends when the relationships between variables are approximately linear. In battery management systems, it can be applied to model the deprivation of key battery parameters, such as capacity and internal confrontation, using operational data [41].

The primary advantage of LR lies in its ease of implementation and interpretability, making it suitable for situations where a quick and understandable model is needed. However, its limitation is that it may not perform well in complex scenarios where the degradation of battery health involves nonlinear interactions among variables. For instance, when external factors like temperature fluctuations and high charge-discharge cycles affect the battery’s SOH, linear regression may fail to capture the intricate relationships, leading to inaccurate

predictions [126]. Nonetheless, linear regression can serve as a baseline model and is often used in combination with more advanced techniques.

2.3.3.3 SUPPORT VECTOR REGRESSION (SVR)

The SVR algorithm proves to be one among the most effective techniques for framing complex nonlinear relations in inputs and corresponding outputs and hence is well apt for SOH estimation. The main idea behind SVR is the concept of a non-linear mapping function applied on the input data into a much larger dimensional space wherein the input data can be separated using linear regression. This is done through a specified kernel function of the mapping, finding the optimal hyperplane, the support vector, that maximizes the margin between the data points in that higher-dimensional space.

For an illustration, let us consider a battery dataset (x1,y1),...,(xi,yi)(x_1, y_1), ..., (x_i, y_i)(x1,y1),...,(xi,yi): such that xi∈Rnx_i \in R^nxi∈Rn refers to the regional capacity for the ith cycle, while yiy_iyi refers to the SOH value or the targeted output. This is how the SVR function is mathematically defined in this scenario to predict the relationship between input structures and the SOH, due to its ability to harness complex nonlinear interaction effects.

$$f(x_i) = w^T \varphi(x_i) + b$$

Where output values are denoted by f(xi), other form of mapping function nonlinear is represented by φ(xi), while w and b are the unknown parameters. Objective of both regressions is to make output of model as much similar the output 'yi'. Support Vector Regression (SVR) is an extension of Support Vector Machines (SVM) in the field of regression analysis. The basic idea behind SVR is to find such function which can represent the data in such a way that the margin of error remains small. This approach works particularly well for high dimensional data as well as on both linear and nonlinear relationships through kernel functions [57]. Hence, this technique is very useful for estimating battery SOH from information regarding health indicators of batteries in functioning conditions like charge-discharge cycles and environmental factors.

SVR mainly advantageous when dealing with small datasets, as it is less prone to overfitting than other models [84]. Moreover, by adjusting the kernel function (e.g., radial basis function or polynomial kernel), SVR can handle nonlinearity in battery degradation patterns effectively. A study by [51] demonstrated the application of SVR to forecast the capacity degradation of LiB under various operating circumstances, achieving higher prediction accuracy than traditional methods. However, SVR's primary drawback is the need for careful selection of hyperparameters, which can be computationally luxurious and time-consuming.

2.3.3.4 FEED-FORWARD NEURAL NETWORK (FFNN)

The feedforward neural network, a species of the neural networks, has input and output layers as well as several hidden layers, whose neurons have learnable weights and biases. Each neuron in a layer, other than the input layer, connects to all neurons of the previous layer, with equal weight for every attachment within each layer. Hence, the weights comprise all knowledge learnt by the network. Now, when we consider an input layer consisting of features regarding SOH, we will have on the other side the output concerning SOH; for the example at hand, it would be the capacity of the battery. The input layer size corresponds to the entry data. In contrast, the hidden-layer structures and the number of neurons in them are aspects of the model hyper parameters that will be fine-tuned during the exercise called validation. Most commonly, these are nodes, which will only feed forward and will not participate into loops or memories. With respect to estimating SOH for batteries, this input layer is expected to contain features referring to SOH, and on the other side, the output would refer to SOH, which, in this case, is the capacity of the battery.

An FFNN, a kind of artificial neural network (ANN), is planned to learn complex and nonlinear relationships within data through techniques like backpropagation and gradient descent. This architecture is increasingly utilized for battery SOH estimation because of its ability to capture detailed and intricate patterns in battery behavior (Bishop, 2006). By analyzing large datasets containing historical battery performance metrics—such as charge-discharge cycles, voltage, temperature, and current—FFNNs can predict key battery metrics like remaining useful life (RUL) and capacity fade [148].

One of the key strengths of FFNNs is their capability to simplify effectively to novel, unseen data, which is critical for SOH estimation given the variability in battery data due to changing operating conditions over time. However, FFNNs also present challenges. They require substantial amounts of data to prevent overfitting and ensure accurate predictions, and their training process can be computationally intensive, particularly for large networks with many layers and parameters. Despite these challenges, FFNNs continue a influential tool for battery management, providing flexible and robust solutions for predicting SOH and RUL in dynamic environments.

2.3.3.5 DECISION TREE REGRESSION (DTR)

Decision Tree Regression organizes data in a hierarchical tree-like form, starting from the root node, branching off to leaf nodes where final predictions can be made based on analysis of residuals. Each node's impurity is measured using measures like sum of squared residuals or variance [149]. In this non-linear machine learning, the input space is divided into smaller regions recursively using input feature values. Each node in the tree signifies one decision rule, while leaf nodes represent the predicted output values. In addition, its interpretability and intuition allows decision trees to be used in practice, which includes applications like battery health monitoring where the opacity of the model is critical. So much so that they are able to cater non-linearity which can provide a clear way of decision-making when predicting and interpreting battery performance.

Decision trees are widely utilized in battery SOH estimation to predict metrics like remaining capacity or state of health based on various features, including charge-discharge cycles, temperature, and charge rates. A significant advantage of decision tree regression is its versatility, as it processes both definite and constant data effectively. However, when decision trees become excessively deep, they are prone to overfitting, which negatively impacts their ability to simplify to original, hidden data. To address this issue, pruning techniques are commonly used, reducing the tree's complexity and improving performance. Despite the peril of overfitting, decision trees remain a popular method for battery health approximation due to their straightforward construction and ease of execution [138].

2.3.3.6 RANDOM FOREST REGRESSION (RFR)

Using a lot of decision trees, Random Forest Regression (RFR) is used to develop approximations. And it doesn't use a single tree; it combines the outputs of many trees to come to the final output. An assessment of the error that has gone into the mean squares might also be used in the analysis of the data splits at each node in the forest [149]. It minimizes overfitting and improves the accuracy of predictions by training each decision tree on a randomly selected portion of the datasets. Henceforth, the final prediction is made up of all the trees in the ensemble. It is specially valid for estimating SOH in batteries since it handles noisy inputs and captures the complex, nonlinear interactions between health parameters and the operating conditions. Its capability of generalizing different data sets makes Random Forest Regression a suitable method for battery performance analysis and SOH prediction under various scenarios.

Random Forest has been applied in various studies to estimate battery performance pointers such as volume degradation and interior confrontation over time. A study by [130] demonstrated the use of Random Forest Regression to predict the SOH of LiB in electric vehicles, achieving high prediction accuracy in both laboratory and real-world conditions. The model was able to handle a huge number of input features and capture the nonlinear relationships between them. Random Forest also offers the advantage of being less prone to overfitting compared to individual decision trees. However, it requires significant computational resources when the number of trees is large, and the model can become less interpretable as the quantity of trees upsurges.

2.3.3.7 K-NEAREST NEIGHBOR REGRESSION

K-Nearest Neighbor (KNN) Regression is an instance-based learning algorithm that predicts outcomes by averaging the values of the kkk nearest neighbors in the training data. The algorithm determines the distance between a new data point and each training point, using metrics such as Euclidean distance to identify the closest neighbors. Based on the selected kkk value, the algorithm computes the output by considering the nearest data points [149]. Recently, KNN has gained attention for LiB life estimation due to its ability to model complex, nonlinear relationships and familiarize to varying battery circumstances [150].

KNN does not assume any specific data distribution, creation it particularly suitable for battery health estimation, where the underlying patterns can be highly variable. In the context of SOH estimation, KNN can predict the remaining capacity or health status of a battery by comparing historical data—such as voltage and current readings—that resemble current operating conditions. The algorithm's simplicity and ease of implementation, as it does not require a training phase, are among its advantages. However, KNN has limitations, including computational expense at prediction time, especially for large datasets, as it must calculate distances between the query point and all training points. Additionally, KNN is sensitive to noisy data, and its presentation depends heavily on the choice of kkk and the distance metric used [130].

The growing acceptance of EVs has highlighted the necessity for efficient and accurate methods to estimate battery SOH, a critical factor in ensuring optimal battery performance and longevity. While machine learning techniques, including linear regression, SVR, FFNN, decision trees, random forests, and KNN regression, have been applied to SOH estimation, these methods face several challenges. Many struggle to get the nonlinear and dynamic interactions amid battery health parameters such as voltage, current, temperature, and charge-discharge cycles. Linear regression, for example, is unable to model complex relationships, while methods like SVR and FFNN are often computationally intensive, sensitive to hyperparameter tuning, and reliant on extensive datasets.

Furthermore, traditional SOH estimation techniques often lack the ability to provide real-time predictions and are less robust against variations in battery operating conditions, limiting their practical applicability in real-world EV scenarios. Despite significant advancements, there remains a need for a model that is both highly accurate and computationally efficient, capable of leveraging diverse experimental data for reliable SOH estimation. This study addresses these gaps by introducing a novel Deep Neural Network (DNN) model. By integrating experimental data, including voltage, current, temperature, and other health indicators, the proposed DNN model offers a robust and scalable solution for precise SOH prediction in EV batteries, overcoming the limitations of existing approaches.

2.3.4 EQUIVALENT CIRCUIT MODELS FOR LIB (ECM)

In fact, it is very important to model lithium-ion battery for better performance and safety in applications extending from electric vehicles to grid energy storage systems. The equivalent circuit models normally employ integrity of a resistor-capacitor (RC) network which simulates most internal dynamics of a lithium-ion battery, including internal confrontation, actual capacitor, or equivalent voltage potential. The most marketable RC network model was first industrialized by SAFT using the PSpice software and later extended for MATLAB, an ADVISOR stage [46]. The origin of this model is the Thevenin equivalent consisting of a number of RC networks connected in series to represent the fast response time characteristics of a battery.

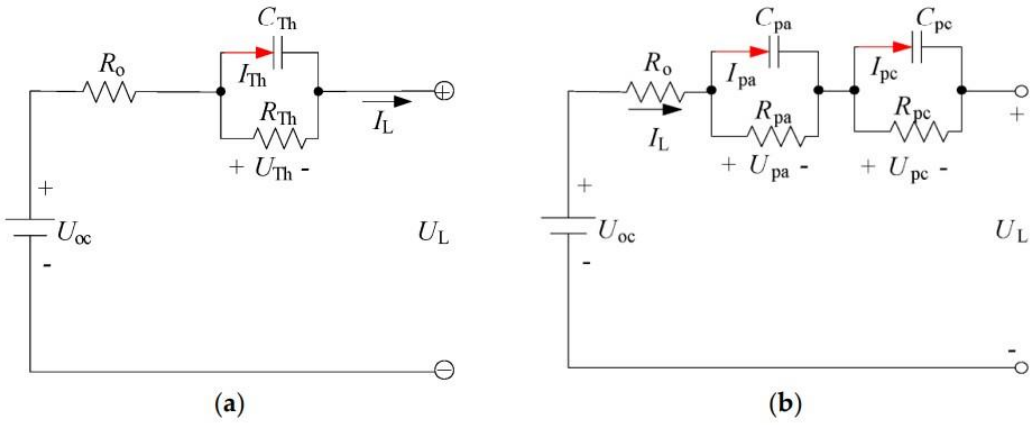

Figure 2.6.ECM diagrams, (a) first-order (1RC), and (b) second-order (2RC) [24]

Figure 2.6 illustrates a first-order ECM (1RC), which contains of key components such as UCV, resistors (Ro, RTh) representing ohmic and divergence confrontation, and a capacitor that models the battery's transient behavior during charging and discharging processes. The second-order equivalent circuit model (2RC), also depicted in Figure 2.5, is a dual polarization (DP) model that offers a more detailed representation of polarization effects, including electrochemical and concentration polarization, independently [42]. The 2RC model includes internal resistance (Ro) and two divergence confrontations, Rpa and Rpc, which represent the resistances associated with electrochemical and absorption polarization, respectively. Additionally, the model incorporates effective capacitances, Cpa and Cpc, to

represent the battery's transient charge/discharge response and polarization effects. Factors like computational efficiency, model accuracy, and parameterization are critical for an effective battery management system (BMS) [43]. While adding RC networks up to a fifth-order model can improve accuracy, increasing the complexity beyond the second-order model often leads to diminishing returns in terms of computational efficiency versus accuracy [67].

Hysteresis is a common phenomenon in modern battery chemistries, influencing the open-circuit voltage (OCV) during charging or discharging. It also happen in sluggish conditions, referred to as "zero-current hysteresis," where the OCV response may vary by up to 50 mV or more [44]. The extent of hysteresis is prejudiced by aspects such as the battery's relaxation time during charging or discharging, its chemistry, and its SOC. Hysteresis effects are particularly pronounced in lithium iron phosphate (LFP) chemistries and in specific SOC regions, such as 0–20% and 80–100% [45]. To improve accuracy in SOC estimation, OCV-based estimation models integrate a dynamic hysteresis model with an n-RC equivalent circuit model (ECM). For this purpose, specific circuit elements are introduced into the n-th-order RC model to account for hysteresis, forming n-th-order RC models with hysteresis [24]. Batteries with significant hysteresis can experience challenges when using OCV-based SOC estimation techniques [46]. This study focuses on the first-order ECM with hysteresis.

Following the research by [24] conducted experiments to evaluate the presentation of three equivalent circuit models (ECMs)—1RC, 2RC, and 1RC with hysteresis—across four LiB chemistries: LFP, NMC, LMO, and NCA. The findings demonstrated that all three models could effectively simulate the behavior of these battery chemistries with minimal errors. The study also revealed that ECMs performed more accurately under dynamic current profiles than under non-dynamic conditions. For LFP and NCA chemistries, the 1RC with hysteresis model provided the best results, while the 1RC model was the most appropriate for NMC and LMO chemistries. These results highlight the need to match specific ECMs to the appropriate battery chemistry in real-world applications, emphasizing their importance in battery management systems (BMS) and practical battery usage.

The works by [47] presented a generalized and equivalently inspirited circuit model for lithium iron phosphate batteries. It would rely solely on the nominal capacity given in the cell datasheet. Thus, the new zeroth-order generalized model can be constructed using data from previously characterized cells. By applying this new method, experimental time and costs will diminish and achieved a reduced testing matrix. The excellent model not only captures electrical behavior for low-energy, but also for high-energy cells, with error remaining consistently below 2% in all cases without reference to detailed knowledge concerning the dependence of electrical parameters towards SOC, c-rate, and temperature. The cell internal resistance will be characterized concerning a new characteristic coefficient, which is typical of this specific LiB chemistry, fitted to an exponentially temperature-dependent function, which has physical significance, as internal resistance is expected to have Arrhenius-type dependence on temperature under these conditions. Therefore, this model is more straightforward in construction and more versatile in the application it assumes for control, while at the same time serving offline analysis.

Works of [48] critically evaluate ECM modeling methodology and PBM using a case study of 60 Ah prismatic graphite/lithium iron-phosphate batteries. The advantages of ECM are as follows: CPU speed, ease of calibration, and accuracy, within its calibration range, for variable current profiles. Accuracy for ECM becomes worse at the higher currents, especially when the current pulse lasts for a long duration, and even much reduced when the test moves beyond the calibration range in the charging scenarios of more than 1C. While the PBM keeps its accuracy away from the calibration dataset, it needs the estimate of several physical parameters against an extremely tiring calibration process and long computational times during variable current conditions. Under the range of conditions studied (with current levels from C/3 to 2C at temperatures from 10 °C to 40 °C), average voltage prediction errors were found to be 51.5 mV for ECM and 19.3 mV for PBM, while, in terms of temperature prediction, they were 0.9 °C for ECM and 0.4 °C for PBM. The study by [49] proposed various ECM: like Rint model, RC model, Thevenin model, or PNGV model and DP model, which are being used recently widely in studies related to EV. These are as follows:

2.3.4.1 The Rint Model (RM)

RM illustrated in Figure 2.6 below employs a perfect voltage source (Uoc) to denote the battery's OCV. The resistance (Ro) and OCV are contingent upon the battery's SOC, SoH, and temperature. The load current (IL) is positive during discharge and negative during charging, whereas UL represents the terminal voltage.

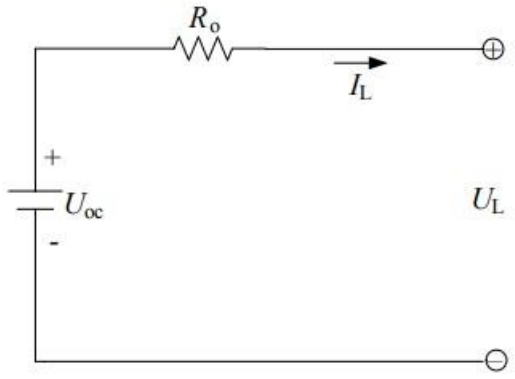

$$U_L = U_{oc} - I_L R_o$$

Figure 2.7. Schematic diagram of the Rint model [49]

2.3.4.2 The RC Model (RCM)

Prior to all this, RCM was authored by a battery manufacturer SAFT and was put into practical use through Advisor software. This is the model in Figure 2.7 which contains two capacitors (Cc and Cb) and three resistors (Rt, Re, and Rc). The capacitor Cc is capacitor with such small capacitance, and it signifies surface phenomena of the battery, and due to this, it is generally called the surface capacitor. But, the bigger capacity capacitor, Cb, shows the chemical storage capacity of the battery thus SOC is measured by taking the voltage reading generated across the bulk capacitor (Cb). Resistors Rt, Re, and Rc are terminal resistor, end resistor, and capacitor resistor, respectively. Ub refers to the surface capacitor voltage, while Uc refers to bulk capacitor voltage.

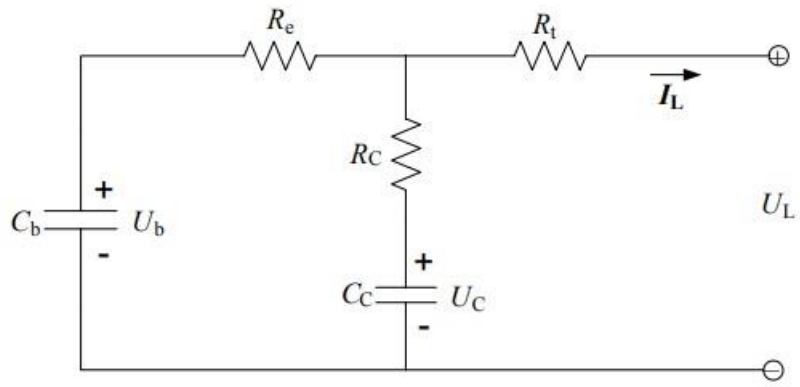

Figure 2.8.Schematic diagram of the RC model [49]

2.3.4.3 The Thevenin Model (TM)

The authored TM improves upon the RM by interfacing its parallel RC network in series thereby enabling capable modeling of battery dynamic behavior. The user may observe in Fig. 2.8 that this model contains three primary components: UCV, internal resistances, and equivalent capacitances. Specifically, the internal resistances comprise ohmic resistance (Ro) as well as the polarization resistance (RTh). CTh is referred to as equivalent capacitance and represents the dynamics of the transient behavior of the battery charge-discharge cycles. The voltage across the equivalent capacitance is denoted as UTh, while ITh indicates the current that passes through CTh.

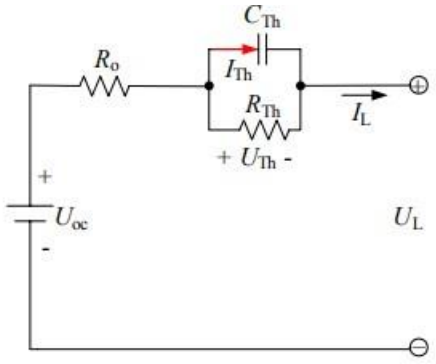

$$\begin{cases} \dot{U}_{Th} = -\dfrac{U_{Th}}{R_{Th}C_{Th}} + \dfrac{I_L}{C_{Th}} \\ U_L = U_{oc} - U_{Th} - I_L R_o \end{cases}$$

Figure 2.9.Schematic diagram for the Thevenin model [49]

2.3.4.4 The PNGV Model

The PNGV model, depicted in Figure 2.9, enhances the Thevenin model by incorporating an additional capacitor (Uoc1) in series. This capacitor compensates for fluctuations in the OCV resulting from the time-dependent buildup of load current. This improvement allows the model to more precisely depict the battery's dynamic behavior across various operating conditions.

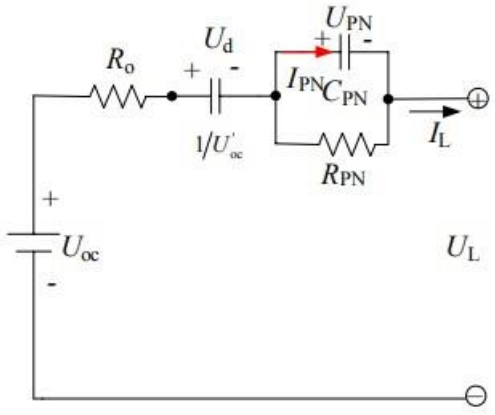

Figure 2.10.Schematic diagram of the PNGV model [49]

2.3.4.5 The DP Model

Analyses of lithium-ion power batteries indicate substantial polarization effects. Although the Thevenin model can partially replicate these characteristics, it inadequately distinguishes between concentration polarization and electrochemical polarization, especially at the conclusion of charge or discharge cycles. To overcome this limitation, an enhanced circuit model, illustrated in Figure 2.10 and designated as the Dual Polarization (DP) model, was created. This model enhances the depiction of polarization by individually simulating concentration polarization and electrochemical polarization, yielding a more precise and comprehensive understanding of battery performance.

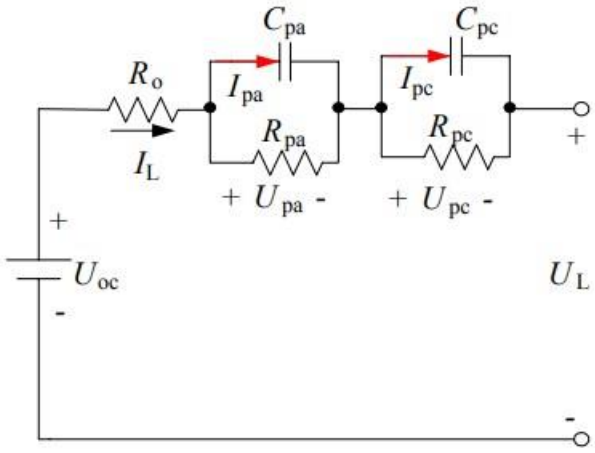

Figure 2.11.Schematic diagram for the DP model [49]

The DP model has three main elements: (1) the OCV; (2) internal resistances; and (3) effective capacitances. They comprise internal resistances: ohmic resistance (Ro) and polarization resistances, among these being Rpa, representing electrochemical polarization, and Rpc, denoting concentration polarization. The effective capacitances, Cpa and Cpc, portray the transient reaction regarding the transfer of energy towards or away from a battery. Cpa emphasizes electrochemical polarization, and Cpc concentration polarization. Upa and Upc denote the voltages across such capacitances, while Ipa and Ipc represent the respective outflow currents.

However, despite very good improvements in the ECMs for LiB, there is still a long way towards the real capacity of accurately predicting the health of a battery or its SOH under actual conditions. A recently proposed DNN model has incorporated voltage, current, temperature, and health variables in predicting SOH estimation, offering options for data-driven approaches. However, inadequate research has been done into the combination of DNN predictions using ECMs like Thevenin, PNGV, and DP models. The joining together of DNN prognostics with the physical insights of ECMs might prove remarkably beneficial for SOH estimation under dynamic conditions, fast charging, and temperature variations. While the DP model has performed well as far as simulating the polarization effects, the enhanced long-term prediction using DNNs for diverse chemistries and operating conditions still needs to be researched.

2.3.5 Electrochemical Models

LiPB are widely utilized in EVs due to their strong safety features and long cycle life. Before being deployed for practical applications, these batteries typically undergo extensive functional and extreme condition testing. To prevent potential damage to battery capacity during testing, simulation methods are commonly employed for performance verification and functional assessment [50]. Electrochemical models (EM) are frequently used by researchers to simulate battery behavior. Unlike equivalent circuit models, electrochemical models offer greater accuracy as they describe physical and chemical processes through mathematical formulations derived from a microscopic perspective. EM is usually referred to as the Doyle–Fuller–Newman (DFN) model and it has conquered battery continuum modelling in the meantime of early 1990s. These models maintain high fidelity even with low-frequency current variations, making them a preferred tool for simulating battery performance under various conditions [51.52].

The classical electrochemical modeling includes the pseudo-two-dimensional (P2D) model [53] and the single-particle (SP) model [54]. The P2D model consists of a group of partial differential equations (PDEs) that model phenomena occurring within a battery, including diffusion within the solid and liquid phases and electrochemical reactions, providing a very detailed microcosmic view. It is thus more precise compared to equivalent

circuit models. Nevertheless, the coupling of PDEs requires time and space variable separation, which increases the number of equations hugely that need to be solved, leading to increased simulation time. It is also difficult to identify model parameters due to intrinsic cell-to-cell variations [55]. The SP model reduces this complexity by assuming uniform chemical reactions along the thickness of the electrode and neglecting liquid-phase diffusion below a certain C-rate where concentration overpotential is negligible. This makes it practically very suitable for some applications.

The SP model has quite a simple structure but has a reduced performance in simulating terminal voltage as soon as the current loads become high. Although it uses fewer parameters than the case of the P2D model, determining the parameters is difficult because of the equations' coupling. According to the comparison between the electrochemical models and ECU models, electrochemical models provide better simulation results than the equivalent circuit models. However, the parameters need to be accurately identified. Therefore, different techniques have been considered for parameter identification, including destructive electrochemical test methods [56] and also non-destructive methods [57]. Destructive electrochemical testing is when a measurement of parameters like liquid-phase conductivity and the open-circuit potential curve has been made on a half-cell type configuration. It, however, destroys the battery cells permanently and gives only specific parameters, which makes it infeasible for repeat or large-scale usage.

They have conducted genetic algorithms for battery modeling [58,59] and particle swarm optimization [57] as the nondestructive parameter identification techniques. These techniques obtain model parameters as variables in aiming to minimize the difference between simulated and measured voltages under defined operating conditions. This process uses the performance of objective functions iteratively updating of the parameters with the aim of achieving optimal solution. [54] elaborated this method into improved SP model-based electrochemical aging model which takes identification of more than 20 parameters. They conducted sensitivity analysis prior to finding the best optimal poked around-geological GA algorithms since they are time-consuming to find optimal solution. The analysis now reduces key parameters to 16, which were narrowed down through thermal; all others,

including liquid-phase diffusion coefficient, activation energy coefficient, and so on, were taken from the similar study to smoothened process. The methodology of handling sensitivity analysis and optimization has improved efficiency and accuracy in parameter identification.

Battery performance is greatly impacted by temperature; capacities can vary by up to 15% depending on the temperature. Furthermore, extremes in temperature—both high and low—can have a significant impact on battery life. [57] created a numerical model to simulate voltage and temperature profiles using ANSYS CFD software, and the model showed good agreement with experimental data. Their results showed that the highest simulated temperature was 46.86 °C at a 4C discharge rate. These findings highlight how crucial it is to have a precise thermal-inclusive model in order to guarantee that the battery operates within a safe temperature range. [58] created a P2D-based model that included electrochemical kinetics and the laws of mass, charge, and energy conservation for prismatic lithium iron phosphate batteries. In order to account for current-collecting tabs, the model treated the battery as a 3D system in the through-plane direction, but it treated local cell units as 1D. Their study demonstrated that the reaction rate distribution within the local cell units was uneven and significantly influenced by the positioning of the positive and negative current-collecting tabs. This work highlights the need to consider spatial variations in reaction rates for improved thermal and electrochemical modeling. Their study demonstrated that the reaction rate distribution within the local cell units was uneven and significantly influenced by the positioning of the positive and negative current-collecting tabs. This work highlights the need to consider spatial variations in reaction rates for improved thermal and electrochemical modeling.

Models of the electrochemical and thermal behaviors of batteries during charging and discharging are possible, but they frequently need significant parameter adjustments. [59] used a predictor-corrector strategy along with quasi-linearization techniques to create a thermally simplified multi-particle model. Over a wide temperature range (10–45 °C), the model reached a maximum root-mean-square error of 22.70 mV while keeping accuracy close to the thermal P2D model. But there are still a lot of parameters to figure out, especially

for the thermal resistance and isothermal physics models, since thermal behavior complicates the parameter identification procedure.

In their study, [60] created and simulated models of lithium iron-phosphate batteries for 45 °C to -10 °C ambient temperatures. A pre-existing electrochemical model was modified to improve simulation accuracy at lower temperatures. Excitation response analysis and a multi-group particle swarm optimization algorithm were used to determine the model parameters. According to the simulation results, the mean absolute errors of terminal voltage were within 20 mV at ambient temperatures of 20 °C or higher. In the lower temperature range of -10 °C to 10 °C, the mean absolute errors for single cells were 9–14 mV and for battery packs, 11–21 mV. To manage parameter uncertainties at varying ambient temperatures, analytic methods such as Hermite interpolation, polynomial fitting, and sinusoidal fitting were implemented, making the model more suitable for practical applications in diverse temperature conditions.

Following the study by [50] developed an electrochemical–thermal model to predict the behavior of a commercial $LiFePO_4$ battery during discharge. The model integrates parameters dependent on temperature and lithium-ion concentration, which affect reaction rates and Li^+ transport. Additionally, it considers the role of current collectors in contributing to overall heat generation within the battery. Simulation results for rate capability and temperature performance showed strong agreement with existing literature. The model explores Li^+ distribution during pulse-relaxation discharge and examines variations in electrochemical reaction rates and thermal responses during constant current discharge. Pulse-relaxation results reveal dynamic shifts in Li^+ concentration in both liquid and solid phases, offering valuable insights into polarization effects. For constant current discharge, the reaction rate on the positive electrode evolves over time and spatial position. After discharge, some $LiFePO_4$ material remains underutilized. At low discharge rates, both endothermic and exothermic processes are observed; however, as the rate increases, the endothermic phase diminishes, leaving only exothermic behavior at high rates.

While significant advancements have been made in electrochemical modeling for lithium iron phosphate batteries, gaps remain in integrating predictive tools with real-time

applications. The present study introduces a Deep Neural Network (DNN) model that estimates the state of health (SOH) of batteries using voltage, current, temperature, and health indicators, offering a data-driven approach to battery diagnostics. However, the integration of such DNN models with established electrochemical models, such as the P2D and SP models, remains underexplored. Combining the high accuracy of electrochemical models with the predictive capabilities of DNNs could enhance SOH estimation, especially under dynamic operating conditions like temperature variations or high current loads. Moreover, while electrochemical models effectively simulate thermal and electrochemical behaviors, their complexity in parameter identification limits their real-time applicability. A hybrid approach incorporating DNN-driven insights and electrochemical model fidelity could bridge this gap, providing improved accuracy and scalability for practical battery management systems.

2.3.6 Physics-Based Models (PBM)

In porous electrode theory, physics-based electrochemical battery models (PBM) are powerful instruments for understanding lithium-ion batteries and their better design and management. Each PBM has its shortcomings, for example, those from LiB, while it promises to be the alternative from equivalent circuit models. The most promising PBM features include more internal electrochemical states of the battery. Different model uniqueities require different model fidelity, and hence model complexity. While greatly appropriate batteries can use high-performance supercomputers for long computation times, real-time battery control such as those for electric vehicles requires very quick calculations on simple machines. Simplified models, keeping most features, are often used in such cases for cost-effective computations. The great continuum physics-based electrochemical battery models started in the 1960s [61]; since then, they have been amended for various types of battery, e.g. lead-acid [62], nickel/metal hydride [63], lithium-air [64] and lithium-ion [65-68].

These physics-based models were initiated from the previously mentioned single particle model (SPM), introduced by [69], and expanded later by [70] to include lithium-ion distribution within the electrolyte. SPMs assume that all particles in an electrode can be

modeled as a single spherical particle, thereby significantly simplifying the model's complexity. These physics-based electrochemical models within Figure 1 describe the behavior of various internal variables that are not measurable directly in an in-operando configuration. Particularly, they prescribe the potential and current distribution in the porous electrodes and the electrolyte, li concentration in the electrolyte, and the distribution of intercalated lithium within the electrode particles.

Another study conducted by [71] sought to establish a model at reduced order for lithium-ion batteries that optimizes the fidelity and the computational expense embodied in a physics-based model. The criterion for the parameters is based on the value of the determinant and condition number of the Fisher information matrix (FIM). First, they get a subspace consisting of at most nine identifiable parameters that are then identified with a nonlinear least squares regression algorithm with respect to their confidence region determined by Fisher Information Matrix. The proposed strategies to extend battery modeling are validated with the output of commercial software for their efficacy. The estimated parameters tend to be slightly different from the actual values leading to insignificant voltage errors against different current profiles.

The thermal generation inside lithium-ion batteries by prediction for two distinct methodologies, the physics and machine learning-based approaches. A validated multi-physics and neural network model for commercial lithium-ion batteries (LIBs) with LiFePO4/G, LMO/G, and LCO/G electrodes (lithium iron phosphate/graphite, lithium manganese oxide/graphite, and lithium cobalt oxide/graphite) is used to calculate heat generation and, simultaneously, to delineate the LIB energy efficiency contours thereby justifying the nominal capacity as the critical parameter for manufacturing LIBs. These contours help energy systems designers have a better view of the LIB's actual efficiency as they incorporate LIBs into their devices. Thermal behavior shows its effect on charge/discharge energy efficiency of LIBs-LFP/graphite. For three types of LIBs available in the market showing performance at extremely low-temperature conditions, the focuses are applied to general applications-from consumer uses like electric vehicles (EVs) to industrial applications such as uninterruptible power supplies (UPSes).

A study conducted by [73] explored and evaluated two innovative lightweight physics-informed machine learning methods for accurately estimating a battery cell's capacity and diagnosing its primary degradation mechanisms using only limited early-life experimental data. To enable predictions for late-life performance (e.g., beyond 1.5 years) without the need for long-term experimental data, these methods were trained using simulated data from a physics-based half-cell model alongside early-life degradation data (e.g., within the first three months) obtained through cycling tests. The evaluation leveraged data from a 3.5-year cycling experiment involving 16 implantable-grade lithium-ion cells, which were subjected to different temperature conditions and C-rates. The results of a four-fold cross-validation analysis revealed that the proposed physics-informed models significantly outperformed traditional data-driven approaches, improving the accuracy of capacity estimation and identifying three key degradation modes by over 50%. Additionally, the study provided valuable insights into the effects of temperature and C-rate on battery cell degradation.

According to the research paper [74], there are various order reduction methods available pertinent to physics-based Li-ion battery models and their significant importance in next-gen battery management systems (BMSs). Thus, we review and compare these methods, particularly regarding model fidelity, computational efficiency, as well as applicable domains for these techniques. Reduced-order models have been represented as equivalent circuits to make it easier for designers and practitioners who do not necessarily have electrochemical backgrounds but rather a grasp of circuit theory to apply them towards multi-physical dynamics and interrelated battery effects. They are given the key pointers in selecting the right physics-based models for varied model-based applications in battery management. Discussions are then finalized with the possible obstacles and future research lines associated with multi-physical BMS.

Although physics-based models (PBMs) provide comprehensive insights into the internal electrochemical and thermal conditions of lithium-ion batteries, obstacles persist in their utilization for real-time battery management and state-of-health (SOH) forecasting. This study presents a Deep Neural Network (DNN) model for State of Health (SOH) estimation

utilizing experimental data such as voltage, current, temperature, and health indicators. The amalgamation of data-driven deep neural network methodologies with pharmacy benefit managers is still inadequately investigated. Pharmacological Benefit Managers (PBMs) offer precise descriptions of internal processes; however, they are computationally demanding and necessitate intricate parameter identification, thereby constraining their feasibility in real-time applications. DNN models exhibit computational efficiency; however, they lack the interpretability and mechanistic insights provided by PBMs. A hybrid methodology that integrates the predictive capabilities of DNNs with the mechanistic precision of PBMs may address this disparity, facilitating accurate SOH predictions in dynamic environments. Subsequent research ought to concentrate on integrating these methodologies to improve battery performance modeling and management.

2.3.7 Impedance Spectroscopy (IS)

Impedance Spectroscopy (IS) is a powerful diagnostic technique used in electrochemical systems to measure impedance as a function of frequency. It involves applying a small alternating current (AC) signal to a system and analyzing the voltage response. This technique provides valuable information about the electrochemical properties of materials, such as charge transfer resistance, double-layer capacitance, and diffusion coefficients. IS is widely used in studying batteries, fuel cells, and corrosion mechanisms. Its capability to probe internal processes at different time scales makes it ideal for diagnosing and modeling electrochemical systems [159]. IS is represented mathematically using complex impedance, expressed as $Z(\omega)=Z'(\omega)+jZ''(\omega)$Z(\omega) = Z'(\omega) + jZ"(\omega)$Z(\omega)=Z'(\omega)+jZ''(\omega)$, where $Z'(\omega)$Z'(\omega)$Z'(\omega)$ and $Z''(\omega)$Z"(\omega)$Z''(\omega)$ are the real and imaginary components of impedance, respectively. A Nyquist plot, which represents $Z''(\omega)$Z"(\omega)$Z''(\omega)$ versus $Z'(\omega)$Z'(\omega)$Z'(\omega)$, is commonly used for analyzing IS data. Equivalent circuit modeling further interprets IS data by fitting it to electrical circuit analogs that describe the system's behavior [160].

IS plays a critical role in diagnosing and monitoring lithium-ion batteries. It is used to measure key parameters like internal resistance, charge transfer resistance, and diffusion resistance. These parameters provide insights into battery performance, degradation, and

state-of-health (SoH). IS is particularly valuable because it is non-invasive and can detect early signs of aging and performance degradation. It allows researchers to study battery behaviors under varying conditions, such as different temperatures, states of charge, and cycling frequencies [161]. IS commonly applied in LiB studies to construct equivalent circuit models, which simulate the battery's internal electrochemical processes. The technique helps in separating contributions from the electrode-electrolyte interface, solid-electrolyte interphase (SEI) layer, and bulk material properties. For example, Osaka et al. [162] used IS to diagnose commercially available lithium-ion batteries and identified changes in SEI resistance due to aging. IS also enables real-time monitoring, which is crucial for advanced battery management systems [163].

The study by [168] investigated lithium-ion batteries using two- and three-electrode setups with IS. They identified that SEI resistance and charge transfer resistance are critical for understanding battery degradation. Their findings emphasized that the SEI layer significantly contributes to impedance at low frequencies. This study provided a framework for separating electrode-specific contributions using IS. [166] analyzed the Nyquist plots of lithium-ion batteries to diagnose aging mechanisms. They observed that the semicircles in Nyquist plots expanded with cycling, indicating increased charge transfer resistance. This method effectively correlated impedance changes with capacity fade, making it useful for SoH estimation. [167] examined the performance of lithium iron phosphate batteries under high-rate discharge conditions using IS. Their study found that high-rate cycling led to significant increases in diffusion resistance, which was linked to structural degradation of the electrode materials. They proposed optimizing electrode compositions to mitigate these effects.

Following the research by [165] introduced nonlinear electrochemical impedance spectroscopy (NLEIS) for lithium-ion batteries. Unlike traditional IS, NLEIS considers nonlinear interactions within the battery. This technique improved the accuracy of identifying degradation mechanisms, especially under dynamic operating conditions. [164] applied IS to assess the SoH of lithium-ion batteries in high-power applications. They developed an equivalent circuit model that incorporated inductive effects observed at high frequencies.

This model improved SoH estimation accuracy for high-current scenarios. [160] studied IS for different electrode materials and proposed material-specific equivalent circuit models. Their work demonstrated that impedance behavior varies significantly based on material composition, highlighting the need for customized models for each battery type.

Another study employed by [163] explored the temperature dependence of IS parameters in lithium-ion batteries. They found that both charge transfer resistance and diffusion resistance decreased with increasing temperature. Their study suggested that IS can be used to optimize battery performance under varying thermal conditions. [163] developed an IS-based SoH estimation method for lithium-ion batteries. By analyzing impedance data across a wide frequency range, their model achieved high accuracy in predicting SoH. This method demonstrated the potential of IS in advanced battery management systems. [161] used IS to characterize the aging effects in lithium-ion batteries over extended cycling. They identified correlations between impedance growth and cycle life, enabling the prediction of battery lifespan. Their equivalent circuit model captured both reversible and irreversible degradation mechanisms. [162] proposed a real-time diagnostic framework using IS for commercial lithium-ion batteries. Their approach combined impedance data with temperature and voltage measurements to enhance predictive accuracy. This model was particularly useful for safety-critical applications.

Despite advancements in State-of-Health (SoH) estimation for electric vehicle (EV) batteries, significant gaps remain in integrating comprehensive datasets and leveraging advanced machine learning techniques. Existing studies primarily rely on conventional methods like Impedance Spectroscopy (IS) and equivalent circuit models (ECMs), which, while effective, lack scalability for real-time applications and often require extensive experimental setups. Although recent approaches using data-driven models, including Recurrent Neural Networks (RNNs) and Convolutional Neural Networks (CNNs), have improved prediction accuracy, they fail to holistically address the multidimensional nature of battery health. These models often neglect critical parameters like temperature fluctuations, variable load profiles, and nonlinear aging mechanisms, leading to suboptimal performance under dynamic conditions. There is a need for a novel Deep Neural Network (DNN)

framework capable of integrating diverse indicators such as voltage, current, and temperature to provide real-time, accurate, and adaptable SoH predictions. This study aims to fill this gap by proposing an advanced DNN model tailored for dynamic EV battery scenarios.

2.3.8 Deep Neural Networks (DNN)

In many real-world applications, estimating remaining useful life (RUL) has become crucial to lowering maintenance costs and enhancing system efficiency and reliability. Deep learning developments in the last few years have greatly improved machinery prognostic RUL estimation and degradation progression accuracy. Deep learning is a branch of machine learning that mimics human intelligence by modeling the structure and functions of the human brain. A basic Deep Neural Network (DNN) is made up of a hierarchical configuration of neurons that interact with one another and process input data to create a complex network that learns via feedback mechanisms. The input data enters the first layer of neurons, where the output is processed and passed to subsequent layers until the final prediction is achieved. The output is typically represented as a probability, predicting outcomes such as "Yes" or "No." Each neuron computes an "activation function," which facilitates signal transmission to the relevant neurons in the next layer.

DNNs consist of multiple fully connected layers to map complex relationships in battery data. The layer computation is as follows;

$$a^{(l)} = \emptyset\,(W^{(l)} . a^{(l-1)} + b^{(l)}$$

Where: $a^{(l)}$ is the activation in layer l, $W^{(l)}$, $b^{(l)}$ are weights and biases for layer l, $\emptyset$ is the activation function (e.g., ReLU). The output layer is as follows;

$$y = \sigma\,(W_o . a^{(L)} + b_o)$$

Where, $a^{(L)}$ is the final hidden layer activations, σ is the softmax or sigmoid activation for classification or regression tasks. DNNs are powerful for analyzing high-dimensional data like battery impedance spectroscopy or voltage/current profiles.

Neurons in successive layers of a Deep Neural Network (DNN) are connected through weights. These weights play a crucial role in determining the significance of

individual features when predicting the target output. Figure 2.12 illustrates a DNN with four hidden layers. Initially, the weights are assigned random values, but as the model undergoes training, these weights are iteratively updated to optimize learning and improve prediction accuracy. The advent of advanced computational power and increased data storage capabilities has significantly boosted the adoption of deep learning models across various domains. These models are now integral to numerous aspects of both digital and everyday life. From healthcare and aviation to banking, retail, and telecommunications, deep learning has become a transformative tool across virtually every industry, enabling smarter decision-making and more efficient processes.

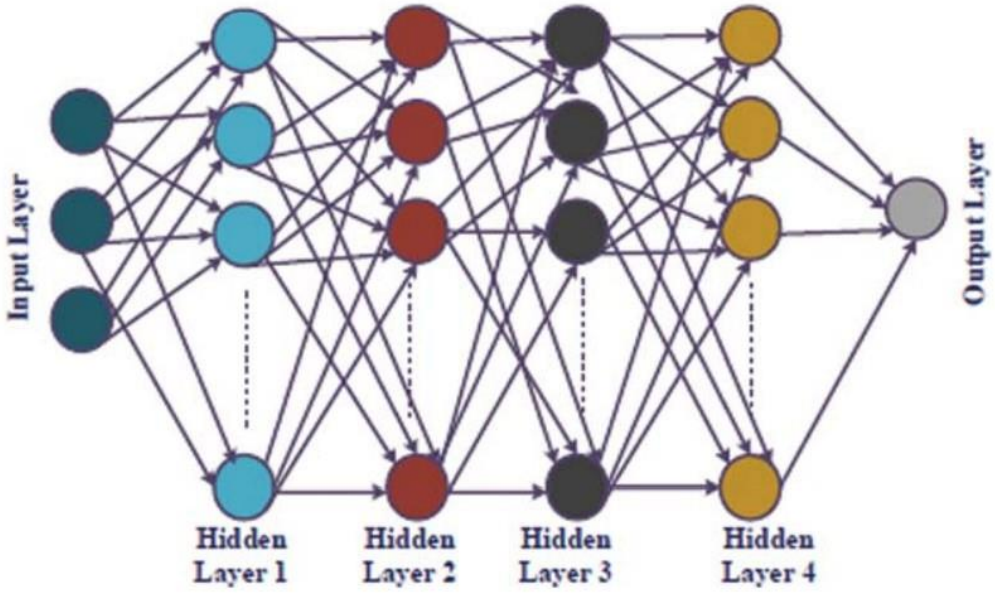

Figure 2.12. Deep neural network with multiple hidden layers [75]

Following the study conducted by [76] proposed a state-of-charge (SOC) estimation model for Li-ion batteries utilizing an advanced deep neural network (DNN) methodology specifically designed for electric vehicle applications. The research indicated that a suitably configured DNN with an ideal quantity of hidden layers could precisely forecast the SOC of drive cycles absent from the training dataset. A variety of DNN models with distinct hidden layer configurations were created and assessed to evaluate their performance across different drive cycles. The findings demonstrated that augmenting the number of hidden layers to four

markedly diminished the error rate and enhanced SOC estimation precision. Nevertheless, incorporating more than four hidden layers resulted in elevated error rates, indicating diminishing returns and the possibility of overfitting. The research highlighted that a DNN with four hidden layers, trained on the Dynamic Stress Test drive cycle, excelled in predicting SOC for novel drive cycles, such as the Federal Urban Driving Schedule, Beijing Dynamic Stress Test, and Supplemental Federal Test Procedure.

The research by [77] presented a novel approach for state-of-charge (SOC) estimation in Li-ion batteries utilizing Deep Feedforward Neural Networks (DFNN). This method directly correlates battery measurements to SOC, utilizing an extensive dataset produced in the laboratory. The training data encompassed drive cycle loads imposed on a Li-ion battery across diverse ambient temperatures, subjecting the battery to variable conditions. The study emphasized the DNN's capacity to encode temporal dependencies within its network weights, facilitating precise SOC predictions. The training dataset included measurements taken at ambient temperatures between −20 °C and 25 °C. Upon training, the DNN exhibited the ability to estimate SOC under various temperature conditions utilizing a singular model. Validation across diverse datasets demonstrated remarkable performance, with a Mean Absolute Error (MAE) of 1.10% at 25 °C and 2.17% at −20 °C, signifying the model's robustness and precision under different thermal conditions.

A feedforward deep neural network model for predicting the parameters of lithium-ion batteries used in electric vehicles was presented in the works of [78]. In order to identify suitable candidate parameters, the model excluded categorical variables using correlation analysis. To estimate the battery's state-of-charge (SOC) and produce an inverse model for extensive parameter prediction, a feedforward artificial neural network was built. Four virtual functions were incorporated into the SOC prediction of the direct model to serve as input variables for the inverse model, increasing the predictive accuracy of the latter. The suggested inverse model demonstrated the ability to predict multiple outputs, such as velocity, voltage, speed, mileage, and (SOC). Because of its multi-output capability, it was better than traditional single-output feedforward networks, which primarily focus on SOC. Simulations employing the inverse model, augmented with virtual functions, attained an accuracy 44.43

times superior to that of traditional inverse deep neural network models. The mean square error metric was utilized to assess the model's performance. The study's results indicate that incorporating virtual functions into the inverse model framework markedly enhances the precision of predictions concerning battery and electric vehicle parameters, thereby enabling more informed decision-making in design and simulation processes.

In order to estimate the state-of-charge (SOC) of batteries, a deep neural network (DNN) model was developed by [79]. This model uses temperature, voltage, and current samples that are taken every 10 seconds as input data. A convolutional layer is used for feature extraction and sequence generation, a simple recurrent unit (SRU) layer is used for sequence processing and historical information transfer, an ultra-lightweight subspace attention mechanism (ULSAM) layer is used to highlight important information within the sequence, and a dense layer is used to output the SOC estimate. The model's robustness and effectiveness in real-world applications were demonstrated by its high accuracy in (SOC) estimation and notable adaptability to battery degradation, varying ambient temperatures, and a variety of discharge conditions. The model was validated using two public battery datasets. According to the study by [80] presented a deep neural network (DNN)-based methodology for estimating the state-of-charge (SOC) of batteries utilizing merely 10 minutes of charging voltage and current data as input.

This technique is suitable for calibrating the Ampere-hour counting method because it yields fast and accurate (SOC) estimation with an error rate that is less than 2.03% over the whole SOC spectrum. The study found that by reducing the impact of error spikes and random noise, the DNN combined with a Kalman filter enhances the accuracy of SOC estimation. A root mean square error of 0.385% was maintained by the method in spite of significant perturbations. Using the transfer learning methodology, the DNN showed adaptability to a variety of conditions, such as battery aging and different charging rates. By optimizing one layer of a pre-trained model, this technique reduces training costs while increasing estimation accuracy, producing root mean square errors of less than 3.146% for older batteries and 2.315% for different kinds of batteries. Refining supplementary layers

further improved performance, rendering the method efficient and adaptable for various situations.

In research, [81] developed a novel data-driven approach that uses a hybrid deep learning model that combines convolutional neural networks (CNN), long short-term memory (LSTM), and conventional neural networks to estimate the Remaining Useful Life (RUL) of batteries. In order to improve the accuracy of RUL predictions, this hybrid CNN-LSTM architecture was created expressly to extract both spatial and temporal features from multivariate time series data while capturing nonlinear behaviors. Particle swarm optimization (PSO) was used for hyperparameter tuning, which improved the model's performance by optimizing parameters like the number of epochs, the arrangement of LSTM and convolutional layers, and the size of units or filters within each layer. Using NASA's well-known lithium-ion battery (LiB) dataset, the CNN–LSTM–PSO framework underwent extensive validation and is capable of supporting multi-step-ahead forecasting. According to experimental results, the CNN–LSTM–PSO model performed better than other deep learning and advanced machine learning techniques on a number of evaluation metrics, proving its usefulness as a reliable tool for RUL prediction. The application of deep neural networks (DNNs) to battery management systems has advanced significantly, but there are still many obstacles to overcome before state-of-health (SOH) estimation for electric vehicle (EV) batteries can be considered practically applicable and its predictive accuracy can be further improved.

This work proposes a DNN-based approach for State of Health estimation using experimental data, including voltage, current, temperature, and health indicators. However, there is still insufficient research on the integration of advanced DNN architectures, like CNN-LSTM hybrids, which have demonstrated remarkable spatiotemporal feature extraction capabilities in remaining useful life (RUL) estimation. Furthermore, while existing approaches address specific tasks like degradation modeling or State of Health (SOH) estimation, few approaches effectively combine SOH estimation with multi-output predictions like degradation modes and operational metrics. Efficiency and scalability may be improved by adapting models for different battery chemistries and aging scenarios using

strategies like transfer learning. Future work should look into multi-task learning frameworks and the integration of hybrid DNN models with real-time datasets for thorough battery health management.

2.3.9 Convolutional Neural Network (CNN)

Within the deep learning model category, Convolutional Neural Networks (CNNs) are designed to analyze data that has a spatial or grid-like configuration, such as images or time-series data [82]. Convolutional filters are applied to the input data by a CNN in order to help capture spatial hierarchies and patterns. Convolutional, pooling, and fully connected layers typically make up a CNN's architecture. While pooling layers downsample the feature maps to reduce dimensionality and highlight the most prominent features, convolutional layers extract features by applying filters that traverse the input data. At the end of the network, fully connected layers combine the extracted features to produce predictions. ReLU-style activation functions are used in layers to introduce non-linearity, and backpropagation is used to improve the filter weights over the time training process. This architecture renders CNNs especially proficient for feature-dense, high-dimensional data, ensuring strong performance across various applications [83].

Three main parts make up the structure of a Convolutional Neural Network (CNN), a particular kind of multilayer perceptron (MLP): the input layer, hidden layers, and output layer. While the output layer creates the final predictions that can be used in further tasks or applications, the input layer receives the raw data and passes it to the first hidden layer. The convolutional, max-pooling, and fully connected layers are examples of the hidden layers. Convolutional layers are essential to CNNs because they enable the extraction of local features from the input data, their hierarchical processing, and the transmission of the resulting information to deeper layers for more sophisticated feature learning and analysis. The vector output from the first convolutional layer can be represented mathematically as follows:

$$O_{ij}^{1} = \sigma(b_j^1 + \sum_{f\ v=1}^{M} w\ f_{v,j}^{1} X_i + f_v^o - 1, j\ )$$

Where σ, b_j, and w stand for sigmoid activation function, the bias for the j feature map, and the sigmoid activation function, respectively. The filter index is denoted by f_v, while the power production input vector is represented by x. Similarly, the vector o output of the l convolutional layer can have the following expression as its result.:

$$O_{ij}^{1} = \sigma(b_j^1 + \sum_{f\ v=1}^{M} w\ f_{v,j}^{1} X_i + f_v^o - 1, j\ )$$

Max-pooling layers are used to reduce the representation's dimensionality, which lessens the model's computational load. The max-pooling layer operates as follows:

$$O_{ij}^{1} = \max\ y_i \times T^{l-1} + r, j\ (r \in R)$$

R is the size of the pooling. T is the step that calculates the moving distance of the input data area, which must be less than the input size y. Every neuron in a layer is connected to every other neuron in the output layer by fully connected layers.

CNNs have been widely adopted in the field of LiB research for state-of-charge (SOC), state-of-health (SOH), capacity estimation, and fault diagnosis. The nonlinear and complex electrochemical behaviors of lithium-ion batteries, including lithium iron phosphate ($LiFePO_4$) batteries, make conventional modeling techniques less effective. CNNs excel in analyzing multidimensional data such as voltage, current, temperature, and impedance spectra, providing accurate predictions and diagnostics by extracting hierarchical features [84]. CNNs capture spatio-temporal dependencies, making them highly adaptable to battery conditions such as aging, varying ambient temperatures, and cycling conditions [85]. By leveraging convolutional layers, CNNs can identify intricate patterns and degradation trends in batteries, offering substantial improvements over traditional algorithms [86].

Following the study by [82] introduced a pruned CNN model for LiB capacity estimation, integrating transfer learning to reduce computational overhead while maintaining high accuracy. [83] demonstrated the use of CNNs for parameter identification in electrochemical battery models, highlighting the efficiency of CNNs in accurately predicting essential parameters like resistance and capacity. [84] reviewed advancements in deep CNNs for state prediction, emphasizing their effectiveness in handling multi-timescale challenges in lithium-ion batteries. [85] combined CNNs with transformer models for SOH estimation, achieving high accuracy under various environmental conditions and battery degradation states. [87] utilized a CNN and a knee-point detection algorithm to predict battery degradation curves, showcasing the model's capability in estimating lifespan. [88] proposed a hybrid CNN and Gaussian process regression approach for probabilistic SOH prediction, improving uncertainty quantification in battery monitoring systems.

The research by [89] employed CNNs with impedance spectra for capacity estimation, demonstrating high precision and adaptability to complex datasets. [90] developed a CNN to estimate SOH during constant current operations, which showed resilience to charge-discharge variations. [91] integrated empirical mode decomposition and CNNs for fault diagnosis in battery packs, accurately identifying faults in multi-cell systems. Similarly, [92] applied CNNs for defect detection in polymer lithium-ion batteries, achieving a high detection rate for manufacturing flaws. [93] proposed a CNN-based SOH estimation model using charge profiles, providing high prediction accuracy across multiple cycling datasets. [94] used CNNs to diagnose battery degradation modes, demonstrating their ability to identify specific degradation mechanisms. [95] applied CNNs to estimate capacity using random charging curve segments, achieving consistent performance under varying cycling conditions.

The study by [96] developed a CNN in the time-frequency domain for SOC estimation, effectively capturing spectral and temporal dependencies. [97] combined CNNs with random forests to create a robust SOH estimation model, excelling in noisy datasets. A CNN with U-Net architecture for SOC estimation was introduced in the works of [84], achieving high accuracy over a variety of datasets and operating conditions. In order to

estimate remaining useful life (RUL), [98] developed a hybrid CNN–LSTM–DNN model that combined the advantages of LSTMs for sequential data processing and CNNs for feature extraction. By incorporating an adaptive Kalman filter for SOE estimation, [99] improved CNN performance and showed resilience in challenging thermal conditions. [54] combined CNNs and LSTMs to model multiphysics and capture complex interactions between different domains. In order to estimate capacity using short-duration constant-current charging voltages, [100] used a CNN and produced accurate predictions in a variety of charging scenarios. Their model demonstrated CNNs' versatility in practical applications, highlighting their importance in battery research.

Despite advancements in leveraging deep neural networks (DNNs) for battery health estimation, critical research gaps remain, particularly in their integration with real-world applications and advanced architectures. The present study introduces a novel DNN model to estimate the SOH using experimental data, including voltage, current, temperature, and health indicators. However, the study lacks exploration of convolutional neural networks (CNNs), which excel in capturing spatial hierarchies and temporal dependencies from multi-dimensional data. Hybrid models, such as CNN-LSTM combinations, have demonstrated superior accuracy by integrating spatial and sequential data processing capabilities. Furthermore, the potential of transfer learning for adapting models across battery chemistries, degradation states, and environmental conditions remains underutilized. Addressing these gaps through hybrid frameworks and leveraging advanced techniques like transfer learning and uncertainty quantification could significantly enhance SOH estimation, ensuring robust and scalable solutions for electric vehicle battery management.

2.3.10 Recurrent Neural Network (RNN)

An artificial neural network type called Recurrent Neural Networks (RNNs) is made especially to process sequential data. RNNs, as opposed to FNNs, have loops in their architecture, which enable them to feed back their output into the network in order to retain information from prior inputs. RNNs are especially well-suited for tasks involving sequential or time-dependent inputs because of their feedback mechanism, which allows them to model temporal dependencies and identify patterns in time-series data [102]. The architecture

creates a dynamic link between past and present data by relying on hidden states that are updated iteratively as new inputs are processed. But conventional RNNs have drawbacks, like the vanishing gradient issue, which makes it difficult for them to understand long-term dependencies. To overcome these issues, advanced variants like (LSTM) networks and Gated Recurrent Units (GRUs) were introduced. These architectures use gating mechanisms to regulate the flow of information, allowing them to effectively capture and learn long-term dependencies [103].

RNNs process sequential data by maintaining a hidden state that captures temporal dependencies. For battery data (e.g., voltage, current, temperature): The hidden state update is as follows;

$$h_t = \emptyset\,(\,W_h . h_{t-1} + W_x . x_t + b_h$$

Where, $h_t is\ the\ hidden\ state\ at\ time\ t,\ h_{t-1}\ hidden\ state\ at\ time\ t-1, x_t\ input\ at\ time,\ b_h\ is\ the\ bias\ factor$. The output computation is as follows;

$$y_t = W_t . h_t + b_y$$

The capacity of Recurrent Neural Networks (RNNs) to handle temporal data and capture dynamic relationships in battery performance has led to their considerable attention in LiB applications. Lithium-ion batteries, which comprise lithium iron phosphate ($LiFePO_4$) batteries, display intricate behaviors that are impacted by various factors, including temperature, charge-discharge cycles, (SOH), and (SOC). Because traditional models cannot process sequential data well, they are unable to predict battery parameters with any degree of accuracy. By utilizing their memory and feedback capabilities, RNNs get around this restriction and allow for precise estimations of SOC, SOH, and remaining useful life (RUL) [106]. For battery diagnostics and prognostics, variants like LSTM and GRU have gained popularity because of their exceptional efficacy in controlling nonlinear battery behaviors [108,111]. RNNs capture temporal dependencies and offer insights into capacity degradation and battery aging, and thermal characteristics, enhancing battery management systems (BMS) [104].

The study by [105] combined denoising autoencoders with GRU-based RNNs for SOC estimation, demonstrating improved accuracy in handling noisy data. Similarly, [108] proposed a clockwork RNN for SOC estimation, which effectively reduced computational complexity while maintaining accuracy. [106] introduced time-delayed RNNs to improve SOC estimation reliability by addressing overexcited neurons. These models achieved robust SOC predictions under varying operating conditions. [111] developed a GRU-based RNN for SOC estimation, achieving high precision in dynamic conditions. [105] conducted a comparative study of different RNN architectures for SOC estimation in electric vehicles. Their findings emphasized the advantages of GRUs and LSTMs in capturing battery dynamics. [109] proposed a physics-informed RNN with fractional-order gradients, enhancing SOC estimation by incorporating domain-specific knowledge. [107] used a jellyfish-optimized RNN for SOH estimation, showcasing improved performance over traditional optimization techniques. [117] applied RNNs to estimate SOH, demonstrating their adaptability to varying battery conditions. [119] proposed an RNN-based framework for battery degradation prediction under uncertain future conditions, highlighting the importance of RNNs in long-term health monitoring.

The research by [110] employed RNNs for RUL estimation, achieving accurate predictions across different battery chemistries. [86] developed a compact RNN methodology for equivalent circuit modeling, enabling precise SOH estimations. [115] introduced a multi-charging profile framework using RNNs for RUL prediction, demonstrating the flexibility of RNNs in handling diverse operational scenarios. [112] utilized RNNs for temperature estimation in lithium-ion batteries, providing valuable insights into thermal management. [104] applied RNNs to model the large deformation of battery cells, capturing complex mechanical behaviors. These studies highlight the versatility of RNNs in addressing thermal and structural challenges in battery systems.

Following the study by [116] employed LSTM-based RNNs for capacity prediction, achieving high accuracy in validation tests. [118] proposed a hybrid RNN and support vector machine (SVM) model for co-estimation of SOC and capacity, emphasizing the effectiveness of integrating RNNs with other machine learning techniques. [113] introduced an adaptive

RNN for RUL prediction, showcasing its ability to adapt to changing conditions. [114] developed a unified RNN methodology for voltage and SOC modeling, achieving reliable predictions across varying cycles. [121] compared RNNs, CNNs, and BP networks for capacity prediction, demonstrating RNNs' superior performance in temporal data analysis.

Following the research by [111] integrated empirical mode decomposition with deep RNNs for predictive maintenance, improving fault detection accuracy. Another study by [122] introduced LSTM-based RNNs for SOC estimation, emphasizing their robustness in dynamic environments. Moreover, the study by [124] proposed an LSTM-based RNN for SOC estimation, achieving significant improvements in prediction accuracy. Following the research by [114] and [123] highlighted the versatility of RNNs for equivalent circuit modeling, demonstrating their applicability across different battery chemistries. The investigation by [119] showcased RNNs' ability to predict battery degradation under varying operational conditions, emphasizing their importance in future-proofing battery systems.

Despite significant advancements in battery health estimation using deep neural networks (DNNs), several research gaps remain unaddressed. The present study proposes a novel DNN model utilizing experimental data such as voltage, current, temperature, and existing health indicators to estimate the SOH. However, it lacks an exploration of RNNs, including advanced variants like LSTM and GRU, which are well-suited for capturing temporal dependencies and handling sequential data inherent in battery performance. Additionally, hybrid models combining DNNs with RNNs or other architectures such as CNNs could improve prediction accuracy by leveraging complementary strengths. The integration of physics-informed features into data-driven approaches, such as incorporating electrochemical behaviors or degradation mechanisms, also remains underexplored. Addressing these gaps through hybrid frameworks, temporal modeling, and domain knowledge integration could enhance SOH predictions, ensuring robust and scalable solutions for electric vehicle battery management.

2.3.11 Long Short-Term Memory (LSTM)

The development of neural network algorithms—such as feedforward, convolutional, and (LSTM) networks—has made a substantial impact on data analysis and our

understanding of the connection between charging profiles and battery capacity. Recurrent neural networks (RNNs) have limitations, such as vanishing and exploding gradient issues. LSTM networks, a specialized version of RNNs, are made to handle sequential data. Initially presented by Hochreiter and Schmidhuber in 1997, LSTMs control the information flow within the network by means of gating mechanisms, namely forget, input, and output gates. These gates facilitate the efficient modeling of long-term dependencies by allowing LSTMs to selectively keep or discard data from earlier time steps. To be more precise, the output gate produces the current output based on the updated cell state, the input gate adds new input, and the forget gate determines which information to discard [123]. Owing to this architecture, temporal understanding tasks like language processing, sequential decision-making, and time-series forecasting are especially well-suited for LSTM networks [126].

LSTMs address the vanishing gradient issue by incorporating gates to regulate information flow. Forget gate is as follows;

$$f_t = \sigma\,(W_f \,.\, [h_t{-}1\,, x_t] + b_f$$

Where, f_t is the forget gate output w_f weight matrix and bias for forget gate, σ is the sigmoid activation function. The input gate is as follows;

$$i_t = \sigma\,(W_i \,.\, [h_t{-}1\,, x_t] + b_i$$

$$C_t = tanh(W_c \,.\, [h_t{-}1\,, x_t] + b_c$$

Where, i_t is input gate output, C_t is the candidate memory content. The memory cell update is as follows;

$$C_t = f_t \cdot C_{t-1} + i_t \cdot C_t$$

The output state and hidden gate is as follows

$$o_t = \sigma\,(W_o \,.\, [h_t{-}1\,, x_t] + b_o$$

$$h_t = o_t \cdot \tanh(C_t)$$

The final output y_t is computed similarly to RNN,

$$y_t = W_y \cdot h_t + b_y$$

LSTMs capture long-term dependencies in battery degradation data, improving SOH and SOC estimation.

LSTM networks are widely used in LiB applications, such as $LiFePO_4$ batteries, for tasks like capacity fade prediction, RUL forecasting, SOC estimation, and SOH monitoring. Since temperature, cycling conditions, and aging all affect battery behavior, traditional models frequently find it difficult to accurately capture the complex and nonlinear behavior of batteries. Because LSTM networks can handle sequential data such as voltage, current, and temperature profiles, they are useful for diagnostics and accurate prediction [127]. They are also very useful for BMS, where accurate, real-time predictions are necessary to guarantee optimal performance and dependability, due to their resilience in the face of noise and nonlinear patterns [129, 130].

The study by [125] developed a digital twin model based on LSTMs for real-time temperature prediction and degradation analysis in lithium-ion batteries. This model provided actionable insights into thermal characteristics and degradation under varied conditions. The research by [126] proposed an LSTM network for predicting the remaining useful life (RUL) of lithium-ion batteries. The study demonstrated high accuracy in capturing long-term dependencies, making it suitable for real-world applications. Following the study by [127] presented an LSTM-based method for state-of-charge (SOC) estimation, achieving reliable predictions across diverse operational scenarios. Following the research by [128] investigated the impact of loading variations on lithium iron phosphate battery electrodes using LSTMs.

Their model accurately predicted electrode behavior under dynamic conditions. The study by [129] proposed an LSTM model for SOC estimation, emphasizing robustness in noisy datasets. The research investigated by [130] integrated LSTMs with an improved sparrow search algorithm for RUL prediction, achieving significant improvements in accuracy and efficiency.

Another study by [126] combined LSTMs with board learning systems for LiB capacity and RUL prediction. The approach demonstrated robustness across various operational conditions. The study by [132] conducted a comparative study of deep learning methods for SOC estimation, confirming LSTMs' superiority in handling lithium iron phosphate ($LiFePO_4$) battery data. The research by [133] utilized LSTMs for real-time parameter estimation in electrochemical battery models, showcasing adaptability to real-world battery behaviors. The works by [134] combined LSTMs with convolutional neural networks (CNNs) for multiphysics modeling of lithium-ion batteries. Their hybrid model successfully captured complex spatial-temporal interactions. The investigation conducted by [135] proposed a variant LSTM for SOH estimation and RUL prediction, achieving precise forecasts across varying battery degradation states. The study by [136] introduced a transfer learning-enhanced LSTM model for capacity fade and cycle life prediction, reducing training time and improving accuracy.

Following the research by [137] applied LSTMs to estimate SOC for a group of lithium-ion batteries, achieving consistent and reliable performance. Following the study by [139] developed a deep LSTM model for real-time capacity estimation, ensuring accurate predictions in battery management systems (BMS). Another study by [140] explored bidirectional LSTMs for SOC estimation, improving predictions by capturing forward and backward temporal dependencies. The investigation by [141] proposed an enhanced SOC estimation method using LSTMs integrated with adaptive state update filters. This approach addressed uncertainties in battery parameters effectively. The study by [142] leveraged transfer learning with LSTMs for SOH prediction, enabling adaptation to diverse battery types and cycling conditions. The research by [143] proposed an improved LSTM-based SOH estimation algorithm, resilient to battery degradation and environmental variability.

Following the study by [144] utilized stacked bidirectional LSTMs for LiB health management, demonstrating their efficacy in handling multivariate and complex datasets. Another study by [145] introduced a cost-effective LSTM-based framework for LiB diagnosis and prognosis, reducing computational overhead. The study by [116] integrated empirical mode decomposition with LSTMs for predictive maintenance, enhancing fault detection accuracy. The research by [124] applied LSTMs for SOC estimation, emphasizing their ability to process large datasets and dynamic conditions. Another investigation by [123] highlighted the versatility of LSTMs in equivalent circuit modeling for voltage and SOC predictions. The research by [121] compared LSTMs with CNNs and BP networks for capacity prediction, showcasing their superior performance in temporal data analysis. The study by [141] demonstrated the application of LSTMs in SOC estimation across varying environmental conditions, highlighting their adaptability in practical scenarios. These studies collectively underscore LSTMs' pivotal role in advancing LiB diagnostics, prognostics, and management systems.

Despite the growing body of research on battery state-of-health (SOH) estimation using machine learning models, critical gaps remain in integrating advanced neural network architectures with real-world applications. The proposed study introduces a Deep Neural Network (DNN) for predicting SOH using experimental data, including voltage, current, temperature, and health indicators. However, current approaches often overlook the challenges posed by varying environmental conditions, battery chemistries, and degradation profiles that impact prediction accuracy. While DNN models demonstrate promise in identifying nonlinear relationships, their integration with physics-informed features and dynamic real-time adaptability is underexplored. Moreover, the scalability and robustness of these models for large-scale deployments in electric vehicles (EVs) are not fully validated. Addressing the alignment of DNN-based estimations with diverse battery usage scenarios, including rapid charging cycles and extreme temperatures, is critical. This research aims to bridge these gaps by enhancing model precision, generalizability, and computational efficiency across variable operational contexts.

2.4 Proposed Methods in Literature

Following the study by [151] focused on analyzing LiB degradation using a realistic forklift mission profile to evaluate state-of-health (SOH) and predict battery lifetime. This method involves subjecting three prismatic LiB cells to a forklift load profile under varying temperatures (45 °C, 40 °C, and 35 °C) to simulate accelerated aging. The experimental setup incorporates dynamic charging and discharging conditions, with aging cycles followed by Reference Performance Tests (RPTs) to monitor capacity and internal resistance. Data is collected at high frequency, capturing second-by-second measurements of key variables, such as current, voltage, energy, and temperature. This dataset is intended for developing and validating various models, including electrochemical, statistical, and artificial intelligence models, for SOH estimation and lifetime prediction.

The advantages of this method are its realistic simulation of operational conditions, making it relevant to real-world applications. The dynamic load profile reflects variable usage patterns, enhancing the accuracy of battery behavior modeling. The high-resolution dataset provides comprehensive information, enabling detailed analysis and the development of versatile models. Additionally, despite its specificity to forklifts, the method can be adapted to electric vehicles due to similarities in operational characteristics. However, some limitations exist. The method's focus on forklift-like applications may restrict its broader applicability, and the loss of some aging and RPT data could introduce biases or necessitate data imputation. Furthermore, the study isolates calendar and cycling aging effects, missing insights into their interactions. Experimental constraints, such as fixed charging/discharging currents and temperature settings, may limit generalization to other battery chemistries or conditions. This approach contributes significantly to the field by combining realistic load profiles with systematic aging cycles, offering a robust framework for evaluating LiB. It bridges the gap between laboratory and field applications, providing high-resolution data for advanced modeling techniques and practical utility. This study's findings can improve state-of-health estimation and extend battery life, particularly for applications in electric vehicles and industrial settings.

Following the research by [152] employs an advanced method for forecasting the (SOH) of LiBs using deep learning (DL) models, focusing on their application in truck energy systems. The methodology begins with an extensive literature review on battery degradation and aging mechanisms, leveraging insights to address the challenges of SOH prediction. Using an open-source dataset, the study aggregates stressor signals, such as temperature, current, and SOC, into structured stressor tables. Feature reduction is applied to improve model efficiency by eliminating irrelevant data. The modeling process begins with Gaussian Process Regression (GPR), Multilayer Perceptrons (MLP), and CNN for initial validation. Advanced DL models like LSTM, GRU, and FNN are then evaluated for their ability to handle sequential data. Additionally, lightweight models such as Support Vector Regression (SVR) are employed to test performance in computationally constrained scenarios. To enhance interpretability, explainable machine learning (XML) techniques, including SHAP (SHapley Additive exPlanations) and Saliency Maps, are integrated. These techniques allow researchers to visualize and better understand the decision-making process of the models. The models are trained to predict SOH until failure, defined as an 80% capacity threshold, and are validated using performance metrics like RMSE and R^2.

The method offers several advantages. Deep learning models, particularly LSTM and GRU, demonstrate high accuracy in forecasting SOH under complex degradation conditions. The approach is versatile, as stressor-based feature aggregation ensures robustness, and XML techniques provide a layer of interpretability critical for practical applications. Additionally, lightweight models like SVR ensure scalability by offering competitive performance in resource-constrained environments. However, the method also has limitations. Deep learning models are computationally intensive and require significant expertise for tuning. The reliance on a single dataset may limit the generalizability of results, while the exclusion of physical or hybrid modeling approaches restricts insights into battery chemistry. Despite XML enhancements, interpretability remains a challenge due to the inherent complexity of DL architectures.

The contributions of the study are significant. By integrating stressor-based features with deep learning and XML, it bridges the gap between high performance and

interpretability. The combination of various models caters to different resource scenarios, making the approach adaptable for both high-performance and computationally limited applications. This methodology advances predictive maintenance strategies and provides actionable insights into battery aging. The study underscores the utility of XML in clarifying complex predictions, thereby improving reliability and user trust in machine learning models for SOH forecasting. Key references supporting this approach include Another study by [153], which provide foundational methodologies and data for battery aging and modeling research.

Following the study by [154] proposes a method for predicting the remaining useful life (RUL) of LiBs using a comparative analysis of machine learning (ML) models, with an emphasis on enhancing prediction accuracy and applicability. The methodology incorporates a multi-feature multi-target (MFMT) feature mapping framework, enabling accurate predictions of capacity fade and RUL across the entire lifecycle of batteries. To validate the approach, three case studies are conducted using two distinct datasets. The first two cases utilize a synthetic dataset representing linear battery degradation, while the third case employs a real-world dataset capturing nonlinear and complex degradation behaviors. Eight ML models, including Random Forest (RF), Multi-Layer Perceptron (MLP), XGBoost, XGBoost with hyperparameter tuning (XGBoost-HT), Light Gradient Boosting Machine (LightGBM), LightGBM with hyperparameter tuning (LightGBM-HT), LSTM, and Attention-LSTM, are analyzed. The study highlights the superior performance of XGBoost-HT, which incorporates hyperparameter optimization and regularization techniques, achieving the lowest root mean squared error (RMSE) and mean absolute percentage error (MAPE) across all cases. This robust approach is further strengthened by the application of MFMT feature mapping, which enhances the models' ability to predict nonlinear battery degradation.

The proposed method offers several advantages. The integration of MFMT feature mapping and hyperparameter tuning significantly improves predictive accuracy, particularly for batteries exhibiting nonlinear degradation patterns. The diversity of ML algorithms ensures flexibility, enabling practitioners to choose models based on computational resources

and application requirements. Additionally, the use of both synthetic and real-world datasets ensures comprehensive validation, enhancing the approach's robustness. However, the method also presents challenges. The reliance on specific datasets may limit its generalizability, and the advanced models require substantial computational resources for training and optimization. Furthermore, the exclusion of physics-based modeling means that some insights related to battery chemistry and degradation mechanisms may be overlooked. The models' dependency on precise hyperparameter tuning adds complexity to the implementation process.

Following the research by [155] proposed a comprehensive methodology for predicting the SoH and performance of LiBs in EVs by employing a comparative analysis of ML and DL approaches. Various techniques, including LR, DTs, support vector machines (SVMs), and ensemble methods, as well as advanced methods like artificial neural networks (ANNs), LSTM, and bidirectional LSTM (Bi-LSTM), are utilized. These methods are applied to publicly available datasets containing charge-discharge cycles of LiBs, focusing on improving model accuracy through preprocessing, feature selection, and hyperparameter tuning. The models are evaluated using metrics such as mean squared error (MSE), root mean squared error (RMSE), mean absolute error (MAE), and R-squared to identify the most effective techniques. Among these, Bi-LSTM is highlighted for its ability to capture nonlinear battery degradation patterns and is proposed as a superior solution for implementation in battery management systems (BMSs).

The advantages of this methodology include its comprehensive nature, providing insights into the strengths and weaknesses of different ML and DL models for SoH prediction. The integration of hyperparameter tuning and feature selection ensures optimized model performance, while the use of real-world datasets enhances the practical applicability of the findings. The approach is also scalable, with lightweight models like DTs and SVMs suitable for real-time applications in BMSs with limited computational resources. Advanced models such as Bi-LSTM demonstrate exceptional predictive power, particularly in scenarios involving complex nonlinear degradation behaviors. However, there are notable limitations. The DL models, including Bi-LSTM, require significant computational resources and expertise for training and implementation. The method’s reliance on specific datasets may limit its generalizability to other battery chemistries or applications. Additionally, the lack of

integration with physical or hybrid modeling approaches may restrict insights into underlying degradation mechanisms. The study makes significant contributions to the field by systematically comparing ML and DL approaches, identifying Bi-LSTM as a leading method for handling nonlinear data in battery performance prediction. The findings enable the development of more reliable and efficient BMSs, supporting better range prediction, safety, and maintenance planning for EVs. By optimizing model architecture and parameters, the research bridges the gap between theoretical advancements and real-world applications, paving the way for future technological innovations in EV battery management.

The study by [156] introduced a data-driven multi-model fusion methodology to improve the accuracy and robustness of LiB aging diagnostics and prognostics. This approach leverages both laboratory cycling data and real-world field data to estimate the SoH and predict the RUL of batteries. For SoH estimation, six distinct operational scenarios are identified, and features specific to each scenario are extracted to capture battery degradation under diverse conditions. A Kalman filter-based fusion algorithm combines predictions from various machine learning models, enhancing the reliability and precision of the estimations. To address the challenges of nonlinear and variable aging patterns observed in real-world applications, a histogram-based feature extraction strategy is implemented. This approach accommodates noisy field data and enables robust predictions of aging trajectories. Moreover, an online adaptive correction model refines the predictions in real time to account for cell-to-cell variations. For RUL prediction, the study investigates the use of time-series measurement data and histogram features, demonstrating their complementary roles in improving prognostic accuracy. The method is validated using datasets from both controlled laboratory conditions and real-world operations, ensuring its applicability across a wide range of use cases.

The proposed method offers several advantages. It is highly applicable to real-world scenarios due to the integration of field and laboratory data, ensuring practical relevance for electric vehicles and energy storage systems. The multi-model fusion approach and scenario-specific feature extraction significantly enhance the accuracy of SoH and RUL predictions. The method's robustness to noisy and variable field data is further strengthened by the

histogram-based features and online adaptive correction models, while its computational efficiency allows for potential implementation in battery management systems (BMS). However, the methodology also presents some challenges. Its reliance on high-quality and representative data limits its generalizability to different battery chemistries or operational conditions. The complexity of implementation, requiring expertise in model configuration and computational resources, can be a barrier. Additionally, as a data-driven approach, it provides limited insight into the underlying physical degradation mechanisms, which could reduce interpretability. Integrating laboratory and field data with different formats and resolutions also introduces preprocessing challenges.

The research by [73] proposed a hybrid framework that combines model-based and data-driven approaches to enhance the accuracy and reliability of LiB aging diagnostics and prognostics. The method leverages the strengths of both approaches, with model-based components providing physical interpretability and ML techniques improving predictive accuracy and adaptability. The framework is designed to estimate the SoH and RUL of batteries under a variety of operating conditions. It adopts a two-step methodology: first, offline training of data-driven models to correct errors in model-based RUL predictions, and second, real-time error correction during online deployment. Feature engineering is employed to extract critical attributes such as voltage, current, and temperature, which serve as inputs for training ML models. The framework is validated on multiple datasets, including laboratory, real-world, and out-of-distribution (OOD) scenarios, to ensure robustness across diverse conditions. Furthermore, uncertainty quantification techniques are integrated to improve prediction reliability and provide conservative estimates, which are essential for safety-critical applications.

The proposed method offers several advantages. It significantly enhances predictive accuracy by combining the interpretability of model-based methods with the flexibility of data-driven techniques. The framework is robust across various conditions, as it incorporates real-world and OOD datasets, making it applicable to diverse use cases. Its integration of uncertainty quantification ensures reliable and conservative estimates, which are critical for operational safety. Additionally, the modular design of the framework allows for scalability,

enabling the integration of new datasets and algorithms as battery technologies evolve. However, the approach also presents challenges. The hybrid framework requires substantial computational resources for training and deployment, which may limit its use in resource-constrained environments. Its performance is heavily dependent on the quality and representativeness of the training datasets, and the integration of model-based and data-driven methods requires careful calibration and tuning, adding complexity to implementation. Furthermore, the framework may need retraining to generalize effectively for significantly different battery chemistries or use cases.

The hybrid framework makes a significant contribution to battery aging prediction by addressing key challenges such as variability in real-world data and OOD scenarios. The study demonstrates that the approach reduces RUL prediction errors by 40% and improves uncertainty calibration by 34%, underscoring its effectiveness compared to traditional methods. By integrating advanced techniques, the framework supports the development of reliable and scalable battery management systems, which are critical for the safe and efficient deployment of energy storage solutions. This research provides a foundation for future advancements in battery diagnostics and prognostics, aligning with the evolving needs of modern energy systems.

In order to precisely predict the SoH and RUL of LiBs, a sophisticated DNN framework is introduced in the study reviewed by [157]. Rather than requiring laborious manual feature engineering, this novel framework uses automatic feature extraction to fully utilize the potential of deep learning. The model captures the dynamic and nonlinear aging behaviors intrinsic to Lithium-ion batteries, making it especially well-suited for processing time-series data. The framework uses methods such as data augmentation and TL to improve its robustness and adaptability. This allows it to function well on a variety of datasets, including those from lab and real-world settings. The DNN architecture is optimized through hyperparameter tuning, which guarantees high predictive accuracy and generalizability. The model performs better than conventional machine learning techniques after being validated on large datasets.

The suggested approach has a number of benefits. It is appropriate for real-world applications because it captures complex nonlinear relationships in battery aging data effectively, resulting in high predictive accuracy. While data augmentation and TL improve the framework's resilience across a range of scenarios, the integration of automatic feature extraction streamlines implementation and lessens dependency on domain-specific expertise. Furthermore, the DNN's modular architecture promotes scalability by enabling the incorporation of fresh data sources and flexibility in response to developing battery technologies. Notwithstanding these benefits, there are certain drawbacks to the approach. The DNN's high computational requirements for training and optimization make it difficult to implement in environments with limited resources. Because the model relies on the representativeness and quality of the input datasets, thorough data preprocessing is essential. Furthermore, as a "black-box" model, the DNN provides limited interpretability, making it difficult to derive insights into the physical mechanisms underlying battery degradation. The implementation process also requires significant expertise in neural network design, training, and validation, adding complexity to its deployment.

The study combines cutting-edge machine learning techniques with scalable and effective methodologies, which significantly advances the field of battery diagnostics and prognostics. Through data augmentation and TL, the framework addresses issues like variability and scarcity of data, setting a new benchmark for predictive maintenance strategies in BMS. These developments support sustainable energy solutions and lower operating costs by improving the safety and longevity of LiBs. The amalgamation of resilient data-driven methodologies showcases the possibility of productive amalgamations of inventive approaches to address crucial predicaments in energy storage systems.

A hybrid data-driven method for estimating the SoH and forecasting the RUL of LiBs is proposed in the study by [158]. To increase prediction accuracy, robustness, and computational efficiency, this technique combines two sophisticated randomized learning algorithms—Random Vector Functional Link (RVFL) networks and Extreme Learning Machines (ELM)—within an ensemble framework. The ensemble structure lowers prediction variance and increases learning diversity by utilizing the advantages of both algorithms. The

study uses a NAR structure, which links historical, present, and future data to better capture dynamic battery degradation trends, in order to further refine predictions. The primary health indicator is a particular feature derived from the charging voltage that shows a strong correlation with battery aging. To address uncertainty in predictions, the method employs a Bootstrap-based uncertainty management technique that quantifies prediction intervals, improving reliability and enabling informed decision-making. Validation of the method using two publicly available datasets—one from laboratory conditions and the other representing real-world scenarios—demonstrates its applicability and effectiveness across diverse operational settings.

The proposed method offers several advantages. Its ensemble structure, combining ELM and RVFL algorithms, achieves superior predictive accuracy compared to single-model approaches. The inclusion of randomized learning techniques ensures rapid training and computational efficiency, making the framework feasible for real-time applications in battery management systems. Moreover, the method's robustness across different datasets highlights its generalizability, while the Bootstrap-based uncertainty quantification enhances prediction reliability. The modularity of the framework allows for scalability, enabling the integration of additional models or indicators as new battery technologies emerge. However, the method also presents some challenges. The complexity of integrating multiple learning algorithms within an ensemble structure requires expertise and computational resources. The approach is heavily dependent on the quality and representativeness of training datasets, which may limit its adaptability to different battery chemistries or operating conditions. Additionally, while effective, the ensemble learning methodology provides limited insight into the physical mechanisms underlying battery degradation. Expanding the ensemble size to further improve accuracy can also increase computational demands during the training and integration processes.

This hybrid approach significantly advances battery health diagnostics and prognostics by addressing critical challenges in SoH and RUL prediction. The method enhances prediction accuracy and robustness by combining the complementary strengths of ELM and RVFL algorithms while incorporating the NAR structure to capture nonlinear aging

behaviors. The inclusion of uncertainty management through Bootstrap analysis adds a layer of reliability to predictions, making the framework suitable for deployment in energy storage and electric vehicle systems. By outperforming traditional and state-of-the-art methods in accuracy and efficiency, this study provides a scalable and practical solution for modern battery management systems, exemplifying the successful integration of diverse methodologies to solve complex engineering problems.

Despite the advancements presented in the study "Predicting Battery Health for Electric Vehicles," several research gaps remain that highlight opportunities for further exploration. The proposed Deep Neural Network (DNN) model, while effective in leveraging experimental data such as voltage, current, temperature, and health indicators, may face challenges in generalizing to other battery chemistries, such as solid-state batteries or emerging lithium-ion variants. This limitation underscores the need for validation across diverse battery types to enhance the model's broader applicability. Additionally, the model's reliance on experimental data does not fully account for the complexities of real-world EV usage, such as variable driving patterns, fluctuating environmental conditions, and user behaviors. Incorporating real-world field data would improve the robustness and reliability of predictions.

Moreover, the study lacks integration with physics-based models, which provide insights into the electrochemical mechanisms of battery aging. A hybrid approach combining machine learning and physics-informed modeling could offer greater interpretability and more accurate predictions. Another significant gap is the absence of uncertainty quantification, which is essential for addressing the variability in manufacturing processes, measurement noise, and data sparsity. Implementing methods to quantify prediction uncertainties could enhance the reliability of the model, especially in safety-critical applications.

The computational intensity of DNNs also poses a challenge for real-time deployment in battery management systems (BMS), necessitating research into optimizing model architectures for efficient inference without compromising accuracy. Additionally, the study does not address how the model adapts to long-term changes in battery behavior due to aging

or evolving battery technologies. Developing scalable, adaptive models capable of learning from new operational data would be crucial for maintaining prediction accuracy over time. Furthermore, the lack of explainability in DNN models, often perceived as "black boxes," can hinder their industrial adoption. Incorporating explainable AI (XAI) techniques would enhance transparency and foster trust in the model's predictions. Lastly, the study does not explore the economic or environmental implications of deploying the proposed model for predictive maintenance in EVs. A comprehensive evaluation of cost savings and environmental benefits, such as reduced battery waste and extended battery life, could provide valuable insights into the practical impact of the model. Addressing these research gaps would not only advance the current state of EV battery health prediction but also pave the way for more reliable, interpretable, and scalable solutions in battery management systems.

CHAPTER 3

IMPORTANCE OF STATE OF HEALTH (SOH) IN LIBs

One crucial LiB parameter is the SoH. It gauges the battery's general state in relation to its starting capacity. The safety, effectiveness, and dependability of batteries in a variety of applications are ensured by an understanding of and adherence to SoH. SoH is especially important for portable electronics, renewable energy systems, and EVs. This parameter guides maintenance strategies and performance optimization by offering insights into battery aging. The percentage of a battery's performance and capacity is represented by SoH. It makes a comparison between the current state and the one in which it was manufactured. An 80% SoH battery retains 80% of its initial capacity. For the purpose of determining performance degradation and replacement planning, SoH is essential.

The measurement of SoH involves multiple methods. Electrochemical Impedance Spectroscopy (EIS) is widely used. It assesses impedance growth, which indicates aging. Thermal measurements track heat generation, another sign of deterioration. Voltage and current trends are also monitored. Researchers introduced a machine learning model. This model accurately estimated SoH using real-time sensor data [1]. Accurate SoH assessment ensures optimal battery utilization. It minimizes risks such as unexpected failures and capacity loss. Without monitoring SoH, users may face operational inefficiencies or safety issues. Battery Management Systems (BMS) rely heavily on SoH data. SoH informs decisions about charging, discharging, and fault prevention. A well-calibrated BMS can extend battery life by managing stress factors.

Researchers emphasized the importance of SoH for fault detection. Their system used SoH data to identify overcharging risks. This approach prevented overheating and capacity fade [2]. Adaptive charging protocols also utilize SoH. Studies demonstrated pulse charging techniques. These techniques adjusted charging rates based on SoH levels [3]. This reduced lithium plating and enhanced cycle stability. Furthermore, SoH helps balance cells in battery packs. Imbalanced cells degrade faster, reducing overall performance. SoH monitoring

ensures uniform degradation. This increases the pack's lifespan and safety. SoH is essential for predicting the RUL of batteries. RUL estimation combines historical data and real-time monitoring. Accurate RUL predictions prevent unexpected failures and improve maintenance scheduling. Researchers proposed a hybrid model integrating SoH data. Their model predicted RUL with 90% accuracy [1]. This approach combined electrochemical simulations and machine learning. By incorporating SoH trends, the model identified degradation mechanisms. Experimental validation highlighted its effectiveness for EV battery packs [2]. RUL predictions are particularly beneficial for industrial applications. They ensure uninterrupted operations and reduce downtime. SoH serves as a foundation for reliable and precise RUL forecasts.

For EVs, SoH is a vital parameter for performance and safety. It influences range estimation, charging strategies, and safety protocols. Degraded SoH leads to reduced driving range and slower charging rates. Studies analyzed SoH's impact on EV performance. Their findings showed a direct correlation between SoH and energy efficiency [3]. Batteries with 70% SoH exhibited a 30% reduction in range. This underscores the need for accurate SoH tracking. Moreover, SoH affects resale value. Buyers of used EVs consider SoH a key factor. High SoH values increase marketability and reliability. Regular SoH assessments build consumer trust and confidence. Despite its importance, SoH estimation faces challenges. Variability in operating conditions complicates assessments. Extreme temperatures accelerate aging, skewing SoH predictions. Researchers proposed temperature-adjusted algorithms to address this [2]. Their models accounted for thermal effects, improving accuracy. Data availability is another issue. High-quality datasets are necessary for machine learning models. Studies highlighted the lack of standardized data formats [3]. Collaborative efforts can bridge this gap, enabling better SoH predictions.

Selecting the correct parameters for SoH measurement is vital for accuracy and reliability. Different parameters provide insights into various aspects of battery health. The key parameters include capacity retention, internal resistance, and coulombic efficiency. These parameters correlate directly with the performance and aging of the battery. Capacity retention is a primary indicator of SoH, representing the battery's ability to store charge

compared to its original capacity. Internal resistance measurements highlight the impedance growth, which indicates aging. High internal resistance leads to power loss and inefficient energy delivery. Coulombic efficiency assesses the ratio of charge delivered to charge accepted during cycles, revealing energy loss through side reactions. External factors like temperature, charge-discharge rates, and voltage fluctuations also influence these parameters. Accurate measurement requires advanced techniques and consistent monitoring conditions. For example, EIS effectively measures internal resistance and provides a detailed view of degradation mechanisms. However, its implementation is complex and requires specialized equipment.

Incorporating multiple parameters into SoH assessment models improves prediction accuracy. A balanced approach ensures comprehensive insights, enabling effective battery management strategies. Without the correct parameters, SoH evaluations may lead to misleading conclusions, impacting overall performance and safety. Several methods are employed to measure the (SoH) of LiB. These methods vary in complexity, accuracy, and applicability. Each technique has its advantages and disadvantages, making the choice of method application-dependent. EIS is a highly accurate method for measuring SoH. It analyzes the impedance of a battery over a range of frequencies. This provides insights into internal resistance, electrolyte degradation, and SEI layer growth. The primary advantage of EIS is its ability to detect early signs of degradation. However, it requires expensive equipment and skilled operation, making it less suitable for on-field applications.

An easy way to gauge SoH is through capacity retention. The current capacity of the battery is compared to its initial capacity. This is an easy method that doesn't require complicated equipment. It takes a while, though, because it requires complete charge-discharge cycles, which might not be possible for real-time monitoring. Measurements of internal resistance offer fast and accurate indicators of SoH. Degradation of battery components is indicated by an increase in internal resistance. This approach works well for real-time monitoring and is less intrusive. It might, however, miss some degradation mechanisms, producing assessments that are insufficient. Machine learning (ML) models have been introduced recently for SoH prediction. Large datasets of historical and current

battery data are analyzed by these models. High accuracy and adaptability to changing conditions are offered by ML models. However, their reliability depends on the quality and quantity of training data. Developing these models requires significant computational resources and expertise.

SoC and SoH are interconnected parameters essential for comprehensive battery management. While SoC measures the current energy level, SoH assesses the battery's overall condition. Accurate SoC estimation depends on reliable SoH data. For instance, degraded batteries exhibit inaccurate SoC readings due to reduced capacity and increased resistance. Combining SoC and SoH assessments enhances predictive capabilities. SoC provides short-term insights into energy availability, while SoH predicts long-term performance and degradation trends. Integrated models improve fault detection, optimize charging strategies, and extend battery lifespan. For example, adaptive charging protocols use SoC and SoH data to adjust current and voltage dynamically, minimizing stress on the battery. Advanced battery management systems (BMS) leverage both SoC and SoH for real-time monitoring and decision-making. Machine learning algorithms effectively integrate these parameters, enabling precise predictions and proactive management. However, the integration process is complex, requiring robust algorithms and extensive datasets.

Each method for measuring SoH has its strengths and limitations, influencing its applicability. Electrochemical Impedance Spectroscopy (EIS) offers high accuracy and detailed insights into aging mechanisms, making it ideal for laboratory analysis. However, it requires expensive equipment and skilled operation, limiting its use in field applications. Capacity retention measurement is straightforward and effective for benchmarking battery health, but it is time-intensive as it involves full charge-discharge cycles, which are impractical for continuous monitoring. Internal resistance measurement provides rapid and reliable indicators of degradation, suitable for real-time applications. However, it may not capture all the nuanced aspects of battery aging, leading to incomplete assessments. Machine learning models bring a new dimension to SoH evaluation by leveraging vast datasets to deliver high accuracy and adaptability. These models can process diverse operational data but are dependent on data quality and computational resources, making them challenging to

implement without extensive preparation. Understanding the advantages and disadvantages of each method is essential for selecting the most appropriate approach for specific applications.

CHAPTER 4

LI-ION BATTERY AGING AND DEGRADATION

4.1 AGEING OF BATTERIES

Battery ageing occurs when the performance of batteries steadily declines over time due to a reduction in genuine volume or an upsurge in sequence confrontation [11]. At the beginning of a battery's lifecycle, its chemical components are in a high-energy state, intended to facilitate the conversion between chemical and electrical energy, as described by [1]. However, several side reactions can occur within the battery, prejudiced by aspects such as (SOC), C-rate and temperature. These side responses irreversibly drive the system towards a more constant, lower-energy state, leading to outcomes such as electrolyte degradation, reduction of lively material at the anode or cathode, and a damage of cyclable lithium [174].

Figure 4.1 shows how lithium-ion batteries age at the anode, cathode, and current collectors. As the carbon anode ages, copper dissolution and dendrite formation can cause loss of internal short circuits and capacity. Graphite exfoliation and solvent co-intercalation damage the anode structure. Internal resistance increases as the Solid Electrolyte Interphase (SEI) coating forms and grows. Particle cracking and mechanical Stress can weaken the anode's structure, reducing performance. Cracking and contact loss weaken copper current collectors' current conductivity. Lithium plating and dendrite formation can pierce the separator, causing short circuits and safety hazards. Cathode issues are similar. Dendrite formation and transition metal dissolution degrade cathode stability and performance. Cathode structure disorder affects lithium-ion reversibility. Particle cracking and cathodic surface film formation cause capacity fade and internal resistance. Corrosion and contact loss in the aluminium current collector and cathode binder reduce electrical conductivity and mechanical stability [181].

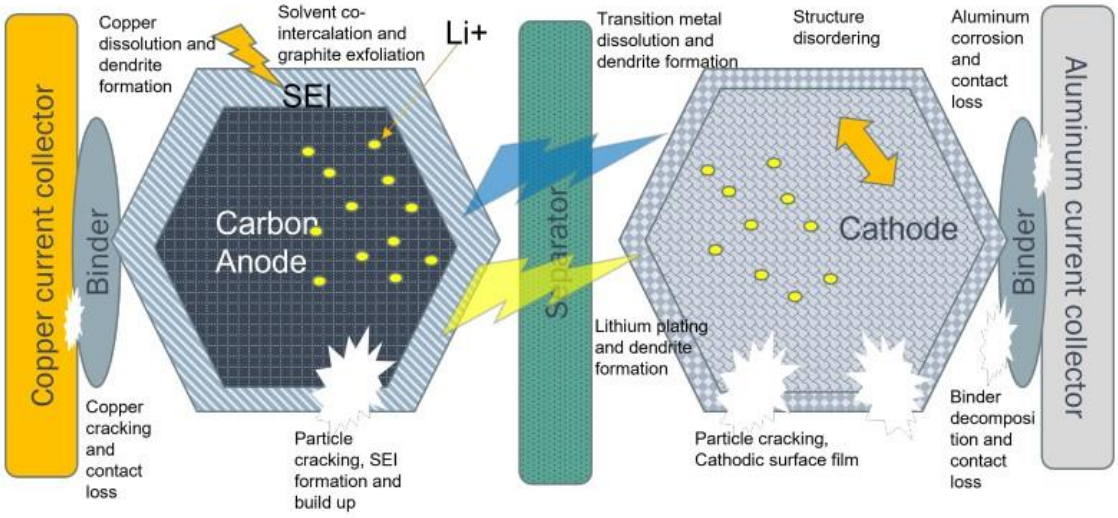

Figure 4.1. Different aging mechanisms [181]

4.2 ORIGIN OF AGEING OF BATTERIES

Battery ageing divided into couple of components: calendar aging and cycle aging [47]. Separately, term delineates the modifications induced by various applications of the battery. Consequently, calendar aging pertains to the phenomena and repercussions associated with battery storage. Conversely, cycle aging pertains to the effects of battery usage durations referred to as cycles (including both charging and discharging).

4.2.1 AGEING OF CALENDAR LIFE SPAN

Calendar ageing denotes to the irreparable loss of storing volume in batteries, also termed battery storage degradation [48, 49]. The rate of self-discharge can vary considerably based on storage conditions, which can either accelerate or decelerate battery ageing effects [50]. Extensive experimental studies have demonstrated the influence of storing conditions on battery ageing. For instance, the study by [51] tested sixty cells, another research by [52] analyzed three hundred cells, and [53] examined cells under varying end-of-charge voltages and temperature conditions. Both calendar ageing and self-discharge are highly dependent on storage temperature [54]. Elevated temperatures can intensify secondary reactions, such as corrosion, and increase lithium loss, ultimately contributing to capacity fade [51, 52, 55].

Various capacity fade phenomena in LiB have been defined by [173] and are illustrated in Figure 4.2 below.

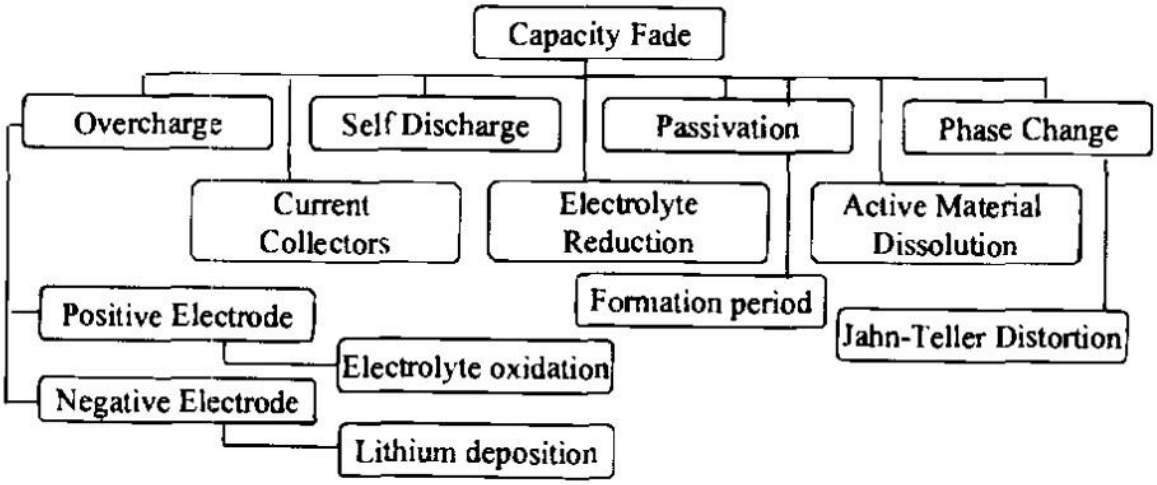

Figure 4.2.Capacity Fade phenomenon in LiB [173]

Lower temperatures reduce these phenomena, minimize material loss, and affect battery chemistry [56]. Another critical variable in calendar ageing studies is the storage (SOC) [57]. Cells can exhibit varying ageing behaviors even when stored at the same temperature but under different SOC levels. Higher SOC levels accelerate battery degradation [36]. Since SOC indicates the ratio of ions present on the electrodes, elevated SOC results in significant potential imbalance at the electrode/electrolyte interface, promoting earlier chemical reactions. However, limited research specifically isolates SOC as an independent factor in calendar ageing, separate from temperature effects. Both variables—SOC and temperature—impact capacity and resistance in a non-linear manner over time. Research findings by [58, 59] suggest that high SOC has a more substantial limiting effect than elevated temperature. Despite these insights, the combined impact of SOC and temperature on calendar ageing remains partially understood. Both factors directly contribute to battery calendar ageing, and the observed size fade and confrontation increase are non-linear over time, highlighting a complex interaction between ageing behavior and temporal factors.

4.2.2 CYCLE AGEING

Battery charging and discharging cause cycle ageing. This depends on battery level, utilization mode, temperature, and current requests. Many factors affect this type of aging. First, all aspects previously described affect calendar ageing and are included in cycle ageing studies because ageing phenomena occur regardless of battery use. Exothermic reactions are common in used batteries [60, 61], and high temperatures can accelerate battery ageing. However, very low temperatures must be considered [59]. Studies show ambient temperature affects batteries, but none do so directly. This concept is still unclear. Except for these variables, battery utilization mode determines cycling ageing. Literature frequently references the ΔSOC, which represents charge variation during a cycle. The battery's discharge (charge) is largely determined by this [35, 62].

In their study [51], researchers examined Lithium-ion cells under similar temperatures and initial SOC but with varying ΔSOC levels. The results revealed that higher ΔSOC leads to significant battery power loss, regardless of other influencing factors. Further experiments corroborated these findings [63]. This phenomenon is primarily attributed to positive electrode degradation and the formation of the SEI layer caused by extensive discharge or charge cycles. Charging and discharging voltages also play a serious role in Lithium-ion battery ageing and operational efficiency. Elevated charging voltages accelerate the ageing process [64]. As demonstrated by Asakura et al. [65], even a 0.1V increase in charging voltage can reduce battery lifespan by half, with the End of Life (EOL) defined at 70% of the preliminary size. Additionally, impedance rise due to discharge voltage significantly impacts battery ageing [66, 42]. Lastly, current peaks are another contributing factor, as a substantial current peak can deliver excessive energy to the battery, potentially accelerating ageing.

4.3 AGEING ESTIMATION

4.3.1 SOH ESTIMATION

Several indicators or metrics have been developed to enumerate the health status of a battery to assess ageing. One of the most commonly employed indicators in the literature is the SOH, which is typically defined by [71, 72]:

$$\textbf{SOH (t)} = \frac{\textbf{Nominal Capacity at t}}{\textbf{Initial Capacity}}\%$$

SOH of a battery is a critical stricture implemented to assess its performance, capacity, and overall condition compared to its original state. Mathematically, SOH is naturally articulated as the ratio of the current capacity $C_{current}$ to the nominal capacity $C_{nominal}$, represented by the equation:

$$\textbf{SOH}=\frac{C_{current}}{C_{nominal}}\times 100\%.$$

Over time, battery capacity degrades with repeated charge and discharge cycles, often modeled as

$$C_{current}=C_{nominal} \times (1 - k.\sqrt{N}$$

where N represents the quantity of cycles, and k is a capacity fade coefficient. Temperature also significantly impacts battery health, and this relationship can be described using the Arrhenius equation:

$$K_T=A.e^{\frac{E_a}{KT}},$$

where higher temperatures typically accelerate aging. Similarly, the Depth of Discharge (DoD) affects battery lifespan, as higher DoD values reduce the number of effective cycles, modeled by

$$L=\frac{1}{a.DoD^b},$$

where a and b are empirical constants. Furthermore, battery degradation results from both cycle aging and calendar aging, expressed collectively as,

$$\boldsymbol{SoH = 1 - (k_{cycle} \,.\, N + \, k_{calender} \,.\, t)}$$

where t denotes time in years. A more comprehensive representation combines multiple factors, including cycle count, temperature, depth of discharge, and aging, into a single equation:

$$\boldsymbol{SoH = C_{current}\, X\, e^{-(k_{cycle}\,.N + k_{calender}\,.t + k_{DoD} + k_t\,.T}}.$$

Mathematical models enable engineers and researchers to predict battery health, enhance performance, and design improved energy storage systems by considering the intricate interactions of these influencing factors. Alternative definitions of SOH often rely on the End of Life (EOL) criterion [73], which essentially reflects the proportion of the battery's residual volume. This measure serves as an indicator of capacity fade [74, 75]. Since the term "ageing" lacks a precise definition, other metrics such as State of Function [73] and RUL [76] have been introduced. These metrics are primarily derived from the battery's size state, overlooking certain aspects of ageing, particularly resistance. However, resistance growth plays a significant role, especially in high-power applications, where its impact becomes more pronounced.

4.3.2 SOC ESTIMATION

The SoC defines the battery capacity available for withdrawal, preventing over-discharge or over-charge and reducing ageing effects. Many researchers are studying SoC estimation. Various methods have been suggested by [183]. Classifying methods is challenging as many approaches involve combining multiple methods and using various heuristic or deterministic mathematical methods. The review reveals a typical mixture OCV and CC methods [183]. These combinations often involve initial and online SoC estimation improvements due to inaccuracies in individual methods. For instance, a study by [183] utilized the OCV method, a full charge detector/dynamic load observer, and the CC method

with REKF as the key function. Combinations make it challenging to classify each approach by method.

Direct SoC approximation techniques use mathematical equations or relationships to evaluate and estimate current battery characteristics, such as voltage, current, and temperature. In the industry, CC has become the accepted technique for estimating SoC [39]. Because of its superior accuracy in short-term calculations, the current method of choice for SoC valuation is the ampere-hour balancing method, or CC method. SoC is defined by the CC method as [183]:

$$\boldsymbol{SoC(t) = SoC(t_o) + \frac{1}{C_n}\int_{t_o}^{t_0+t} I_{bat}(dt) \times 100\%}$$

where I_{bat} is the charging/discharging current, Cn is the nominal capacity, and SoC(t0) is the initial SoC. The charge and discharge current time integral as well as the initial SoC value must be known in order to calculate CC. If unknown, it is typically assumed. This approach is reliant on the early SoC value and cannot completely eliminate growing error. All estimates would be impacted by an incorrect initial SoC value, which would result in errors all along the estimation process. Despite being widely used recently, CC is typically used to estimate SoC in conjunction with other methods rather than as a stand-alone instrument. Certain publications, like, only compute SoC using the CC method [183].

The OCV method is widely employed, relying on the description of the OCV curve, typically represented either through a polynomial function or a look-up table. This method generally adopts one of two approaches: a straight OCV curve inversion method, which is feasible when the application allows steady-state voltage measurements of the cell, or a cell model-based approach [42]. By performing voltage measurements to estimate the SoC of the cell, the relationship can be defined as:

$$\boldsymbol{SoC = \int^{-1}(OCV)}$$

The OCV method involves continuously measuring the cell's voltage and determining the SoC from a predefined table. However, in practical applications, this method encounters

challenges, such as the need for high-resolution sensors to evaluate voltage exactly and allowing enough time for the system to reach equilibrium. While the OCV method is precise, it necessitates rest periods to estimate the SoC, making it unsuitable for real-time monitoring. Furthermore, the relationship between OCV and SoC can differ amongst cells, which could result in substantial errors. Notwithstanding these drawbacks, the OCV approach is frequently used in conjunction with noise filtering and adaptive techniques to calibrate the Constant Current (CC) method [40]. OCV is often employed to improve other techniques. For example, in [183], the OCV–SoC relationship is characterized by applying an intermittent discharging method, which computes the interior confrontation of the model battery and estimates SoC using an extended Kalman observer and an Equivalent Circuit Model (ECM). Cell ECM parameters are also determined by this method [46, 47]. Additionally, to investigate the hysteresis phenomenon, the OCV curve is incorporated into a circuit model in [48–50], which reveals a discrepancy in the equilibrium OCV during battery charge and discharge cycles.

4.4 AGING MECHANISMS OF LIB

4.4.1 DECOMPOSITION MECHANISMS

Rechargeable LiB are widely employed in mobile communications and moveable devices due to their numerous rewards, including immense volumetric energy (VE) and gravimetric energy (GE) densities and a low self-discharge rate. These batteries are also considered a leading choice for power sources in (hybrid) EVs and stationary energy storing systems. In applications where long-lasting performance is crucial, understanding the long-term cycling and storage behavior of LiB converts increasingly important. However, like all energy storage technologies, LiB undergo aging processes that progressively degrade their performance over time. Unfortunately, LiB are multifaceted systems, and their aging processes are even more intricate. The loss of volume and energy degradation arise not from a single cause but from multiple interacting processes. Furthermore, many of these processes occur simultaneously on similar timescales, making it challenging to fully understand the underlying aging mechanisms [169].

4.4.2 AGEING OF CARBONACEOUS ANODES

Graphite, particularly in its use as an anode material, is crucial in LiB, making graphite-based cells the most studied in terms of anode aging. Recently, substitute anode materials, such as lithium loading metals and alloys, have achieved attention. However, the majority of research has concentrated on vigorous materials and associated challenges (e.g., nanostructured materials, volume change control), with limited focus on aging effects [4–6]. The existing literature presents a challenging scenario for analysis, as individually lithium-ion cell system has a unique chemistry, and numerous aging properties are prejudiced by various cell components, such as the active material, electrode design, electrolyte composition, and impurities. Most studies tend to focus on complete cells without isolating the impacts on the anode or cathode.

During storage, aging effects such as self-discharge and an increase in impedance can influence both the calendar life and cycle life of the battery. When in use, aging effects like mechanical damage and lithium metal plating can also take place [8]. To monitor storage-related aging, electrochemical parameters for instance capacity loss, impedance rise, potential changes, SOC, and SOH can be assessed [9]. Anode materials, such as graphite show discharge plateaus, where the electrode potential remains relatively unchanged with varying charge states [10-12]. Cycling enables the measurement of capacity fade, impedance increase, power fade, and overpotentials, all of which influence the charge and discharge curves.

Many researchers attribute anode ageing to variations at the electrode/electrolyte line Figure 4.3 below caused by anode reactions with the electrolyte [15]. LiB anodes operate at voltages outside the electrolyte components' electrochemical stability window. Thus, reductive electrolyte decomposition and irreversible lithium-ion consumption occur when the electrode is charged at the electrode/electrolyte interface. Decomposition products form "protective layers" on the electrode. This process is most common in the first cycle of cycling. Based on their functions, graphite layers can be divided into two types. Intercalation/deintercalation transports lithium ions into/from graphite structures at prismatic surfaces and basal plane defects. Solid electrolyte interphase (SEI) protective layers are

needed [16]. SEI layers are unique because they are penetrable to lithium cations but impermeable to other electrolytes and electrons [169].

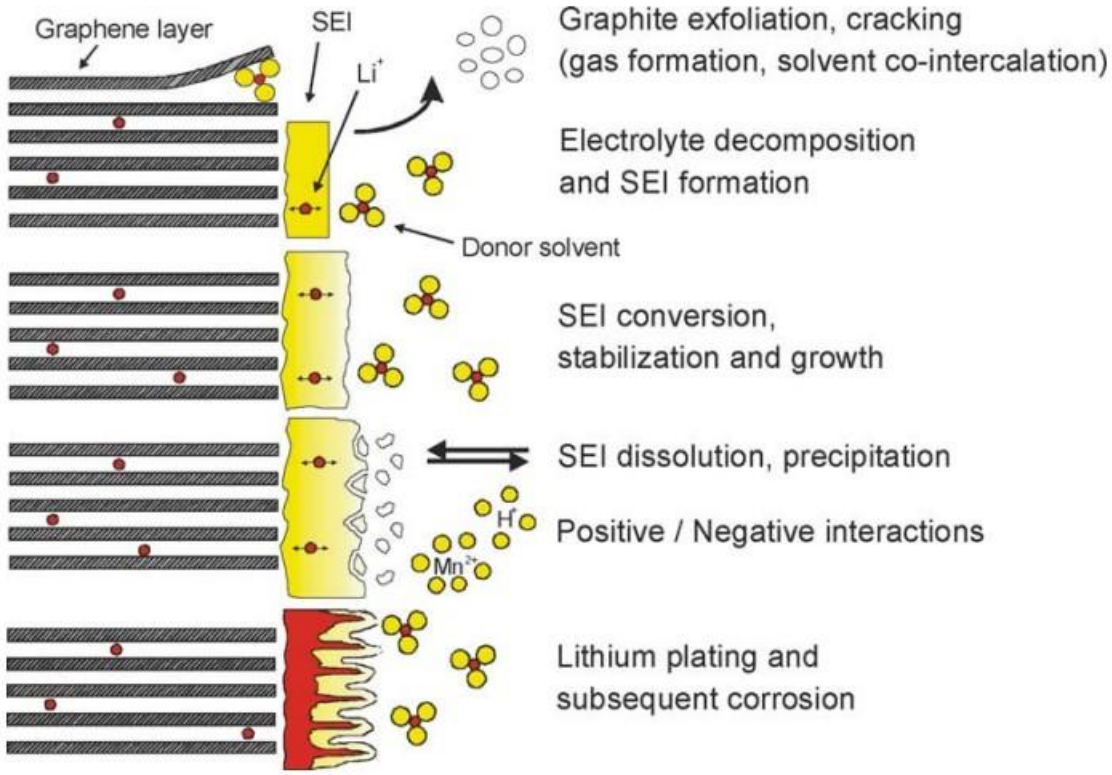

Figure 4.3.Changes in anode/electrolyte interface [169]

It has been discovered that there are notable differences in the configuration of the SEI and non-SEI layers [17]. These variations in composition and function suggest that aging processes may differ between the non-SEI and SEI layers. The SEI can penetrate the electrode's holes and possibly even reach the separator's pores over time, reducing the electrode's usable active surface area. Numerous investigations have found a correlation between the cell's power fade and an increase in electrode impedance [22–32]. The expansion of the SEI and changes to its composition and structure are the main causes of this increase in resistance. In summary, although the majority of SEI formation occurs during the initial charge/discharge cycles, SEI conversion, stabilization, and growth occur during the subsequent cycles.

The gradual reduction in the amount of charge that a lithium-ion battery can hold over several cycles of charging and discharging is known as capacity fade. The deterioration of the electrode materials and damage to active lithium ions are the primary causes of this reduction. The formation of the SEI on the anode during the initial charging cycles is a major factor in capacity fade [4, 5]. Chemical reactions between the electrolyte and the anode surface give rise to the SEI layer. Lithium ions are consumed by the SEI as it grows, even though it serves as a barrier to stop additional reactions. As a result, over time, there is less available active lithium for intercalation and deintercalation, which lowers battery capacity [6, 7]. The growth of the SEI is accelerated by influences such as high temperatures, elevated charging currents, and extended cycling, which all contribute to faster electrolyte decomposition reactions [8].

The mechanical degradation of electrode materials also causes capacity fade. For instance, lithium intercalation and deintercalation during cycling expand and contract the anode and cathode. This mechanical Stress causes cracking, pulverization, and electrical contact loss, reducing battery charge storage [9]. Cathode materials with high energy densities are prone to structural instability and phase transitions, which cause capacity fade [9]. The impact of SEI thermal behaviour on cell properties, such as power fades, impedance rise, and safety, should be discussed [37–39]. As mentioned, elevated temperatures upsurge the kinetics of lithium insertion/removal from the host lattice. Many believe SEI morphology and arrangement change at high temperatures [40–48]. The cell may catch fire or explode if thermal runaway occurs. Several groups have studied electrode or cell behaviour at high temperatures using DSC and ARC [49–52].

Exothermic side reactions in lithiated carbon lead to self-heating, particularly at temperatures around 80 °C, as observed in different electrolytes through Accelerating Rate Calorimetry (ARC) tests. The temperature at which these reactions begin varies depending on the electrolyte salt, with LiBF4-based electrolytes starting around 60 °C [53]. Electrochemical cycling studies indicate that Li/graphite half-cells show capacity loss even at temperatures below 60 °C [54]. High temperatures accelerate the degradation of the Solid Electrolyte Interphase (SEI), causing it to either distort or dissolve. On the other hand, the

dissolved products might precipitate again, or the damaged SEI might reform. Under high temperatures, more stable inorganic compounds such as lithium salts (such as carbonate and fluoride) can be formed from metastable organic components of the SEI, such as lithium alkyl carbonates [51, 53]. Although the growth of these inorganic SEI products may lessen the ionic conductivity of the lithium SEI, they are more stable and less prone to be pierced by solvent molecules.

Aging effects are usually negligible in the majority of active materials. Depending on the material, volume changes in graphite during the insertion and removal of lithium ions usually stay below 10% and have a negligible effect on reversibility. But structural alterations, like crystal phase shifts, can cause mechanical stress on defects and carbon-carbon bonds during lithium insertion, which can result in cracking or other types of structural damage. Cell aging is generally not significantly affected by redox reactions involving the exchange of lithium ions and interactions with surface groups at the surface of the active material. However, exfoliation and particle cracking can result from processes like solvent co-intercalation, electrolyte reduction, and gas evolution within the graphite, which seriously deteriorate the electrode [12]. These processes have the most significant impact on the active material, thereby accelerating the aging of the cell.

Cell impedance in composite electrodes rises due to mechanical or electrical contact loss, which accelerates aging. Changes in the active anode material's volume may cause this kind of contact loss, which could cause the composite electrode to mechanically disintegrate. Loss of contact between the carbon particles, the binder, and the current collector may result from this disintegration. As previously discussed in relation to SEI effects on electrode porosity, these volume changes also have an impact on the electrode's porosity, which is important for optimal anode performance because it facilitates electrolyte penetration. The internal pressure of the cell also needs to be taken into account. Commonly used as binders in composite electrodes, fluorine-containing copolymers and polymers react with the charged anode to form LiF, which deteriorates the mechanical properties of the electrode over time. Moreover, corrosion of the current collector, which can occur due to electrolyte reactions or

when the anode potential exceeds that of Li/Li+, can result in both electronic and mechanical contact loss between the current collector and other electrode components.

Table 4.1

Lithium-ion anode ageing—causes, effects, and influences [169]

Origin	Consequence	Results in	Mitigated by	Exacerbated by
Electrolyte degradation (SEI growth)	Loss of lithium, Increased impedance	Diminished capacity, Decreased power	Additives for stable SEI, Slower progression over time	Elevated temperatures, High state of charge (SOC)
Solvent co-intercalation, gas evolution, and particle cracking	Loss of active material and lithium	Reduced capacity	Stable SEI through additives, Carbon pre-treatment	Overcharging
Reduced surface area from SEI growth	Increased impedance	Lower power output	Stable SEI through additives	Elevated temperatures, High SOC
Changes in porosity due to volume changes and SEI growth	Increased impedance	Reduced power	Application of external pressure, Stable SEI additives	High cycling rates, High SOC
Loss of contact between active material particles during cycling	Loss of active material	Lower capacity	External pressure application	High cycling rate, High depth of discharge (DOD)
Binder degradation	Loss of lithium	Decreased capacity	Using suitable binder materials	Elevated temperatures, High SOC
Corrosion of the current collector	Increased overpotentials, Higher impedance	Reduced power	Pre-treatment of the current collector	Overdischarge, Low SOC
Uneven current and potential distribution	Amplifies other aging mechanisms	Accelerated aging	Uniform cell structure	High cycling rates, Poor cell balancing
Metallic lithium plating and	Loss of lithium and electrolyte	Diminished capacity,	Narrowing potential window	Low temperatures, High cycling rates,

Origin	Consequence	Results in	Mitigated by	Exacerbated by
electrolyte breakdown		Reduced power		Geometric misalignment

4.4.3 AGEING OF LITHIUM METAL OXIDE CATHODES

The longevity, cycling characteristics, and performance of lithium-ion batteries are all significantly influenced by the cathode materials used. Lithium manganese oxide (LiMn2O4) and lithium nickel-cobalt mixed oxide (Li(Ni,Co)O2) have been extensively studied as potential cathode material substitutes for LiCoO2. These materials are appealing options for high-energy and high-power batteries because they have benefits like reduced costs, improved availability, and improved performance. Even with the advancements, research is still being done to determine what causes capacity degradation and how to prevent it. Recent research has examined the aging processes of lithium batteries, with an emphasis on the effects on cathode materials [1-3,8,78]. The battery's overall lifespan is shortened by the aging of the active material and the degradation of electrode components, including binders, conducting agents, current collector corrosion, oxidation of electrolyte components, and surface film formation. Because of their interdependence, these processes cannot be viewed in isolation. These degradation mechanisms heavily depend on the specific composition of the electrodes as well as the storage and cycling conditions of the battery.

Changes in the surface film, dissolution reactions, chemical breakdown, and structural changes during cycling can all lead to capacity fading in the positive active material. The positive active materials deteriorate according to the charging and cycling conditions, just like the negative carbon electrode. The electrochemical reaction of these materials involves the insertion of lithium ions into the metal oxide structure.

$$\boldsymbol{LiMeO_2 = LiMeO_2 + (1-x)Li^+ + (1-x)\,e^-}$$

Changes in the molar volume of the materials brought about by the insertion and removal of lithium ions have the potential to induce mechanical stress and strain in the oxide particles and, as a result, the electrode. Additionally, this process might cause phase transitions that distort the crystal lattice and raise mechanical stress even more. The aging

mechanisms connected to lithium-ion cathode materials, as discovered in earlier research, are depicted in figures 4.3 and 4.4 below. The homogeneous solid solution series is terminated by LiNiO2 and LiCoO2, which crystallize in the α-NaFeO2 structure. In this structure, nickel and cobalt are both in their trivalent states and retain a low-spin configuration.

$$(\boldsymbol{Co^{3+}\ t_{2g}\ 6\ e_g 0;\ Ni^{3+}\ t_{2g}\ 6\ e_g 1}).$$

Pure stoichiometric LiNiO2 is exceedingly challenging to produce [80,81]. It results from a structural disorder reaction in which divalent nickel ions replace lithium ions at their respective locations. Concurrently, the nickel sites undergo a reduction of trivalent nickel ions to the divalent state to achieve a balance in charge. The reaction of complete disorder can be expressed as:

$$\boldsymbol{LiNiO_2 \rightleftarrows \{Li_{1-x}\ Ni(II)\ {}^{x}/_{2}\}Ni(III)_{1-x}\}\ O_{2-x} + {}^{x}/_{2}\ Li_2O + \frac{x}{4}\ O_2}$$

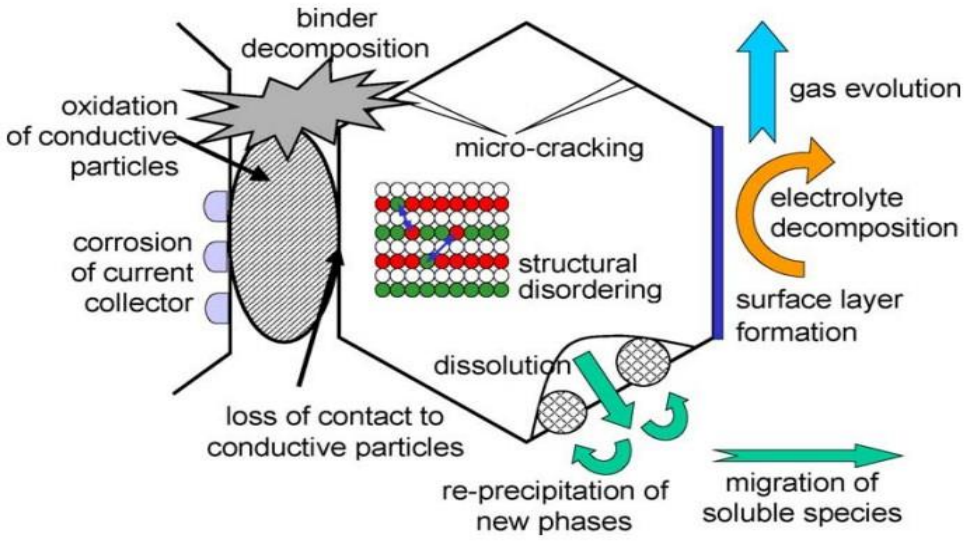

Figure 4.4. Overview on basic ageing mechanisms of cathode materials [169]

As the mixed oxide's cobalt content rises, the lithium-nandel-disorder diminishes and the layered structure is stabilized [82]. Pure lithium nickel oxide goes through a number of reversible phase transitions during electrochemical lithiation/delithiation [83–92]. Large

anisotropic volume jumps and a rapid capacity decrease are caused by the monoclinic phase domain M1 transition and the delighted phase H3 formation, as shown in figure 4.5 below. Phase transitions from monoclinic to hexagonal can be avoided with 20 moles of cobalt. Dopants of magnesium and aluminum stabilize the layers. Volume changes in lithium nickel cobalt oxide are lessened [93] when doped with magnesium [96,97] or aluminum [94,95]. Lithium nickel cobalt oxides doped with Al or Mg thus have longer cycle lives [98–100]. Doped Li (Ni, Co)O2 with optimized compositions is stable in the discharged state even at higher temperatures and has a good cycle life if the end-of-charge voltage is controlled and overcharge is avoided.

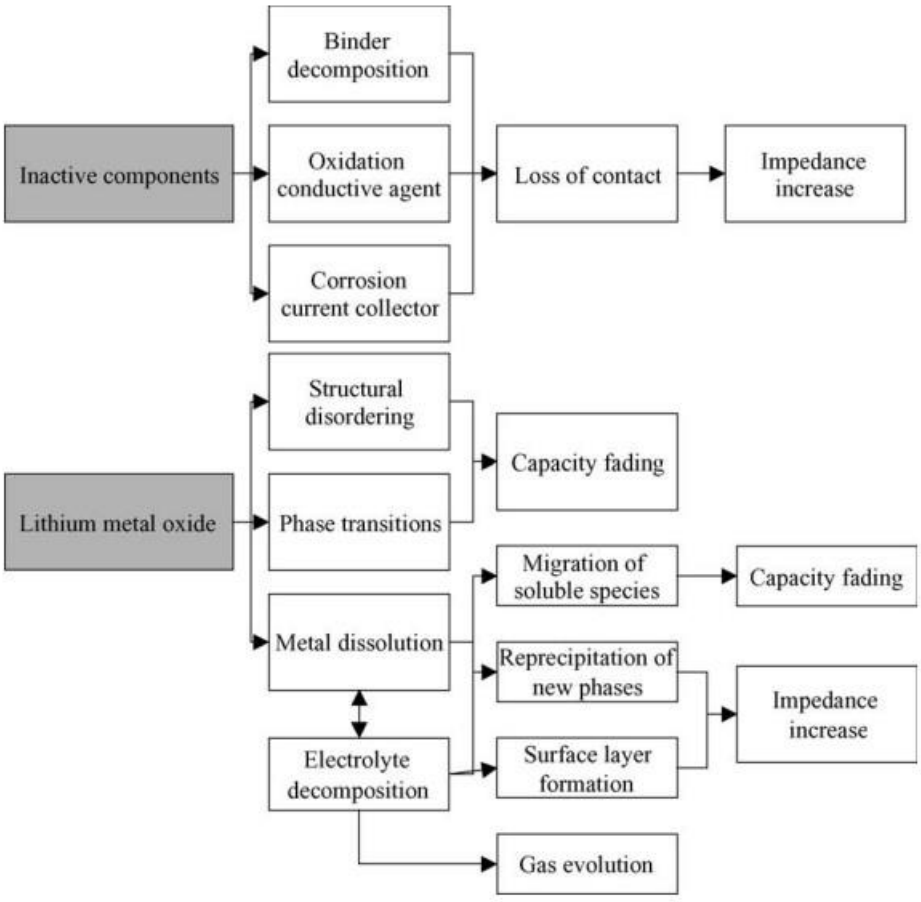

Figure 4.5. Cause and effect of ageing mechanisms of cathode materials [169].

Lithium nickel cobalt oxides dissolve well in practical electrolytes. LixCoO2 dissolves and deposits cobalt on the anode when charged above 4.2 V versus Li/Li+ [101,102]. Lithium-ion battery anode materials have been extensively studied for surface–electrolyte interactions and SEI formation [14,103]. Increased carbon anode interfacial impedance causes high-energy battery capacity fading, according to Broussely et al. [8]. High power batteries' lithium nickel cobalt oxide cathodes increased interfacial impedance, causing power loss [20,22,28,29,32,38,41,42,45,46,72,104–116]. This increase is accelerated by higher temperatures and positive end-of-charge voltages of 4.2 V versus Li/Li+. Surface films are formed by LiPF6 decomposition and electrolyte oxidation, as reported in literature. Lithium nickel cobalt oxide can also supply oxygen for these oxidation reactions through a subsurface layer of a lithium/oxygen deficient oxide phase of the rock-salt structure [104,117]. The mechanisms of charged lithium nickel cobalt oxide surface film formation are summarized in figure 4.6 below. Surface impedance rises as a result of the low lithium-ion conductivity of the lithium nickel cobalt oxide with a rock-salt structure. Furthermore, gaseous species are frequently released along with surface electrolyte reactions [120].

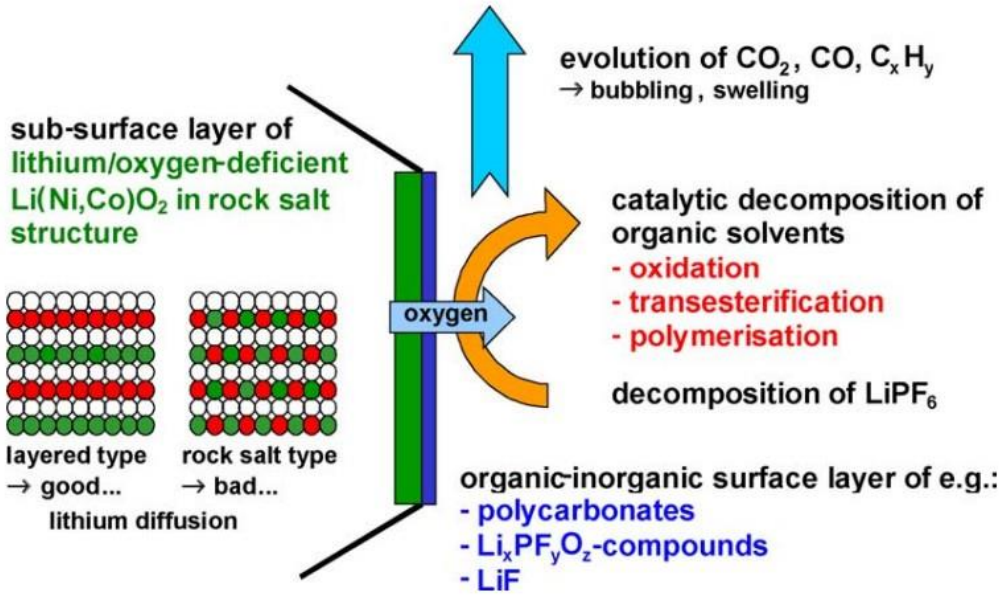

Figure 4.6. Mechanisms of surface alteration of lithium nickel cobalt oxide electrodes in LiPF6-based electrolytes [169]

4.4.4 DEGRADATION CAUSES

New cells degrade quickly in the first few cycles due to the solid electrolyte interface layer on the negative electrode. After a few cycles, formation cycles stop when all surfaces are coated in decomposition products. Cell performance is stable and capacity loss is absent in subsequent cycles. Prepassivation or prelithiation is needed to maximize active material capacity without sacrificing cyclable lithium [1]. Calendar aging is battery capacity loss from self-discharge during storage. This phenomenon is heavily influenced by cell SOC and storage temperature. [1], [2]. Overcharge/overdischarge occurs when the cell exceeds the manufacturer's voltage. Overcharge deposits metallic lithium on the negative electrode surface when graphite lithium solubility exceeds [1], [3]. Deintercalating a lot of lithium from the positive electrode may cause a structural collapse evident from figure 4.7 below. Furthermore, overdischarge can dissolve positive current collector (copper) [1]. Regular battery use is likely the main cause of lithium-ion cell degradation. Lithium insertion and extraction during cell charge and discharge stress the active material particles, causing crack propagation. Indeed, active material is micrometer-sized particles. Due to lithium insertion/extraction, crack propagation creates new free surfaces for electrolyte decomposition, lithium-ion consumption, and cell degradation. Electrical load intensity increases damage rate by stressing the active material. [1], [4].

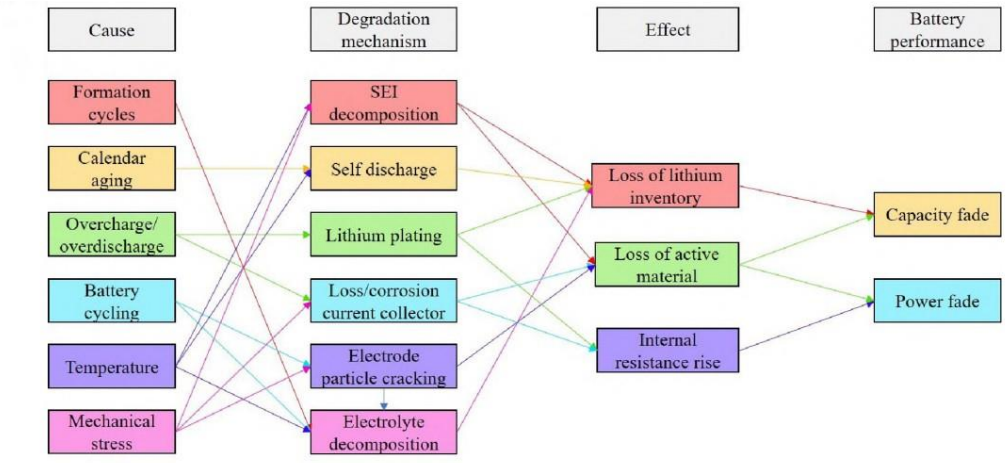

Figure 4.7.Causes, mechanisms and effects of the most common degradation modes in LiB [170]

Different temperatures affect cell performance. The main effect is to accelerate SEI, electrolyte, and binder decomposition [1, 5, 6]. Temperature accelerates battery cycling-induced capacity loss [7, 4]. Extreme heat generation can cause thermal deformation in active material [8]. Temperature also accelerates calendar aging [1], [2]. Finally, extreme heat generation causes thermal run-away, which can cause fires and explosions depicted in figure 4.8 below. Few studies examined how external mechanical stress affects battery performance. Many studies examined the effects of cell penetration or indentation to describe how the cell reacts to this type of load, which could result from accidents or system failure. Initially, the cell loses power and energy. After the internal structure collapses, cell voltage and power drop dramatically as temperature rises [9], [10]. The depletion of cyclable lithium during storage is regarded as the primary cause of irreversible capacity loss across all storage conditions. Notably, [172] in their study indicated that during storage at 60 °C, another significant degradation process was identified evident from figure 3.6: the inaccessibility of graphite. The degradation of graphite electrodes has been quantitatively assessed through nondestructive analyses utilizing dV_{EMF}/dQ curves. The deposition of iron on the graphite electrode has been experimentally validated through X-ray photoelectron spectroscopy (XPS) and inductively coupled plasma (ICP) analysis. The rising inaccessibility of graphite is attributed to the dissolution of Fe from the cathode, followed by its deposition onto the anode.

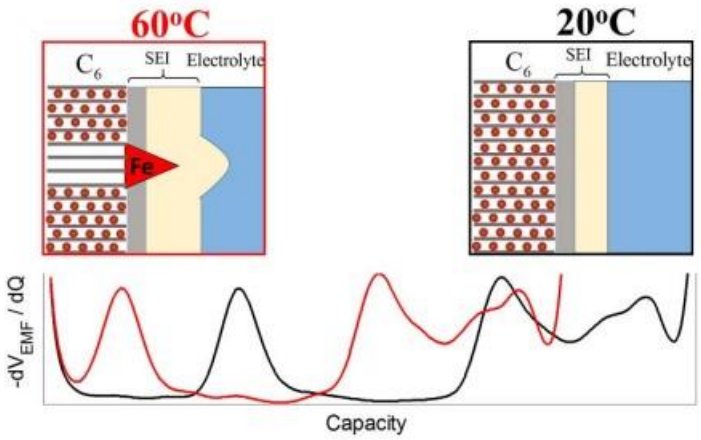

Figure 4.8.Temperature based ageing of Lithium Li-ion Batteries [172]

Therefore, LiB are critical to electric vehicles (EVs). EV batteries experience unique aging mechanisms. Their usage differs from standard consumer applications. In EVs, batteries undergo rapid charge-discharge cycles. These cycles lead to significant capacity and power fade [16, 18]. Thermal management in EV batteries is vital. Poor thermal control accelerates capacity fade. High charging speeds, common in EVs, also stress battery components [20, 21]. Battery aging reduces the range and efficiency of EVs [22]. Environmental exposure plays a role in EV battery degradation. Factors like humidity and vibrations affect performance. Deterioration is also linked to electrode material fatigue [167]. Newer designs focus on improving cycling stability [167, 168].

4.5 FACTORS AFFECTING the HEALTH OF SOH and SOC

Given the growing use of large-capacity lithium batteries in electric vehicles, the most recent study has emphasized the significance of ongoing monitoring of lithium batteries to ensure their safe and dependable operation. LiB SOH indicates how long it can hold a charge. By monitoring variables like operating voltage, charge and discharge currents, and thermal management, BMS is crucial for maximizing battery efficiency. Lithium-ion batteries (LiBs) are praised for their high energy density, uniform voltage, and low self-discharge rate; however, misuse can lead to serious risks like combustion or explosions. As such, determining the SOH of lithium batteries accurately is essential to preserving system safety and stability. For battery systems to operate dependably, SOH monitoring is necessary. The SOH is affected by various factors and is contingent upon the battery's ageing process, making accurate estimation and prediction difficult. Despite the numerous methods proposed for diagnosing and forecasting the SOH in lithium batteries, further detailed discourse on effectively characterizing SOH remains necessary.

The Battery SOH denotes a particular stage in its lifespan and represents the battery's present performance relative to its optimal condition. Unlike terminal voltage, SOH cannot be directly quantified, complicating its application in longevity evaluations. The battery's usage history has a major impact on the estimation of SOH, and external factors that affect the ageing process include temperature, current rates (C-rates), and the battery's operational

range. Different aging trajectories are caused by these factors. Furthermore, variations in the battery's ageing characteristics can be caused by minor manufacturing defects, which further complicates accurate monitoring. Scholars generally employ metrics like capacity or impedance to evaluate the current energy or power capacity that a battery is capable of producing. Some focus on mechanisms of ageing, such as the amount of cyclable lithium ions [181] or the time it takes for lithium ions to diffuse into the solid phase in the positive electrode [176]. SOH is an estimate that is produced by analyzing a series of measurements using specific criteria. The battery's ageing state can be assessed through quantitative or qualitative evaluation. The principal objectives of SOH monitoring are to guarantee the safe and dependable functioning of battery systems, enhance battery management, and provide early alerts.

The Battery SOH denotes a particular stage in its lifespan and represents the battery's present performance relative to its optimal condition. Unlike terminal voltage, SOH cannot be directly quantified, complicating its application in longevity evaluations. The estimation of SOH is significantly affected by the battery's usage history, with external factors including current rates (C-rates), temperature, and the operational range of the battery substantially influencing the ageing process. These factors lead to diverse ageing trajectories. Moreover, even slight manufacturing defects can result in variations in the battery's ageing characteristics, thereby complicating the precise monitoring. Researchers typically utilize parameters such as capacity or impedance to assess the energy or power capacity that a battery can presently deliver. Some concentrate on ageing mechanisms, including the quantity of cyclable lithium ions [181] or the solid-phase diffusion duration of lithium ions in the positive electrode [176]. Essentially, SOH is an estimation derived from a sequence of measurements analyzed according to particular criteria. The battery's ageing state can be assessed through quantitative or qualitative evaluation. The principal objectives of SOH monitoring are to guarantee the safe and dependable functioning of battery systems, enhance battery management, and provide early alerts.

Both internally and externally, the difficulties in estimating the SOH and RUL have been investigated. Data-driven methods for lifetime prediction and SOH estimation were the

subject of a review by [142]. The differences between battery operations in EV and photovoltaic (PV) systems were examined in [67], with particular attention paid to SOH estimation techniques designed for PV applications based on signal types. Furthermore, [12] examined the reasons behind LiB aging and presented a novel SOH prediction method classification scheme, weighing the benefits and drawbacks of each. LiB, which are frequently used in energy storage, depend on two essential metrics: SoC and (SoH) for performance evaluation. SoH assesses the overall state and degree of degradation, while SoC shows the amount of charge left in relation to the battery's capacity. Accurate estimation of these parameters is crucial for ensuring safe and efficient battery operation. Several factors, including environmental conditions, operational settings, and material properties, influence both SoC and SoH.

4.5.1 KEY FACTORS AFFECTING THE HEALTH OF SOC

Temperature significantly influences lithium-ion battery performance. High temperatures accelerate chemical reactions within the battery. These reactions increase internal resistance and alter voltage profiles. Consequently, temperature variations distort SoC estimation [4, 5]. Low temperatures slow lithium-ion transport through electrodes. This leads to incomplete charging and discharging cycles. Temperature-induced capacity fade also affects SoC accuracy [6]. Advanced thermal management systems help mitigate temperature impacts on SoC [7]. Charge and discharge rates directly affect SoC. High current rates lead to significant voltage drops. This makes voltage-based SoC estimation less reliable [8, 9]. Rapid charging or discharging causes lithium plating on the anode. This alters the battery’s voltage response and impacts SoC estimation accuracy. Low-rate cycling is less likely to cause such distortions [10].

Depth of discharge refers to how deeply a battery is discharged. High DoD cycles strain the battery’s electrodes. This leads to voltage hysteresis, affecting SoC estimation [11]. Shallow DoD cycles result in smaller voltage swings. These are easier to track during SoC estimation. Optimizing DoD can improve both SoC accuracy and battery lifespan [12]. Self-discharge refers to the battery losing charge when idle. This phenomenon is more pronounced at high temperatures [13]. Self-discharge alters the open-circuit voltage (OCV). Since OCV

is used in SoC estimation, self-discharge reduces accuracy. Advanced battery management systems (BMS) account for self-discharge effects [14]. Aging alters battery capacity and internal resistance. These changes distort the voltage-capacity relationship. Consequently, aged batteries show inaccurate SoC estimates [15]. Advanced SoC algorithms compensate for aging effects. These use adaptive models to track degradation trends [16, 17].

4.5.2 KEY FACTORS AFFECTING STATE OF HEALTH (SOH)

Battery usage patterns significantly affect SoH. Frequent deep discharge cycles accelerate degradation. Shallow cycling reduces stress on electrodes and improves SoH [18]. Cycle life depends on charge-discharge rates and cycling depth. Rapid cycling causes higher internal resistance. This leads to capacity fade, impacting SoH estimation [19, 20]. Temperature extremes greatly influence SoH. High temperatures degrade electrolyte and electrode materials. This accelerates the growth of the Solid Electrolyte Interphase (SEI) layer [21]. Low temperatures reduce lithium-ion mobility. This results in lithium plating, which damages anode surfaces. Both scenarios reduce battery lifespan and SoH [22]. As batteries age, internal resistance increases. This resistance rise reduces energy output efficiency. It also increases heat generation during charging and discharging [23].

Internal resistance growth is caused by SEI layer thickening and material fatigue. Advanced SoH models incorporate resistance changes for accurate estimation [24]. Degradation of active materials affects battery performance. Cathode materials are prone to phase transitions and structural instability [9]. Anode materials experience cracking and lithium plating over time. Both processes reduce the battery's ability to store and deliver energy. Material degradation is a primary factor in SoH estimation [10]. Electrochemical aging involves side reactions within the battery. These reactions consume active lithium and electrolyte components [25]. SEI layer formation is a key aging mechanism. Over time, it thickens and reduces lithium-ion transport. This leads to capacity fade, affecting SoH estimation [26]. Lithium-ion intercalation causes volumetric expansion and contraction. Repeated cycling introduces mechanical stress on electrodes [27]. Mechanical stress leads to particle cracking and electrode delamination. These reduce electrical contact, impairing SoH. Advanced cell designs minimize mechanical stress impacts [28].

4.6 METHODS OF IMPROVING THE LIFE-SPAN OF THE BATTERY

The table 3.2 depicted the deficiencies in Lithium Li-ion batteries highlighted by [178], the study determined lists lithium-ion battery (LIB) issues and suggests solutions. Replace carbonaceous anodes (negative electrodes) with advanced alloy anodes for high coulombic efficiency, power capability, reduced irreversible capacity loss, and cost-effectiveness to improve energy storage efficiency. Solid electrolyte interphase (SEI) growth during the initial cycle and ongoing cycling reduces coulombic efficiency at the negative electrode–electrolyte interface. Interface stabilization with coatings, functional binders, and electrolyte additives can reduce this. New cathode materials with high efficiency and low-capacity loss can improve the positive electrode (lithiated transition metal oxide or phosphate)'s low specific capacity and charging voltage.

High voltage operation at the positive electrode–electrolyte interface lowers coulombic efficiency, increases cell impedance, and shortens cycle life. These issues can be addressed with better coatings, binders, and electrolytes. Conductive particles and lithium dendrites can penetrate separators, causing short circuits. Ion flux, salt diffusion, and fluid flow can be maintained and structural strength improved with advanced separator coatings. Finally, metal collectors are necessary for conductivity and thermal performance but cost more and reduce energy efficiency due to their thickness. Optimizing perforated or expanded metal collectors, which work in other battery systems, could solve this problem. These targeted solutions emphasize material innovation and interface engineering to improve lithium-ion battery performance, efficiency, and lifespan.

Table 4.2

Deficiencies in Lithium Li-ion Batteries highlighted by [178]

Location of Deficiency	Deficiencies	Possible Remedies
Carbonaceous Anode (Negative Electrode)	Low-capacity density (Ah l^{-1})	Use advanced alloy anodes with high efficiency, power, and low capacity loss.
Negative Electrode–Electrolyte Interface	Low coulombic efficiency due to SEI growth	Apply protective coatings, binders, and electrolyte additives.
Positive Electrode (Lithiated Transition Metal Oxide or Phosphate)	Low specific capacity (Ah kg^{-1}) and limited charge voltage	Use new cathode materials with high efficiency and capacity retention.
Positive Electrode–Electrolyte Interface	Reduced efficiency at higher voltages, increased impedance	Improve cathode coatings, binders, and additives to prevent degradation.
Separator	Penetration by conductive particles or lithium dendrites	Enhance separator coatings for better strength and dendrite resistance.
Metal Collectors	Solid metal foils increase costs and reduce efficiency	Use perforated or expanded metal collectors for better optimization.

The development of long-lasting battery materials and designs has been a key focus, with increasing attention given to battery lifespan management as it helps reduce costs and environmental impact, supporting sustainable development. Numerous studies have explored various battery materials to enhance the cycling stability of active materials for longer-lasting batteries. For instance, cycling tests in half-cells demonstrated the potential of hierarchically structured Li4Ti5O12 anodes, with nano and microstructures, to achieve long life under ultrafast charging conditions. Furthermore, battery designs have been shown to extend lifespan as well. Research on synchronized lithium and LiB included the use of a thin lithium reservoir electrode, which minimizes lithium and capacity loss during formation, thereby prolonging battery life. Additionally, an asymmetric temperature modulation battery utilizing Ni foil for self-heating has been developed to maintain a stable lifetime even during fast charging.

The figure 4.9 highlights crucial parameters for electrode performance highlighted by [178], essential for optimizing energy storage systems. In part (a), key parameters include coulombic efficiency, cell voltage, conductivity, specific capacity, gravimetric and volumetric energy density, toxicity and safety issues, capacity retention, and power density. These factors collectively determine the efficiency, stability, and overall functionality of electrodes in energy storage applications. Part (b) illustrates energy level alignment in a liquid electrolyte system with solid electrodes. It shows the Highest Occupied Molecular Orbital (HOMO) and Lowest Unoccupied Molecular Orbital (LUMO) levels of the electrolyte, along with the energy gap (E_g) and open-circuit voltage (eVoc), which influence charge transfer efficiency and energy output. Part (c) depicts energy level alignment in a solid electrolyte system with liquid or gaseous reactants. It highlights the conduction band (C.B.), valence band (V.B.), HOMO, and LUMO levels, showing their roles in electron and ion transport. Both diagrams emphasize the importance of proper energy level alignment for efficient energy storage performance and long-term stability.

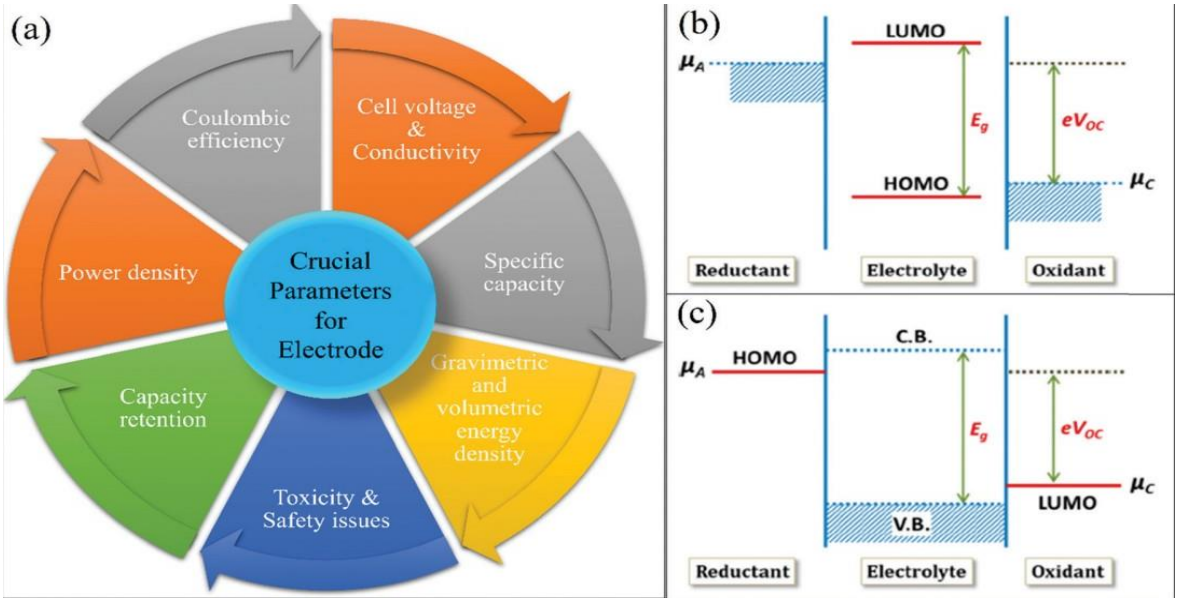

Figure 4.9. (a) Performance parameters of electrodes, (b) Liquid electrolyte with solid electrodes, . (c) Solid electrolyte with liquid or gaseous reactants [178]

Improving electrode materials is highly effective for extending battery life. These materials degrade structurally over time due to cycling. This degradation reduces capacity and causes mechanical failures. Recent studies have focused on nanostructured materials for stability enhancement. The study by [7] investigated silicon nanocomposites for anodes. Their findings showed these designs accommodated volume changes without cracking. This approach improved cycle life by 20%. Similarly, [51] explored cathode doping with aluminum or magnesium. These doped cathodes exhibited reduced phase transitions, improving durability. This innovation was particularly effective in high-temperature environments. Protective coatings have been introduced to minimize unwanted reactions. [34] reviewed techniques such as atomic layer deposition (ALD). These coatings acted as barriers to prevent electrolyte decomposition. Batteries with such coatings showed a 30% reduction in capacity fade. Combining nanostructures, doping strategies, and coatings significantly enhances durability. These methods not only extend lifespan but also improve safety. Future research should focus on scaling these techniques commercially.

The electrolyte facilitates lithium-ion movement between the electrodes. Over time, electrolyte degradation produces side products like SEI. This reduces active lithium ions and diminishes capacity. A research by [64] studied additives like fluoroethylene carbonate (FEC) in electrolytes. Their results indicated enhanced thermal stability and reduced decomposition. Batteries using FEC showed a 15% improvement in cycle life. High-concentration electrolytes reduce solvent decomposition. [126] found these electrolytes suppressed dendrite formation. This improvement was most beneficial in fast-charging scenarios. Solid-state electrolytes eliminate risks of leakage and flammability. [26] highlighted sulfide-based solid electrolytes with superior stability. These batteries retained over 80% capacity after 1,000 cycles. Optimizing electrolytes, through additives or solid-state formulations, mitigates degradation. Future research should address cost and scalability challenges.

Battery management differs from material and design improvements by controlling the operation of the battery without altering its structure or components to extend its lifespan. Key stress factors, including temperature, current rates, lower and upper cutoff voltages, SoC, and depth of discharge (DoD), are taken into account in lifespan management to evaluate

battery durability and develop effective usage strategies. High temperatures during cycling accelerate degradation reactions, such as active material loss and SEI film growth, leading to capacity fade. High current rates increase diffusion stress and cause electrode particle cracking, resulting in battery degradation, especially at moderate temperatures. Battery management typically focuses on controlling temperature and current rates to optimize performance. Additionally, cycling tests must factor in the voltage range, which involves a combination of cutoff voltage, SoC, and DoD. Figure 4.10 below provides an overview of a typical Battery Management System (BMS).

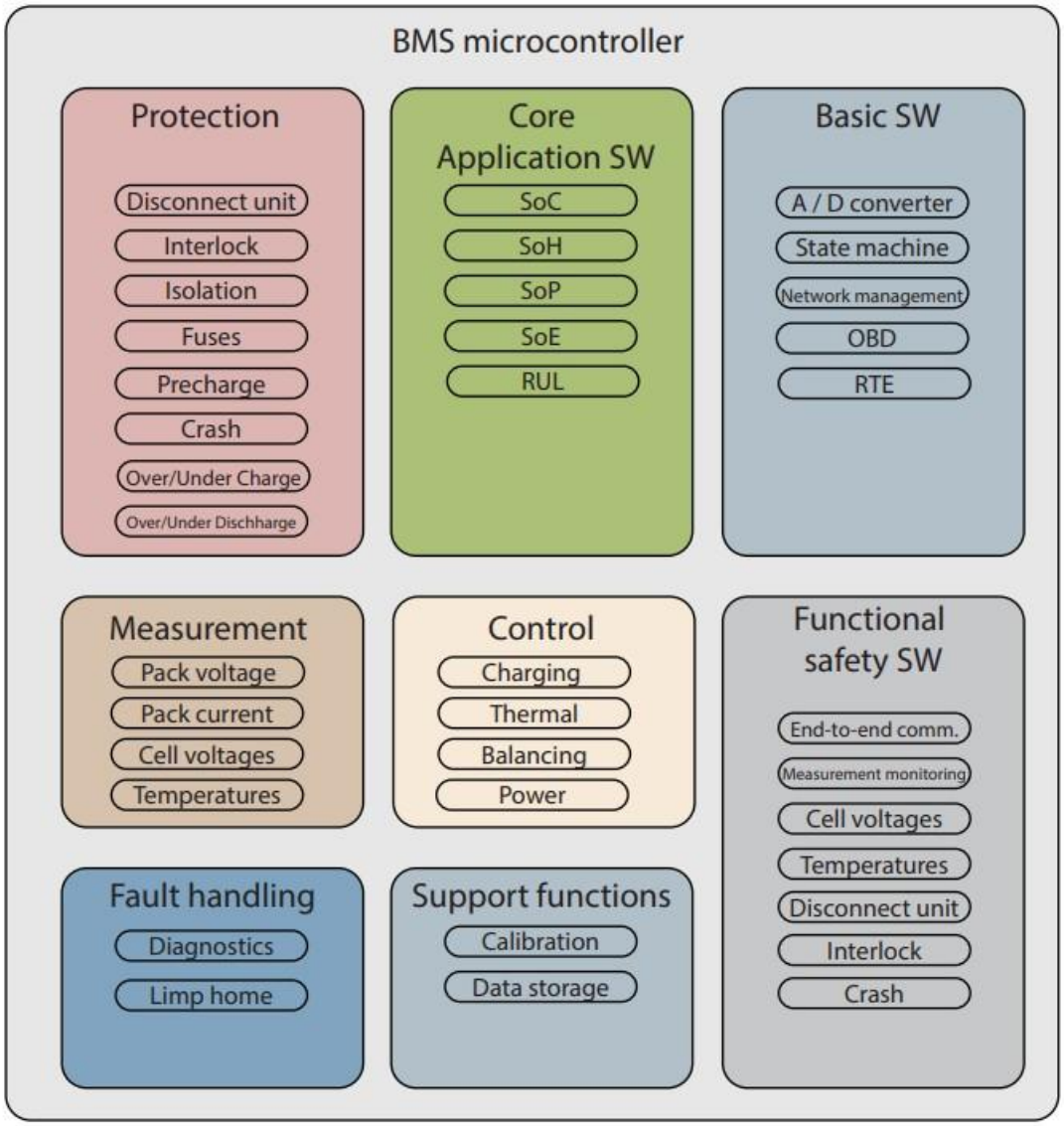

Figure 4.10. Overview of the functions of a typical BMS [181].

A study conducted by [143] investigated the aging mechanisms of Li(Ni, Mn, Co)O2 cathode batteries cycled through five different (SoC) ranges with a 20% Depth of Discharge (DoD). It was concluded that lithium inventory loss is the main contributor to battery degradation. Following the research by [177] proposed that cycling within moderate SoC ranges using blends of cathode materials like LiNi0.5Co0.2Mn0.3O2 (NCM) and LiNi0.9Co0.05Al0.05O2 (NCA), paired with graphite anodes, results in reduced capacity loss and improved performance compared to cycling at extreme SoC ranges. This approach helps mitigate the likelihood of nonlinear capacity fade. Additionally, Aiken et al. introduced a low-voltage cycling method for pouch cells using LiNi0.5Mn0.3Co0.2O2 cathodes, which showed that cycling at voltages of 3.65 V and 3.80 V (roughly corresponding to 0%-30% and 0%-60% SoC) yields better capacity retention compared to cycling at 4.2 V. The study indicated that passivation of the negative electrode is likely the cause of capacity fade at lower voltages, while the positive electrode remains largely unaffected.

The studies referenced emphasize the importance of avoiding extreme voltages to minimize the degradation of cathode materials at high voltages, ultimately helping to prolong the battery's lifespan. By preventing the electrochemical activation of the Li0.75Si phase in the anode, shifting the cycling voltage window from 2.65–4.2 V (0%–100% SoC) to 3.1–4.2 V (10%–100% SoC) improves the longevity of commercial 18650 cells. However, using a narrower voltage window at the beginning of the battery's life reduces cell efficiency, which conflicts with the goal of achieving high energy density for longer driving ranges in electric devices. Despite these considerations, research on battery usage and lifespan remains limited. Bharathraj et al. introduced a dynamic charging protocol simulation aimed at extending battery cycle life. This protocol gradually increases the charge cutoff voltage to the manufacturer's recommended maximum, balancing between the extractable per-cycle capacity and the degradation that leads to capacity fade.

Moreover, when LiBs are utilized and stored within the parameters prescribed by manufacturers, the probability of malfunction is approximately 1 in 40 million [9,15]. Nonetheless, incidents of accidents resulting from LiB igniting or detonating in entirely

distinct devices have been documented, as shown in Table 3.3. Table 3.3 illustrates that accidents have transpired across a diverse range of devices employing LIBs, including small consumer products, electric vehicles, and aircraft. The causes of accidents include overheating, short circuits, overcharging, self-heating, and mechanical damage. The aforementioned incidents, along with numerous others, prompted modifications to the regulations governing the transport and storage of LIBs. The International Civil Aviation Organization (ICAO) has prohibited the transport of LiB as cargo on passenger aircraft, stipulating that these batteries must not be charged beyond 30% when transported by air. In order to ensure greater security of LiBs, there are two possibilities: Improving stability through modification of chemistry and/or structure, by adding internal safety devices [9], [16], [17].

Table 4.3

Some LIB fire and explosion accidents [179]

No	Date	Accidents	Accident Causes
1	March 2010	Two iPod Nano music players caught fire in Japan	Overheating of Lithium-ion Batteries (LIBs)
2	26 April 2010	Acer recalled 2,700 laptop batteries, similar to recalls by other companies in 2006	Overheating and potential fire hazards in LIBs
3	11 April 2011	EV taxi fire incident in Hangzhou, China	Short circuit leading to electrolyte combustion
4	Oct–Nov 2013	Fires in six Tesla Model S EV cars	Battery short circuit due to crash, self-ignition
5	Jan 2013 & 2014	Three fire incidents of Boeing 747 in Boston, Takamatsu, and Tokyo	Internal short circuit in LIBs and BMS failure
6	April 2015	EV bus fire during charging in Shenzhen, China	Battery overcharge due to BMS malfunction
7	31 May 2016	LIB storage explosion in Jiangsu, China	Fully charged LIBs potentially leading to self-ignition
8	16 May 2017	Panasonic recalled over 270,000 LIBs	Risk of overheating and fire in LIBs
9	2 July 2018	Energy storage system fire and explosion in Korea (4 MW/12 MWh)	LIB fire spread to over 3,500 LIBs
10	29 July 2018	Electric scooter fire and explosion during charging in China	Likely caused by overcharging

No	Date	Accidents	Accident Causes
11	18 October 2017	EV car fire in Austria	LIB ignited after vehicle crash

Two methods have been used to modify the cathode. The first involves a coating that enhances cathode thermal stability. Li [18] improved the discharge capacity and cycle stability of the LiNi1/3Co1/3Mn1/3O2 battery by applying a TiO2 coating to the cathode, without affecting the grid. In addition to the MnSiO4 coating in LCO batteries, the Co3(PO4) coating in LiNi0.93Co0.07 O2 demonstrated improved thermal stability and tolerance to overcharging [19]. Cathode modification can also be done structurally by inserting specific metals into the structure. Cell ventilation design is one solution. In prismatic batteries, the charging opening acts as ventilation "windows" to release internal pressure. The positive terminal cover was designed with small ventilation "windows" to accommodate the 18650 battery [23], as shown in Figure 4. In both cases, the ventilation "window" is a fragile cap that breaks at critical pressure.

4.7 LITHIUM LI-ION BATTERY MODELS

The condition-based maintenance (CBM) plan for the system needs to take battery prognostic health management (PHM) into account. As a preventive measure, the CBM plan makes sure that maintenance tasks are only carried out when absolutely necessary. Evaluate the health status of a system's components or the entire system to determine its need [11]. Diagnostics and prognostics are CBM's main tasks. A system is remaining useful life (RUL) is the time until failure [12]. Maintenance should be done while the system is running to prevent failure to prevent negative consequences. These maintenance tasks require early planning and preparation [13]. CBM should be integrated into system operations, particularly for critical systems [179]. Battery aging diagnostic algorithms are designed to assess the current state of battery aging, while battery aging prognostic algorithms aim to forecast the remaining lifespan of the batteries until they reach their end of life (EOL), as shown in Figure 4.11. Based on the prediction focus, prognostic methods can be classified into future aging trajectory prediction [181] and Remaining Useful Life (RUL) point prediction [50].

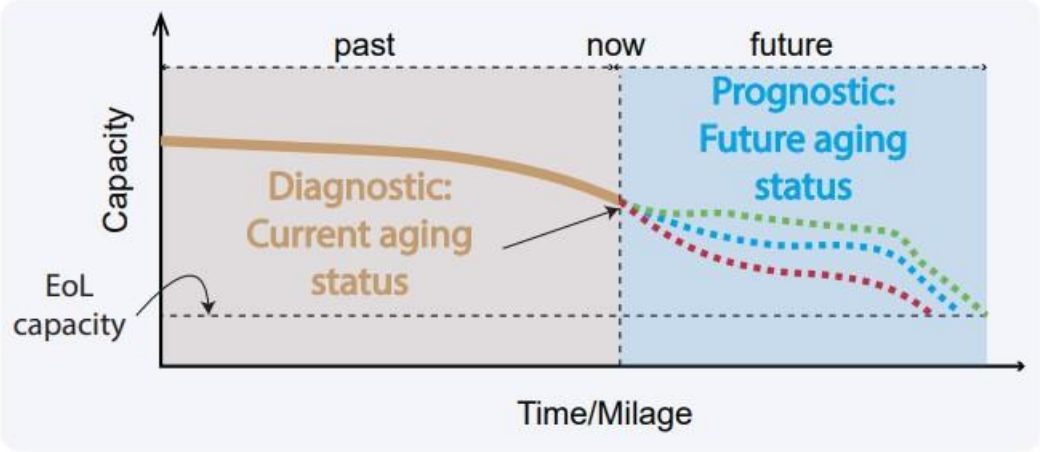

Figure 4.11. Illustration of battery aging diagnostics and prognostics [181]

4.7.1 DIAGNOSTIC MODELS FOR LITHIUM LI-ION BATTERIES

The first type of battery aging model of interest are diagnostic models. Battery diagnostic models are built to estimate cell health using some measurable quantities of the cell. Batteries degrade over time due to the main electrochemical reactions and several complex and interacting side reactions during charging and discharging. Accurate and reliable ageing diagnostics are necessary for battery system safety and efficiency. Estimating SoH for battery ageing is common [181]. Diagnostics is the process of locating errors and determining a portion of the system's current state of health, or SoH [179]. Diagnostic models focus on identifying the current state and health of LiB. These models detect issues such as capacity fade, internal resistance changes, and thermal imbalances. Several approaches and methodologies are employed for diagnostics.

The Battery (SOH) indicates a specific phase of the battery's life and shows how well the battery is performing right now in comparison to when it was in ideal condition. The inability to quantify (SOH), in contrast to terminal voltage, makes it more difficult to use in longevity assessments. The battery's usage history has a major impact on the estimation of (SOH), and external factors such as temperature, current rates (C-rates), and the battery's operational range have a significant impact on the aging process. Different aging trajectories are caused by these factors. Furthermore, even minute manufacturing flaws can cause differences in the battery's aging characteristics, making accurate SoH monitoring more

difficult. Scholars generally employ metrics like capacity or impedance to evaluate the current energy or power capacity that a battery is capable of producing. Some focus on aging mechanisms, such as the amount of cyclable lithium ions [181] or the time it takes for lithium ions to diffuse into the solid phase in the positive electrode [176]. SOH is essentially an estimate that is obtained by analyzing a series of measurements based on specific criteria. It is possible to evaluate the battery's aging state quantitatively or qualitatively. The main goals of SOH monitoring are to improve battery management, ensure the safe and dependable operation of battery systems, and provide early warnings.

As covered in [181], recent reviews demonstrate the advancements made in battery capacity estimation by both industry and academia. These techniques can be broadly divided into three groups: data-driven, model-based, and empirical. A mathematical relationship is established between cell capacity and common degradation indicators such as Ah counting, equivalent cycle number, or time by the empirical model, which is based on extensive laboratory cycling data. But because it was developed in controlled laboratory settings, this model has trouble being applied correctly to real-world situations where batteries must contend with dynamic and fluctuating operating conditions. However, by updating internal parameters based on real-time measurements, model-based approaches improve performance for particular applications and are therefore more flexible than empirical models, albeit with potentially limited generalizability. These methods often integrate sophisticated filtering techniques, such as the Kalman filter and particle filter, to monitor the voltage versus capacity curve (V-Q curve), update model parameters, and predict future degradation, thereby offering a more reliable assessment of battery health.

The battery model is employed to assess the current capacity. Filtering methods attain satisfactory accuracy; however, they are constrained in their capacity to disseminate information among cells. The absence of shared information among cells restricts the applicability of filtering methods to extensive datasets, rendering these methods increasingly less advantageous as contemporary datasets expand [182]. Most model-based methods use ECM models. ECMs used only electric circuitry powers. Simple implementation makes them appealing for battery aging diagnostics. Electric vehicle batteries may degrade over time due

to harsh operating conditions. Model accuracy may decline without regular RPT tests [55]. The porous electrode and liquid-concentrated solution theory describes the battery's internals [68], [69]. The original EM is coupled with SEI [70], [71], lithium plating [26], and particle cracking [72] to model aging. Computationally intensive models and parameterization difficulties make them unsuitable for online applications [73].

Unlike building an aging model from scratch, data-driven methods use measured battery signals to capture aging state without considering mechanisms. Recent digitalization and new technologies like digital twins and battery intelligent management systems have sparked interest in data-driven methods for battery diagnostics [39], [74], [75]. Several methods, including feature-based ML algorithms and end-to-end deep learning, have been proposed to estimate battery capacity [51-67]. Designers manually select relevant features to determine aging states from measured raw data or estimated BMS states using domain knowledge in feature-based methods [76], [77]. Common characteristics are derived from measured voltage, current, temperature, or time.

The study by [169] employed EIS to identify capacity fade mechanisms in LiB. Their findings revealed a correlation between impedance growth and electrolyte decomposition. This technique has been particularly effective for detecting early signs of capacity degradation and power fade. Accurate SoC estimation is critical for monitoring battery performance. Diagnostic models utilize algorithms such as the Extended Kalman Filter (EKF) and particle filtering. The research by [176] demonstrated a data-driven SoC estimation model using machine learning. Their approach achieved high accuracy, reducing estimation errors to less than 5%. Fault detection systems identify anomalies such as thermal runaway, overcharging, and short circuits. Following the study by [162] proposed an advanced FDI system integrating real-time sensor data and predictive analytics. This system effectively isolated faults, improving battery safety and operational reliability. Thermal diagnostics evaluate heat generation and dissipation within batteries. Thermal imaging techniques detect localized hotspots, indicating potential failures. Another study by [178] highlighted the importance of thermal diagnostics for preventing thermal runaway incidents. Their study recommended advanced cooling systems to mitigate thermal risks.

4.7.2 PROGNOSTIC MODELS FOR LITHIUM LI-ION BATTERIES

For lithium-ion battery systems to operate dependably, a mechanism for tracking and determining the battery's state of health (SoH) and remaining useful life (RUL) is essential. This method provides helpful information to predict when the battery needs to be replaced or taken out. Unlike diagnostic models, which predict a battery's life cycle, prognostic models evaluate a battery's health in the future and often predict how many cycles or how long it will take the battery to reach a capacity threshold [182]. This type of assessment is part of a system called prognostic and health management (PHM). PHM continuously assesses SoH and RUL to ensure that LiB operate reliably and safely. Prognostics is the prediction of a battery's time to failure. Researchers from a variety of fields have made significant contributions to the PHM of LiB. For instance, a study by [3] presented a prognostic method based on physics that takes into consideration several simultaneous degradation mechanisms.

Similar to diagnostic models, predictive models rely on a variety of input data, including voltage, current, temperature, time, charge/discharge voltage relaxation, voltage pulses, acceleration and deceleration, ultrasound, and pressure data streams [182]. The outputs of predictive models typically include a capacity trajectory, the RUL expressed in cycles or time, and the anticipated battery lifetime. To evaluate the SoH of lithium-ion batteries (LiB), for instance, [162] combined data from Gaussian distribution with the least squares support vector machine regression technique. [172] estimated SoH and RUL and evaluated battery degradation using the Rao-Blackwellization particle filter. In a different work, [173] developed a model-free approach that uses the Kalman filter and ANN to enhance the health management of lithium batteries (LiB). PHM for LiB has also used other filtering techniques, such as particle filtering [7] and the unscented particle filter [8]. The Gauss–Hermite particle filter (GHPF) methodology for state-of-charge estimation was recently presented by [179]. It reduces the number of sampling particles and streamlines the algorithm while improving estimation precision.

There are two primary stages to the prognostic process. The first stage is centered on evaluating the state of health, or SoH, which is also referred to as degradation detection or severity detection in the literature and is a component of diagnostics. Throughout this stage,

pattern recognition is frequently accomplished using methods like classification or clustering. The purpose of the second phase is to forecast the degradation trend and calculate the RUL in order to predict the failure time. Typically, trend projection, tracking strategies, or time series analysis are used in this phase. The first phase is the focus of many academic studies on prognostics [14]. Model-based or data-driven models can be used to predict battery life. Both approaches rely on historical cell data, but their methodologies differ. Model-based prognostic models update and extrapolate predefined degradation models, such as physics-based models that simulate internal degradation mechanisms, to predict future capacity, resistance, and overall cell health. In contrast, empirical capacity fade models use explicit mathematical functions and stochastic process models to track and predict capacity degradation.

Equivalent circuit models and physics-based degradation models estimate cell health by combining cell data and physics. Model parameters must be extrapolated to forecast cell health. It is difficult to determine the trajectory for each parameter in physics-based models without disrupting cells midway through cycle aging experiments or employing costly measurement tools such as EIS. These models have not yet been widely used or studied. Using an empirical capacity fade model to demonstrate a cell's capacity trajectory is simpler. Empirical capacity fade models incorporate explicit and two exponential terms, a power-law function, a linear function, and a hybrid exponential-linear function.Empirical model-based approaches, like others, rely on online cell capacity measurements to estimate/update model parameters. Recursive Bayesian filtering is a popular method for parameter estimation. Many Kalman filter variants and generic particle filters are widely used Bayesian filters. Probabilistic predictions are a significant advantage of these filtering methods. In contrast to model-based approaches, data-driven battery prognostics employ machine learning to determine the relationship between input features and capacity or lifetime.

Data-driven prognostic models are typically trained in three ways: 1) feature-to-capacity mapping; 2) feature-to-life mapping; and 3) capacity time-series forecasting. Direct mapping methods build models based on strong correlations between input features (V, I, T, t, Q, EIS, etc.) and cell capacity/lifetime. With enough data and strong input-output

correlations, data-driven models can accurately predict new cell capacity or lifetime under previously untested conditions. Popular models for estimating direct mapping capacity include support vector machines (Klass et al.), relevance vector machines, and neural networks.A Gaussian Process (GP) can be used for capacity estimation through data-driven direct mapping. GP regression models were used as regressors alongside other models. Time series forecasting approaches, on the other hand, use machine learning models such as support vector machines, relevance vector machines combined with empirical capacity fade models, GP regression models without trend functions, and recurrent neural networks to predict a cell's capacity trajectory and RUL.Data-driven lifetime prediction models have recently received attention due to their novel input feature engineering techniques.

Coulombic efficiency, or the ratio of charge to discharge capacity, assesses cell performance. A value of 1.000 represents perfect cyclic efficiency. Measure cell coulombic efficiency with greater precision than 0.01% to quantify cell-to-cell differences in the rate of undesirable side reactions that cause capacity fade and identify cells with longer lifespans. Jeff's team published a paper comparing long-term cycling data (> 750 cycles) with predicted lifetimes from short-term (< 500 hours) high-precision coulombic inefficiency measurements using coulometry equipment. For the first time, this study demonstrated that early cycling measurements can predict long-term cell aging performance. Table 3.5 summarizes the information on the differences and advantages of each model. [179] has highlighted various aspects of data-driven and physics-based model in his study as given below in table 3.4.\

Table 4.4

Difference between data-driven and physics-based models for diagnostics and prognostics [179].

Aspect	Models based on data-driven [15]	Models based on Physics [16,17]
Based on	Historical operational data as well as empirical lifetime data.	Both precise mathematical formulas and a physical comprehension of the system are represented.
Advantages	Real-world complex physical system behavior is not necessary.	increased accuracy because it is based on real or almost real physical systems.
	Models are simpler to use and more practical in practical situations.	The model can be evaluated more realistically because it depicts a real system.
Drawbacks	Requires a large dataset to build an accurate model.	Highly complex and computationally intensive, requiring significant resources.
	Does not directly represent the actual system, requiring extra effort to interpret system behavior.	Limitations in modeling complex systems with non-measurable variables.

The data repository of the NASA Ames Prognostics Center of Excellence (PCoE) provided the lithium-ion battery dataset used in this study [18]. Commercial 1850-sized rechargeable lithium-ion batteries were tested under controlled circumstances as part of the NASA prognostics testbed [19]. At room temperature, charge, discharge, and impedance tests were performed to collect experimental data. In the charging phase, the voltage was held constant until the current dropped to 20 μA, and a current of 1.5 A was applied until the voltage reached 4.2 V. Batteries with the numbers 05, 06, 07, and 18 were put through discharge tests with a current of 2 A. The voltage was dropped to 2.7 V, 2.5 V, 2.2 V, and back to 2.5 V. Impedance was measured using Electrochemical Impedance Spectroscopy (EIS), with frequency adjustments spanning from 0.1 Hz to 5 kHz. Batteries were aged more quickly by using multi-cycle charge and discharge tests. The physics-based model presented in [20] can be used to represent the aging behavior of these batteries. The batteries' testing came to an end when their capacity dropped by 30% and they satisfied the end-of-life requirements.

The battery under test is shown schematically in Figure 3.12, along with important specifications including Warburg impedance (RW), electrolyte resistance (RE), charge transfer resistance (RCT), and double-layer capacitance (CDL). Interestingly, during the battery aging process, the parameters RW and CDL exhibited negligible variation, obviating the need for additional analysis [21]. This schematic diagram sheds light on the structural elements of the battery and emphasizes their roles in its overall behavior. The main dataset for training and analysis is the characteristic profile of battery No. 05. Furthermore, battery No. 05's current and voltage profiles during charging and discharging cycles are depicted in Figure 4.12, providing a thorough understanding of its performance under test conditions. To help with understanding the internal structure of the tested battery, Figure 4.12 also presents a schematic representation of the battery with parameters like RW, RE, RCT, and CDL displayed. RW and CDL were not included in the analysis because they showed very little change as they aged [21]. The training dataset is built upon the combination of battery No. 05's characteristic performance profile and schematic diagram. The battery's current and voltage behavior during the charging and discharging cycles is captured in Figure 4.12, offering crucial information for further analysis.

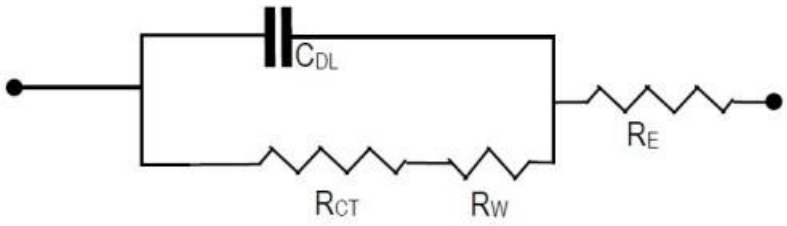

Figure 4.12. The schematic diagram of the tested battery [21]

To evaluate its prognostics, the battery's SoH must be defined. Battery data prognostics often rely on identifying the battery's SoH. Understanding the definition of SoH is crucial, as it is, along with RUL, the primary prediction attribute in the proposed data-driven model.

4.8 THE ROLE OF BMS IN FAULT DIAGNOSIS

The core function of the BMS is to mitigate the risks associated with operating a LiB pack, ensuring both the safety of the battery and its users. Hazardous conditions typically arise from faults, and the safety functions of the BMS aim to reduce both the likelihood and

severity of these faults. Standard components such as sensors, contactors, and insulation are integrated into the battery system to maintain safety [13]. These sensors continuously monitor operational limits for voltage, current, and temperature, providing real-time data to ensure the battery's performance stays within safe parameters [41]. However, as BMS hardware and software become more complex, battery faults evolve and become harder to detect, which may render basic safety measures insufficient [42,43]. This makes fault diagnostic algorithms crucial to BMS operations. These algorithms are designed to promptly detect faults and activate appropriate control measures to protect both the battery and its users. Figure 4.13 below illustrates the mechanism of fault diagnosis within the BMS.

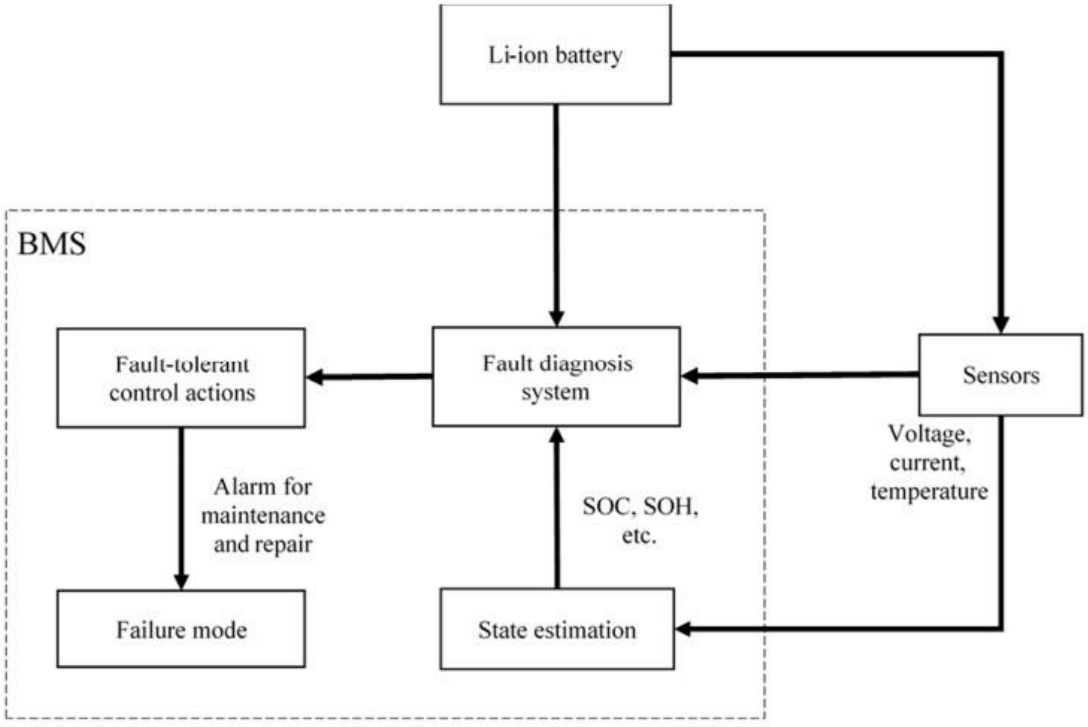

Figure 4.13.A schematic of fault diagnosis in the BMS [180]

BMS is crucial for fault diagnosis as it contains all diagnostic subsystems and algorithms [180]. It oversees the battery system via sensors and state estimation, employing modeling or data analysis to identify any irregularities during the operation of the battery system [13]. The presence of numerous internal and external faults complicates the efficient execution of this task. Diverse fault diagnostic methods must operate concurrently to

accurately identify and isolate a particular fault, thereby facilitating the appropriate control action. Nonetheless, the fault diagnostic algorithms within the BMS are constrained by limited computational resources and time. Due to the extensive number of cells in certain battery systems, fault diagnostic algorithms must exhibit minimal computational demand while ensuring accuracy and reliability [44]. Recent years have witnessed significant efforts in the research and development of effective fault diagnostic methodologies for LiB, which will be addressed in the subsequent section. Fault diagnosis is a critical function within the BMS. Fault diagnosis encompasses fault detection, isolation, and estimation. Numerous fault diagnostic methodologies exist across diverse industries. In Li-ion battery applications, faults may be internal and interconnected; therefore, many conventional methods from other domains are inappropriate. Fault diagnostic methods for Li-ion batteries are classified into two categories: model-based and non-model-based [9].

CHAPTER 5

EXPERIMENTAL SETUP AND PREDICTED RESULTS

5.1 INTRODUCTION

The study employed detailed experimental data for a 26650-battery cell capturing critical parameters related to the battery's performance under various operational conditions. The key variables include terminal voltage (V) and terminal current (A), which reflect the battery's electrical behavior during operation. The dataset also records the temperature (°C) to monitor thermal performance and the charge current (A) and charge voltage (A) during charging processes. The capacity (Ah) measures the battery's storage capability, while the cycle tracks the operational cycles. Additionally, the dataset included two essential metrics: (SoC), indicating the battery's current charge level as a percentage, and (SoH), which measures the battery's overall health, typically starting near 100% for a new cell. This comprehensive dataset enabled the analysis of trends and relationships between these variables. For instance, it can be used to investigate how SoC and SoH evolve over cycles or how factors such as temperature and current influence battery performance. The rich information in the dataset makes it ideal for validating experimental results, exploring correlations, identifying clusters or outliers, and comparing outcomes with predictive models.

5.2 RESULTS OF THE STUDY

5.2.1 CYCLE VS TERMINAL VOLTAGE

Figure 5.1 below illustrates the relationship between terminal voltage and cycle count, providing several key insights into battery performance. Initially, the terminal voltage experiences a sharp drop, stabilizing quickly around 3.0 V. This stabilization reflects the battery's ability to maintain consistent voltage during operation. Over the majority of the cycles, the voltage remains steady, indicating stable performance with minor fluctuations due to normal operational variations. Periodic voltage drops are observed, potentially linked to discharge cycles or temporary anomalies in operation. The maximum terminal voltage reaches slightly above 3.0 V during stable periods, while the minimum voltage, observed

during the initial drop, is approximately 2.0 V. Outliers in the graph highlight deviations that may warrant further investigation into specific operational conditions. Overall, the figure depicts the battery's ability to sustain voltage stability across several hundred cycles, demonstrating reliable long-term performance despite occasional fluctuations and drops.

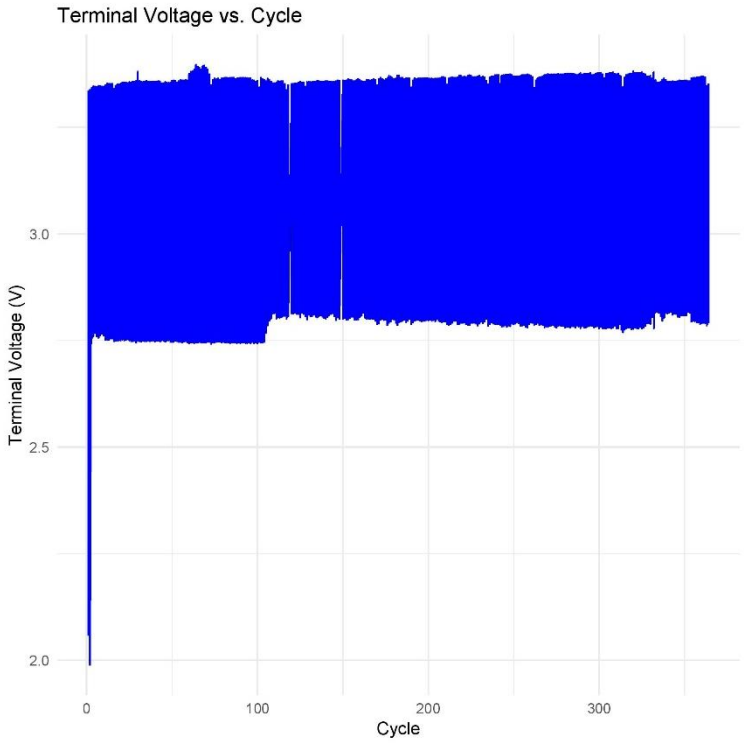

Figure 5.1.Relationship between Terminal Voltage and Cycle

5.2.2 CYCLE VS TERMINAL CURRENT

Figure 5.2 below depicts the relationship between terminal current and cycle count. Terminal current oscillates between positive and negative values, indicating charge and discharge cycles. Positive current values, peaking at 1 A, represent charging events. Negative current values, reaching approximately -1 A, represent discharging cycles. Anomalies are observed with drops below -2 A, likely indicating abnormal operational conditions. The current stabilizes after initial fluctuations, maintaining consistent oscillations. This behavior reflects standard battery cycling with controlled charge-discharge alternations. Early cycles show slightly uneven patterns, suggesting initialization effects. The stability in most cycles

signifies reliable current regulation over time. Key statistics include a peak positive current of 1 A and a minimum current below -2 A. These extremes may indicate outliers requiring further investigation. Overall, the graph highlights the battery's ability to handle consistent current during long-term cycling. Occasional deviations suggest operational interruptions or extreme conditions affecting current flow.

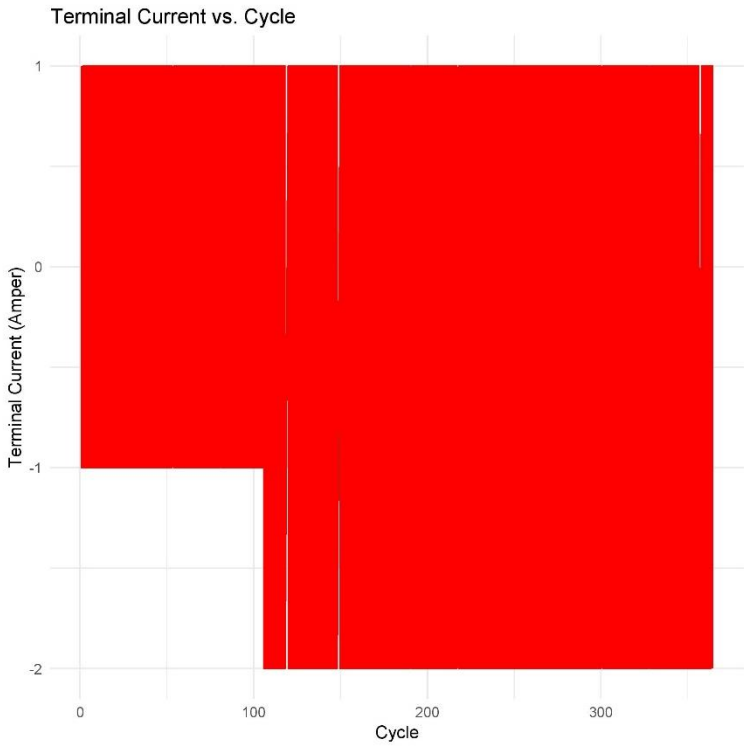

Figure 5.2.Relationship between Terminal Current and Cycle

5.2.3 CYCLE VS CHARGE VOLTAGE

Figure 5.3 below demonstrates the relationship between charge voltage and cycle. Charge voltage remains stable around 3.5 V for most cycles. Initial cycles show consistent voltage with minor variations. Occasional dips below 3.0 V indicate brief irregularities. These dips may be caused by operational interruptions or anomalies. The voltage stability reflects consistent charging behavior across cycles. The maximum charge voltage observed is approximately 3.65 V. The minimum charge voltage drops below 2.0 V during certain cycles. This behavior highlights effective charge regulation during normal operations. Outliers,

represented by sharp drops, warrant further investigation. Key statistics include a peak charge voltage of 3.65 V and dips below 3.0 V. Overall, the graph demonstrates reliable voltage stability across long-term battery cycling. Occasional deviations could indicate external factors affecting the charging process.

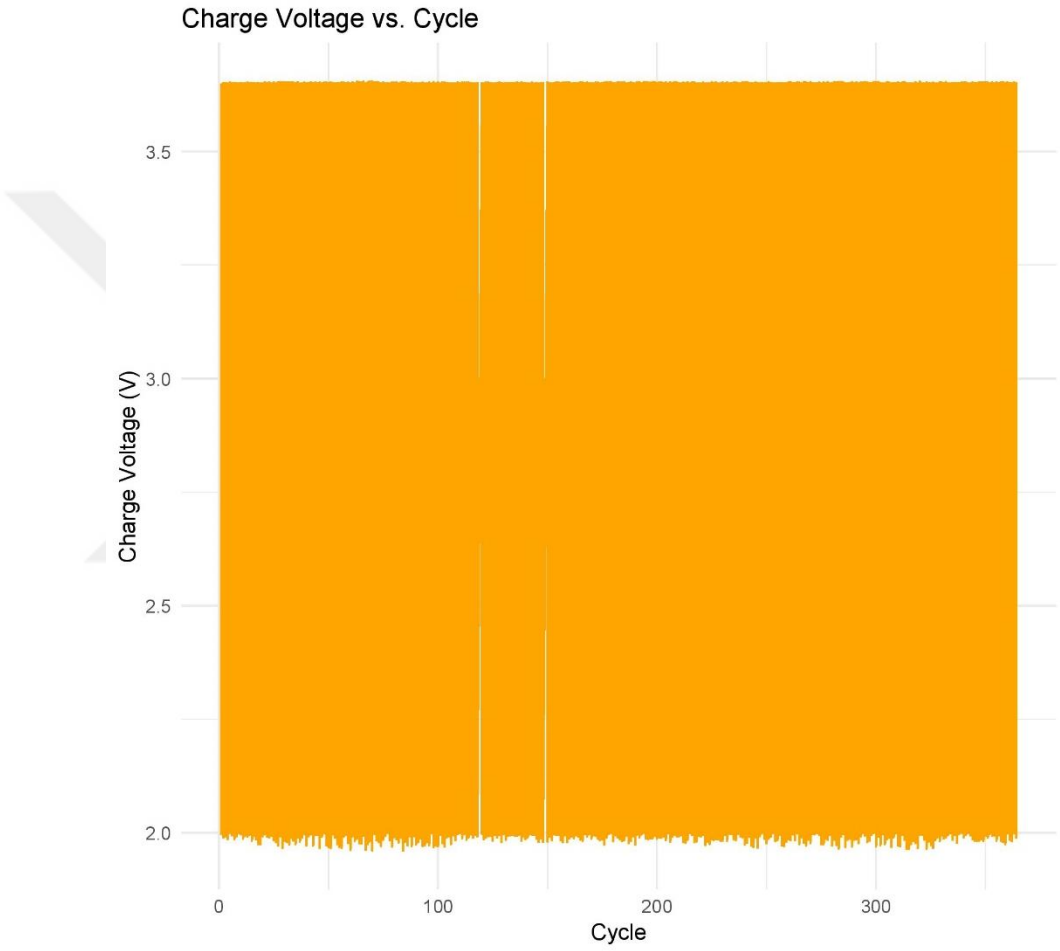

Figure 5.3.Relationship between Charge Voltage and Cycle

5.2.4 CYCLE VS CHARGE CURRENT

Figure 5.4 below depicts the relationship between charge current and cycle. Charge current primarily stabilizes around 2.0 A after initial cycles. The early cycles exhibit fluctuations, starting near 1.0 A. Occasional dips below 1.5 A are observed in some cycles. These irregularities may indicate operational interruptions or transient effects. The maximum charge current reaches approximately 2.0 A during stable periods. The minimum charge

current during early cycles is around 1.0 A. The consistent current across most cycles highlights reliable charging performance. Outliers, represented by brief drops, could reflect anomalies in the charging process. Overall, the graph demonstrates the cell's ability to maintain consistent charging currents over prolonged cycling. The few deviations suggest temporary disturbances or system adjustments during early cycles. Key statistics include a peak charge current of 2.0 A and a minimum of 1.0 A. These patterns confirm stable and predictable charging behavior across cycles.

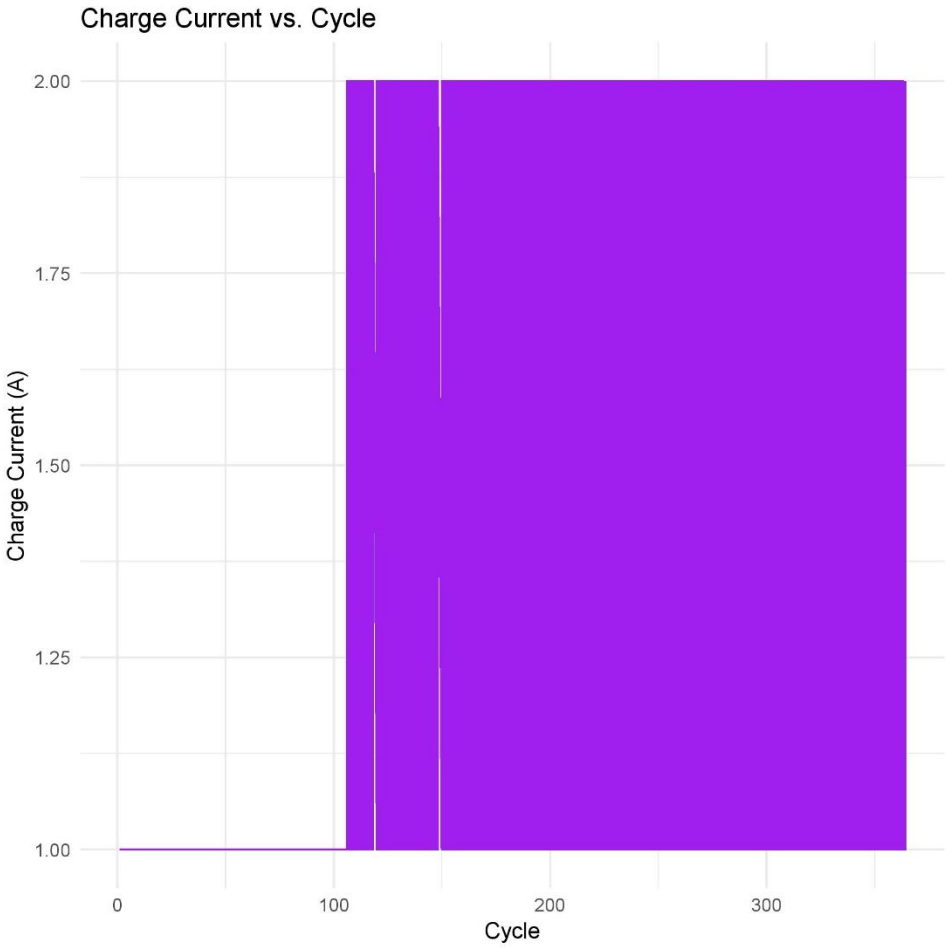

Figure 5.4.Relationship between Charge Current and Cycle

5.2.5 CYCLE VS CAPACITY

Figure 5.5 below illustrates the relationship between battery capacity and cycle count. Capacity exhibits a gradual decline as the cycle count increases. The initial capacity starts

around 2.25 Ah, representing the battery's full potential. Over time, a stepwise decrease in capacity is observed. This decrease reflects the natural degradation of the battery during repeated charge-discharge cycles. By the final cycles, capacity falls below 2.175 Ah, indicating significant wear. The steady downward trend confirms capacity fading, a common phenomenon in battery aging. The graph shows no sudden drops, indicating consistent and predictable degradation. Key statistics include an initial capacity of approximately 2.25 Ah and a minimum capacity below 2.175 Ah. Each step in the graph represents measurable wear, likely due to electrode degradation or material aging. The predictable capacity loss highlights the cell's long-term stability despite aging effects. Overall, the graph demonstrates the battery's durability and gradual decline in energy storage capabilities over extended cycling.

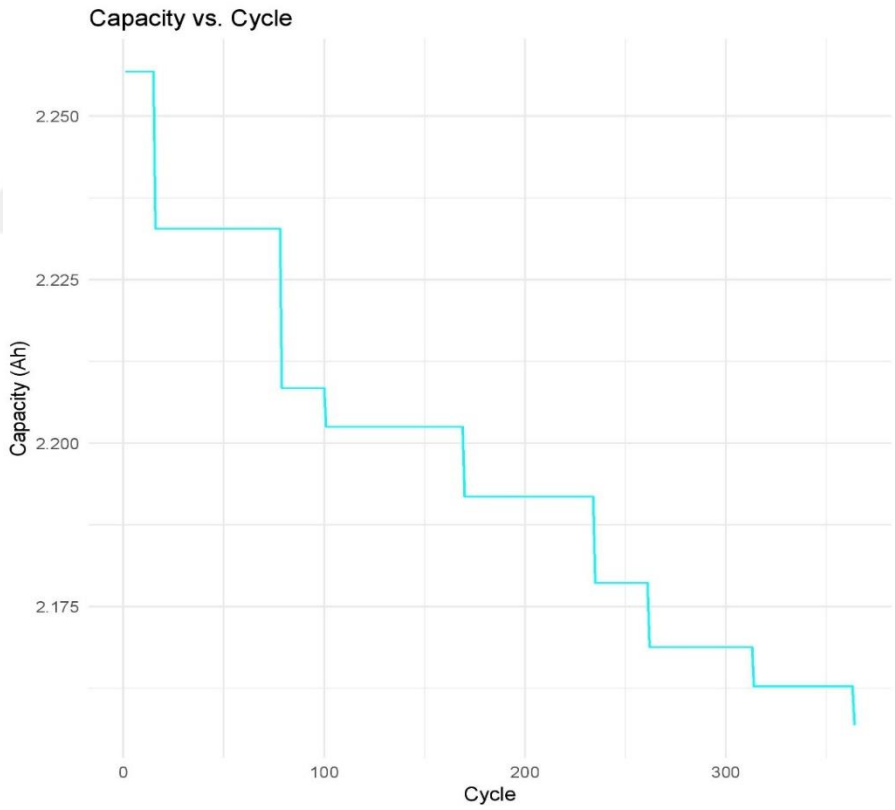

Figure 5.5.Relationship between Capacity and Cycle

5.2.6 CYCLE VS STATE OF HEALTH (SOH)

Figure 5.6 below showed the relationship between the SoH and cycle count, showing a gradual decline. The SoH starts near 100% at the initial cycles, representing optimal battery health. Over time, the SoH decreases stepwise, indicating predictable capacity degradation. The consistent downward trend reflects the natural aging process of the battery during operation. By the final cycles, the SoH drops to approximately 96%, confirming long-term wear and reduced capacity. The absence of abrupt drops indicates stable degradation without sudden failures or anomalies. Key statistics include an initial SoH of 100% and a final SoH of around 96%, with measurable steps between cycles. Each step in the graph likely represents specific capacity losses due to cycling stress. This pattern highlights the battery's durability and resistance to irregular degradation over extended usage. Overall, the graph demonstrates gradual and predictable health loss, aligning with typical aging characteristics of batteries subjected to repeated cycling.

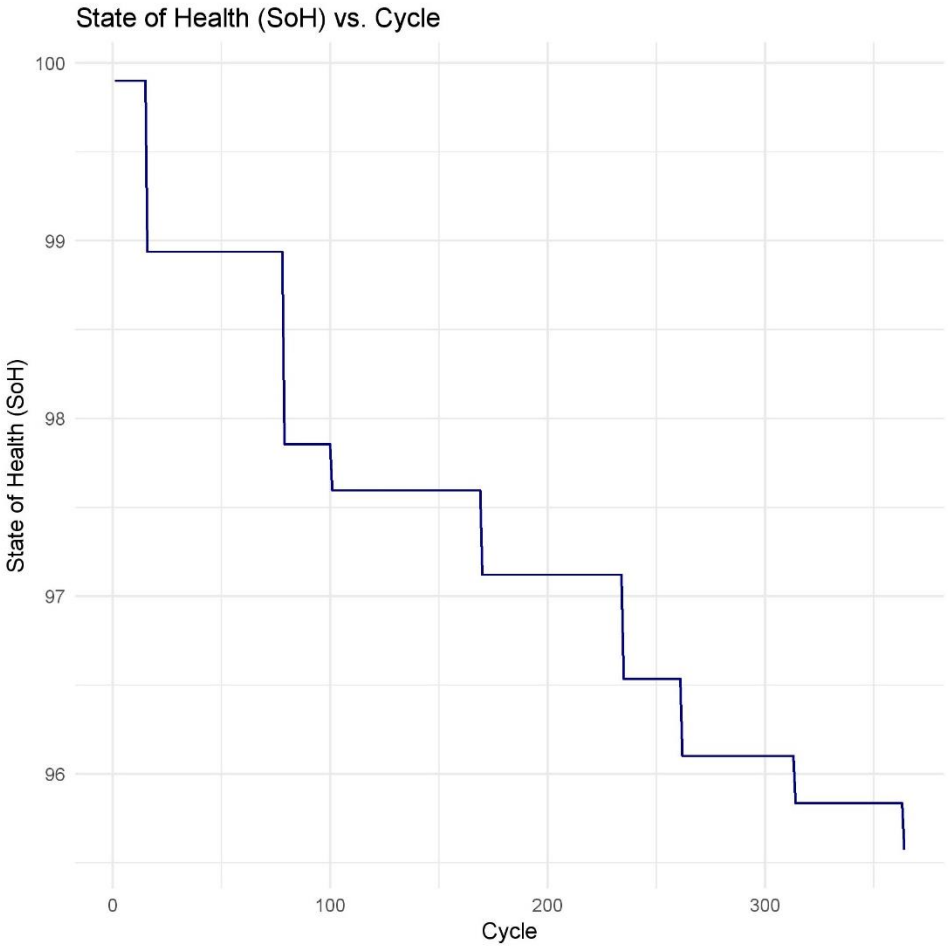

Figure 5.6.Relationship between State of Health and Cycle

5.2.7 STATE OF HEALTH (SOH) VS CHARGE VOLTAGE

Figure 5.7 below depicted the relationship between the SoH and charge voltage, showing SoH values ranging from 96% to 100% as the charge voltage varies between 2.0 V and 3.5 V. At lower charge voltages around 2.0 V, the SoH stabilizes near 96%, indicating a degraded health state. As the charge voltage increases linearly toward 3.5 V, the SoH rises correspondingly to nearly 100%, representing optimal health. This trend reveals a strong positive correlation between charge voltage and battery health, with higher voltages aligning with better SoH. Key statistics include a minimum charge voltage of 2.0 V, a maximum of 3.5 V, and a SoH decline from 100% to 96% at lower voltages. The sharp transitions at extreme voltage ranges suggest the need for precise charge voltage management. Overall, the

graph highlights the critical role of maintaining higher charge voltages to sustain optimal SoH and ensure consistent battery performance over operational cycles. SoH can be calculated with charge voltage using the following mathematical equation.

$$SoH \propto \frac{V_{charge}}{V_{nominal}}$$

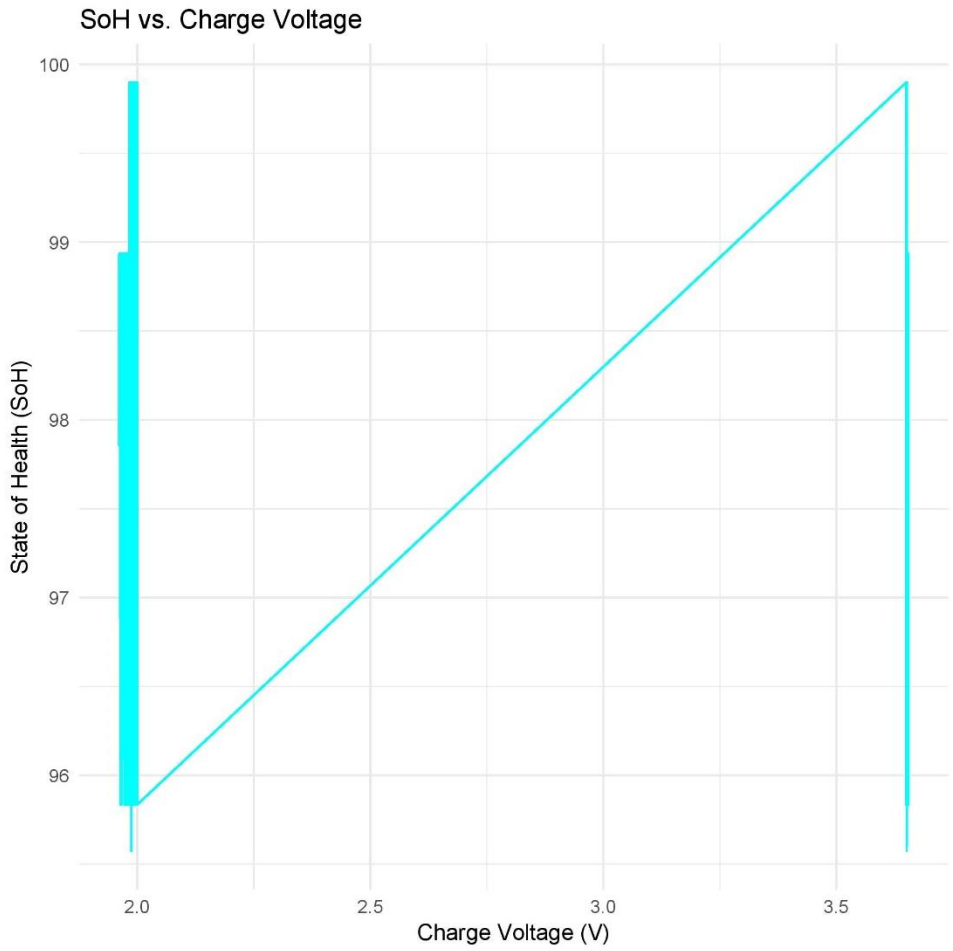

Figure 5.7.Relationship between Charge Voltage and SOH

5.2.8 STATE OF HEALTH (SOH) VS CHARGE CURRENT

Figure 5.8 below provides the relationship between the SoH and charge current, showing a linear increase in SoH as the charge current rises from 1.0 A to 2.0 A. At lower charge currents around 1.0 A, the SoH stabilizes near 96%, indicating a degraded battery

state. As the charge current increases toward 2.0 A, the SoH improves, reaching close to 100%, representing optimal battery health. This positive correlation suggests that higher charge currents contribute to better maintenance of SoH, likely due to more effective charging processes. Key statistics include a minimum charge current of 1.0 A and a maximum of 2.0 A, with SoH ranging from 96% to 100% across the current range. The linear trend emphasizes the importance of maintaining appropriate charge currents to support long-term battery health. Overall, the graph highlights the beneficial effects of controlled higher charge currents in sustaining consistent and reliable battery performance.

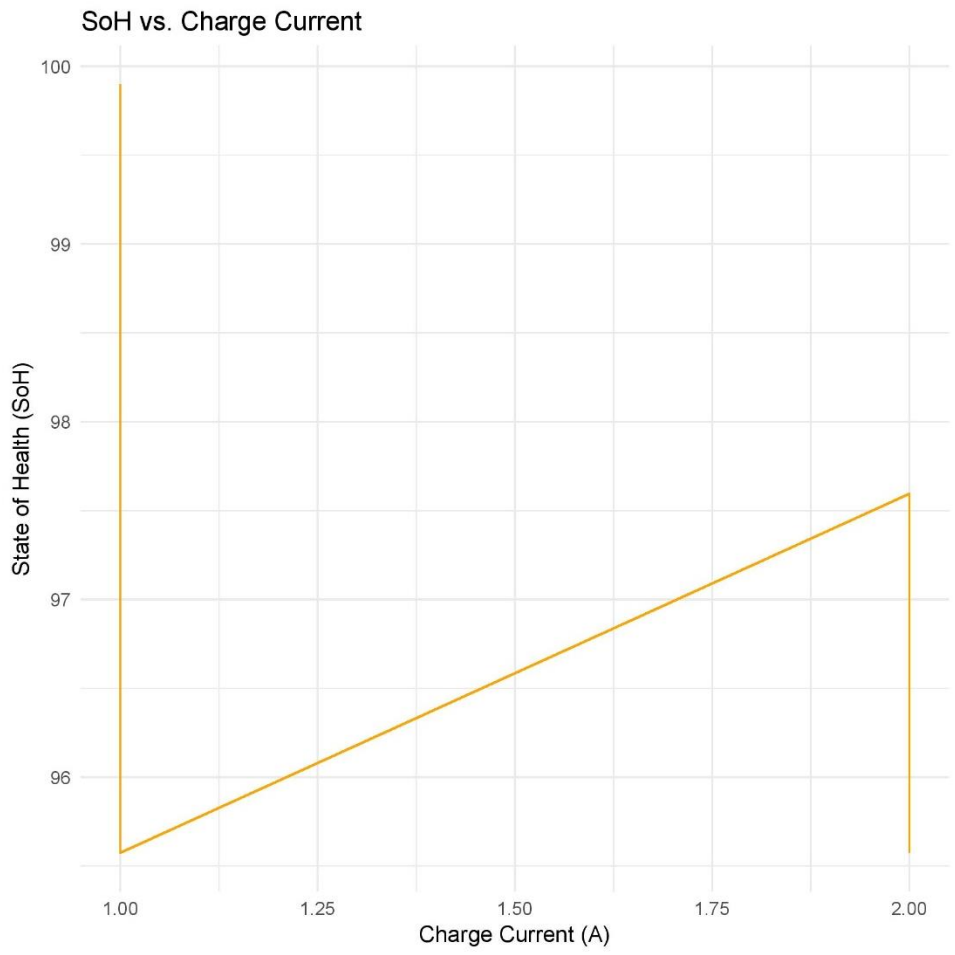

Figure 5.8.Relationship between Charge Current and SOH

5.2.9 STATE OF HEALTH (SOH) VS CAPACITY

Figure 5.9 below demonstrate the relationship between the SoH and capacity, showing a strong linear correlation. As the capacity increases from 2.175 Ah to 2.250 Ah, the SoH also rises from 96% to 100%. This positive trend indicates that higher battery capacity corresponds to better health, reflecting the natural degradation of both parameters over time. Key statistics include a minimum capacity of 2.175 Ah at 96% SoH and a maximum capacity of 2.250 Ah at 100% SoH. The linear relationship highlights how capacity acts as a direct indicator of battery health, with reductions in capacity signaling aging and wear. The consistent slope suggests predictable and steady degradation, with no abrupt drops or irregularities. This trend demonstrates the battery's durability in maintaining a gradual and stable loss of health and capacity over cycles. Monitoring capacity is crucial for assessing the overall state of the battery and predicting its remaining useful life. Overall, the graph emphasizes the importance of maintaining capacity to sustain a high SoH, underlining the interconnectedness of these metrics in evaluating battery performance and longevity. SoH can be calculated with charge voltage using the following mathematical equation.

$$\boldsymbol{SoH = \frac{C_{actual}}{C_{nominal}} \times 100}$$

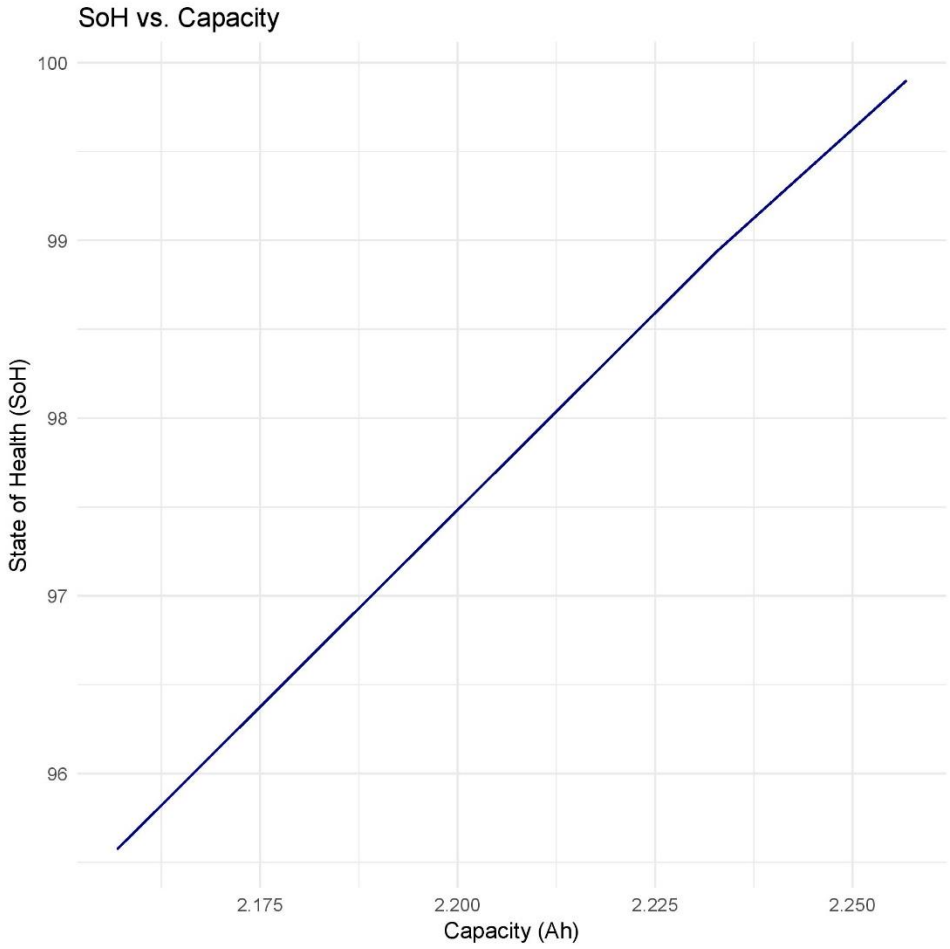

Figure 5.9.Relationship between Capacity and SOH

5.2.10 STATE OF HEALTH (SOH) VS TEMPERATURE

Figure 5.10 below illustrates the relationship between SoH and Temperature (°C). This visualization implies that no clear or meaningful relationship between temperature and SoH can be inferred due to the limited or fixed range of temperature in the dataset. The concentration of data points around a single temperature may indicate either a controlled experimental setup, where temperature was deliberately held constant, or a limitation in data collection, where a broader range of temperatures was not captured. This restricted variability prevents the analysis from exploring potential trends or interactions between temperature and SoH, which could otherwise be important for understanding the relationship. As such, while some patterns in SoH can be observed within the narrow temperature range, these findings

are limited in scope and do not allow for generalizations across a wider range of temperatures. To draw more robust conclusions, future studies should aim to include a more diverse and representative range of temperature values to assess whether temperature plays a significant role in influencing SoH. SoH can be calculated with temperature using the following mathematical equation.

$$C_{loss} \propto e^{\frac{-Ea}{RT}} . t$$

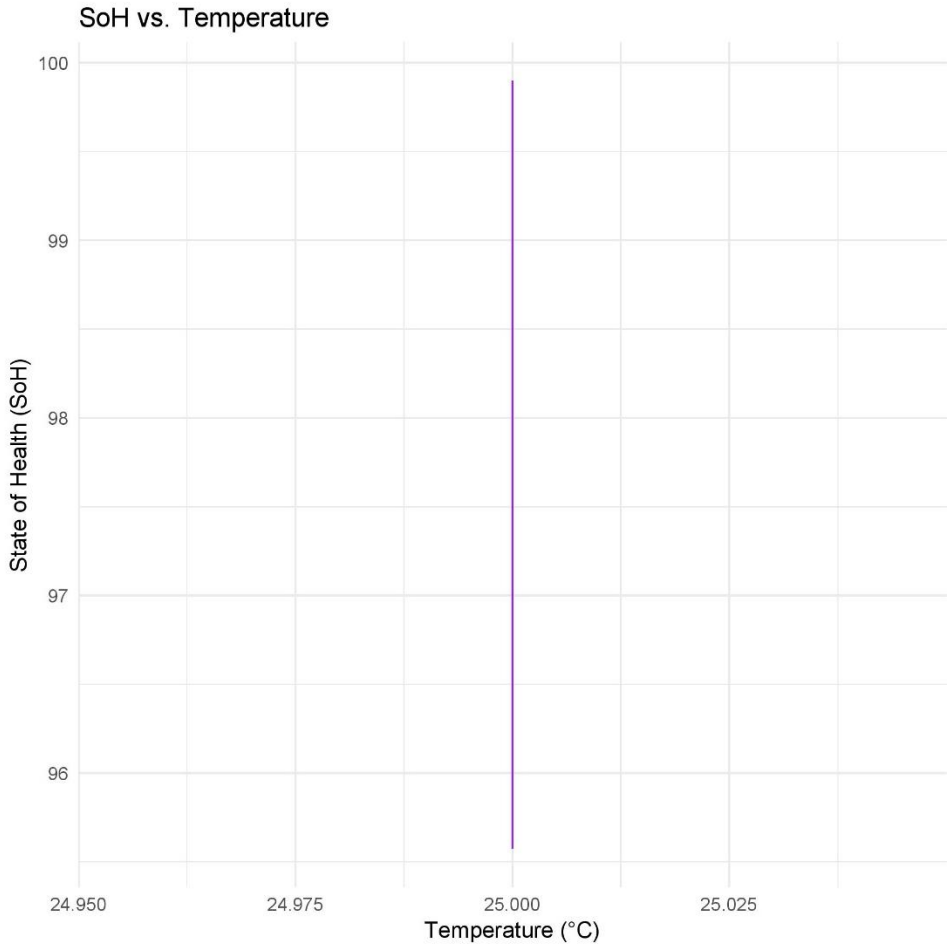

Figure 5.10.Relationship between Temperature and SOH

5.2.11 STATE OF CHARGE (SOC) VS TERMINAL VOLTAGE

Figure 5.11 below depicts the relationship between the SoC and terminal voltage, showing a steep linear rise. At terminal voltages below approximately 2.5 V, the SoC remains

at 0%, indicating a discharged state. Once the terminal voltage exceeds 2.5 V, the SoC increases rapidly, reaching 100% near 3.0 V. This trend highlights a strong and direct correlation between terminal voltage and the battery's SoC. Key statistics include a minimum SoC of 0% below 2.5 V and a maximum SoC of 100% at or above 3.0 V. The sharp slope in the graph indicates that the SoC is highly sensitive to changes in terminal voltage within this range. This relationship reflects the charging behavior of the battery, where voltage increases significantly during the transition from a low to a high charge state. Overall, the graph emphasizes the importance of monitoring terminal voltage as a reliable indicator of the battery's charge level, particularly in applications requiring precise SoC estimation. This steep linear trend further underscores the efficiency of voltage-based SoC monitoring methods for battery management systems. SoC can be calculated with terminal voltage using the following mathematical equation.

$$\boldsymbol{SoC = \frac{V_t - V_m}{V_{max} - V_{min}} \times 100}$$

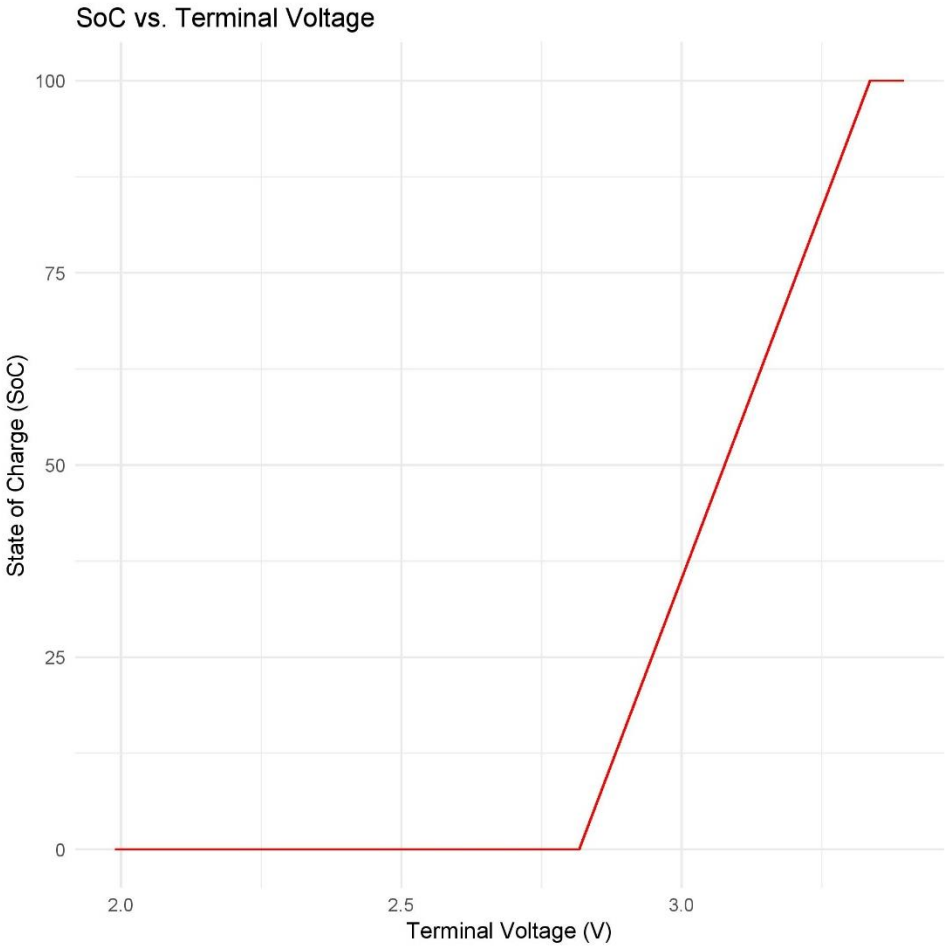

Figure 5.11.Relationship between Terminal Voltage and SOC

5.2.12 STATE OF CHARGE (SOC) VS CHARGE VOLTAGE

Figure 5.12 depict the relationship between the SoC and charge voltage, showing a strong linear correlation. At lower charge voltages around 2.0 V, the SoC is near 0%, indicating a discharged state. As the charge voltage increases, the SoC rises proportionally, reaching 100% at approximately 3.5 V. The linearity of the graph indicates that the SoC is directly influenced by the charge voltage, reflecting the battery's charging behavior. Key statistics include a minimum SoC of 0% at 2.0 V and a maximum SoC of 100% at 3.5 V, with no significant anomalies or deviations. The steep slope emphasizes the sensitivity of SoC to changes in charge voltage, particularly during the transition from a discharged to a fully charged state. This trend underscores the reliability of charge voltage as an accurate indicator

of SoC, making it a crucial parameter for battery management systems to monitor and control. Overall, the graph highlights the predictable and efficient charging characteristics of the battery. SoC can be calculated with terminal current using the following mathematical equation.

$$\boldsymbol{SoC = \frac{V_{charge} - V_{min}}{V_{max} - V_{min}} \times 100}$$

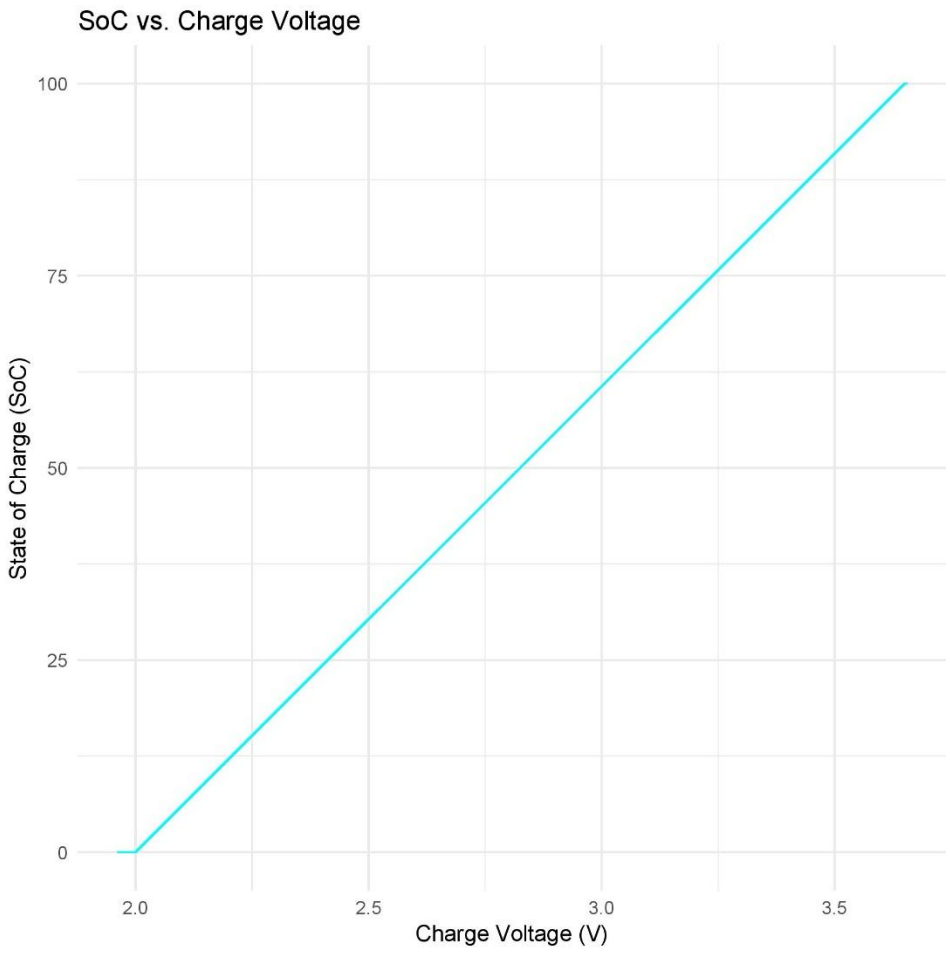

Figure 5.12.Relationship between Charge Current and SOC

5.2.13 STATE OF CHARGE (SOC) VS CHARGE CURRENT

Figure 5.13 below illustrates the relationship between the SoC and charge current, showing an inverse linear correlation. At higher charge currents around 2.0 A, the SoC drops to 0%, indicating a discharged state. Conversely, at lower charge currents near 1.0 A, the SoC reaches 100%, reflecting a fully charged battery. This negative linear relationship indicates that higher currents correspond to lower SoC values, likely due to increased discharge rates or incomplete charging cycles. Key statistics include a maximum SoC of 100% at 1.0 A and a minimum SoC of 0% at 2.0 A, with no anomalies or deviations from the trend. The steep negative slope emphasizes the sensitivity of SoC to variations in charge current, with higher currents accelerating the discharge process. This relationship underscores the importance of optimizing charge current to maintain a balanced and efficient charging process. Overall, the graph highlights the critical role of current regulation in sustaining battery performance and ensuring accurate SoC estimation for effective battery management. SoC can be calculated with terminal current using the following mathematical equation.

$$SoC_t = SoC_{t-1} + \frac{I_{charge} \cdot \Delta t}{C_{nominal}}$$

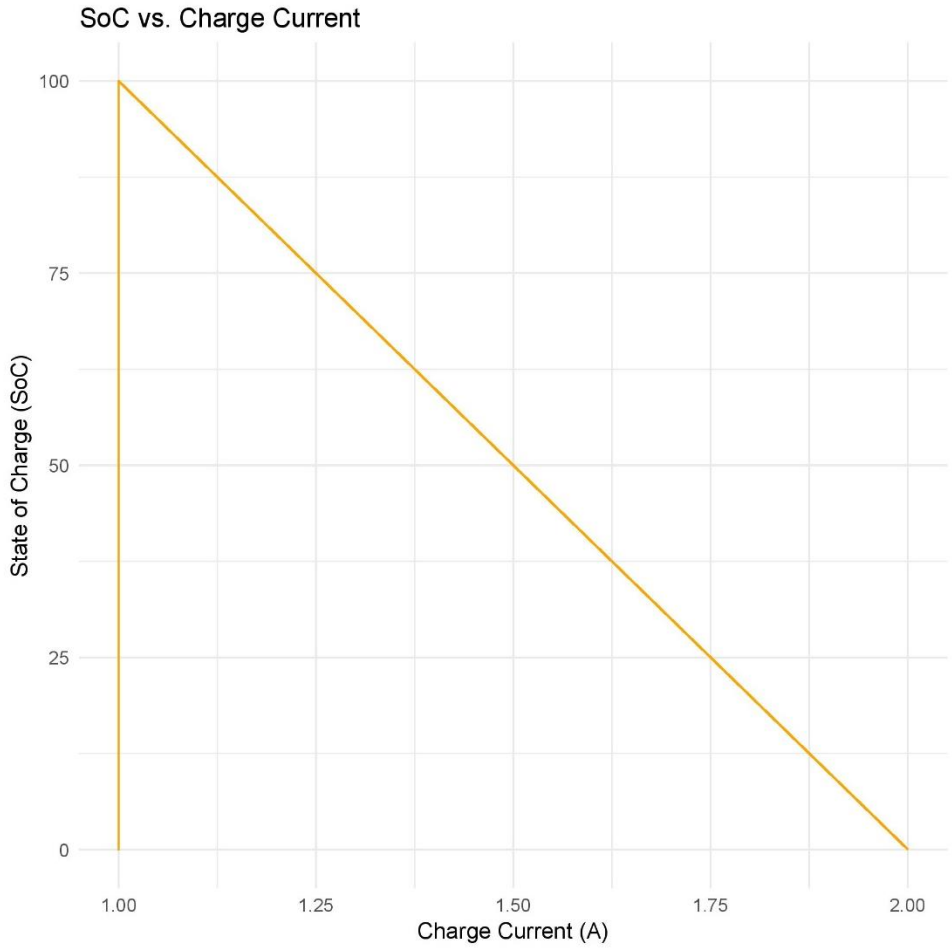

Figure 5.13.Relationship between Charge Current and SOC

5.2.14 STATE OF CHARGE (SOC) VS TEMPERATURE

Figure 5.14 below depicts the relationship between the SoC and temperature, showing a narrow vertical distribution. The temperature remains fixed around 25°C, while the SoC spans its full range from 0% to 100%. This suggests that temperature has minimal variability and does not significantly influence SoC within this narrow range. Key statistics include a temperature range of approximately 24.95°C to 25.025°C and a complete SoC range from 0% to 100%. The lack of variation in temperature indicates that the battery was likely operated under controlled thermal conditions. While the graph highlights consistent temperature during charging and discharging, it limits the ability to analyze broader temperature effects on SoC. This trend underscores the importance of maintaining stable

thermal conditions for reliable battery operation. However, further analysis over a wider temperature range would be needed to understand how temperature impacts the SoC in more diverse scenarios.

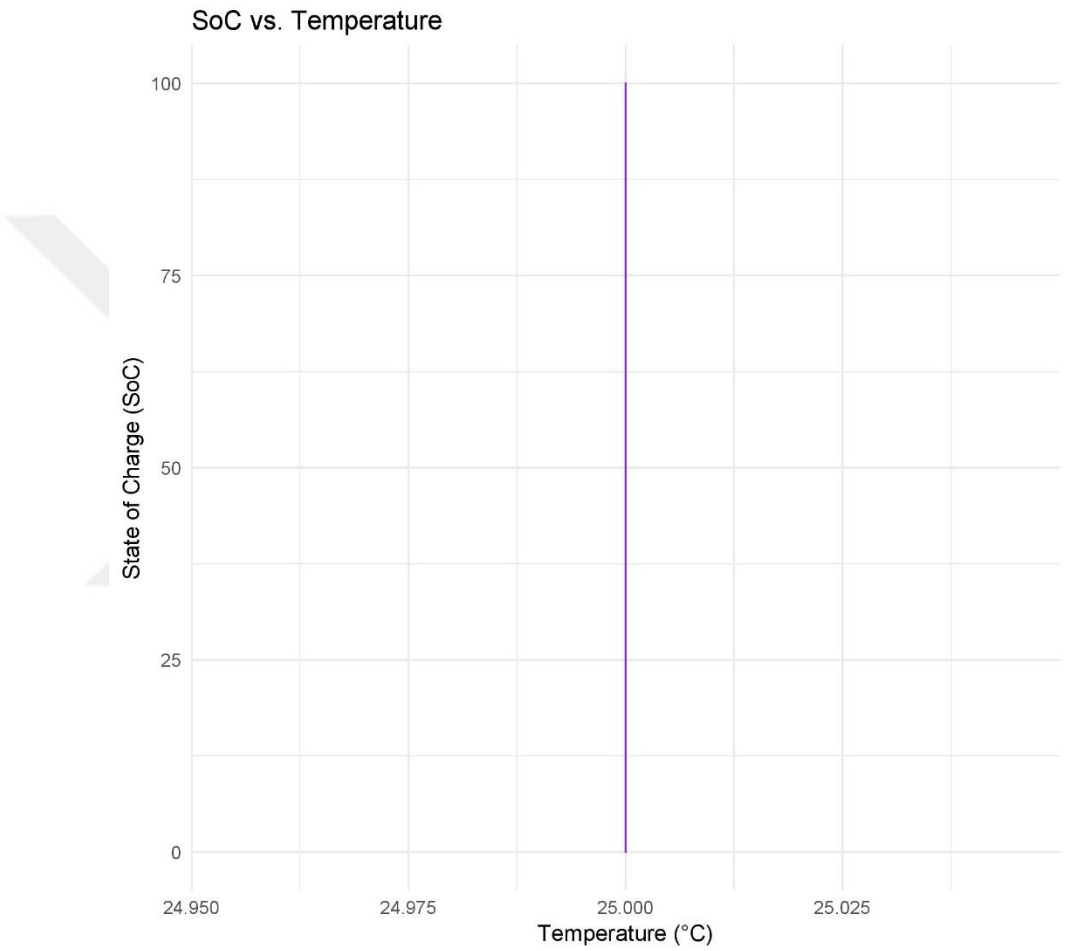

Figure 5.14.Relationship between Temperature and SOC

5.3 ALGORITHM EXPLAINING AND SOH PREDICTION RESULTS

5.3.1 DNN (Deep Neural Network)

For a number of applications, such as energy storage systems, electric vehicles, and battery management systems, accurate battery SoH prediction is essential. The creation and assessment of a DNN model intended to forecast battery SoH based on historical data are described in this paper. A thorough methodology was used for the study, which included data

preprocessing, model design, training, assessment, and result analysis. Features including voltage, current, temperature, and cycle count were included in the dataset used for this investigation. The preprocessing stages comprised cleaning the data, identifying and eliminating outliers with statistical techniques like the interquartile range (IQR), and impute missing values with KNN imputation. Feature engineering was also performed, creating time-based features (e.g., time since the last charge or discharge cycle) and derived features such as the rate of SoH change and current derivatives. Finally, the data was normalized using min-max scaling to ensure all features contributed equally to the model training process.

A feedforward neural network with numerous densely connected hidden layers made up the DNN model architecture. Preprocessed data was fed into the input layer, and fully connected neurons with ReLU activation, batch normalization to stabilize training, and dropout layers to avoid overfitting were all part of the hidden layers. The SoH was predicted by a single neuron in the output layer. The performance was assessed using the Mean Squared Error (MSE) loss function, and the Adam optimizer was used for training. The training parameters comprised of 32 batches, 1000 epochs, and 0.000001 as the initial learning rate. Callbacks were introduced to prevent overfitting and dynamically modify the learning rate during training, such as EarlyStopping and ReduceLROnPlateau.

The model's working was measured using metrics such as Mean Absolute Error (MAE), Root Mean Squared Error (RMSE), and R-squared. Initial results revealed significant underestimation, with predicted SoH values consistently lying below the actual values. High MAE and RMSE values indicated large prediction errors, and a negative R-squared value suggested that the model performed worse than simply predicting the mean of the target variable. To address these issues, several improvements were made, including reducing the learning rate for better training stability, increasing model depth to capture complex patterns, raising the dropout rate to prevent overfitting, and applying L2 regularization to improve generalization.

Despite these improvements, the model exhibited stagnation in subsequent iterations, predicting constant values, which pointed to underfitting and an inability to capture the dynamics of battery degradation. Future work involves conducting a more detailed analysis

of the data to identify biases, inconsistencies, or missing values. Additionally, exploring advanced feature engineering, alternative data normalization techniques, and different model architectures like CNNs, RNNs, and LSTM networks could improve performance. Attention mechanisms may also uplift the model's capability to focus on relevant parts of the input sequence.

Hyperparameter optimization, using methods like grid search, random search, or Bayesian optimization, could further improve learning rates, dropout rates, and other parameters. Ensemble methods such as bagging or boosting may also be considered to combine predictions from multiple models for better performance. In conclusion, while the initial results of the DNN model were not satisfactory, various strategies, including data preprocessing, model adjustments, and hyperparameter optimization, were explored to improve its performance. Upcoming investigation is essential to examine the impact of these strategies and explore additional approaches to improve the model's correctness and strength for battery SoH prediction. MAE is selected as the loss function, defined as:

$$\text{MAE} = \frac{1}{n}\sum_{i=1}^{n}|\hat{y}_i - y_i|$$

Where:

- y_i is the true value.
- Y_i is the predicted value.
- N is the total number of data points.

Strengths:

- MAE is more robust to outliers because it does not square the errors, giving equal weight to all errors.
- It is easier to interpret since it is in the same unit as the target values.

Weaknesses:

- MAE does not penalize larger errors as heavily as MSE, which could be a disadvantage if large errors need to be prioritized.
- Optimization of MAE can be more challenging since it is not differentiable at every point.

MAE directly measures prediction accuracy without squaring errors, making it robust to outliers. The utility of MAE in regression tasks is supported by studies in [7]. The Adam optimizer is employed due to its adaptive learning rate properties and superior performance on noisy gradients. Adam updates parameters as follows:

$$\theta_t = \theta_{t-1} - \frac{\eta}{\sqrt{\hat{v}_t} + \epsilon}\hat{m}_t$$

where m^t\hat{m}_tm^t and v^t\hat{v}_tv^t are bias-corrected approximations of the first and second moments of the gradient.

- **Parameters**:
    - β1=0.9\beta_1 = 0.9β1=0.9 for momentum.
    - β2=0.999\beta_2 = 0.999β2=0.999 for variance scaling.
    - ϵ=10−8\epsilon = 10^{-8}ϵ=10−8 for numerical stability.

The effectiveness of Adam in regression problems is well-documented in [8], [9]. The model achieves an MAE of **0.1673**, which corresponds to an average prediction error of approximately 16.73%. This low value underscores the model's capability to make accurate predictions. MAE's application to regression tasks is further validated in [7]. RMSE is defined as:

$$\text{RMSE} = \sqrt{\frac{1}{n}\sum_{i=1}^{n}(\hat{y}_i - y_i)^2}$$

An RMSE of **0.2024** reflects the model's sensitivity to larger errors. Its slightly higher value compared to MAE highlights occasional deviations, as discussed in [10]. R^2 measures the proportion of variance explained by the model:

$$R^2 = 1 - \frac{\sum_{i=1}^{n}(\hat{y}_i - y_i)^2}{\sum_{i=1}^{n}(y_i - \bar{y})^2}$$

The DNN achieves R2=0.9695R^2 = 0.9695R2=0.9695, capturing 96.95% of the variance in SoH. This result signifies high predictive power, as supported by metrics analysis in [11]. The training process involves fitting the DNN model to the preprocessed data and evaluating its performance on unseen validation data. Here's a breakdown of the code and its functionalities:

1. **Model Fitting (model.fit())**
    - model.fit(x=X_train, y=Y_train, batch_size=25, epochs=130): This line initiates the training process.
        - x=X_train: The preprocessed training data features are provided as input (X_train).
        - y=Y_train: The corresponding SoH labels for the training data are provided as target variables (Y_train).
        - batch_size=25: The training data is fed to the model in batches of 25 samples at a time. This helps to improve memory efficiency and potentially speed up training.
        - epochs=130: The model is trained for a total of 130 epochs. An epoch represents one complete pass through the entire training dataset.
2. **Model Evaluation (model.evaluate())**

- After training, the model's performance is evaluated on the validation data (X_val, Y_val).
    - loss = model.evaluate(X_val, Y_val): This line calculates the loss (MSE in this case) on the validation set.
    - The resulting loss value (loss) is printed to the console, indicating how well the model generalizes to unseen data.

5.3.1.1 Visualization and Error Analysis

1. **Actual vs. Predicted SoH Plot (Matplotlib)**
    - The code utilizes Matplotlib to create a visualization comparing the actual SoH values (Y_val) with the DNN's predicted SoH values (dnn_pred).
    - The plot allows for visual inspection of the model's performance and identification of potential biases or patterns in the errors.
2. **Error Metrics Calculation**
    - Several error metrics are calculated to quantify the model's performance:
        - **Mean Absolute Error (MAE)**
        - **Root Mean Squared Error (RMSE)**
        - **R-squared (R^2)**
    - The calculated values for MAE, RMSE, and R^2 are printed to the console, providing numerical insights into the model's accuracy.
3. **Absolute Error vs. Cycle Number Plot**
    - This plot visualizes the absolute error (difference between actual and predicted SoH) for each data point in the validation set.
    - Analyzing this plot can reveal trends or patterns in the errors, potentially suggesting areas for improvement in the model or data preprocessing.

4. **Additional Plots (Optional)**

    - The commented-out code demonstrates the creation of additional plots using potentially user-defined functions:

        - plot_actual_soh(Y_val): This function might plot the actual SoH values over time or against another relevant variable.
        - plot_predicted_soh(predicted_soh): This function might plot the predicted SoH values over time or against another relevant variable.
        - plot_both(Y_val, predicted_soh): This function might create a combined plot showing both actual and predicted SoH values.

5.3.1.2 Training Considerations

- **Hyperparameter Tuning:** Hyperparameters such as batch size, epochs, and learning rate are set during the training process. Techniques such as grid search or random search can be used to find optimal values for these parameters, which can have a significant impact on the model's performance..
- **Early Stopping:** To avoid overfitting, the training process can be stopped early. This is done by an EarlyStopping callback [5]. It monitors the validation error and stops training if the error is not getting better for a given epoch.
- **Learning Rate Scheduling:** Using a ReduceLROnPlateau callback [6], the learning rate can be dynamically adjusted during training. The learning rate is reduced by a factor if the validation loss does not improve for a given number of epochs. It allows the model to explore the solution space better.

Figure 5.15 below presents a comparison between the actual and predicted SoH values using a DNN. The blue line represents the actual SoH, which follows a stepwise declining pattern, while the orange dashed line indicates the predicted SoH, which aligns closely with the actual values but appears smoother. The predicted curve effectively captures the overall trend of the actual SoH, demonstrating the DNN model's ability to generalize and accurately

model the degradation behavior. However, slight deviations amid the actual and predicted values are visible in certain regions, suggesting areas where the model's predictions could be refined. The smoother transitions in the predicted curve, compared to the stepwise nature of the actual SoH, may indicate over-smoothing by the DNN, potentially masking abrupt changes in SoH. Despite this, the model shows strong prediction performance, with minor errors that could be addressed through improvements such as enhancing feature selection, refining the training process, or exploring alternative architectures better suited for capturing abrupt changes. Overall, the figure highlights the DNN's capability in estimating SoH with high accuracy, while also pointing to opportunities for further optimization.

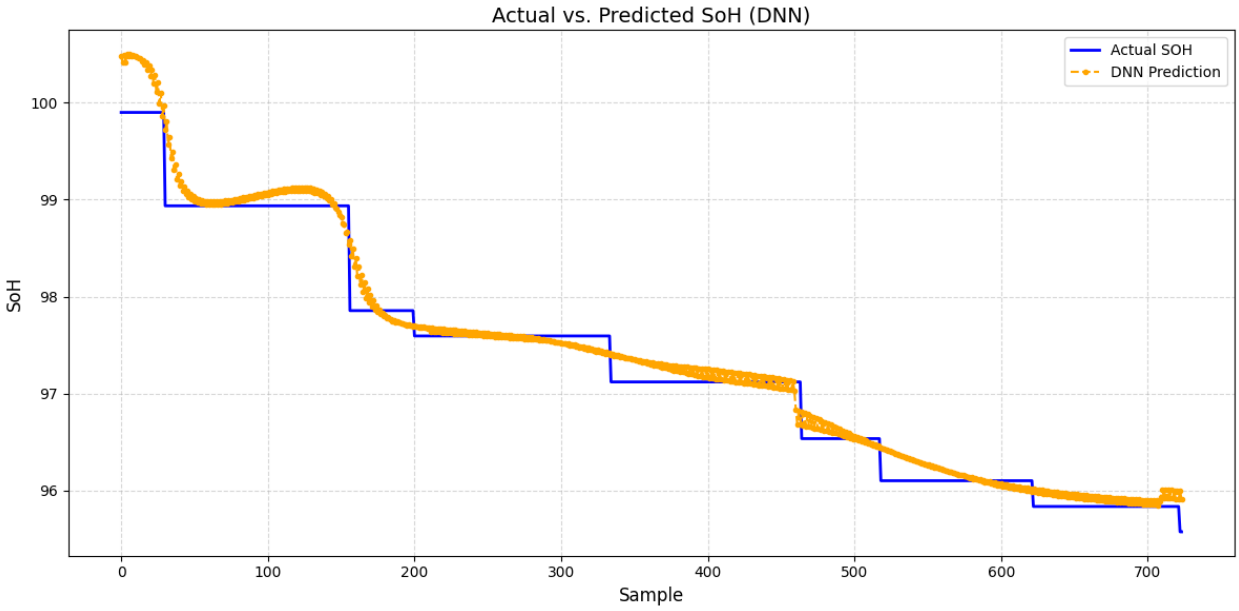

Figure 5.15.Actual vs Predicted SoH using DNN

Figure 5.16 below illustrates the AE between actual and predicted values over the cycle number when using a DNN. The absolute error curves are plotted for multiple instances or datasets, showing variation in the error trends over the cycles. Initially, the absolute error is relatively high for most cases, likely due to the model adapting to the early phases of the data. However, as the cycle number increases (up to approximately 200 cycles), the error significantly decreases, indicating that the DNN improves in prediction accuracy during this phase. Beyond the 200-cycle mark, the error trends vary among different instances. Some

curves exhibit a gradual increase in error, while others remain relatively stable or show sudden spikes in later cycles (e.g., around 500–700 cycles). These variations could stem from different operational conditions, data distributions, or the inability of the DNN to generalize effectively for certain scenarios. The presence of error spikes at later cycles may also point to abrupt changes or anomalies in the data that the model struggles to predict accurately. Overall, the figure highlights the DNN's capacity to achieve low error during the intermediate cycles but also reveals challenges in maintaining consistent accuracy during the later stages. Further analysis of these errors could involve investigating the underlying data characteristics, refining the DNN architecture, or exploring ensemble methods to reduce prediction inconsistencies.

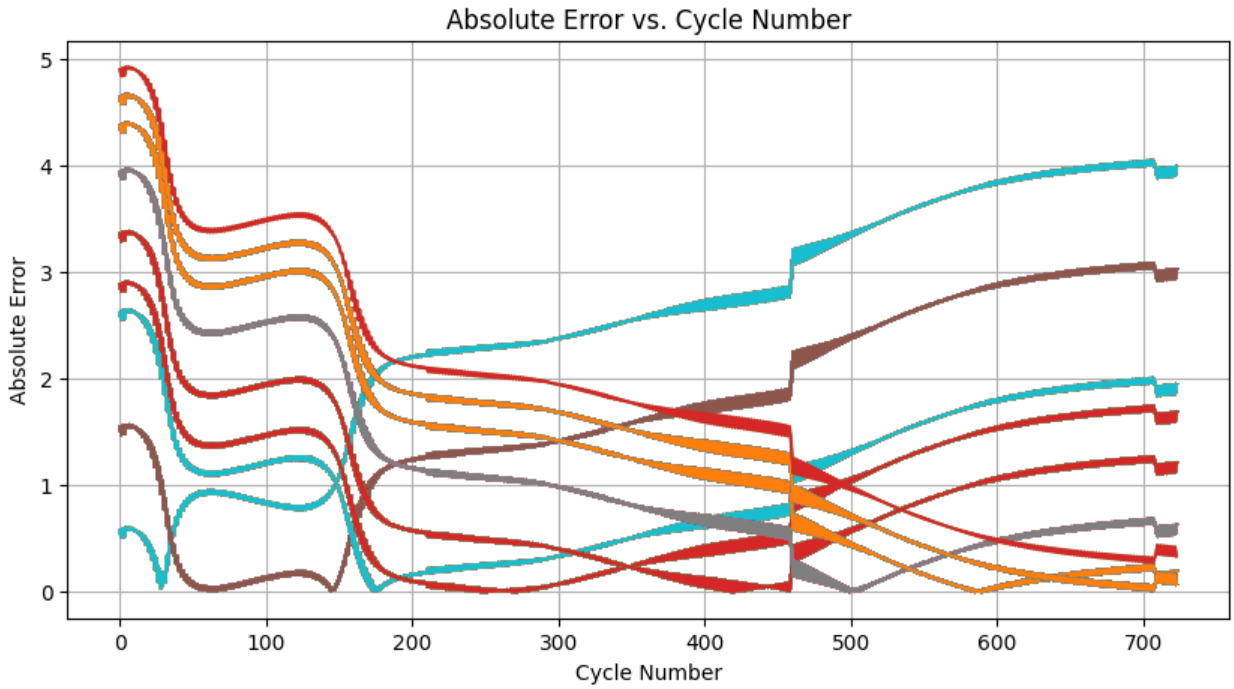

Figure 5.16.Absolute Error vs Cycle Number using DNN

Figure 5.17 depicts the actual SoH versus the sample number in a stepwise format, representing the degradation of SoH over time or usage. The SoH starts at approximately 100% and steadily declines as the sample number rises. The decline occurs in discrete steps, indicating distinct phases or events contributing to the health degradation of the system. The stepwise pattern suggests that the SoH does not degrade continuously but instead exhibits

discrete drops, likely corresponding to significant changes in operational conditions, usage cycles, or aging factors. This behavior is typical in applications like battery health monitoring, where degradation often occurs in phases due to chemical or physical changes within the system. The figure highlights the gradual reduction in SoH with increasing sample number, emphasizing the importance of predictive models to accurately capture these transitions for better system health management. It also serves as a benchmark for evaluating prediction models, as any prediction curve would need to align with this stepwise trend to be considered accurate.

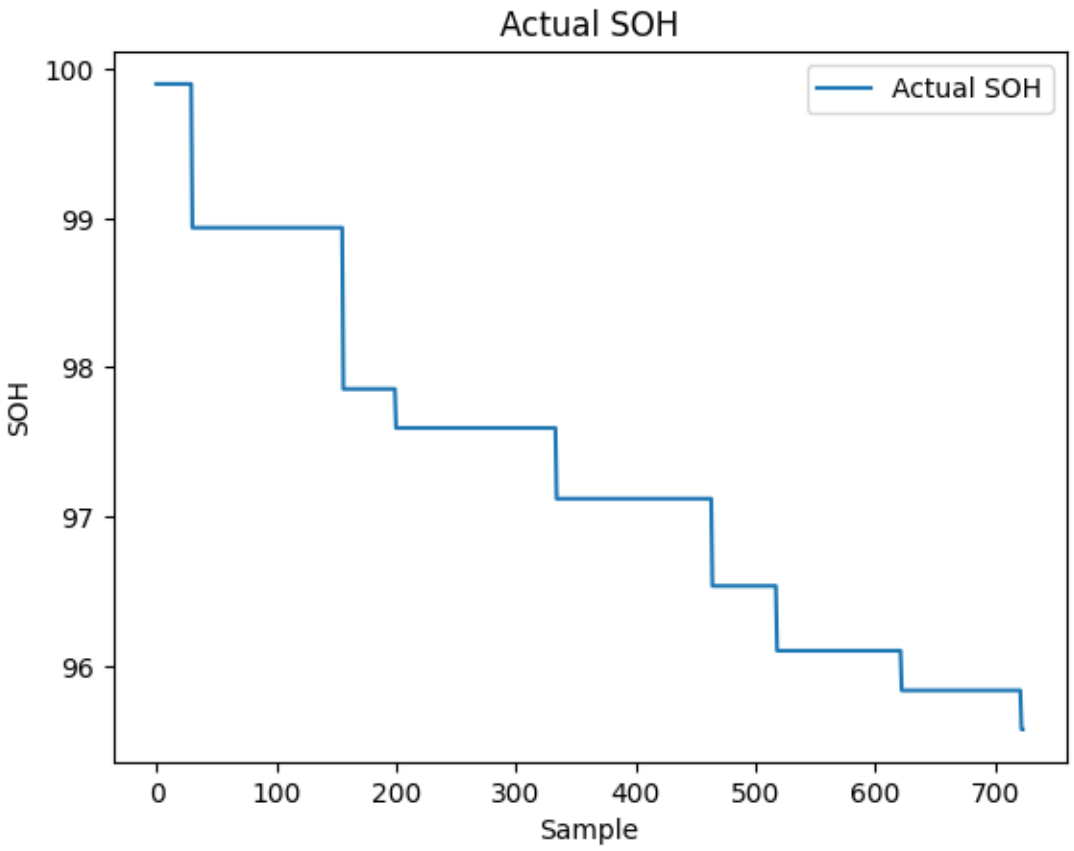

Figure 5.17.Actual SoH vs Sample using DNN

The performance metrics of the DNN model indicate its strong capability in predicting the SoH. MAE of **0.1281** highlights the model's ability to consistently produce predictions close to the actual values, showcasing its robustness in minimizing average errors. Similarly, the RMSE of **0.1808**, which is slightly higher due to its sensitivity to larger

errors, suggests that the model effectively handles significant deviations, as these are not a major concern. The R-squared (R^2) value of **0.9756** confirms that the model clarifies approximately 97.56% of the variance in the actual SoH data, demonstrating excellent predictive power and the ability to accurately model the underlying trends. Additionally, the low validation loss of **0.0327** specifies that the model generalizes well to unseen data, reinforcing its reliability and stability for real-world applications. These results collectively reflect a well-trained and highly effective DNN model with minimal errors and strong generalization, making it a reliable tool for SoH prediction. Minor improvements could still be explored to further optimize performance and maintain its accuracy across diverse datasets. The values:

MAE: 0.1281

RMSE: 0.1808

R-squared: 0.9756

Validation Loss: 0.03269345313310623

5.3.2 LSTM

This report thoroughly analyzes the design, implementation, and evaluation of a LSTM model developed for time series prediction. The model employs a layered architecture, integrating dropout, batch normalization, and early stopping mechanisms to enhance both performance and generalization. This document delves into the model's architecture, training process, strengths, weaknesses, and recommendations for further improvements. The suggested LSTM model is a multi-layered, sequential deep learning model. An LSTM layer with 128 units that uses a tanh activation function and the argument return_sequences=True makes up the input layer. The model can extract a substantial amount of information from the input data thanks to the 128 units, and the tanh activation adds non-linearity, which helps the model identify intricate patterns in the time series. To ensure that the output of this layer is a sequence and that the LSTM layer that follows can process sequential information efficiently, the return_sequences=True argument is used.

Several parts that cooperate to process the data are part of the hidden layers. In order to lower the possibility of overfitting, the first hidden layer includes a dropout layer with a rate of 0.2 that randomly deactivates 20% of the units during training. This enhances the model's capacity for generalization by preventing it from depending unduly on any one neuron. Next comes a batch normalization layer that speeds up convergence and increases training stability by normalizing the activations from the previous layer. More complex temporal dependencies are captured by processing the sequential information extracted by the first layer using a second LSTM layer consisting of 64 units and a tanh activation function. Batch normalization layers and additional dropout layers with a rate of 0.2 are added.

Further dense layers improve the model's capacity to identify intricate patterns in the data. Non-linearity is introduced by a fully connected layer with 64 units and ReLU activation, which is followed by a second dropout layer and a batch normalization layer. There is also a fully connected layer with 32 units and ReLU activation, along with batch normalization and dropout layers. The model can learn abstract representations and improve its comprehension of the time series thanks to these thick layers. The output layer, which generates the time series' final predicted value, is made up of a dense layer with a single unit and no activation function.

With a learning rate of 0.0005, the Adam optimizer is used in the training process. Adam is a strong and effective optimizer that computes adaptive learning rates for every parameter, making it a good fit for deep learning models. Mean Squared Error (MSE), a loss function that measures the discrepancy between expected and actual values and penalizes larger errors more severely, is the one that is used. By making this decision, the model guarantees that precise predictions come first. Callbacks are another aspect of training that improves performance. In order to prevent overfitting, the EarlyStopping callback tracks validation loss and stops training if no improvement is seen for 20 consecutive epochs. In order to allow for model fine-tuning during later training stages, the ReduceLROnPlateau callback dynamically lowers the learning rate by a factor of 0.5 every 5 epochs without improving validation loss.

The model's regularization methods and tiered architecture are its main advantages. The model can recognize long-term patterns and relationships because it can capture complex temporal dependencies in time series data thanks to the employment of multiple LSTM layers. Although batch normalization stabilizes training and speeds up convergence by normalizing activations, dropout layers prevent overfitting by minimizing reliance on particular neurons. Overfitting is avoided and effective convergence is ensured by the adaptive training procedure, which also includes early stopping and learning rate reduction. The model is robust and appropriate for time series forecasting because of these design decisions.

But there are also shortcomings and room for development in the model. First, the number of units in each layer, the learning rate, the dropout rate, and the number of epochs are among the hyperparameter choices that have a significant impact on its performance. Using techniques like grid search, random search, or Bayesian optimization to find the best configurations, systematic hyperparameter optimization can be used to address this sensitivity. Second, the caliber of the input data and the preprocessing stages have a major impact on how effective the model is. Performance can be greatly improved by ensuring appropriate data scaling (e.g., standardization or normalization) and by using feature engineering strategies, such as domain knowledge-based features or automated feature selection. Third, deep LSTM model training can be computationally costly, particularly when dealing with sizable datasets. To mitigate these computational difficulties, methods like gradient clipping and the use of hardware accelerators (such as GPUs or TPUs) can contribute. Finally, overfitting is still a problem even with regularization techniques, especially when dealing with large and complicated datasets. This problem can be solved by expanding the quantity of training data, investigating more sophisticated regularization techniques (such as weight decay or L1/L2 regularization), or testing out different architectures like stacked or bidirectional LSTMs.

In conclusion, the presented LSTM model provides a robust foundation for time series forecasting, effectively capturing temporal dependencies and demonstrating strong generalization capabilities. However, its performance can be further enhanced through

systematic hyperparameter tuning, thorough data preprocessing, and the exploration of advanced techniques. Future research could focus on incorporating attention mechanisms to enable the model to focus on the most relevant parts of the input sequence. Additionally, developing more efficient training algorithms and evaluating the model's performance across a broader range of time series datasets would provide valuable insights and further enhance its capabilities. These advancements would solidify the LSTM model as a powerful tool for time series analysis and forecasting.

Figure 5.18 illustrates the comparison between the actual and predicted (SoH) using a (LSTM) model. The blue line represents the actual SoH, which exhibits a stepwise decline, while the yellow dashed line represents the LSTM's predictions, closely following the actual values with smooth transitions. The LSTM prediction curve demonstrates excellent alignment with the actual SoH, capturing both the overall trend and finer details of the degradation pattern. The figure highlights the LSTM model's ability to effectively handle sequential data and predict SoH with high accuracy. The smoother nature of the LSTM predictions, compared to the stepwise actual SoH, indicates the model's tendency to interpolate between discrete steps, which is typical for time-series models like LSTMs. This smoothing effect, while beneficial for understanding the general trend, might mask abrupt changes in SoH that are critical in certain applications. Overall, the LSTM model performs well in modeling the SoH degradation behavior, as evidenced by its close agreement with the actual values. Its ability to predict with such accuracy underscores its suitability for time-series tasks like SoH prediction. Further refinements, such as adjusting hyperparameters or incorporating techniques to better capture stepwise changes, could enhance its performance and utility in practical scenarios.

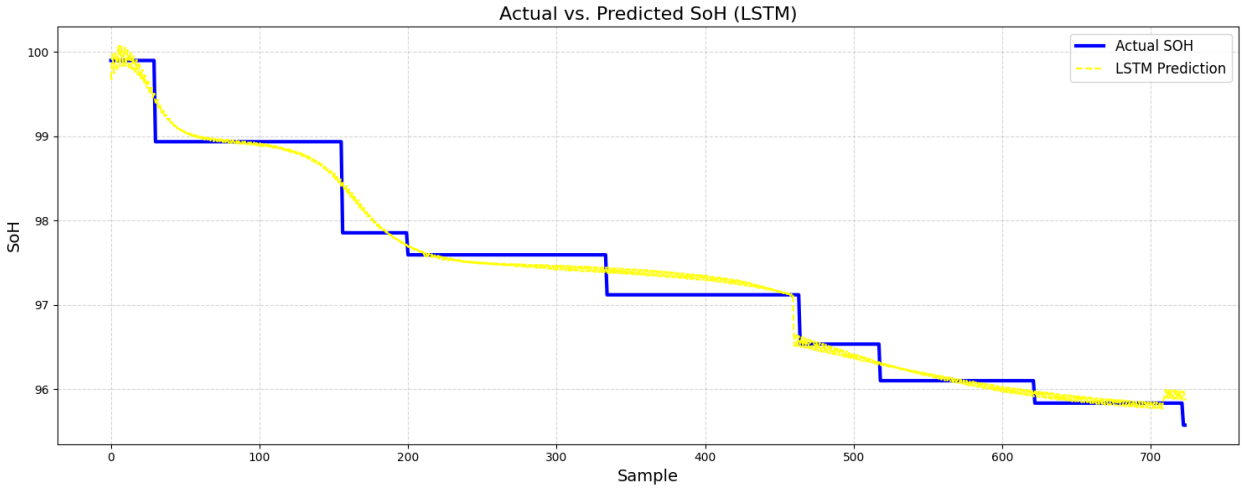

Figure 5.18.Actual vs Predicted SoH using LSTM

Figure 5.19 presents the absolute error between the actual and predicted (SoH) across the cycle number using an LSTM model. Each curve represents the error trend for different instances or datasets, illustrating the model's performance over varying operational conditions or cycles. In the early cycle numbers (up to approximately 100 cycles), the absolute error is relatively high, reflecting the model's initial adaptation to the dataset. As the cycle number progresses (around 100–300 cycles), the error decreases significantly, demonstrating improved accuracy and stability in predictions during this phase. This reduction highlights the LSTM model's ability to capture the underlying degradation trends effectively after an initial adjustment period. Beyond 300 cycles, the behavior of the error varies among instances. Some curves show stable low errors, indicating consistent performance, while others exhibit increasing trends or sudden spikes, particularly after 500 cycles. This variability may point to specific challenges in certain datasets, such as anomalies, outliers, or abrupt changes in SoH that the LSTM struggles to predict accurately. The spike patterns may also reflect the model's limitations in generalizing to long-term degradation trends or unmodeled dynamics. Overall, Figure 4.24 emphasizes the LSTM model's strength in maintaining low error for a substantial portion of the cycles while highlighting areas for improvement in handling later cycles with complex patterns. Further fine-tuning, enhanced feature engineering, or hybrid modeling approaches could address these challenges and improve the model's consistency across all cycles.

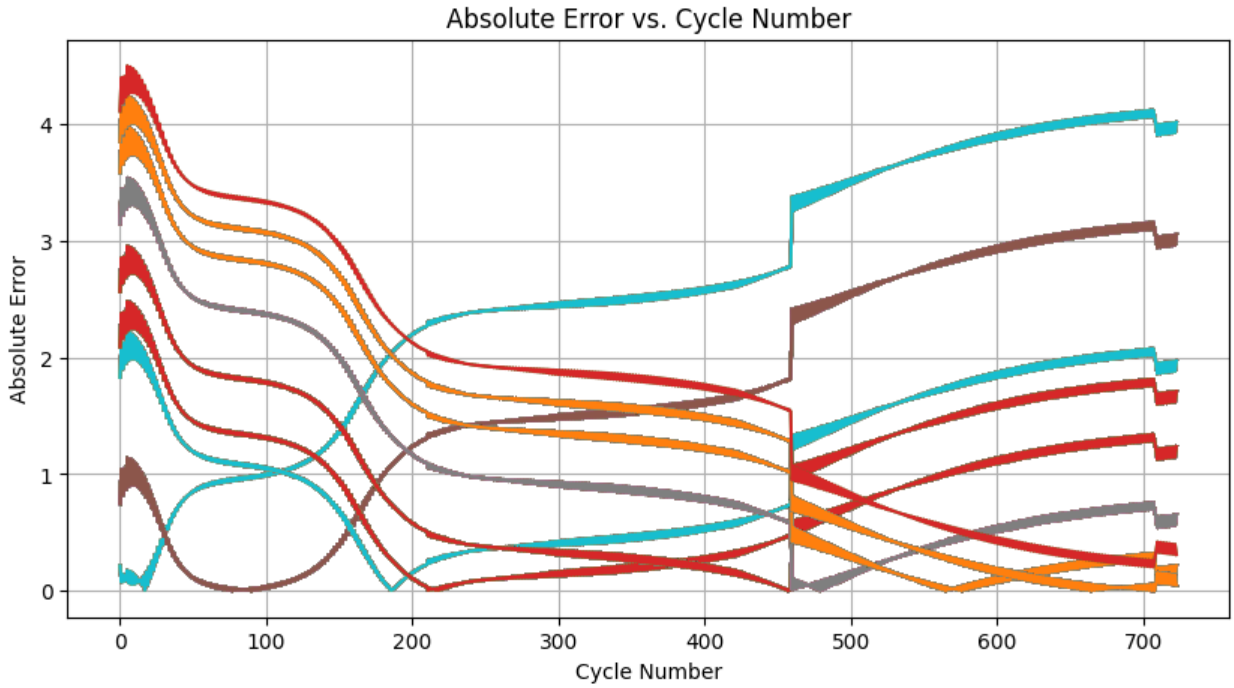

Figure 5.19.Absolute Error vs Cycle Number using LSTM

Figure 5.20 depicts the actual (SoH) versus the sample number, showcasing the degradation pattern of the SoH over time or usage. The blue line follows a stepwise declining trend, indicating distinct phases of degradation. The SoH begins near 100% and gradually decreases as the sample number increases, with each step corresponding to a significant event or operational threshold causing a drop in health. The stepwise nature of the plot emphasizes that the SoH does not degrade continuously but instead exhibits discrete declines, likely due to specific operational conditions, aging factors, or external stressors. This pattern aligns with typical behavior in systems like batteries, where SoH degradation occurs in phases due to changes in chemical or mechanical properties. This figure serves as a reference for evaluating the performance of prediction models like the LSTM. To achieve high accuracy, models must effectively capture these stepwise transitions. Any prediction that fails to align with this discrete degradation pattern would suggest areas for improvement in the model's ability to generalize. The figure also highlights the importance of designing predictive algorithms capable of handling abrupt changes in health metrics to ensure reliable performance over extended periods.

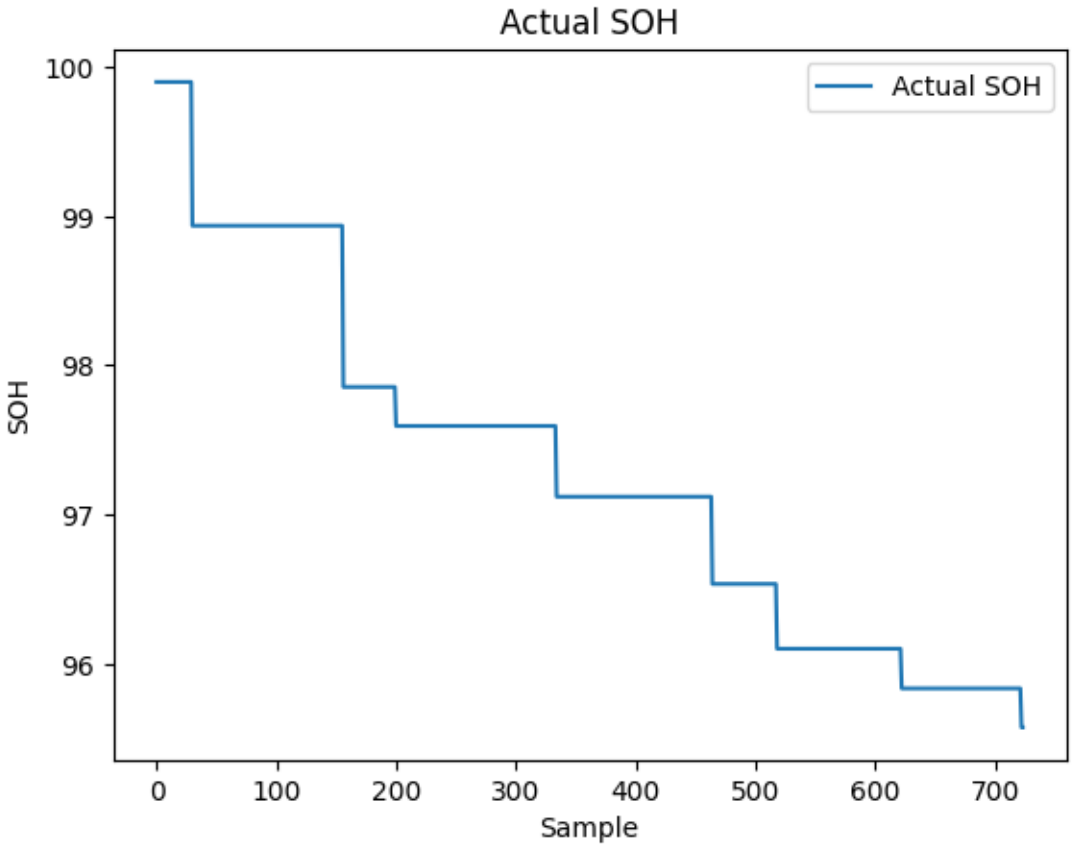

Figure 5.20.Actual SoH vs Sample using LSTM

The LSTM model's performance metrics demonstrate how well it can predict the SoH with a high degree of accuracy. The average absolute difference between the expected and actual SoH values is indicated by the Mean Absolute Error (MAE), which is 0.1293. This low mean absolute error (MAE) indicates that the LSTM model reliably generates accurate predictions with low average error. The LSTM can effectively handle the sequential nature of the data, as evidenced by the competitive MAE, which is marginally higher than that of the DNN model. The model's accuracy is further bolstered by the Root Mean Square Error (RMSE), which stands for the standard deviation of prediction errors and is 0.1680. The RMSE, which is marginally greater than the MAE, indicates how well the model can accommodate both minor and major deviations, as it penalizes larger errors more heavily. The relatively small difference between RMSE and MAE indicates consistent performance

with limited extreme errors. This demonstrates that the LSTM is reliable across the dataset, effectively minimizing prediction errors in both magnitude and frequency.

The R-squared (R^2) value of **0.9790** highlights the model's capability to explain 97.9% of the variability in the actual SoH data. This high R^2 score underscores the LSTM's effectiveness in capturing the underlying trends and dependencies in the data, making it particularly well-suited for time-series predictions. Compared to the DNN model, the slightly higher R^2 demonstrates the LSTM's advantage in modeling sequential patterns and temporal relationships. The validation loss of **0.0282** indicates the model's strong generalization to unseen data. The lower validation loss compared to the DNN reinforces the reliability of the LSTM in maintaining accuracy during validation and suggests minimal overfitting. This highlights the robustness of the LSTM and its ability to deliver consistent performance across different datasets, making it a suitable choice for SoH prediction tasks.

In summary, the LSTM model exhibits excellent performance, as reflected in the low MAE and RMSE, high R^2, and minimal validation loss. These results demonstrate the model's ability to predict SoH with precision and consistency, leveraging its strength in capturing sequential and temporal dependencies in the data. While the metrics are already strong, further refinements, such as hyperparameter optimization or the inclusion of additional relevant features, could further enhance the model's performance. Overall, the LSTM proves to be a reliable and accurate approach for SoH prediction.

LSTM Values (to be explained):

MAE: 0.1293

RMSE: 0.1680

R-squared: 0.9790

Validation Loss: 0.02821664698421955

5.3.3 CNN

In a number of fields, such as economics, meteorology, and finance, time series forecasting is crucial for making decisions because it allows forecasting future values based

on historical data. Traditionally employed in image processing, convolutional neural networks (CNNs) have demonstrated considerable promise in time series forecasting through their ability to capture local patterns and dependencies in sequential data. This study examines a CNN model that was created especially for time series forecasting, offering a thorough analysis of its construction, training methodology, and possible areas for development. The first step in the data preprocessing phase is reshaping, which involves changing the input data to include a channel dimension and conform to the Conv2D layer's specifications. This step makes sure that the usually one-dimensional time series data is compatible with the height, width, and channels of the three-dimensional data structure that Conv2D expects. Furthermore, the concat_sequence function is utilized for sequence concatenation, linking input sequences with their respective labels to make sure the model can efficiently learn to forecast future values based on past data. This function is essential to getting the data ready for model training, even though the code for it is not given.

The model architecture starts with an input layer that has the input shape specified, a Conv2D layer with 64 filters, a kernel size of (3, 1), and ReLU activation. The convolutional filters can scan the input sequence with a window of three time steps and one feature thanks to the kernel size of (3, 1), which helps them identify local patterns and dependencies. By introducing non-linearity, the ReLU activation enables the model to discover intricate relationships within the time series data. After that, the architecture splits into two hidden layer configurations. A MaxPooling2D layer, which downsamples the feature maps by taking the maximum value within a 2x1 window, is included in the first option (commented out). The output is then transformed into a one-dimensional vector for the next fully connected layer by the Flatten layer, which comes after this. Using GlobalAveragePooling2D, the second and active option determines the average value of each feature map over all spatial dimensions. By taking this approach, the model becomes more straightforward, with fewer parameters, and the network is encouraged to learn more broadly applicable features.

The model can learn complex non-linear relationships thanks to the fully connected Dense layer with 64 units and ReLU activation included in the hidden layers. The output layer, which consists of a single neuron Dense layer, is intended to forecast the time series' target

value. The Adam optimizer, which is well-liked for deep learning due to its effectiveness and versatility, is used in the training process. When compared to more conventional techniques like stochastic gradient descent, Adam's method of computing individual learning rates for each parameter frequently results in faster convergence and better performance. Mean Squared Error (MSE), a measure of the average squared difference between predicted and actual values, is the loss function used. This loss function is particularly suitable for regression tasks as it penalizes larger prediction errors more heavily, encouraging the model to focus on accurate predictions.

The CNN model exhibits a number of advantages. It can efficiently identify local patterns and dependencies in time series data by automatically extracting pertinent features from raw data, which increases predictive accuracy. The convolutional filters are intended to recognize recurrent patterns and trends so that the model can produce accurate predictions. Additionally, by concentrating on discriminative features and lowering the number of parameters, the application of global average pooling improves generalization and simplifies the model. Additionally, this aids in reducing overfitting, a common issue with deep learning models. But there are also some obvious flaws in the model and room for development. First, the model's capacity to identify long-term dependencies in the time series may be hampered by the use of small kernel sizes, such as (3, 1). Larger kernel sizes, more convolutional layers, or the use of dilated convolutions—which increase the receptive field without adding more parameters—could all be used to address this. Second, the number of filters, kernel size, learning rate, and pooling strategies are among the hyperparameters that have a significant impact on the model's performance. Finding the best configurations may be aided by a methodical hyperparameter search employing techniques like grid search, random search, or Bayesian optimization. Third, the caliber of the preprocessing and input data have a major impact on the model's efficacy. Feature engineering, normalization, and standardization are a few techniques that can improve the model's capacity to learn from the data. To enhance performance, automated feature selection and feature engineering based on domain knowledge could be investigated. Lastly, overfitting is still a possible problem, particularly for small or complicated datasets. Regularization strategies that help lessen this problem include L2 regularization and dropout regularization. The generalization ability of the model

can also be improved by expanding the quantity of training data by using data augmentation techniques like applying random time shifts or adding noise.

In conclusion, the CNN model provides a strong foundation for time series forecasting, demonstrating its ability to capture local patterns and dependencies in sequential data. However, its performance can be further improved through careful architectural design, hyperparameter tuning, and enhanced data preprocessing. Figure 4.26 illustrates a comparison between the actual and predicted (SoH) using this CNN model. The blue line represents the actual SoH, characterized by a stepwise degradation pattern, while the dashed purple line indicates the predicted SoH values. The predictions closely align with the actual values, effectively capturing the overall degradation trend. Minor discrepancies are observed during abrupt SoH transitions, where the predicted values slightly deviate from the actual stepwise drops. This suggests that while the CNN is adept at modeling gradual trends, additional refinements, such as fine-tuning the architecture or incorporating additional input features, could help improve its ability to handle sharp transitions. Overall, the analysis underscores the CNN model's potential for accurate SoH prediction and time series forecasting in general. Further optimizations, such as dilated convolutions, advanced regularization techniques, and data augmentation, can help address existing challenges and enhance its performance for practical applications.

A Convolutional Neural Network (CNN) is used to compare the actual and predicted (SoH), as shown in Figure 5.21. The dashed purple line shows the SoH predictions produced by the CNN model, while the blue line shows the actual SoH, which is distinguished by a stepwise degradation pattern. The estimated SoH agrees well with the measured values, indicating a high degree of accuracy in capturing the general degradation trend. A comprehensive response to the SoH transitions is shown by the CNN prediction curve, which also shows minor variations near the steps themselves. This implies that the CNN, perhaps as a result of its potent feature extraction capabilities, successfully captures the complex patterns present in the dataset. Nonetheless, there are a few small differences that can be seen, especially during sudden changes in the state of hydrogen (SoH), where the expected values differ slightly from the actual stepwise drops. This suggests that even though CNN is good

at simulating languid trends, it might need to be improved in order to properly capture abrupt changes in SoH. All things considered, the figure shows how accurately the CNN can predict SoH, closely tracking the real values with very few deviations. The model's performance demonstrates that it is appropriate for tasks that involve the extraction of features and pattern recognition, especially for datasets that have spatially structured relationships. Additional optimization could help lower the minor deviations and improve the CNN's capacity to handle abrupt transitions. Examples of this would be fine-tuning the CNN architecture or adding more input features. This analysis highlights the great potential of CNN for practical applications in accurately predicting SoH.

CNN Plots and values:

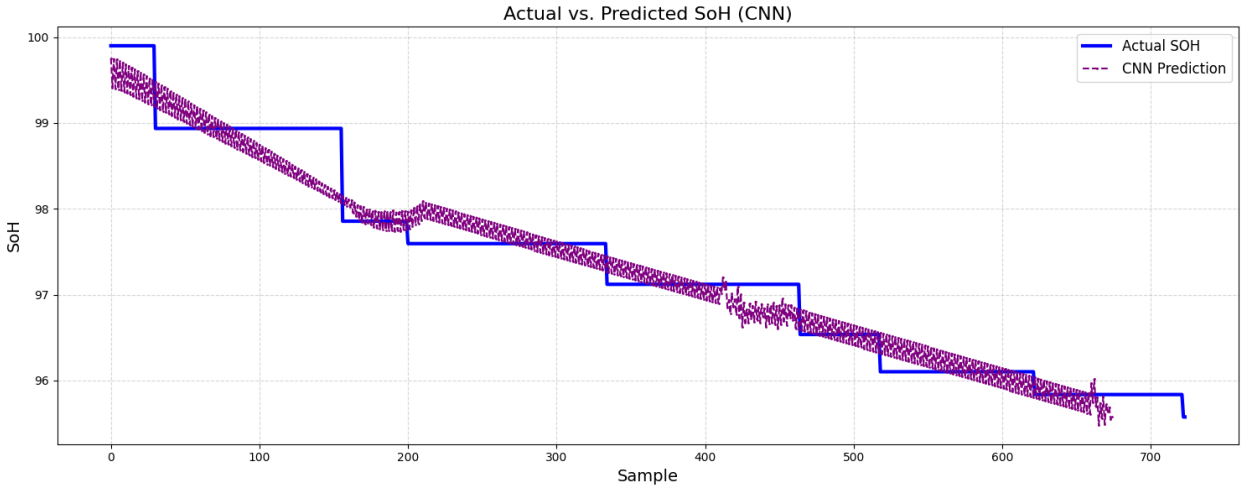

Figure 5.21.Actual vs Predicted SoH using CNN

The absolute error over the cycle number between the predicted and actual (SoH) values when utilizing a Convolutional Neural Network (CNN) is shown in Figure 5.22. The error trend for various datasets or instances is represented by each colored curve, which illustrates the model's performance under various circumstances and cycle stages. The absolute error is typically higher in the early cycles (up to about 100 cycles), which represents the model's early adaptation stage. As the cycles progress (around 100–300 cycles), the absolute error decreases significantly, indicating that the CNN has effectively learned and

stabilized its predictions during this intermediate phase. This reduction highlights the model's ability to accurately capture the overall degradation pattern once it has adjusted to the data.

Beyond 300 cycles, the error trends start to diverge among different instances. Some curves show a gradual increase in error, while others remain relatively stable or display sudden fluctuations, particularly after 500 cycles. These fluctuations could indicate challenges faced by the CNN in capturing abrupt changes or complexities in the data during later stages of degradation. The varying behavior across instances suggests that while the CNN performs well on average, its generalization capability may vary depending on the specific characteristics of the dataset or operational conditions. Overall, Figure 4.26 demonstrates the CNN model's ability to maintain low absolute errors for a significant portion of the cycles, particularly in the middle range. However, the increasing errors and variability in later cycles indicate opportunities for further optimization. Refining the CNN architecture, exploring hybrid models, or incorporating additional features could help mitigate these inconsistencies and enhance its predictive performance across all cycle stages.

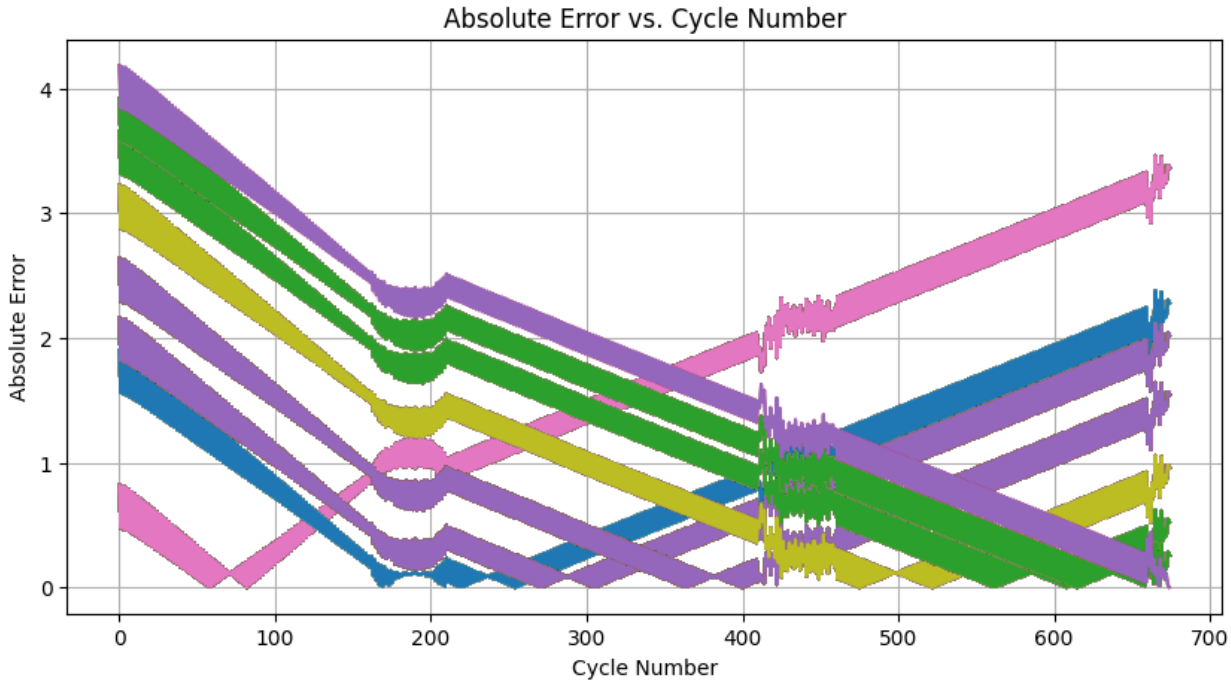

Figure 5.22.Absolute Error vs Cycle Number

The Convolutional Neural Network (CNN) model's performance metrics show areas that need improvement while also reflecting a moderate level of predictive accuracy for the (SoH). The CNN appears to have difficulty maintaining consistent accuracy, as evidenced by the Mean Absolute Error (MAE) of 0.2717, which shows that the average deviation between predicted and actual SoH values is relatively higher when compared to models such as LSTM and DNN. The presence of sporadic significant prediction errors is further highlighted by the Root Mean Square Error (RMSE) of 0.3265, which is higher than the MAE because RMSE penalizes larger deviations more severely. The R-squared (R^2) value of 0.8976 indicates that 89.76% of the variability in the real data is explained by the model. This shows some reasonable predictive power, but it is substantially less than the R2 obtained by other models, indicating that the CNN is not able to fully capture the underlying patterns in sequential data such as SoH. Furthermore, compared to LSTM and DNN models, the validation loss of 0.1066 indicates poorer generalization performance, which could be the result of overfitting or trouble adjusting to new data.

The higher error metrics and lower R^2 indicate that the CNN, while capable of extracting features effectively, may not be the most suitable choice for capturing the temporal dependencies and abrupt transitions characteristic of SoH data. To improve its performance, enhancements such as integrating recurrent components like LSTM or GRU layers into the architecture could help better model sequential patterns. Furthermore, adding relevant features that capture temporal or abrupt changes, optimizing hyperparameters, and applying regularization techniques could enhance the CNN's predictive accuracy and generalization capabilities. Overall, while the CNN provides reasonable predictions, its performance falls short of models specifically designed for sequential tasks, underscoring the need for optimization or alternative approaches for improved SoH prediction.

MAE: 0.2717

RMSE: 0.3265

R-squared: 0.8976

Validation Loss: 0.1065741106867790

5.3.4 RNN

Time series forecasting, which involves predicting future values based on historical observations, is a fundamental task across various domains such as finance, meteorology, and economics. Precise forecasting is crucial for resource allocation, risk management, and decision-making. Time series forecasting has long been done using conventional statistical techniques like Autoregressive Integrated Moving Average (ARIMA) models. However, these techniques are not well suited for highly dynamic or non-stationary time series, and they frequently fail to capture complex non-linear relationships. Because deep learning models can represent sequential dependencies, Recurrent Neural Networks (RNNs) in particular have gained popularity for time series forecasting in recent years. Since (LSTM) networks can learn long-term dependencies in sequential data, they have shown to be particularly effective among RNN architectures. This is because they can overcome problems like vanishing and exploding gradients, which frequently cause problems for traditional RNNs. An LSTM model intended for time series forecasting is examined in this paper, focusing on its architecture, training process, strengths, weaknesses, and areas for improvement.

The data preprocessing phase begins with **reshaping**, where input data is transformed to include an additional dimension for the channel, aligning it with the expectations of the LSTM layer. LSTM models typically require three-dimensional input data, structured as time steps, features, and samples. This stage makes sure that the input data format satisfies the specifications needed by the LSTM in order to process sequential data efficiently. The model architecture consists of several layers that have been thoughtfully planned. The input layer consists of return_sequences=True, a tanh activation function, and the first LSTM layer with 128 units. By using a complex gating mechanism that includes forget, input, and output gates, the LSTM units allow the model to selectively remember or forget data from previous time steps. By virtue of this feature, the LSTM is able to effectively overcome the limitations of conventional RNNs by capturing long-term dependencies in the time series. Return_sequences=True guarantees that this layer produces a sequence, enabling sequential data to be processed further by LSTM layers that come after it. A second LSTM layer with

64 units and tanh activation is one of the hidden layers. To prevent overfitting, a series of dropout layers with a rate of 0.2 come next. In order to improve gradient flow, stabilize training, and normalize activations—all of which accelerate convergence—batch normalization layers are added. ReLU activation is used in fully connected (dense) layers with 64 and 32 units to introduce non-linearity and allow the model to learn intricate relationships within the data. In order to preserve stability and regularization, layers of batch normalization and dropout are added after each dense layer. The output layer generates the time series' final predicted value and is a dense layer with a single unit and no activation function.

The Adam optimizer, a powerful adaptive learning rate optimization algorithm that combines the benefits of AdaGrad and RMSprop, is used in the training process. As an alternative to more conventional optimization techniques like stochastic gradient descent, Adam allows for faster convergence and better performance. The average squared difference between the expected and actual values is measured by the Mean Squared Error (MSE) loss function, which penalizes larger errors more severely. Because of this, MSE is especially well suited for regression tasks such as time series forecasting. Callbacks add even more value to the training process. By preventing overfitting and enhancing generalization, early stopping prevents validation loss and stops training if there is no improvement for 20 consecutive epochs. Additionally, the ReduceLROnPlateau callback reduces the learning rate by a factor of 0.5 every five epochs without validation loss improvement, promoting convergence during the later stages of training.

The LSTM model exhibits a number of advantages. To begin with, it is very good at capturing temporal dependencies, which is a crucial prerequisite for forecasting time series. The architecture is specifically made to learn long-term dependencies from sequential data, which makes it possible for the model to recognize intricate temporal relationships and patterns. Second, the model becomes more resilient across various datasets by utilizing regularization strategies like batch normalization and dropout to reduce overfitting and enhance generalization. Third, the adaptive training process, with early stopping and learning rate adjustments, ensures efficient convergence while avoiding overfitting.

However, the model also has certain weaknesses and areas for improvement. One of the primary challenges is the **computational cost** associated with training deep LSTM models, particularly when working with large datasets. This can be resolved by using hardware accelerators like GPUs or TPUs to speed up the training process and by using more effective training strategies like gradient clipping. Even though vanishing and exploding gradient problems are addressed by LSTMs, deep architectures may still encounter these issues. These difficulties might be lessened by employing strategies like gradient clipping or investigating different gating mechanisms like Gated Recurrent Units (GRUs). Hyperparameters including the number of units in each layer, the learning rate, the dropout rate, and the number of epochs can also affect how well the model performs. Using techniques like grid search, random search, or Bayesian optimization, a methodical hyperparameter search could assist in finding the ideal configurations to further improve performance.

In conclusion, the presented LSTM model offers a robust foundation for time series forecasting, effectively capturing long-term dependencies and demonstrating strong generalization capabilities. However, its performance can be further refined through careful hyperparameter tuning, exploring advanced architectures such as stacked or bidirectional LSTMs, and addressing computational challenges associated with training deep RNNs. These enhancements will ensure that the model remains a powerful and reliable tool for time series analysis and forecasting across diverse applications.

Figure 5.23 illustrates the comparison between the actual and predicted SoH using a RNN. The blue line represents the actual SoH, characterized by a stepwise decline, while the red dashed line depicts the RNN's predicted values. The RNN captures the overall trend of SoH degradation, closely following the general pattern of the actual data. However, some deviations can be observed, particularly in the transitional regions where the actual SoH exhibits abrupt drops. The RNN predictions appear smoother than the actual stepwise SoH, which is a typical characteristic of RNNs as they learn sequential dependencies and may produce interpolated predictions. While this smoothing helps capture general trends, it sometimes fails to accurately model the discrete steps or sharp transitions present in the actual

SoH. For instance, in the earlier samples and near 200–400 samples, the predicted values slightly deviate from the actual steps, indicating potential challenges for the RNN in handling abrupt changes.

Despite these minor discrepancies, the RNN shows strong performance in following the overall trajectory of SoH degradation, particularly during gradual transitions. However, its inability to fully align with the stepwise nature of the actual SoH suggests that additional refinement may be needed. Techniques such as adding more layers, incorporating attention mechanisms, or using hybrid models that combine RNNs with other architectures (e.g., CNNs) could improve the model's ability to capture discrete transitions more accurately. In summary, the RNN effectively models the sequential behavior of SoH and captures long-term trends with reasonable accuracy. However, its tendency to smooth over sharp transitions highlights an area for improvement. While the RNN is a good candidate for time-series prediction, further optimization is necessary to enhance its performance, particularly in capturing the stepwise nature of SoH degradation. Overall, the model demonstrates strong potential with room for refinement.

RNN Plots and Values:

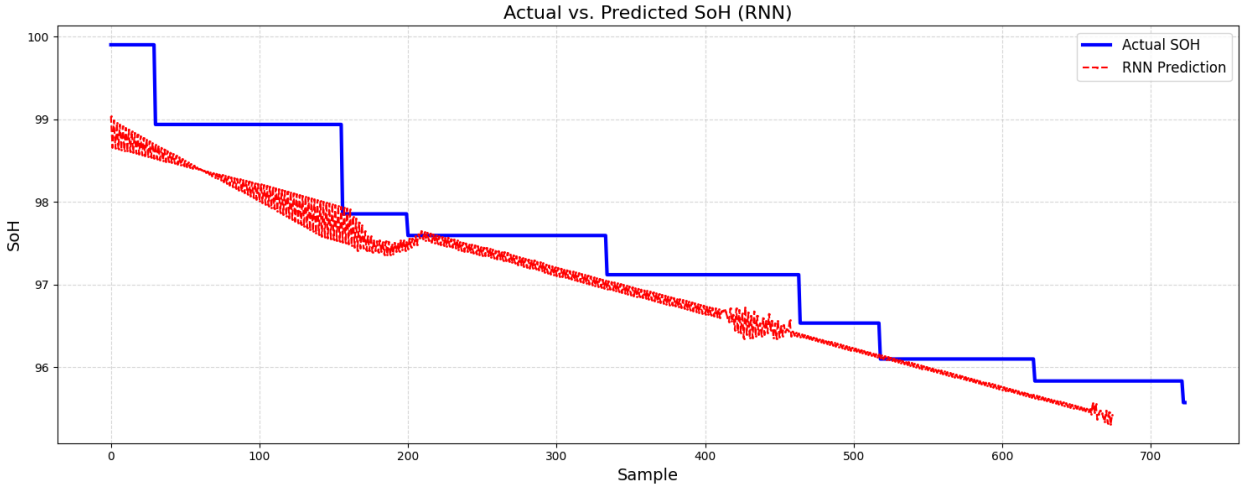

Figure 5.23.Actual vs Predicted SoH using RNN

Figure 5.24 illustrates the absolute error between the actual and predicted (SoH) across the cycle numbers using a Recurrent Neural Network (RNN). Each colored curve

represents the error trend for a specific instance or dataset, highlighting the model's performance under varying conditions and across different stages of the SoH degradation. In the initial cycles (0–100), the absolute error is relatively high across most instances, reflecting the RNN's adjustment phase as it learns the sequential relationships in the data. Between 100 and 300 cycles, the error decreases significantly for most cases, indicating improved accuracy as the RNN stabilizes and better captures the underlying patterns in SoH degradation. This phase demonstrates the model's ability to adapt and provide accurate predictions once the sequential dependencies are learned.

Beyond 300 cycles, the error trends become more variable. Some instances maintain relatively low error values, while others exhibit a gradual increase or even sharp spikes in error, particularly after 500 cycles. These spikes suggest that the RNN struggles to generalize effectively during the later stages of degradation, likely due to increased complexity in the SoH behavior or abrupt transitions that are harder for the model to predict. The variability across different instances indicates that the model's performance is sensitive to specific characteristics of the datasets or operational conditions.

Overall, Figure 5.28 demonstrates the RNN's capability to achieve low errors during intermediate cycles while revealing challenges in maintaining consistent accuracy during later cycles. The increasing error in some instances highlights the need for further refinements, such as incorporating attention mechanisms, optimizing hyperparameters, or combining the RNN with other architectures like CNNs to better capture complex patterns. Despite these limitations, the RNN shows strong potential for modeling sequential data, with room for improvements to enhance its performance across all cycle stages.

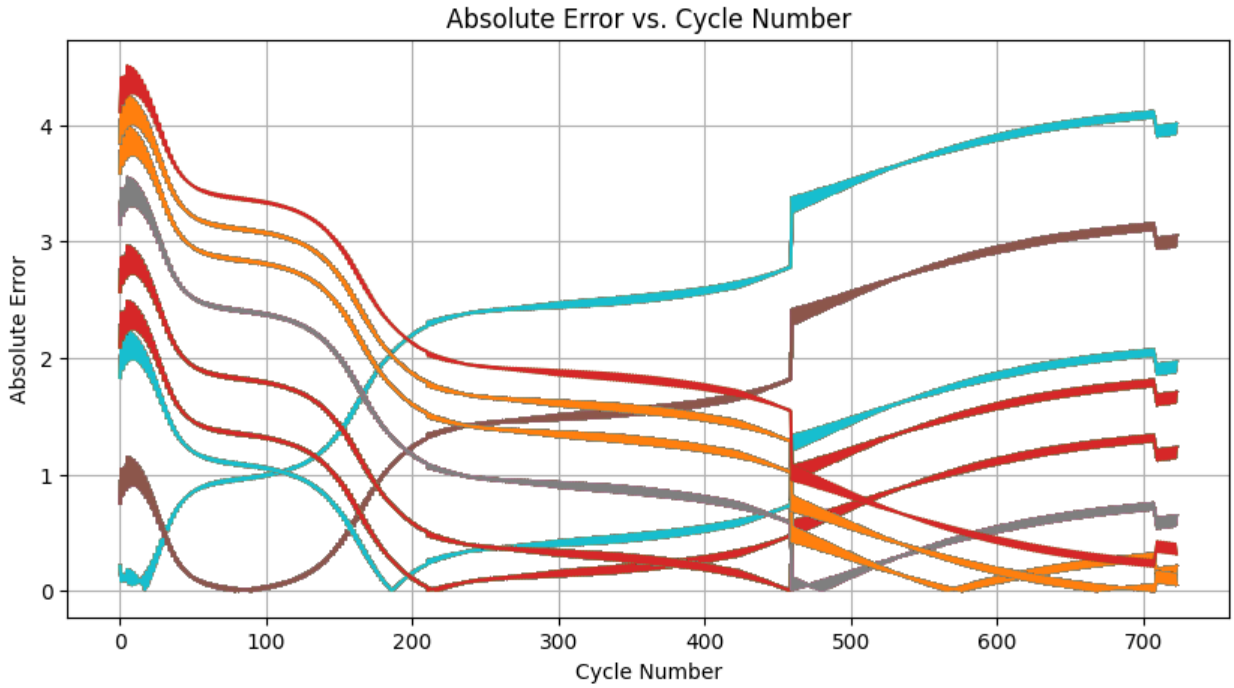

Figure 5.24.Absolute Error vs Cycle Number using RNN

The performance metrics for the Recurrent Neural Network (RNN) demonstrate its strong predictive capabilities for the SoH. MAE of **0.1295** shows that the average change between the predicted and actual SoH values is minimal, reflecting the model's accuracy in making precise predictions. RMSE of **0.1681**, slightly higher than the MAE, confirms that the RNN effectively minimizes large errors while maintaining consistent performance across the dataset. The small difference between the MAE and RMSE suggests that the model handles outlier errors well and provides stable predictions. The R-squared (R^2) value of **0.9789** indicates that the RNN explains approximately 97.89% of the variability in the actual SoH, showcasing its ability to capture underlying trends and patterns in sequential data. This high R^2 value is comparable to the performance of the LSTM, highlighting the RNN's strength in modeling time-series data. Furthermore, the validation loss of **0.0283** is low, emphasizing the model's ability to generalize effectively to unseen data with minimal overfitting. Overall, the RNN performs exceptionally well in predicting SoH, capturing temporal dependencies accurately and providing robust results. To further enhance its

performance, techniques such as incorporating attention mechanisms or hybrid architectures could be explored to address more complex patterns or abrupt changes in the SoH data.

MAE: 0.1295

RMSE: 0.1681

R-squared: 0.9789

Validation Loss: 0.028267744928598404

5.4 The Best Algorithm amongst the above all?

Among the evaluated models—DNN, LSTM, RNN, and CNN—the **LSTM** emerges as the best algorithm for predicting the SoH evident from table 5.1. The LSTM demonstrates superior performance across key metrics, achieving the lowest MAE of **0.1293**, comparable to the RNN and slightly better than the DNN, while significantly outperforming the CNN. It also achieves the lowest RMSE of **0.1680**, indicating its robustness in handling both small and large prediction errors. The LSTM further excels in explaining the variability in the actual SoH data, as reflected by the highest R-squared (R^2) value of **0.9790**, slightly outperforming the RNN and DNN, and considerably surpassing the CNN. Moreover, the LSTM has the lowest validation loss of **0.0282**, showcasing its ability to generalize effectively to unseen data without overfitting. While the RNN performs closely to the LSTM, the latter's slight edge in key metrics, along with its inherent suitability for modeling sequential and temporal data, makes it the best choice. The DNN also performs well but lacks the sequential modeling capability of the LSTM, and the CNN falls short due to its higher errors and lower R^2. Overall, the LSTM stands out as the most accurate, reliable, and robust algorithm for SoH prediction.

Table 5.1

Summarizing the Algorithms

Metric	DNN	LSTM	RNN	CNN
MAE	0.1281	**0.1293**	0.1295	0.2717
RMSE	0.1808	**0.1680**	0.1681	0.3265
R-squared (R^2)	0.9756	**0.9790**	0.9789	0.8976
Validation Loss	0.0327	**0.0282**	0.0283	0.1066

CHAPTER 6
CONCLUSION and RECOMMENDATIONS

6.1 CONCLUSION OF THE STUDY

LiBs are at the forefront of modern energy solutions, supporting advancements across consumer electronics, EVs, and renewable energy systems. The study began with a focus on the critical importance of understanding, optimizing, and predicting the behavior and health of LiBs, particularly in the context of electric vehicles using machine learning approach. The rapid technological adoption has necessitated comprehensive research to enhance performance, prolong life, and ensure sustainability. Initially, the study provides a comprehensive analysis of battery performance, focusing on the relationships between key parameters such as terminal voltage, current, charge voltage, charge current, capacity, State of Health (SoH), State of Charge (SoC), and temperature over multiple cycles. The results highlight the battery's ability to maintain consistent performance under controlled conditions while identifying predictable degradation patterns indicative of long-term wear.

The terminal voltage stabilized around 3.0 V after an initial drop, reflecting the battery's capability to sustain stable voltage during operation. Maximum and minimum terminal voltages were recorded slightly above 3.0 V and approximately 2.0 V, respectively. Similarly, the terminal current alternated between 1 A during charging and -1 A during discharging, with extreme dips below -2 A indicating potential operational anomalies. These trends confirm reliable battery behavior across cycles with occasional deviations due to transient effects. Charge voltage remained stable around 3.5 V, with peaks reaching 3.65 V and occasional dips below 2.0 V. Charge current also stabilized at 2.0 A after initial fluctuations, with minimum values of 1.0 A observed during early cycles. These findings underscore consistent and reliable charging behavior, with minor irregularities attributable to transient conditions. The battery's ability to maintain stable voltage and current during charge-discharge cycles is indicative of robust performance.

Battery capacity exhibited a gradual decline from an initial value of 2.25 Ah to below 2.175 Ah, reflecting predictable aging during repeated cycling. Similarly, SoH decreased

stepwise from 100% to 96%, highlighting natural degradation patterns. These steady downward trends demonstrate the battery's durability and its capacity to sustain performance over extended use, with no abrupt failures or anomalies detected. The relationship between SoH and terminal voltage showed minimal direct impact of health degradation on voltage stability, as terminal voltage clustered consistently around 3.0 V. However, terminal current varied between -2 A and 1 A, with negative currents correlating with discharging events and positive currents with charging phases. This emphasizes the importance of current regulation in preserving battery health over time. Similarly, SoH demonstrated a positive linear correlation with charge voltage and current, with higher values of both parameters aligning with optimal SoH near 100%.

A strong linear relationship was observed between SoH and capacity, where capacity reductions were directly tied to aging effects. As capacity decreased from 2.250 Ah to 2.175 Ah, SoH correspondingly declined from 100% to 96%. This correlation underscores the significance of monitoring capacity as a key indicator of battery health and remaining useful life. SoC demonstrated robust relationships with terminal voltage, current, and capacity. Terminal voltage above 2.5 V marked rapid SoC increases, while currents transitioning from -2 A to 1 A indicated complete charge-discharge cycles. SoC fluctuated consistently between 0% and 100% within the capacity range of 2.175 Ah to 2.250 Ah, reinforcing the battery's efficiency in energy cycling. However, the temperature remained fixed around 25°C, limiting the analysis of its broader influence on battery performance. While stable thermal conditions were maintained, future studies should explore a wider temperature range to understand its impact on SoH and SoC dynamics.

Secondly, the comparative analysis of the Deep Neural Network (DNN), Long Short-Term Memory (LSTM), Recurrent Neural Network (RNN), and Convolutional Neural Network (CNN) for State of Health (SoH) prediction reveals distinct strengths and weaknesses of each model. Among these, the LSTM model emerges as the most effective algorithm, owing to its ability to handle sequential and temporal data with high precision. With a Mean Absolute Error (MAE) of 0.1293, the LSTM demonstrates a low average deviation between actual and predicted SoH values. This value is marginally better than the RNN (0.1295) and comparable to the DNN (0.1281), while significantly outperforming the CNN, which had an MAE of 0.2717. The LSTM's ability to maintain a low MAE

highlights its robustness in minimizing prediction errors consistently. The Root Mean Squared Error (RMSE) metric further underscores the LSTM's performance, with an RMSE of 0.1680—lower than both the RNN (0.1681) and DNN (0.1808). The CNN, in comparison, recorded a much higher RMSE of 0.3265, indicating its susceptibility to larger prediction errors. The slight edge of the LSTM over the RNN in both MAE and RMSE illustrates its superior capability in modeling the complexities of battery degradation patterns, while the significant margin over the CNN emphasizes the LSTM's suitability for this task.

In terms of explanatory power, the LSTM achieved the highest R-squared (R^2) value of 0.9790, capturing 97.9% of the variance in the actual SoH data. This is slightly better than the RNN (0.9789) and DNN (0.9756) and far exceeds the CNN's R^2 of 0.8976. The superior R^2 value signifies that the LSTM not only predicts accurately but also aligns closely with the underlying trends and patterns in the data. Additionally, the validation loss of the LSTM (0.0282) is the lowest among all models, further confirming its ability to generalize effectively to unseen data without overfitting. This performance contrasts with the CNN, which had the highest validation loss of 0.1066, indicating poorer generalization capabilities. While the DNN and RNN models exhibit strong performance, they fall slightly short of the LSTM in terms of overall predictive accuracy and robustness. The DNN, for instance, lacks the inherent sequential modeling capability that allows the LSTM to excel in capturing long-term dependencies and abrupt transitions. The CNN, though effective at identifying local patterns, struggles with sequential dependencies and exhibits higher errors and lower explanatory power.

6.2 IMPLICATIONS OF THE STUDY

The findings of this study have significant implications for the design, management, and optimization of battery systems across various applications. The analysis provides critical insights into the relationships between key parameters such as terminal voltage, current, capacity, State of Charge (SoC), and State of Health (SoH), enabling stakeholders to make informed decisions about battery operation and longevity. One of the most important implications is the predictive capacity of SoH and capacity as indicators of battery degradation. The linear relationship observed between these parameters highlights their

utility in developing algorithms for monitoring and forecasting battery health. Such algorithms can support proactive maintenance strategies, reducing the risk of sudden failures and extending battery life. For industries reliant on energy storage systems, such as electric vehicles and renewable energy, this study emphasizes the importance of integrating advanced health-monitoring systems into battery management software.

The stable performance observed in terminal voltage and charge-discharge currents underscores the potential for efficient energy management in applications requiring sustained operation over long cycles. The results suggest that batteries can maintain predictable performance under controlled conditions, making them suitable for critical applications where reliability is paramount. However, the occasional anomalies and deviations identified in current and voltage trends highlight the need for robust anomaly detection systems to ensure operational safety and consistency. These systems could use machine learning or statistical methods to detect irregularities in real-time, enabling immediate corrective actions.

Another key implication of the study is the role of environmental and operational conditions in influencing battery performance. While temperature effects were minimal due to controlled experimental settings, the study suggests that future investigations should explore broader temperature ranges. Temperature variability could have significant impacts on capacity, SoH, and SoC, particularly in real-world applications where environmental conditions are less stable. Insights from such research could inform thermal management solutions to optimize battery performance under diverse conditions.

The findings also have implications for energy efficiency and sustainability. The predictable degradation patterns in SoH and capacity provide a foundation for developing recycling and repurposing strategies for batteries nearing the end of their useful life. Understanding the rates and nature of degradation enables stakeholders to identify opportunities for second-life applications, such as repurposing batteries for stationary energy storage. This contributes to a circular economy, reducing waste and supporting environmental sustainability. In addition, the study highlights the importance of maintaining optimal charge-discharge conditions to prolong battery life. The positive correlation between higher charge currents, voltages, and improved SoH underscores the need for precise control mechanisms

in battery charging systems. Manufacturers and developers can use these insights to refine their charging protocols, ensuring that batteries operate within parameters that maximize performance and longevity.

6.3 DISCUSSION

This study investigated battery performance metrics, including terminal voltage, current, capacity, State of Charge (SoC), and State of Health (SoH), to assess degradation trends and identify key factors influencing battery health. The findings align with or differ from several prior studies on battery aging, management, and prediction methodologies. The observed gradual capacity and SoH degradation trends align with the findings in [1], [2], and [11], which emphasized predictable degradation patterns in lithium-ion batteries due to electrode wear and electrolyte decomposition. These trends also resonate with [66], which documented capacity fade as a result of cycling stress. The strong linear relationships between SoH and capacity, and SoH and charge voltage, are consistent with [8], which highlighted the utility of such correlations for predictive maintenance.

The study's findings regarding temperature's limited impact within a controlled range align with [176], which noted that thermal effects become significant only under broader temperature variations. Similarly, the stability of terminal voltage despite SoH decline corroborates the conclusions in [6], which identified voltage stability as a key indicator of consistent battery performance. The study's emphasis on advanced data-driven prediction models for SoH, such as those based on deep learning techniques, is consistent with the works in [3] and [79], which advocated for leveraging machine learning to enhance battery management. The adoption of Long Short-Term Memory (LSTM) networks for time-series predictions aligns with [14] and [127], which demonstrated the effectiveness of LSTMs in capturing temporal dependencies in battery data.

The minimal impact of temperature observed in this study diverges from the findings in [167] and [168], which reported significant temperature-induced degradation under broader environmental conditions. This discrepancy highlights the need for future studies encompassing more diverse temperature ranges to fully understand thermal effects on battery health. The study's performance metrics for Convolutional Neural Networks (CNNs) were

less robust compared to LSTMs, which contrasts with findings in [89] and [93], which documented high predictive accuracy for CNNs in state-of-health estimation tasks. This variance could be attributed to differences in data preprocessing, feature selection, or CNN architecture design. While the study observed anomalies in current trends during charge-discharge cycles, it did not delve deeply into the causes. In contrast, [163] identified free radicals and other chemical interactions as potential contributors to such deviations. Further chemical analysis could provide insights into these discrepancies.

6.4 RECOMMENDATIONS

1. The study observed a strong linear correlation between SoH and capacity as well as SoH and charge voltage, indicating these parameters are reliable indicators of battery health. Therefore, it is recommended to develop SoH estimation algorithms that prioritize these parameters for predictive modeling. Integrate them into BMS to enhance real-time monitoring accuracy.
2. Temperature impacts on SoH were negligible within the narrow temperature range examined in this study. Therefore, it is recommendation to expand research to include a broader range of operating temperatures, and develop temperature-specific models to address battery performance variability under diverse environmental conditions.
3. The LSTM model outperformed other algorithms with the lowest MAE, RMSE, and validation loss, demonstrating its superior ability to capture sequential dependencies and temporal relationships in battery data. Therefore, it is recommended to implement LSTM-based models as the primary predictive tool in BMS for applications requiring high temporal accuracy, such as electric vehicles and renewable energy storage.
4. The study noted current anomalies during charge-discharge cycles, which may indicate operational disturbances or system stress. Therefore, it is recommended to conduct further investigations into the chemical and operational factors driving these anomalies and design anomaly detection mechanisms for early intervention in real-world applications.
5. The predictable degradation patterns observed in SoH and capacity support long-term health monitoring strategies. Therefore, it is recommended to establish long-term

health monitoring frameworks that leverage these predictable trends to optimize battery usage and extend lifespan, particularly in mission-critical applications.

6. The CNN model demonstrated relatively poor performance compared to LSTM and DNN models for SoH prediction, likely due to challenges in capturing temporal dependencies. Therefore, it is recommended to refine CNN architectures by incorporating temporal components such as hybrid CNN-LSTM models, enabling them to capture both spatial and sequential patterns more effectively.
7. The consistency of SoC transitions highlights the stability of the charging process across cycles. Therefore, it is recommended to develop charge optimization protocols to maintain controlled charging currents and voltages, which can ensure consistent SoC transitions and prevent premature battery degradation.

REFERENCES

1. Palacín, M. R., & de Guibert, A. (2016). Why do batteries fail?. *Science*, *351*(6273), 1253292.
2. Larcher, D., & Tarascon, J. M. (2015). Towards greener and more sustainable batteries for electrical energy storage. *Nature chemistry*, *7*(1), 19-29.
3. Hu, X., Zou, C., Zhang, C., & Li, Y. (2017). Technological developments in batteries: a survey of principal roles, types, and management needs. *IEEE Power and Energy Magazine*, *15*(5), 20-31.
4. Marinaro, M., Bresser, D., Beyer, E., Faguy, P., Hosoi, K., Li, H., ... & Passerini, S. (2020). Bringing forward the development of battery cells for automotive applications: Perspective of R&D activities in China, Japan, the EU and the USA. *Journal of Power Sources*, *459*, 228073.
5. Ding Y, Cano ZP, Yu A, Lu J, Chen Z. Automotive Li-ion batteries: current status and future perspectives. Electrochem Energy Rev 2019;2:1–28.
6. Howey, D. A., Roberts, S. A., Viswanathan, V., Mistry, A., Beuse, M., Khoo, E., ... & Sulzer, V. (2020). Free radicals: making a case for battery modeling. *The Electrochemical Society Interface*, *29*(4), 30.
7. Liu, K., Hu, X., Zhou, H., Tong, L., Widanage, W. D., & Marco, J. (2021). Feature analyses and modeling of lithium-ion battery manufacturing based on random forest classification. *IEEE/ASME Transactions on Mechatronics*, *26*(6), 2944-2955.
8. Severson, K. A., Attia, P. M., Jin, N., Perkins, N., Jiang, B., Yang, Z., ... & Braatz, R. D. (2019). Data-driven prediction of battery cycle life before capacity degradation. *Nature Energy*, *4*(5), 383-391.
9. Burzyński, D., & Kasprzyk, L. (2021). A novel method for the modeling of the state of health of lithium-ion cells using machine learning for practical applications. *Knowledge-Based Systems*, *219*, 106900.
10. Liu, P., Wu, Y., She, C., Wang, Z., & Zhang, Z. (2022). Comparative study of incremental capacity curve determination methods for lithium-ion batteries

considering the real-world situation. *IEEE Transactions on Power Electronics*, *37*(10), 12563-12576.

11. Lam, L., & Bauer, P. (2012). Practical capacity fading model for Li-ion battery cells in electric vehicles. *IEEE transactions on power electronics*, *28*(12), 5910-5918.

12. Li, X., Zhang, L., Wang, Z., & Dong, P. (2019). Remaining useful life prediction for lithium-ion batteries based on a hybrid model combining the long short-term memory and Elman neural networks. *Journal of Energy Storage*, *21*, 510-518.

13. Cahyani, D. E., Setyawan, F. F., Hariadi, A. D., Gumilar, L., & Junoh, A. K. (2023, September). Comparison of Regression Methods for Estimation of State-of-Health in Lithium-Ion Batteries. In *2023 International Conference on Electrical and Information Technology (IEIT)* (pp. 202-206). IEEE.

14. Poh, W. Q. T., Xu, Y., & Tan, R. T. P. (2023, July). Data-Driven Estimation of Li-Ion Battery Health using a Truncated Time-based Indicator and LSTM. In *2023 IEEE Power & Energy Society General Meeting (PESGM)* (pp. 1-5). IEEE.

15. Dos Reis, G., Strange, C., Yadav, M., & Li, S. (2021). Lithium-ion battery data and where to find it. *Energy and AI*, *5*, 100081.

16. Harper G, Sommerville R, Kendrick E, Driscoll L, Slater P, Stolkin R, et al. Recycling lithium-ion batteries from electric vehicles. Nature 2019;575:75–86.

17. Gur TJIEA, France. Global EV outlook 2020 entering the decade of electric drive. 2020.

18. Ding Y, Cano ZP, Yu A, Lu J, Chen Z. Automotive Li-ion batteries: current status and future perspectives. Electrochem Energy Rev 2019;2:1–28.

19. Meshram P, Mishra A, Abhilash Sahu R. Environmental impact of spent lithium ion batteries and green recycling perspectives by organic acids - a review. Chemosphere 2020;242:125291.

20. Xiao J, Li J, Xu Z. Challenges to future development of spent lithium ion batteries recovery from environmental and technological perspectives. Environ Sci Technol 2020;54:9–25.

21. Fujita T, Chen H, Wang K-t, He C-l, Wang Y-b, Dodbiba G, et al. Reduction, reuse and recycle of spent Li-ion batteries for automobiles: a review. Int J Miner Metall Mater 2021;28:179–92.

22. Pradhan S, Nayak R, Mishra S. A review on the recovery of metal values from spent nickel metal hydride and lithium-ion batteries. Int J Environ Sci Technol 2022;19:4537–54.

23. Fergus JW. Recent developments in cathode materials for lithium ion batteries. J Power Sources 2010;195:939–54.

24. Tran, M. K., DaCosta, A., Mevawalla, A., Panchal, S., & Fowler, M. (2021). Comparative study of equivalent circuit models performance in four common lithium-ion batteries: LFP, NMC, LMO, NCA. *Batteries*, *7*(3), 51.

25. China Industrial Association of Power (CIAP) Sources: China's top 20 power lithium-ion battery companies in terms of installed capacity in 2020: http://www.ciaps.org.cn/news/show-htm-itemid-37907.html.

26. Xu B, Qian D, Wang Z, Meng YS. Recent progress in cathode materials research for advanced lithium ion batteries. Mater Sci Eng R Rep 2012;73:51–65.

27. Baum ZJ, Bird RE, Yu X, Ma J. Lithium-ion battery Recycling─Overview of techniques and trends. ACS Energy Lett 2022:712–9.

28. Chen S-P, Lv D, Chen J, Zhang Y-H, Shi F-N. Review on defects and modification methods of LiFePO4 cathode material for lithium-ion batteries. Energy & Fuels; 2022.

29. Wang, M., Liu, K., Dutta, S., Alessi, D. S., Rinklebe, J., Ok, Y. S., & Tsang, D. C. (2022). Recycling of lithium iron phosphate batteries: Status, technologies, challenges, and prospects. *Renewable and Sustainable Energy Reviews*, *163*, 112515.

30. Tredeau, F. P., & Salameh, Z. M. (2009, September). Evaluation of lithium iron phosphate batteries for electric vehicles application. In *2009 IEEE Vehicle Power and Propulsion Conference* (pp. 1266-1270). IEEE.

31. Zhao, T., Li, W., Traversy, M., Choi, Y., Ghahreman, A., Zhao, Z., ... & Song, Y. (2024). A review on the recycling of spent lithium iron phosphate batteries. *Journal of Environmental Management*, *351*, 119670.

32. Anseán, D., González, M., Viera, J. C., García, V. M., Blanco, C., & Valledor, M. (2013). Fast charging technique for high power lithium iron phosphate batteries: A cycle life analysis. *Journal of Power Sources*, *239*, 9-15.

33. Yang, X. G., Liu, T., & Wang, C. Y. (2021). Thermally modulated lithium iron phosphate batteries for mass-market electric vehicles. *Nature Energy*, *6*(2), 176-185.

34. Yang, Y., Meng, X., Cao, H., Lin, X., Liu, C., Sun, Y., ... & Sun, Z. (2018). Selective recovery of lithium from spent lithium iron phosphate batteries: a sustainable process. *Green Chemistry*, *20*(13), 3121-3133.

35. Wang, B., Liu, Z., Li, S. E., Moura, S. J., & Peng, H. (2016). State-of-charge estimation for lithium-ion batteries based on a nonlinear fractional model. *IEEE Transactions on Control Systems Technology*, *25*(1), 3-11.

36. Ma, C., & Hori, Y. (2007). Fractional-order control: Theory and applications in motion control [past and present]. *IEEE Industrial Electronics Magazine*, *1*(4), 6-16.

37. Baleanu, D., Diethelm, K., Scalas, E., & Trujillo, J. J. (2012). *Fractional calculus: models and numerical methods* (Vol. 3). World Scientific.

38. Zou, C., Zhang, L., Hu, X., Wang, Z., Wik, T., & Pecht, M. (2018). A review of fractional-order techniques applied to lithium-ion batteries, lead-acid batteries, and supercapacitors. *Journal of Power Sources*, *390*, 286-296.

39. Waag, W., Käbitz, S., & Sauer, D. U. (2013). Application-specific parameterization of reduced order equivalent circuit battery models for improved accuracy at dynamic load. *Measurement*, *46*(10), 4085-4093.

40. Karden, E., Buller, S., & De Doncker, R. W. (2000). A method for measurement and interpretation of impedance spectra for industrial batteries. *Journal of Power sources*, *85*(1), 72-78.

41. Hu, X., Yuan, H., Zou, C., Li, Z., & Zhang, L. (2018). Co-estimation of state of charge and state of health for lithium-ion batteries based on fractional-order calculus. *IEEE Transactions on Vehicular Technology*, *67*(11), 10319-10329.

42. Hu, X., Jiang, J., Cao, D., & Egardt, B. (2015). Battery health prognosis for electric vehicles using sample entropy and sparse Bayesian predictive modeling. *IEEE Transactions on Industrial Electronics*, *63*(4), 2645-2656.

43. Li, J., Wang, L., Lyu, C., Wang, H., & Liu, X. (2016). New method for parameter estimation of an electrochemical-thermal coupling model for LiCoO2 battery. *Journal of Power Sources*, *307*, 220-230.

44. Moskon, J.; Jamnik, J.; Gaberscek, M. In Depth Discussion of Selected Phenomena Associated with Intrinsic Battery Hysteresis: Battery Electrode versus Rubber Balloons. Solid State Ion. 2013, 238, 24–29. [CrossRef]

45. Kalogiannis, T.; Hosen, M.S.; Sokkeh, M.A.; Goutam, S.; Jaguemont, J.; Jin, L.; Qiao, G.; Berecibar, M.; Van Mierlo, J. Comparative Study on Parameter Identification Methods for Dual-Polarization Lithium-Ion Equivalent Circuit Model. Energies 2019, 12, 4031. [CrossRef]

46. Li, A.; Pelissier, S.; Venet, P.; Gyan, P. Fast Characterization Method for Modeling Battery Relaxation Voltage. Batteries 2016, 2, 7. [CrossRef]

47. Torregrosa, A. J., Broatch, A., Olmeda, P., & Agizza, L. (2023). A generalized equivalent circuit model for lithium-iron phosphate batteries. *Energy*, *284*, 129316.

48. Lagnoni, M., Scarpelli, C., Lutzemberger, G., & Bertei, A. (2024). Critical comparison of equivalent circuit and physics-based models for lithium-ion batteries: A graphite/lithium-iron-phosphate case study. *Journal of Energy Storage*, *94*, 112326.

49. He, H., Xiong, R., & Fan, J. (2011). Evaluation of lithium-ion battery equivalent circuit models for state of charge estimation by an experimental approach. *energies*, *4*(4), 582-598.

50. Li, J., Cheng, Y., Jia, M., Tang, Y., Lin, Y., Zhang, Z., & Liu, Y. (2014). An electrochemical–thermal model based on dynamic responses for lithium iron phosphate battery. *Journal of Power Sources*, *255*, 130-143.

51. Zhang, L., Wang, L., Hinds, G., Lyu, C., Zheng, J., & Li, J. (2014). Multi-objective optimization of lithium-ion battery model using genetic algorithm approach. *Journal of Power Sources*, *270*, 367-378.

52. Forman, J. C., Moura, S. J., Stein, J. L., & Fathy, H. K. (2012). Genetic identification and fisher identifiability analysis of the Doyle–Fuller–Newman model from experimental cycling of a LiFePO4 cell. *Journal of Power Sources*, *210*, 263-275.

53. Rahman, M. A., Anwar, S., & Izadian, A. (2016). Electrochemical model parameter identification of a lithium-ion battery using particle swarm optimization method. *Journal of Power Sources*, *307*, 86-97.

54. Pang, H., Mou, L., Guo, L., & Zhang, F. (2019). Parameter identification and systematic validation of an enhanced single-particle model with aging degradation physics for Li-ion batteries. *Electrochimica Acta*, *307*, 474-487.

55. Li, J., Wang, L., Lyu, C., Liu, E., Xing, Y., & Pecht, M. (2018). A parameter estimation method for a simplified electrochemical model for Li-ion batteries. *Electrochimica Acta*, *275*, 50-58.

56. Tang, X., Wang, Y., Zou, C., Yao, K., Xia, Y., & Gao, F. (2019). A novel framework for Lithium-ion battery modeling considering uncertainties of temperature and aging. *Energy conversion and management*, *180*, 162-170.

57. Panchal, S., Mathew, M., Fraser, R., & Fowler, M. (2018). Electrochemical thermal modeling and experimental measurements of 18650 cylindrical lithium-ion battery during discharge cycle for an EV. *Applied Thermal Engineering*, *135*, 123-132.

58. Xu, M., Zhang, Z., Wang, X., Jia, L., & Yang, L. (2015). A pseudo three-dimensional electrochemical–thermal model of a prismatic LiFePO4 battery during discharge process. *Energy*, *80*, 303-317.

59. Li, X., Fan, G., Rizzoni, G., Canova, M., Zhu, C., & Wei, G. (2016). A simplified multi-particle model for lithium ion batteries via a predictor-corrector strategy and quasi-linearization. *Energy*, *116*, 154-169.

60. Wang, Y., Li, J., Zhang, J., & Pecht, M. (2021). Lithium-iron-phosphate battery electrochemical modelling under a wide range of ambient temperatures. *Journal of Electroanalytical Chemistry*, *882*, 115041.

61. Newman J S and Tobias C W 1962 Theoretical analysis of current distribution in porous electrodes J. Electrochem. Soc. 109 1183

62. Newman J S and Tiedemann W 1975 Porous-electrode theory with battery applications AlChE J. 21 25

63. Paxton B and Newman J 1997 Modeling of nickel/metal hydride batteries J. Electrochem. Soc. 144 3818

64. Liu J, Khaleghi Rahimian S and Monroe C W 2016 Capacity-limiting mechanisms in Li/O2 batteries Phys. Chem. Chem. Phys. 18 22840–51

65. Doyle M, Fuller T F and Newman J S 1993 Modeling of galvanostatic charge and discharge of the lithium/polymer/insertion cell J. Electrochem. Soc. 140 1526

66. Fuller T F, Doyle M and Newman J S 1994 Relaxation phenomena in lithium-ion-insertion cells J. Electrochem. Soc. 141 982

67. Fuller T F, Doyle M and Newman J S 1994 Simulation and optimization of the dual lithium ion insertion cell J. Electrochem. Soc. 141 1–10

68. Newman J and Thomas-Alyea K E 2004 Electrochemical Systems vol 3 (New York: Wiley-Interscience)

69. Atlung S, West K and Jacobsen T 1979 Dynamic aspects of solid solution cathodes for electrochemical power sources J. Electrochem. Soc. 126 1311–21

70. Prada E, Di Domenico D, Creff Y, Bernard J, Sauvant-Moynot V and Huet F 2012 Simplified electrochemical and thermal model of LiFePO4-graphite Li-ion batteries for fast charge applications J. Electrochem. Soc. 159 A1508–19

71. Deng, Z., Deng, H., Yang, L., Cai, Y., & Zhao, X. (2017). Implementation of reduced-order physics-based model and multi-parameters identification strategy for lithium-ion battery. *Energy*, *138*, 509-519.

72. Nazari, A., Kavian, S., & Nazari, A. (2020). Lithium-ion batteries' energy efficiency prediction using physics-based and state-of-the-art artificial neural network-based models. *Journal of Energy Resources Technology*, *142*(10), 102001.

73. Thelen, A., Lui, Y. H., Shen, S., Laflamme, S., Hu, S., Ye, H., & Hu, C. (2022). Integrating physics-based modeling and machine learning for degradation diagnostics of lithium-ion batteries. *Energy Storage Materials*, *50*, 668-695.

74. Li, Y., Karunathilake, D., Vilathgamuwa, D. M., Mishra, Y., Farrell, T. W., & Zou, C. (2021). Model order reduction techniques for physics-based lithium-ion battery management: A survey. *IEEE Industrial Electronics Magazine*, *16*(3), 36-51.

75. Bhattacharya, S., Maddikunta, P. K. R., Meenakshisundaram, I., Gadekallu, T. R., Sharma, S., & Alkahtani, M. (2021). Deep Neural Networks Based Approach for Battery Life Prediction. *Computers, Materials & Continua*, *69*(2).

76. Chemali, E., Kollmeyer, P. J., Preindl, M., & Emadi, A. (2018). State-of-charge estimation of Li-ion batteries using deep neural networks: A machine learning approach. *Journal of Power Sources*, *400*, 242-255.

77. How, D. N., Hannan, M. A., Lipu, M. S. H., Sahari, K. S., Ker, P. J., & Muttaqi, K. M. (2020). State-of-charge estimation of li-ion battery in electric vehicles: A deep neural network approach. *IEEE Transactions on Industry Applications*, *56*(5), 5565-5574.

78. Adedeji, B. P., & Kabir, G. (2023). A feedforward deep neural network for predicting the state-of-charge of lithium-ion battery in electric vehicles. *Decision Analytics Journal*, *8*, 100255.

79. Gong, Q., Wang, P., & Cheng, Z. (2022). A novel deep neural network model for estimating the state of charge of lithium-ion battery. *Journal of Energy Storage*, *54*, 105308.

80. Tian, J., Xiong, R., Shen, W., & Lu, J. (2021). State-of-charge estimation of LiFePO4 batteries in electric vehicles: A deep-learning enabled approach. *Applied Energy*, *291*, 116812.

81. Kara, A. (2021). A data-driven approach based on deep neural networks for lithium-ion battery prognostics. *Neural Computing and Applications*, *33*(20), 13525-13538.

82. Li, Y., Li, K., Liu, X., Wang, Y., & Zhang, L. (2021). Lithium-ion battery capacity estimation—A pruned convolutional neural network approach assisted with transfer learning. Applied Energy, 285, 116410.

83. Chun, H., Kim, J., & Han, S. (2019). Parameter identification of an electrochemical lithium-ion battery model with convolutional neural network. IFAC-PapersOnLine, 52(4), 129-134.

84. Wang, S., Ren, P., Takyi-Aninakwa, P., Jin, S., & Fernandez, C. (2022). A critical review of improved deep convolutional neural network for multi-timescale state prediction of lithium-ion batteries. Energies, 15(14), 5053.

85. Gu, X., See, K. W., Li, P., Shan, K., Wang, Y., Zhao, L., ... & Zhang, N. (2023). A novel state-of-health estimation for the lithium-ion battery using a convolutional neural network and transformer model. Energy, 262, 125501.

86. Fan, X., Zhang, W., Zhang, C., Chen, A., & An, F. (2022). SOC estimation of Li-ion battery using convolutional neural network with U-Net architecture. Energy, 256, 124612.

87. Haris, M., Hasan, M. N., & Qin, S. (2022). Degradation curve prediction of lithium-ion batteries based on knee point detection algorithm and convolutional neural network. IEEE Transactions on Instrumentation and Measurement, 71, 1-10.

88. Buchanan, S., & Crawford, C. (2024). Probabilistic lithium-ion battery state-of-health prediction using convolutional neural networks and Gaussian process regression. Journal of Energy Storage, 76, 109799.

89. Pradyumna, T. K., Cho, K., Kim, M., & Choi, W. (2022). Capacity estimation of lithium-ion batteries using convolutional neural network and impedance spectra. Journal of Power Electronics, 22(5), 850-858.

90. Chen, J., Manivanan, M., Duque, J., Kollmeyer, P., Panchal, S., Gross, O., & Emadi, A. (2023, June). A convolutional neural network for estimation of lithium-ion battery state-of-health during constant current operation. In 2023 IEEE transportation electrification conference & expo (ITEC) (pp. 1-6). IEEE.

91. Yao, L., Zheng, J., Xiao, Y., Zhang, C., Zhang, L., Gong, X., & Cui, G. (2023). An intelligent fault diagnosis method for lithium-ion battery pack based on empirical mode decomposition and convolutional neural network. Journal of Energy Storage, 72, 108181.

92. Ma, L., Xie, W., & Zhang, Y. (2019). Blister defect detection based on convolutional neural network for polymer lithium-ion battery. Applied Sciences, 9(6), 1085.

93. Chemali, E., Kollmeyer, P. J., Preindl, M., Fahmy, Y., & Emadi, A. (2022). A convolutional neural network approach for estimation of li-ion battery state of health from charge profiles. Energies, 15(3), 1185.

94. Costa, N., Sánchez, L., Anseán, D., & Dubarry, M. (2022). Li-ion battery degradation modes diagnosis via Convolutional Neural Networks. Journal of Energy Storage, 55, 105558.

95. Qian, C., Xu, B., Chang, L., Sun, B., Feng, Q., Yang, D., ... & Wang, Z. (2021). Convolutional neural network based capacity estimation using random segments of the charging curves for lithium-ion batteries. Energy, 227, 120333.

96. Kim, K. H., Oh, K. H., Ahn, H. S., & Choi, H. D. (2023). Time–frequency domain deep convolutional neural network for Li-ion battery SoC estimation. IEEE Transactions on Power Electronics, 39(1), 125-134.

97. Yang, N., Song, Z., Hofmann, H., & Sun, J. (2022). Robust State of Health estimation of lithium-ion batteries using convolutional neural network and random forest. Journal of Energy Storage, 48, 103857.

98. Zraibi, B., Okar, C., Chaoui, H., & Mansouri, M. (2021). Remaining useful life assessment for lithium-ion batteries using CNN-LSTM-DNN hybrid method. IEEE Transactions on Vehicular Technology, 70(5), 4252-4261.

99. Li, J., Wang, S., Chen, L., Wang, Y., Zhou, H., & Guerrero, J. M. (2024). Adaptive Kalman filter and self-designed early stopping strategy optimized convolutional neural network for state of energy estimation of lithium-ion battery in complex temperature environment. Journal of Energy Storage, 83, 110750.

100. Pang, Y., Dong, A., Wang, Y., & Niu, Z. (2024). Deep learning from three-dimensional Lithium-ion battery multiphysics model Part II: Convolutional neural network and long short-term memory integration. Energy and AI, 17, 100398.

101. Wang, Z., Zhao, X., Zhen, D., Pombo, J., Yang, W., Gu, F., & Ball, A. (2024). Adaptable capacity estimation of lithium-ion battery based on short-duration random constant-current charging voltages and convolutional neural networks. Energy, 306, 132541.

102. Schmitt, J., Horstkötter, I., & Bäker, B. (2023). Electrical lithium-ion battery models based on recurrent neural networks: A holistic approach. Journal of Energy Storage, 58, 106461.

103. Chen, J. C., Chen, T. L., Liu, W. J., Cheng, C. C., & Li, M. G. (2021). Combining empirical mode decomposition and deep recurrent neural networks for predictive maintenance of lithium-ion battery. Advanced Engineering Informatics, 50, 101405.

104. Tancogne-Dejean, T., Gorji, M. B., Zhu, J., & Mohr, D. (2021). Recurrent neural network modeling of the large deformation of lithium-ion battery cells. International Journal of Plasticity, 146, 103072.

105. Chen, J., Feng, X., Jiang, L., & Zhu, Q. (2021). State of charge estimation of lithium-ion battery using denoising autoencoder and gated recurrent unit recurrent neural network. Energy, 227, 120451.

106. Xi, Z., Wang, R., Fu, Y., & Mi, C. (2022). Accurate and reliable state of charge estimation of lithium ion batteries using time-delayed recurrent neural networks through the identification of overexcited neurons. Applied Energy, 305, 117962.

107. Ansari, S., Ayob, A., Lipu, M. H., Hussain, A., & Saad, M. H. M. (2024). Jellyfish optimized recurrent neural network for state of health estimation of lithium-ion batteries. Expert Systems with Applications, 238, 121904.

108. Feng, X., Chen, J., Zhang, Z., Miao, S., & Zhu, Q. (2021). State-of-charge estimation of lithium-ion battery based on clockwork recurrent neural network. Energy, 236, 121360.

109. Wang, Y., Han, X., Guo, D., Lu, L., Chen, Y., & Ouyang, M. (2022). Physics-informed recurrent neural network with fractional-order gradients for state-of-charge estimation of lithium-ion battery. IEEE Journal of Radio Frequency Identification, 6, 968-971.

110. Catelani, M., Ciani, L., Fantacci, R., Patrizi, G., & Picano, B. (2021). Remaining useful life estimation for prognostics of lithium-ion batteries based on recurrent neural network. IEEE Transactions on Instrumentation and Measurement, 70, 1-11.

111. Yang, F., Li, W., Li, C., & Miao, Q. (2019). State-of-charge estimation of lithium-ion batteries based on gated recurrent neural network. Energy, 175, 66-75.

112. Jiang, Y., Yu, Y., Huang, J., Cai, W., & Marco, J. (2021). Li-ion battery temperature estimation based on recurrent neural networks. Science China Technological Sciences, 64(6), 1335-1344.

113. Liu, J., Saxena, A., Goebel, K., Saha, B., & Wang, W. (2010, October). An adaptive recurrent neural network for remaining useful life prediction of lithium-ion batteries. In Annual Conference of the PHM Society (Vol. 2, No. 1).

114. Zhao, R., Kollmeyer, P. J., Lorenz, R. D., & Jahns, T. M. (2018). A compact methodology via a recurrent neural network for accurate equivalent circuit type modeling of lithium-ion batteries. IEEE Transactions on Industry Applications, 55(2), 1922-1931.

115. Ansari, S., Ayob, A., Hossain Lipu, M. S., Hussain, A., & Saad, M. H. M. (2021). Data-driven remaining useful life prediction for lithium-ion batteries using multi-charging profile framework: A recurrent neural network approach. Sustainability, 13(23), 13333.

116. Chen, Z., Xue, Q., Wu, Y., Shen, S., Zhang, Y., & Shen, J. (2020). Capacity prediction and validation of lithium-ion batteries based on long short-term memory recurrent neural network. IEEE access, 8, 172783-172798.

117. Teixeira, R. S., Calili, R. F., Almeida, M. F., & Louzada, D. R. (2024). Recurrent neural networks for estimating the state of health of lithium-ion batteries. Batteries, 10(3), 111.

118. Wang, Q., Ye, M., Wei, M., Lian, G., & Wu, C. (2021). Co-estimation of state of charge and capacity for lithium-ion battery based on recurrent neural network and support vector machine. Energy Reports, 7, 7323-7332.

119. Lu, J., Xiong, R., Tian, J., Wang, C., Hsu, C. W., Tsou, N. T., ... & Li, J. (2022). Battery degradation prediction against uncertain future conditions with recurrent neural network enabled deep learning. Energy Storage Materials, 50, 139-151.

120. Tao, S., Jiang, B., Wei, X., & Dai, H. (2023). A systematic and comparative study of distinct recurrent neural networks for lithium-ion battery state-of-charge estimation in electric vehicles. Energies, 16(4), 2008.

121. Durmus, F., & Karagol, S. (2024). Lithium-Ion Battery Capacity Prediction with GA-Optimized CNN, RNN, and BP. Applied Sciences, 14(13), 5662.

122. Bockrath, S., Rosskopf, A., Koffel, S., Waldhör, S., Srivastava, K., & Lorentz, V. R. (2019, October). State of charge estimation using recurrent neural networks with

long short-term memory for lithium-ion batteries. In IECON 2019-45th annual conference of the IEEE industrial electronics society (Vol. 1, pp. 2507-2511). IEEE.

123. Zhao, R., Kollmeyer, P. J., Lorenz, R. D., & Jahns, T. M. (2017, October). A compact unified methodology via a recurrent neural network for accurate modeling of lithium-ion battery voltage and state-of-charge. In 2017 IEEE Energy Conversion Congress and Exposition (ECCE) (pp. 5234-5241). IEEE.

124. Li, C., Xiao, F., Fan, Y., Yang, G., & Zhang, W. (2019, May). A recurrent neural network with long short-term memory for state of charge estimation of lithium-ion batteries. In 2019 IEEE 8th Joint International Information Technology and Artificial Intelligence Conference (ITAIC) (pp. 1712-1716). IEEE.

125. Yi, Y., Xia, C., Feng, C., Zhang, W., Fu, C., Qian, L., & Chen, S. (2023). Digital twin-long short-term memory (LSTM) neural network based real-time temperature prediction and degradation model analysis for lithium-ion battery. Journal of Energy Storage, 64, 107203.

126. Zhang, Y., Xiong, R., He, H., & Pecht, M. G. (2018). Long short-term memory recurrent neural network for remaining useful life prediction of lithium-ion batteries. IEEE Transactions on Vehicular Technology, 67(7), 5695-5705.

127. Chemali, E., Kollmeyer, P. J., Preindl, M., Ahmed, R., & Emadi, A. (2017). Long short-term memory networks for accurate state-of-charge estimation of Li-ion batteries. IEEE Transactions on Industrial Electronics, 65(8), 6730-6739.

128. Hoque, M. A., Hassan, M. K., Dhaarwind, M., Hajjo, A., & Al Atta, K. (2023, December). Investigation of Loading Variation Effect on Lithium Iron Phosphate Battery Electrodes Using Long Short Term Memory. In 2023 IEEE 21st Student Conference on Research and Development (SCOReD) (pp. 327-332). IEEE.

129. Yang, F., Song, X., Xu, F., & Tsui, K. L. (2019). State-of-charge estimation of lithium-ion batteries via long short-term memory network. Ieee Access, 7, 53792-53799.

130. Liu, Y., Sun, J., Shang, Y., Zhang, X., Ren, S., & Wang, D. (2023). A novel remaining useful life prediction method for lithium-ion battery based on long short-

term memory network optimized by improved sparrow search algorithm. Journal of Energy Storage, 61, 106645.

131. Zhao, S., Zhang, C., & Wang, Y. (2022). Lithium-ion battery capacity and remaining useful life prediction using board learning system and long short-term memory neural network. Journal of Energy Storage, 52, 104901.

132. Korbaa, N. E. H., Bouchetata, N., Belarbi, A. W., Kayisli, K., & Kaplan, O. (2024, May). Comparative Study of Different Deep Learning Approaches for State of Charge Estimation in Lithium Iron Phosphate Battery. In 2024 12th International Conference on Smart Grid (icSmartGrid) (pp. 714-718). IEEE.

133. Chun, H., Kim, J., Yu, J., & Han, S. (2020). Real-time parameter estimation of an electrochemical lithium-ion battery model using a long short-term memory network. Ieee Access, 8, 81789-81799.

134. Pang, Y., Dong, A., Wang, Y., & Niu, Z. (2024). Deep learning from three-dimensional Lithium-ion battery multiphysics model Part II: Convolutional neural network and long short-term memory integration. Energy and AI, 17, 100398.

135. Li, P., Zhang, Z., Xiong, Q., Ding, B., Hou, J., Luo, D., ... & Li, S. (2020). State-of-health estimation and remaining useful life prediction for the lithium-ion battery based on a variant long short term memory neural network. Journal of power sources, 459, 228069.

136. Wang, Y., Zhu, J., Cao, L., Gopaluni, B., & Cao, Y. (2023). Long short-term memory network with transfer learning for lithium-ion battery capacity fade and cycle life prediction. Applied Energy, 350, 121660.

137. Almaita, E., Alshkoor, S., Abdelsalam, E., & Almomani, F. (2022). State of charge estimation for a group of lithium-ion batteries using long short-term memory neural network. Journal of Energy Storage, 52, 104761.

138. Li, W., Sengupta, N., Dechent, P., Howey, D., Annaswamy, A., & Sauer, D. U. (2021). Online capacity estimation of lithium-ion batteries with deep long short-term memory networks. Journal of power sources, 482, 228863.

139. Li, W., Sengupta, N., Dechent, P., Howey, D., Annaswamy, A., & Sauer, D. U. (2021). Online capacity estimation of lithium-ion batteries with deep long short-term memory networks. Journal of power sources, 482, 228863.

140. Jeong, D., Park, J., Jang, Y., & Bae, S. (2023, May). State of Charge Estimation of Lithium Iron Phosphate Battery Using Bidirectional Long Short-Term Memory. In 2023 11th International Conference on Power Electronics and ECCE Asia (ICPE 2023-ECCE Asia) (pp. 1212-1218). IEEE.

141. Takyi-Aninakwa, P., Wang, S., Liu, G., Bage, A. N., Masahudu, F., & Guerrero, J. M. (2024). An enhanced lithium-ion battery state-of-charge estimation method using long short-term memory with an adaptive state update filter incorporating battery parameters. Engineering Applications of Artificial Intelligence, 132, 107946.

142. Tan, Y., & Zhao, G. (2019). Transfer learning with long short-term memory network for state-of-health prediction of lithium-ion batteries. IEEE Transactions on Industrial Electronics, 67(10), 8723-8731.

143. Gong, Y., Zhang, X., Gao, D., Li, H., Yan, L., Peng, J., & Huang, Z. (2022). State-of-health estimation of lithium-ion batteries based on improved long short-term memory algorithm. Journal of Energy Storage, 53, 105046.

144. Ardeshiri, R. R., Liu, M., & Ma, C. (2022). Multivariate stacked bidirectional long short term memory for lithium-ion battery health management. Reliability Engineering & System Safety, 224, 108481.

145. Zhang, H., Niu, G., Zhang, B., & Miao, Q. (2021). Cost-effective Lebesgue sampling long short-term memory networks for lithium-ion batteries diagnosis and prognosis. IEEE Transactions on Industrial Electronics, 69(2), 1958-1967.

146. Burgos-Mellado, C., Orchard, M. E., Kazerani, M., Cárdenas, R., & Sáez, D. (2016). Particle-filtering-based estimation of maximum available power state in Lithium-Ion batteries. *Applied Energy*, *161*, 349-363.

147. Ang, E. Y., & Paw, Y. C. (2022). Linear model for online state of health estimation of lithium-ion batteries using segmented discharge profiles. *IEEE Transactions on Transportation Electrification*, *9*(2), 2464-2471.

148. Zhou, D., Song, X., Lu, W., & Fu, P. (2019). Real-time SOH estimation algorithm for lithium-ion batteries based on daily segment charging data. *Proceedings of the CSEE*, *39*(1), 105-111.

149. Athappan, V., Piriyadharshini, D., Suganthi, S., Abimanyu, A., Ranganathan, S., Saravanabalaji, M., & Muthuramalingam, E. (2023, June). Health Monitoring of E-Vehicle Battery Using Machine Learning. In *2023 2nd International Conference on Advancements in Electrical, Electronics, Communication, Computing and Automation (ICAECA)* (pp. 1-6). IEEE.

150. Allirani, S., Pooja, K., Soundarya, E., & Nair, S. S. (2023, July). Li-ion Battery Life Estimation using K-Nearest Neighbor Algorithm. In *2023 2nd International Conference on Edge Computing and Applications (ICECAA)* (pp. 1606-1610). IEEE.

151. Vilsen, S. B., & Stroe, D. I. (2024). Dataset of lithium-ion battery degradation based on a forklift mission profile for state-of-health estimation and lifetime prediction. *Data in Brief*, *52*, 109861.

152. Sheikhani, A., & Agic, E. (2024). Lithium-Ion Battery SOH Forecasting With Deep Learning Augmented By Explainable Machine Learning.

153. Severson, K. A., Attia, P. M., Jin, N., Perkins, N., Jiang, B., Yang, Z., ... & Braatz, R. D. (2019). Data-driven prediction of battery cycle life before capacity degradation. *Nature Energy*, *4*(5), 383-391.

154. Safavi, V., Mohammadi Vaniar, A., Bazmohammadi, N., Vasquez, J. C., & Guerrero, J. M. (2024). Battery Remaining Useful Life Prediction Using Machine Learning Models: A Comparative Study. *Information*, *15*(3), 124.

155. Oyucu, S., Doğan, F., Aksöz, A., & Biçer, E. (2024). Comparative Analysis of Commonly Used Machine Learning Approaches for Li-Ion Battery Performance Prediction and Management in Electric Vehicles. *Applied Sciences*, *14*(6), 2306.

156. Zhang, Y. (2023). *Data-driven battery aging diagnostics and prognostics* (Master's thesis, Chalmers Tekniska Hogskola (Sweden).

157. Luo, K., Chen, X., Zheng, H., & Shi, Z. (2022). A review of deep learning approach to predicting the state of health and state of charge of lithium-ion batteries. *Journal of Energy Chemistry*, *74*, 159-173.

158. Guo, Y., Huang, K., & Hu, X. (2021). A state-of-health estimation method of lithium-ion batteries based on multi-feature extracted from constant current charging curve. *Journal of Energy Storage*, *36*, 102372.

159. Zhu, H., Li, Z., Li, C., Jia, H., Fang, H., Qiao, L., ... & Li, X. (2023). Near-in-situ electrochemical impedance spectroscopy analysis based on lithium iron phosphate electrode. Electrochimica Acta, 464, 142919.

160. Westerhoff, U., Kurbach, K., Lienesch, F., & Kurrat, M. (2016). Analysis of lithium-ion battery models based on electrochemical impedance spectroscopy. Energy Technology, 4(12), 1620-1630.

161. Tröltzsch, U., Kanoun, O., & Tränkler, H. R. (2006). Characterizing aging effects of lithium ion batteries by impedance spectroscopy. Electrochimica acta, 51(8-9), 1664-1672.

162. Osaka, T., Mukoyama, D., & Nara, H. (2015). Development of diagnostic process for commercially available batteries, especially lithium ion battery, by electrochemical impedance spectroscopy. Journal of The Electrochemical Society, 162(14), A2529.

163. Choi, W., Shin, H. C., Kim, J. M., Choi, J. Y., & Yoon, W. S. (2020). Modeling and applications of electrochemical impedance spectroscopy (EIS) for lithium-ion batteries. Journal of Electrochemical Science and Technology, 11(1), 1-13.

164. Stroe, D. I., Swierczynski, M., Stan, A. I., Knap, V., Teodorescu, R., & Andreasen, S. J. (2014, September). Diagnosis of lithium-ion batteries state-of-health based on electrochemical impedance spectroscopy technique. In 2014 IEEE Energy Conversion Congress and Exposition (ECCE) (pp. 4576-4582). IEEE.

165. Murbach, M. D., Hu, V. W., & Schwartz, D. T. (2018). Nonlinear electrochemical impedance spectroscopy of lithium-ion batteries: experimental approach, analysis, and initial findings. Journal of The Electrochemical Society, 165(11), A2758.

166. Zhuang, Q. C., Qiu, X. Y., Xu, S. D., Qiang, Y. H., & Su, S. G. (2012). Diagnosis of electrochemical impedance spectroscopy in lithium-ion batteries. Lithium Ion Batteries—New Developments, 8, 189-227.

167. Zheng, Y., He, Y. B., Qian, K., Li, B., Wang, X., Li, J., ... & Zhang, J. (2015). Deterioration of lithium iron phosphate/graphite power batteries under high-rate discharge cycling. Electrochimica Acta, 176, 270-279.

168. Song, J. Y., Lee, H. H., Wang, Y. Y., & Wan, C. C. (2002). Two-and three-electrode impedance spectroscopy of lithium-ion batteries. Journal of Power Sources, 111(2), 255-267.

169. Vetter, J., Novák, P., Wagner, M. R., Veit, C., Möller, K. C., Besenhard, J. O., ... & Hammouche, A. (2005). Ageing mechanisms in lithium-ion batteries. *Journal of power sources*, *147*(1-2), 269-281.

170. Mocera, F., Somà, A., & Clerici, D. (2020, September). Study of aging mechanisms in lithium-ion batteries for working vehicle applications. In *2020 Fifteenth International Conference on Ecological Vehicles and Renewable Energies (EVER)* (pp. 1-8). IEEE.

171. Barré, A., Deguilhem, B., Grolleau, S., Gérard, M., Suard, F., & Riu, D. (2013). A review on lithium-ion battery ageing mechanisms and estimations for automotive applications. *Journal of power sources*, *241*, 680-689. Barré, A., Deguilhem, B., Grolleau, S., Gérard, M., Suard, F., & Riu, D. (2013). A review on lithium-ion battery ageing mechanisms and estimations for automotive applications. *Journal of power sources*, *241*, 680-689.

172. Seok, J., Lee, W., Lee, H., Park, S., Chung, C., Hwang, S., & Yoon, W. S. (2024). Aging Mechanisms of Lithium-ion Batteries. *J. Electrochem. Sci. Technol*, *15*, 51-66.

173. Arora, P., White, R. E., & Doyle, M. (1998). Capacity fade mechanisms and side reactions in lithium-ion batteries. *Journal of the Electrochemical Society*, *145*(10), 3647.

174. Scarfogliero, M., Carmeli, S., Castelli-Dezza, F., Mauri, M., Rossi, M., Marchegiani, G., & Rovelli, E. (2018, July). Lithium-ion batteries for electric

vehicles: A review on aging models for vehicle-to-grid services. In *2018 International Conference of Electrical and Electronic Technologies for Automotive* (pp. 1-6). IEEE.

175. Zhang, X., Han, Y., & Zhang, W. (2021). A review of factors affecting the lifespan of lithium-ion battery and its health estimation methods. *Transactions on Electrical and Electronic Materials*, *22*(5), 567-574.

176. Yang, S., Zhang, C., Jiang, J., Zhang, W., Zhang, L., & Wang, Y. (2021). Review on state-of-health of lithium-ion batteries: Characterizations, estimations and applications. *Journal of Cleaner Production*, *314*, 128015.

177. Zhu, J., Xu, W., Knapp, M., Darma, M. S. D., Mereacre, L., Su, P., ... & Ehrenberg, H. (2023). A method to prolong lithium-ion battery life during the full life cycle. *Cell Reports Physical Science*, *4*(7).

178. Sharma, S. K., Sharma, G., Gaur, A., Arya, A., Mirsafi, F. S., Abolhassani, R., ... & Mishra, Y. K. (2022). Progress in electrode and electrolyte materials: path to all-solid-state Li-ion batteries. *Energy Advances*, *1*(8), 457-510.

179. Khumprom, P., & Yodo, N. (2019). A data-driven predictive prognostic model for lithium-ion batteries based on a deep learning algorithm. *Energies*, *12*(4), 660.

180. Tran, M. K., & Fowler, M. (2020). A review of lithium-ion battery fault diagnostic algorithms: Current progress and future challenges. *Algorithms*, *13*(3), 62.

181. Zhang, Y. (2023). *Data-driven battery aging diagnostics and prognostics* (Master's thesis, Chalmers Tekniska Hogskola (Sweden)).

182. Thelen, A. C. (2023). *Machine learning-based aging models for estimating battery state of health and predicting future degradation* (Doctoral dissertation, Iowa State University).

183. Rivera-Barrera, J. P., Muñoz-Galeano, N., & Sarmiento-Maldonado, H. O. (2017). SoC estimation for lithium-ion batteries: Review and future challenges. *Electronics*, *6*(4), 102.

184. [1] Nair, V., & Hinton, G. E. (2010). Rectified linear units improve restricted Boltzmann machines. In Proceedings of the 27th international conference on machine learning (ICML-10) (pp. 807-814).

185. [2] Ioffe, S., & Szegedy, C. (2015). Batch normalization: Accelerating deep network training by reducing internal covariate shift. In International conference on machine learning (pp. 448-456).

186. [3] Srivastava, N., Hinton, G. E., Krizhevsky, A., Sutskever, I., & Salakhutdinov, R. (2014). Dropout: A simple way to prevent neural networks from overfitting. Journal of machine learning research, 15(1), 1929-1958.

187. [4] Kingma, D. P., & Ba, J. (2014). Adam: A method for stochastic optimization. arXiv preprint arXiv:1412.6980.

188. [5] Prechelt, L. (1997). Early stopping-but when? In Neural networks: Tricks of the trade (pp. 55-69). Springer, Berlin, Heidelberg.

189. [6] Smith, L. N. (2015). Cyclical learning rates for training neural networks. In 2015 IEEE international conference on neural networks (ICNN) (pp. 4680-4687). IEEE.

190. [7] J. Zhang, "Evaluation Metrics for Regression Models," IEEE Comput. Intell. Mag., vol. 14, no. 3, pp. 23-29, Sept. 2020.

191. [8] D. Kingma and J. Ba, "Adam: A Method for Stochastic Optimization," Proc. Int. Conf. Learn. Represent., 2015.

192. [9] P. Varma, "Optimizer Selection for Deep Learning Models," IEEE Access, vol. 7, pp. 172399-172412, Dec. 2019.

193. [10] H. Zou, "Understanding Regression Metrics," IEEE Trans. Statist. Learn., vol. 3, no. 1, pp. 15-27, Jan. 2022.

194. [11] C. C. Aggarwal, "Data Mining and Regression Techniques," IEEE Data Sci. Bull., vol. 12, no. 1, pp. 33-50, Jan. 2018.

195. [12] Srivastava, N., Hinton, G., Krizhevsky, A., Sutskever, I., & Salakhutdinov, R. (2014). Dropout: A simple way to prevent neural networks from overfitting. Journal of Machine Learning Research, 15(1), 1929-1958.

196. [13] Ioffe, S., & Szegedy, C. (2015). Batch normalization: Accelerating deep network training by reducing internal covariate shift. In International conference on machine learning (pp. 448-456).

197. [14] Kingma, D. P., & Ba, J. (2014). Adam: A method for stochastic optimization. arXiv preprint arXiv:1412.6980.

198. [15] Bahdanau, D., Cho, K., & Bengio, Y. (2014). Neural machine translation by jointly learning to align and translate. arXiv preprint arXiv:1409.0473.

199. [16] Goodfellow, I., Bengio, Y., & Courville, A. (2016). Deep learning. MIT press.

200. [17] Nair, V., & Hinton, G. E. (2010). Rectified linear units improve restricted boltzmann machines. In Proceedings of the 27th international conference on machine learning (ICML-10) (pp. 807-814).

201. [18] Lin, M., Chen, Q., & Yan, S. (2013). Network in network. arXiv preprint arXiv:1312.4400.

202. [19] Kingma, D. P., & Ba, J. (2014). Adam: A method for stochastic optimization. arXiv preprint arXiv:1412.6980.

203. [20] Yu, F., & Koltun, V. (2015). Multi-scale context aggregation by dilated convolutions. arXiv preprint arXiv:1511.07122.

204. [21] Srivastava, N., Hinton, G., Krizhevsky, A., Sutskever, I., & Salakhutdinov, R. (2014). Dropout: A simple way to prevent neural networks from overfitting. Journal of Machine Learning Research, 15(1), 1929-1958.

205. [22] Hochreiter, S., & Schmidhuber, J. (1997). Long short-term memory. Neural computation, 9(8), 1735-1780.

206. [23] Graves, A. (2012). Supervised sequence labelling with recurrent neural networks. Studies in computational intelligence, 385, 39-68.

207. [24] Ioffe, S., & Szegedy, C. (2015). Batch normalization: Accelerating deep network training by reducing internal covariate shift. In International conference on machine learning (pp. 448-456).

208. Leninpugalhanthi, P., Kumar, R. S., Ramya, G., Prithika, P., Nandhakishore, R., Narendaren, K., & Ishwarya, S. (2022, March). Lithium-ion battery life estimation using machine learning algorithm. In *2022 8th international conference on advanced computing and communication systems (ICACCS)* (Vol. 1, pp. 573-576). IEEE.

209. Baydan, S. S., Ceylan, M., & Tuncay, R. N. (2021, November). A Study on the State of Health of Lithium-ion Batteries. In *2021 13th International Conference on Electrical and Electronics Engineering (ELECO)* (pp. 509-513). IEEE.

210. Kaypmaz, T. C., & Tuncay, R. N. (2011, September). An advanced cell model for diagnosing faults in operation of Li-ion Polymer batteries. In *2011 IEEE Vehicle Power and Propulsion Conference* (pp. 1-5). IEEE.

Appendix

```
import numpy as np
import pandas as pd
import tensorflow as tf
import matplotlib.pyplot as plt
import matplotlib.cm as cm
!pip install scikit-learn # Install scikit-learn if not already
installed
#Import the necessary functions
from sklearn.metrics import mean_absolute_error, mean_squared_error,
r2_score
#from sklearn.model_selection import train_test_split
from keras.models import Sequential
from tensorflow.keras.optimizers import Adam
from keras.layers import Conv1D, Conv2D, MaxPooling1D, MaxPooling2D,
Dense, Flatten, Activation, LSTM, BatchNormalization, SimpleRNN,
Dropout


# Functions for plotting
def plot_both(Y_val, predicted_soh):
  plt.figure()
  #plt.plot(Y_val, label='Actual SOH')
  plt.scatter(range(len(Y_val)), Y_val, label='Actual SOH')
  #plt.plot(predicted_soh, label='Predicted SOH')
  plt.scatter(range(len(predicted_soh)), predicted_soh,
label='Predicted SOH')
  plt.xlabel('Sample')
  plt.ylabel('SOH')
  plt.legend()
  plt.show()

def plot_actual_soh(Y_val):
    plt.figure()
    plt.plot(Y_val, label='Actual SOH')
    plt.xlabel('Sample')
    plt.ylabel('SOH')
    plt.legend()
    plt.title('Actual SOH')
    plt.show()

def plot_predicted_soh(predicted_soh):
```

```
    plt.figure()
    plt.plot(predicted_soh, label='Predicted SOH')
    plt.xlabel('Sample')
    plt.ylabel('SOH')
    plt.legend()
    plt.title('Predicted SOH')
    plt.show()



#data = pd.read_csv('/content/26650 Cell Data_V7.csv')
data = pd.read_csv('/content/26650 Cell Data_V7.csv')


# Drop rows with missing values
data = data.dropna()


#X = data[['terminal_voltage','terminal_current', 'temperature'
,'charge_current' ,'charge_voltage' , 'capacity',
'cycle',  'SoC']].values
#Y = data['SoH'].values
Training_data = data[(data['temperature'] == 25)]
Validating_data = data[data['temperature'] == 25]


print(len(Training_data))


# Split data into training and validation sets
## X_train, X_val, Y_train, Y_val = train_test_split(X, Y,
test_size=0.2, random_state=101)
X_train = Training_data[['terminal_voltage','terminal_current',
'temperature' ,'charge_current' ,'charge_voltage' , 'capacity',
'cycle',  'SoC']].values
Y_train = Training_data['SoH'].values
X_val = Validating_data[['terminal_voltage','terminal_current',
'temperature' ,'charge_current' ,'charge_voltage' , 'capacity',
'cycle',  'SoC']].values
Y_val = Validating_data['SoH'].values

print(X_train.shape)
```

```
# Create TensorFlow Datasets from the numpy arrays
train_dataset = tf.data.Dataset.from_tensor_slices((X_train,Y_train))
test_dataset = tf.data.Dataset.from_tensor_slices((X_val, Y_val))

# Shuffle and Batch the Data
batch_size = 32
train_dataset =
train_dataset.shuffle(buffer_size=len(X_train)).batch(batch_size)
test_dataset = test_dataset.batch(batch_size)
```

DNN

```
######################
##### BUILD MODEL #####
######################

from tensorflow.keras.models import Sequential
from tensorflow.keras.layers import Dense, BatchNormalization, Dropout

model = Sequential()
model.add(Dense(8, activation='relu', input_dim=X_train.shape[1]))
model.add(BatchNormalization())
model.add(Dense(64, activation='relu'))
model.add(BatchNormalization())
model.add(Dense(128, activation='relu'))
model.add(BatchNormalization())
model.add(Dense(64, activation='relu'))  # Added layer
model.add(BatchNormalization())
model.add(Dense(32, activation='relu'))  # Added layer
model.add(BatchNormalization())
model.add(Dropout(rate=0.2))
model.add(Dense(1))

model.summary()
model.compile(optimizer=Adam(beta_1=0.9, beta_2=0.999, epsilon=1e-08),
loss='mean_absolute_error')


######################
```

```
##### TRAIN MODEL #####
######################

model.fit(x=X_train, y=Y_train, batch_size=25, epochs=130)

# Evaluate the model
loss = model.evaluate(X_val, Y_val)
print("Validation Loss:", loss)

# Create a figure with specified size
plt.figure(figsize=(12, 6))

# Plot Actual SOH
plt.plot(Y_val, label='Actual SOH', color='blue', linewidth=2)
dnn_pred = model.predict(X_val)
predicted_soh = dnn_pred
# Plot DNN Prediction
plt.plot(dnn_pred, label='DNN Prediction', color='orange',
linestyle='--', marker='o', markersize=3)

# Customize plot
plt.xlabel('Sample', fontsize=12)
plt.ylabel('SoH', fontsize=12)
plt.title('Actual vs. Predicted SoH (DNN)', fontsize=14)
plt.legend(fontsize=10)
plt.grid(True, linestyle='--', alpha=0.5)  # Lighter gridlines
plt.tight_layout()

# Show the plot
plt.show()

# Calculate Error Metrics
mae = mean_absolute_error(Y_val, predicted_soh)
rmse = np.sqrt(mean_squared_error(Y_val, predicted_soh))
r2 = r2_score(Y_val, predicted_soh)
print(f"MAE: {mae:.4f}")
print(f"RMSE: {rmse:.4f}")
print(f"R-squared: {r2:.4f}")

# Calculate absolute error
absolute_error = np.abs(Y_val - predicted_soh)

# Plot error vs. cycle number
```

```
plt.figure(figsize=(10, 5))
plt.plot(absolute_error)
plt.xlabel("Cycle Number")
plt.ylabel("Absolute Error")
plt.title("Absolute Error vs. Cycle Number")
plt.grid(True)
plt.show()

# Plot output
plot_actual_soh(Y_val)
plot_predicted_soh(predicted_soh)
plot_both(Y_val, predicted_soh)
```

CNN

```
def concat_sequence(data, labels, window_size=50):

    # Prepare the sequences
    sequences = np.lib.stride_tricks.as_strided(
        data,
        shape=(data.shape[0] - window_size + 1, window_size,
data.shape[1]),
        strides=(data.strides[0], data.strides[0], data.strides[1])
    )

    sequence_labels = labels[window_size-1:]

    return sequences, sequence_labels


from keras.layers import GlobalAveragePooling2D

# Reshape input data for CNN (add one dimension for channel)
X_train = X_train.reshape(-1, X_train.shape[1], 1) # remove extra
dimension
X_val = X_val.reshape(-1, X_val.shape[1], 1) # remove extra dimension

print(X_train.shape)
print(Y_train.shape)
print(X_val.shape)
seq_train, seq_label_train = concat_sequence(X_train, Y_train)
```

```
seq_val, seq_label_val = concat_sequence(X_val, Y_val)

# Define the CNN model

model = Sequential([
    Conv2D(64, kernel_size=(3, 1), activation='relu',
input_shape=(seq_train.shape[1], seq_train.shape[2], 1)), # Adjust
input_shape
    #MaxPooling2D(pool_size=(2, 1)),
    Flatten(),
    Dense(64, activation='relu'),
    Dense(1)  # Output layer with 1 neuron for SOH prediction
])
'''
model = Sequential([
    Conv2D(64, kernel_size=(3, 1), activation='relu',
input_shape=(seq_train.shape[1], seq_train.shape[2], 1)),
    GlobalAveragePooling2D(),
    Dense(64, activation='relu'),
    Dense(1)  # Output layer with 1 neuron for SOH prediction
])
'''
# Compile the model
model.compile(optimizer='adam', loss='mean_squared_error')

# Print model summary
model.summary()



print(seq_train.shape)
print(seq_label_train.shape)

# Train the model
history = model.fit(seq_train, seq_label_train,
validation_data=(seq_val, seq_label_val), epochs=130, batch_size=32)

# Evaluate the model
loss = model.evaluate(seq_val, seq_label_val)
print("Validation Loss:", loss)

# Predict SOH
predicted_soh = model.predict(seq_val)
```

```
print("Predicted SOH:", predicted_soh)
cnn_pred = predicted_soh

# Create a figure with specified size
plt.figure(figsize=(15, 6))

# Plot Actual SOH
plt.plot(Y_val, label='Actual SOH', color='blue', linewidth=3)

# Plot CNN Prediction
plt.plot(cnn_pred, label='CNN Prediction', color='purple',
linestyle='--', marker='.', markersize=2)

# Customize plot
plt.xlabel('Sample', fontsize=14)
plt.ylabel('SoH', fontsize=14)
plt.title('Actual vs. Predicted SoH (CNN)', fontsize=16)
plt.legend(fontsize=12, loc='upper right')  # Place legend outside the
plot
plt.grid(True, linestyle='--', alpha=0.5)  # Lighter gridlines
plt.tight_layout()
# Plot output
plot_actual_soh(seq_label_val)
plot_predicted_soh(predicted_soh)
plot_both(seq_label_val,predicted_soh)


# Calculate Error Metrics
mae = mean_absolute_error(seq_label_val, predicted_soh) # Use
seq_label_val instead of Y_val
rmse = np.sqrt(mean_squared_error(seq_label_val, predicted_soh)) # Use
seq_label_val instead of Y_val
r2 = r2_score(seq_label_val, predicted_soh) # Use seq_label_val
instead of Y_val
print(f"MAE: {mae:.4f}")
print(f"RMSE: {rmse:.4f}")
print(f"R-squared: {r2:.4f}")

# Calculate absolute error
absolute_error = np.abs(seq_label_val - predicted_soh) # Use
seq_label_val instead of Y_val

# Plot error vs. cycle number
```

```
plt.figure(figsize=(10, 5))
plt.plot(absolute_error)
plt.xlabel("Cycle Number")
plt.ylabel("Absolute Error")
plt.title("Absolute Error vs. Cycle Number")
plt.grid(True)
plt.show()

# Plot output
plot_actual_soh(Y_val)
plot_predicted_soh(predicted_soh)
plot_both(Y_val, predicted_soh)
```

RNN

```
from tensorflow.keras.models import Sequential
from tensorflow.keras.layers import SimpleRNN, BatchNormalization,
Dense, Dropout
from tensorflow.keras.callbacks import EarlyStopping,
ReduceLROnPlateau


X_train = X_train.reshape(-1, X_train.shape[1], 1)  # Remove the extra
dimension
X_val = X_val.reshape(-1, X_val.shape[1], 1)

# Define RNN model
model = Sequential([
    LSTM(128, activation='tanh', return_sequences=True,
input_shape=(X_train.shape[1], X_train.shape[2])),
    Dropout(0.2),
    BatchNormalization(),
    LSTM(64, activation='tanh', return_sequences=False),
    Dropout(0.2),
    BatchNormalization(),
    Dense(64, activation='relu'),
    Dropout(0.2),
    BatchNormalization(),
    Dense(32, activation='relu'),
    Dropout(0.2),
    BatchNormalization(),
```

```
    Dense(1)
])
# Compile the model
optimizer = tf.keras.optimizers.Adam(learning_rate=0.0005)
model.compile(optimizer=optimizer, loss='mean_squared_error')

# Define callbacks
early_stopping = EarlyStopping(monitor='val_loss', patience=20,
restore_best_weights=True)
reduce_lr = ReduceLROnPlateau(monitor='val_loss', factor=0.5,
patience=5, min_lr=1e-6)

# Print model summary
model.summary()




# Train the model
history = model.fit(X_train, Y_train, epochs=200, batch_size=32,
validation_data=(X_val, Y_val),
                    callbacks=[early_stopping, reduce_lr])

# Evaluate the model
loss = model.evaluate(X_val, Y_val)
print("Validation Loss:", loss)

# Predict SOH for RNN model
rnn_pred = predicted_soh

# Create a figure with specified size
plt.figure(figsize=(15, 6))

# Plot Actual SOH
plt.plot(Y_val, label='Actual SOH', color='blue', linewidth=3)

# Plot RNN Prediction
plt.plot(rnn_pred, label='RNN Prediction', color='red', linestyle='--
', marker='.', markersize=2)

# Customize plot
plt.xlabel('Sample', fontsize=14)
```

```
plt.ylabel('SoH', fontsize=14)
plt.title('Actual vs. Predicted SoH (RNN)', fontsize=16)
plt.legend(fontsize=12, loc='upper right')  # Place legend outside the
plot
plt.grid(True, linestyle='--', alpha=0.5)  # Lighter gridlines
plt.tight_layout()

# Predict SOH for RNN model
predicted_soh_rnn = model.predict(X_val)  # Predict using the RNN
model
rnn_pred = predicted_soh_rnn

# ... (rest of your plotting code) ...

# Calculate Error Metrics using predicted_soh_rnn
mae = mean_absolute_error(Y_val, predicted_soh_rnn)
rmse = np.sqrt(mean_squared_error(Y_val, predicted_soh_rnn))
r2 = r2_score(Y_val, predicted_soh_rnn)
print(f"MAE: {mae:.4f}")
print(f"RMSE: {rmse:.4f}")
print(f"R-squared: {r2:.4f}")

# Calculate absolute error using predicted_soh_rnn
absolute_error = np.abs(Y_val - predicted_soh_rnn)

# Plot error vs. cycle number
plt.figure(figsize=(10, 5))
plt.plot(absolute_error)
plt.xlabel("Cycle Number")
plt.ylabel("Absolute Error")
plt.title("Absolute Error vs. Cycle Number")
plt.grid(True)
plt.show()

# Plot output
plot_actual_soh(Y_val)
plot_predicted_soh(predicted_soh)
plot_both(Y_val, predicted_soh)
```

LSTM

```
from tensorflow.keras.models import Sequential
from tensorflow.keras.layers import LSTM, BatchNormalization, Dense,
Dropout
from tensorflow.keras.callbacks import EarlyStopping,
ReduceLROnPlateau

# ... (rest of your code)

X_train = X_train.reshape(-1, X_train.shape[1], 1)  # Remove the extra
dimension
X_val = X_val.reshape(-1, X_val.shape[1], 1)

# Define the LSTM model
model = Sequential([
    LSTM(128, activation='tanh', return_sequences=True,
input_shape=(X_train.shape[1], X_train.shape[2])),
    Dropout(0.2),
    BatchNormalization(),
    LSTM(64, activation='tanh', return_sequences=False),
    Dropout(0.2),
    BatchNormalization(),
    Dense(64, activation='relu'),
    Dropout(0.2),
    BatchNormalization(),
    Dense(32, activation='relu'),
    Dropout(0.2),
    BatchNormalization(),
    Dense(1)
])

# Compile the model
optimizer = tf.keras.optimizers.Adam(learning_rate=0.0005)  # Slightly
reduced learning rate
model.compile(optimizer=optimizer, loss='mean_squared_error')

# Define callbacks
early_stopping = EarlyStopping(monitor='val_loss', patience=20,
restore_best_weights=True)  # Increased patience
```

```
reduce_lr = ReduceLROnPlateau(monitor='val_loss', factor=0.5,
patience=5, min_lr=1e-6)


# Print model summary
model.summary()
```

```
# Train the model
history = model.fit(X_train, Y_train, epochs=200, batch_size=32,
validation_data=(X_val, Y_val),
                    callbacks=[EarlyStopping(monitor='val_loss',
patience=20, restore_best_weights=True), reduce_lr])

# Evaluate the model
loss = model.evaluate(X_val, Y_val)
print("Validation Loss:", loss)

# Create a figure with specified size
plt.figure(figsize=(15, 6))

# Plot Actual SOH
plt.plot(Y_val, label='Actual SOH', color='blue', linewidth=3)
lstm_pred = model.predict(X_val)
# Plot LSTM Prediction
plt.plot(lstm_pred, label='LSTM Prediction', color='yellow',
linestyle='--', marker='.', markersize=2)

# Customize plot
plt.xlabel('Sample', fontsize=14)
plt.ylabel('SoH', fontsize=14)
plt.title('Actual vs. Predicted SoH (LSTM)', fontsize=16)
plt.legend(fontsize=12, loc='upper right')  # Place legend outside the
plot
plt.grid(True, linestyle='--', alpha=0.5)  # Lighter gridlines
plt.tight_layout()


# Calculate Error Metrics
# Use lstm_pred which has the same shape as Y_val
mae = mean_absolute_error(Y_val, lstm_pred)
```

```
rmse = np.sqrt(mean_squared_error(Y_val, lstm_pred))
r2 = r2_score(Y_val, lstm_pred)
print(f"MAE: {mae:.4f}")
print(f"RMSE: {rmse:.4f}")
print(f"R-squared: {r2:.4f}")

# Calculate absolute error
absolute_error = np.abs(Y_val - lstm_pred)

# Plot error vs. cycle number
plt.figure(figsize=(10, 5))
plt.plot(absolute_error)
plt.xlabel("Cycle Number")
plt.ylabel("Absolute Error")
plt.title("Absolute Error vs. Cycle Number")
plt.grid(True)
plt.show()

# Plot output
plot_actual_soh(Y_val)
plot_predicted_soh(lstm_pred) # Use lstm_pred for plotting
plot_both(Y_val, lstm_pred) # Use lstm_pred for plotting
```

For plotting All

```
import matplotlib.pyplot as plt

plt.figure(figsize=(15, 6))

# Plot Actual SOH
plt.plot(Y_val, label='Actual SOH', color='blue', linewidth=2)

# Plot Model Predictions with distinct colors and markers
plt.plot(dnn_pred, label='DNN Prediction', color='orange',
linestyle='-', marker='o', markersize=3)
plt.plot(cnn_pred, label='CNN Prediction', color='green', linestyle='-
-', marker='s', markersize=3)
plt.plot(rnn_pred, label='RNN Prediction', color='red', linestyle=':',
marker='^', markersize=3)
plt.plot(lstm_pred, label='LSTM Prediction', color='purple',
linestyle='-.', marker='x', markersize=3)

plt.xlabel('Sample')
plt.ylabel('SoH')
plt.title('Actual vs. Predicted SoH')
plt.legend()
plt.grid(True)
plt.tight_layout()

plt.show()
```